Universidad de Valladolid

Escuela de Doctorado Universidad de Valladolid

PROGRAMA DE DOCTORADO EN INVESTIGACIÓN BIOMÉDICA

TESIS DOCTORAL

Sarcoplasmic reticulum Ca^{2+} dynamics in aging *Drosophila* and correlation with sarcopenia

Presentada por Alba Del Río Lorenzo para optar al
grado de
Doctor/a por la Universidad de Valladolid

Dirigida por:

Dr. Javier García-Sancho Martín
Dra. María Teresa Alonso Alonso

Valladolid, 2020

A mis padres Javier y Milagros

“Educar la mente sin educar el corazón no es educar en absoluto”

Aristóteles

Para empezar una tesis hace falta valentía, vocación y motivación, pero para acabarla hace falta perseverancia, constancia, disciplina, fuerza y paciencia. Por tanto, en primer lugar quiero agradecer a mis directores de tesis, a Maite y a Javier, por haberme dado esta oportunidad cuando llegué a Valladolid llena de esa vocación y esa motivación. Además agradecerles que me han mantenido llena de ilusión y ganas de aprender ciencia a lo largo de estos años. Siempre serán mis "padres científicos".

Por otro lado, para afrontar el día a día, hace falta todo un equipo que encaje a nivel científico y personal, y hay que decir no podría haber tenido uno mejor. Miriam, que me abrió las puertas el día que llegué, que me ha enseñado a manejarme en el laboratorio y que me ha ayudado como una madre a nivel personal. A Jonathan, que es otro padre científico para mí y que siempre ha dejado de hacer sus cosas por prestarme su incalculable ayuda y atención. A Paloma, que siempre ha sido un referente para mí, ya que, desde que llegué quería alcanzar el lugar al que ella había llegado. A Macarena, que ha sabido entenderme a la perfección a nivel personal y científico y con la que he pasado momentos inolvidables. A Raquel, con la que anduve los primeros pasos de la mano y que resultó ser un ejemplo de trabajo y bondad. A Jesús, por estar siempre dispuesto a ayudar y por los buenos momentos de las tardes de prácticas. A Karla y a Patry con las que he aprendido a enseñar, y que me han sabido ayudar, animar y llevar en la etapa más difícil del camino, el final. Gracias a las dos, por vuestro cariño y por todo lo que me habéis hecho crecer a nivel emocional.

Otro ingrediente importante para poder afrontar el día a día son los amigos, y yo no puedo haberme rodeado de mejores personas en esta etapa. Todos juntos, hemos sido, sin duda, todo un equipazo que ha sabido apoyarse en los momentos duros y divertirse como los que más siempre. Sin duda, sois lo mejor de esta etapa y se me queda corto este manuscrito para agradeceros todo lo que me habéis hecho crecer y sentir. Nagore, eres la mejor amiga que se puede desear. Eres, sin duda, todo un referente personal para mí y nuestra conexión mental es tan increíble que hablamos sin palabras. Alberto, eres un esencial en este camino, una de las personas que más me conoce y cuyo apoyo ha sido siempre infinito. Patri, eres de esas personas únicas, capaz de levantar el ánimo a cualquiera y

que ven el interior de los demás. Lucía, capaz de dar hasta que se queda sin nada para ella misma, inagotable es tu fuente de amor por los demás. Eu, eres la persona más fuerte y leal que conozco y precisamente por eso la que más he echado de menos en esta última etapa aunque nuestra amistad es un para siempre. Iván, la persona con la que más conversaciones científicas transcendentales he tenido y cuyos consejos tengo siempre presentes. Miguel, que siempre te recuerda qué es lo más importante en la vida. Laura, mi descubrimiento más tardío pero que me ha ayudado a alcanzar la meta como no lo habría hecho nadie, con sus palabras, sus risas, su amor y su increíble forma de ser. Sergio, que siempre lo ve todo con perspectiva y le pone una nota de humor. Y Nuria, que me recuerda a mis comienzos y cuya risa siempre te alegra el día. Gracias a toda la gente del IBGM, a Lola y Diego por responder a todas mis preguntas de moscas y a Miriam por nuestras charlas en el pasillo y en cultivos. A todo nuestro grupo de comer que siempre me hacen olvidarme de los problemas cotidianos: Sara, Jorge, Elisa, Aida, Sendoa y Vero.

Una de las experiencias clave en este periodo es la estancia. Yo tuve la suerte de realizarla en Múnich en el laboratorio de la Dr. Fabiana Perocchi, a la que agradezco que me acogiera y me dedicara parte de su tiempo. Pero lo más importante de esta parte imprescindible del doctorado es el crecimiento tanto científico como personal. El ver cómo hacen ciencia en otro país te abre la mente y te prepara para el futuro. Por otro lado conocer a tanta gente con culturas y educaciones diferentes supone un gran enriquecimiento personal. Fueron unos meses increíbles en los que estuve muy bien acompañada y en los que hice amistades muy especiales. Anja, siempre dispuesta a ayudar con cualquier tipo de problema fue mi guía en la cuidad y en el Helmholtz. Sandra y Val, con las que conocí todas las ciudades cercanas a Múnich viviendo momentos increíbles. Elena, mi compañera de confesiones y cervezas. Irem, la que más me ha enseñado y apoyado en todo momento. Kontxe, la persona más dulce que jamás conoceré en mi vida y el resto de compañeros, cada uno ha aportado su granito de arena en mi crecimiento personal: Fran, Ruth, Theresa, René, Guisseppe, Daniela y Tina.

Gracias a mis amigas, las de toda la vida, mi grupo de “miss you” que me acompañan en cada paso de mi vida desde que tengo uso de razón. A mis

“supernenas”, que aunque lejos, están siempre en mí día a día, y que me sacan sonrisas aunque haya tenido el peor de los días. A Lucía Montero, que con su fuerza y su cariño siempre es capaz de levantarme cuando me caigo y que siempre es un aliento de vida. Gracias por haberme incluido en “tu mundo” cuando más lo necesitaba y presentarme a todas tus personas increíbles que tan buenos momentos me han dado, gracias chicas. A mis “biogirls”, con las que entré en este mundo de la bioquímica y en especial a Bea Ranz, que siempre ha sido como una hermana para mí.

Por último, gracias a toda mi familia. A mi tío Gustavo que siempre me anima a alcanzar mis metas, a mi tía Rous que siempre será mi hada madrina y a mi abuela Rosa, que siempre me recuerda que el pasado nunca vuelve y hay que vivir el presente. Gracias a mis abuelos, Paula y Luis, que estarían muy orgullosos de mí. A mi hermana, Coral, que es una inyección de amor puro. Pero sobretodo, gracias a mis padres, a los que va dedicada esta tesis. Gracias, por enseñarme todo lo que sé. Por brindarme una magnífica educación, de la que estaré eternamente agradecida. Por inculcarme los valores más importantes y por vivir siempre en un hogar de amor. Gracias, porque me habéis hecho la persona que soy.

Some of the results exposed in this memory have been published in the following journals:

- **Delrio-Lorenzo, A**., Rojo-Ruiz, J., Alonso, M. T., & García-Sancho, J. (2020). Sarcoplasmic reticulum Ca^{2+} decreases with age and correlates with the decline in muscle function in *Drosophila*. *Journal of cell science*, 133(6), jcs240879.

Communications have also been presented at the following conferences:

- **Delrio-Lorenzo, A**., Rojo-Ruiz, J., Alonso, M. T., & García-Sancho, J. *In vivo* Ca^{2+} imaging in *Drosophila melanogaster* reveals correlation between decreased sarcoplasmic reticulum content and sarcopenia in aging. The 8^{th} workshop of the European Calcium Society on Calcium Signaling in Aging and Neurodegenerative Diseases. Coimbra 2019. Oral communication.
- **Delrio-Lorenzo, A**., Rojo-Ruiz, J., Alonso, M. T., & García-Sancho, J. GAP, flies, sarcoplasmic reticulum and aging. The 8^{th} workshop of the European Calcium Society on Calcium Signaling in Aging and Neurodegenerative Diseases. Coimbra 2019. Symposium.

Table of contents

List of figures

List of tables

Abbreviations

$[Ca^{2+}]$: Ca^{2+} concentration

$[Ca^{2+}]_C$: cytosolic Ca^{2+} concentration

$[Ca^{2+}]_{ER}$: endoplasmic reticulum Ca^{2+} concentration

$[Ca^{2+}]_{SR}$: sarcoplasmic reticulum Ca^{2+} concentration

A-IFM: asynchronous indirect flight muscle

ATP: adenosine triphosphate

BiP: immunoglobulin protein

CaBP: Calcium-Binding-Protein

CCh: carbachol

CNS: central nervous system

CEPIA: Calcium-measuring organelle-Entrapped Protein IndicAtors

CR: calreticulin

DHPR: dihydropyridine receptors

DLM: dorsal longitudinal muscle

DNA: deoxyribonucleic acid

DR: dynamic range

EGTA: Ethylene Glycol Tetraacetic Acid

Elav: embryonic lethal abnormal visual system

ER: endoplasmic reticulum

Fig: Figure

FKBP: FK506 binding proteins

GAL4: galactose-induced gene 4

GAP: GFP-Aequorin-Protein

GCaMP: (Green fluorescent protein-CalModulin Protein)

GECI: genetically encoded Ca^{2+} indicator

GF: giant fiber

GFP: Green Fluorescent Protein

HRP: horseradish peroxidase

IP_3: Inositol 1,4,5-triphosphate

IP_3R: Inositol 1,4,5-triphosphate receptors

Mhc: myosin heavy chain

NCX: Na^+/Ca^{2+} exchanger

Abbreviations

NCKX: $Na^+/Ca^{2+}/K^+$ exchanger

NMJ: neuromuscular junctions

PBS: phosphate-buffered saline

PMCA: Plasma Membrane Ca^{2+}-ATPase

R: fluorescence ratio of two individual wavelengths

R_{min}: minimal fluorescence ratio

R_{max}: maximal fluorescence ratio

R_0: basal fluorescence ratio

ROI: region of interest

ROS: Radical oxygen species

RT: room temperature

RyR: Ryanodine receptor

SERCA: the sarco/endoplasmic reticulum Ca^{2+}-ATPase

SOCE: Store-Operated Ca^{2+} Entry

SR: sarcoplasmic reticulum

SEM: standard error of the mean

SDS: sodium dodecyl sulphate

TBH: 2,5-di(tert-butyl)-1,4-benzohydroquinone

TC: terminal cisternae

UAS: upstream activating sequence

VOCC: Voltage-Operated Calcium Channel

WT: wild type

Summary

Aging still remains a mystery of biology and one of the most affected tissues in aging is skeletal muscle, whose loss of muscle mass and strength is called sarcopenia. Age-dependent sarcopenia is not restricted to mammals, as it affects other animal species including nematodes or flies. Cytosolic Ca^{2+} ion is the intracellular second messenger that triggers muscle contraction. The sarcoplasmic reticulum is the store of Ca^{2+} in the muscle cell, and it releases Ca^{2+} to the cytosol when muscle contracts. Sarcopenia has been linked to the loss of Ca^{2+} homeostasis that trigger muscle contraction, but mechanistic details remain unsolved.

Here we explore the hypothesis that an alteration of the Ca^{2+} content within the sarcoplasmic reticulum (SR) is at the origin of this loss of Ca^{2+} homeostasis observed in sarcopenia. For investigating this hypothesis, we generated transgenic flies that express the ratiometric low affinity Ca^{2+} indicator GAP3 targeted to the muscle sarcoplasmic reticulum (erGAP3), and we developed a new method to calibrate erGAP3 fluorescent signals into SR/ER Ca^{2+} concentrations ($[Ca^{2+}]_{SR/ER}$). With these tools we measured resting $[Ca^{2+}]_{SR}$ *in vivo* along the fly life, and found a progressive decrease with aging that results in a tenfold reduction in the $[Ca^{2+}]_{SR}$ in the oldest flies. Then, to explore the molecular mechanisms involved in this decrease of $[Ca^{2+}]_{SR}$ we studied the expression levels of the main proteins involved in $[Ca^{2+}]_{SR}$ resting levels. In old muscle, we found a slight non-significant increase in the ryanodine receptors (RyR) and in the immunoglobulin protein (BiP) expression whereas the expression of the sarco/endoplasmic reticulum Ca^{2+}-ATPase (SERCA) decreased by 35%. Moreover, the loss of function of the skeletal muscle was monitored by the well-characterized climbing assay, and found a strong correlation between the Ca^{2+} content of the sarcoplasmic reticulum and fly climbing ability with aging. Furthermore, to assess whether the reduction of $[Ca^{2+}]_{SR}$ content in the aged flies also affected the $[Ca^{2+}]_{C}$ transients, we studied the cytosolic Ca^{2+} dynamics during muscle contraction in transgenic flies expressing the cytosolic Ca^{2+} sensor GCaMP in the muscle tissue. This experiments showed that old flies released less Ca^{2+} to the cytosol in comparison to young flies and, thus, these results validated those obtained in the SR.

In order to investigate whether the reduction of SR Ca^{2+} content observed in muscle was a universal phenomenon of aging that occurred also in other tissues

we studied the progression of $[Ca^{2+}]_{ER}$ in brain neurons and in the peripheral sensory wing neurons using the pan neuronal transgenic line, which expresses erGAP3 in all types of neurons. The $[Ca^{2+}]_{ER}$ of the brain neurons did not change significantly with age, and remained stable along the whole fly life. However, the behaviour is different in other neurons as we can also appreciate a decrease in the $[Ca^{2+}]_{ER}$ of the sensory wing neurons, similar to what occurs in the skeletal muscle. Regarding the key molecular players, in contrast to the muscle, SERCA levels remained unchanged in brain neurons whereas BiP and RyR levels are increased in the aging brain.

Resumen

El envejecimiento se define como la pérdida gradual de la función de los tejidos y órganos, que, con el tiempo, lleva finalmente a la muerte. A nivel molecular, implica cambios graduales que llevan a la pérdida de la homeostasis lo que predispone a las patologías asociadas al envejecimiento como, por ejemplo, la sarcopenia o la pérdida de masa y fuerza muscular. La sarcopenia no es un fenómeno exclusivo de humanos, sino que ocurre también en los invertebrados, entre ellos los nemátodos y la mosca de la fruta, *Drosophila melanogaster*. Los mecanismos moleculares responsables de la sarcopenia no se han elucidado completamente. Una de las teorías con evidencias más sólidas postula que existe una deficiencia en el acoplamiento excitación-contracción muscular debido a la pérdida de la homeostasis del Ca^{2+}. El Ca^{2+} es el ion señalizador por excelencia y estas señales se producen en forma de picos o aumentos de la concentración de calcio citosólico ($[Ca^{2+}]_C$) que desencadenan una gran variedad de procesos fisiológicos, entre ellos la contracción muscular.

La hipótesis principal de este trabajo es que la pérdida de la homeostasis del Ca^{2+} observada en la sarcopenia asociada al envejecimiento se debe a una alteración del contenido de Ca^{2+} del retículo sarcoplásmico (RS). Siguiendo esta línea de trabajo nos propusimos realizar medidas de la $[Ca^{2+}]_{RS}$ *in vivo* en un modelo de *Drosophila melanogaster*. Para ello, generamos moscas transgénicas que expresan el sensor de Ca^{2+} de baja afinidad GAP3 dirigido al retículo sarcoplásmico (erGAP3), y desarrollamos un nuevo método para calibrar la señal fluorescente de erGAP3 en concentraciones de Ca^{2+} en el RS/RE. Con estas herramientas medimos la $[Ca^{2+}]_{RS}$ basal *in vivo*, y encontramos una disminución progresiva a lo largo de la vida de las mosca. Los niveles basales de $[Ca^{2+}]_{RS}$ alcanzaron valores de 600 µM en las moscas más jóvenes y disminuyeron hasta diez veces, a una concentración de 50 µM, en las moscas más viejas. Esta disminución de la $[Ca^{2+}]_{RS}$ se correlacionaba fuertemente con la pérdida de función del músculo esquelético en el envejecimiento, monitorizada mediante el ensayo de escalada. Posteriormente, para explorar los mecanismos moleculares implicados en la disminución de $[Ca^{2+}]_{RS}$, estudiamos los niveles de expresión de las principales proteínas involucradas en el mantenimiento de los niveles basales de $[Ca^{2+}]_{RS}$. En el músculo de las moscas viejas, encontramos una disminución de un 35% en la expresión de la ATPasa de Ca^{2+} del retículo (SERCA), que, aunque

significativo no puede explicar por sí solo la disminución de 10 veces en los niveles basales de $[Ca^{2+}]_{RS}$. Por otro lado, también encontramos un aumento leve, pero no significativo de la expresión de la chaperona BiP y del receptor de rianodina (RyR). Además, comprobamos si la reducción de la $[Ca^{2+}]_{RS}$ basal en las moscas envejecidas también afectaba a la $[Ca^{2+}]_{C}$. Para ello, estudiamos la dinámica del Ca^{2+} citosólico durante la contracción muscular en moscas transgénicas que expresan el sensor GCaMP en el músculo. Estos resultados demostraron que el RS de las moscas viejas libera menos contenido de Ca^{2+} al citosol, en comparación con las moscas jóvenes, lo cual está en coherencia con los resultados obtenidos en el RS.

Con el fin de investigar si la reducción de la $[Ca^{2+}]_{RS}$ observada en el músculo envejecido ocurría también en otros tejidos, estudiamos la progresión de $[Ca^{2+}]_{RE}$ en las neuronas del sistema nervioso central y en las neuronas sensoriales del ala, utilizando una línea de mosca transgénica que expresa el sensor erGAP3 en todo tipo de neuronas. El $[Ca^{2+}]_{RE}$ de las neuronas cerebrales no varió significativamente con la edad, y se mantuvo estable durante toda la vida de la mosca. Acorde con estos resultados, los niveles de SERCA se mantienen estables en las neuronas cerebrales con el envejecimiento. Sin embargo, el comportamiento fue diferente en otro tipo de neuronas, como las neuronas sensoriales del ala, donde se apreció una disminución en la $[Ca^{2+}]_{RE}$, similar a lo descrito en el músculo esquelético.

Introduction

1. Physiological aging

The inevitability of aging and death has preoccupied humanity for more than 5.000 years; however aging still remains a mystery of biology. Aging began to be viewed as capable of being extended or shaped in the 1980s, with the discovery of single gene mutations that extended lifespan in the nematode *Caenorhabditis elegans*. Nowadays, hundreds of mutant genes can increase longevity in model organisms, including nematodes, yeast (*Saccharomyces cerevisiae*), fruit flies (*Drosophila melanogaster*) and mice (*Mus musculus*). Most of these genes intervene in the evolutionarily conserved pathways that regulate growth, energy metabolism, nutrient sensing or reproduction. These recent discoveries in the biology of aging indicate that lifespan can be manipulated by genetic, nutritional or pharmacological intervention (Vijg and Campisi, 2008).

Aging is defined as the gradual loss of function of tissues and organs that ultimately results in death. This progressive deterioration is associated with many human pathologies including cancer, diabetes, cardiovascular disorders or neurodegenerative diseases (Kennedy et al., 2014). Understanding these age-related disorders is complicated but necessary to define the complexity of the aging phenotype, in contrast to the ease of defining single gene mutations. However, although some aging phenotypes are visible in laboratory models, they vary among mice strains or individuals and, more importantly some of them are not as obvious in invertebrates. This is the main reason why aging research should focus on searching for biomarkers to better define and characterize the degenerative processes underlying mortality (Vijg and Campisi, 2008).

1.1. The hallmarks of aging

Aging is a multifactorial process involving the interaction of genetic and environmental factors. Experts in the field have attempted to identify and categorize the molecular hallmarks of aging in mammals (López-Otín et al., 2013). They propose nine aging hallmarks (**Fig. 1**) that occur in normal aging and its experimental aggravation or deterioration accelerate or ameliorate aging,

respectively. Moreover, they can be classified in three categories: primary, antagonistic and integrative. **Primary hallmarks** include: genomic instability that involves random deoxyribonucleic acid (DNA) damage and failure in the DNA repair mechanisms; telomere attrition or shortening; epigenetic alterations, such as changes in the DNA methylation patterns; and, impaired protein homeostasis (termed proteostasis); and they produce negative effects. **Antagonistic hallmarks** refer to the mechanisms that are initially beneficial but become deleterious at chronic high levels. This class includes mitochondrial dysfunction, which results in increased generation of radical oxygen species (ROS); cellular senescence, defined as a stable arrest from the cell cycle; and deregulated nutrient sensing. By interconnecting the two groups, a new category of hallmarks arises, the **integrative** that are responsible for the progressive loss of tissue function observed in aging. Among these, stem cell exhaustion as a decline in the regenerative property of tissues, and altered intercellular communication, including endocrine, neuronal or neuroendocrine.

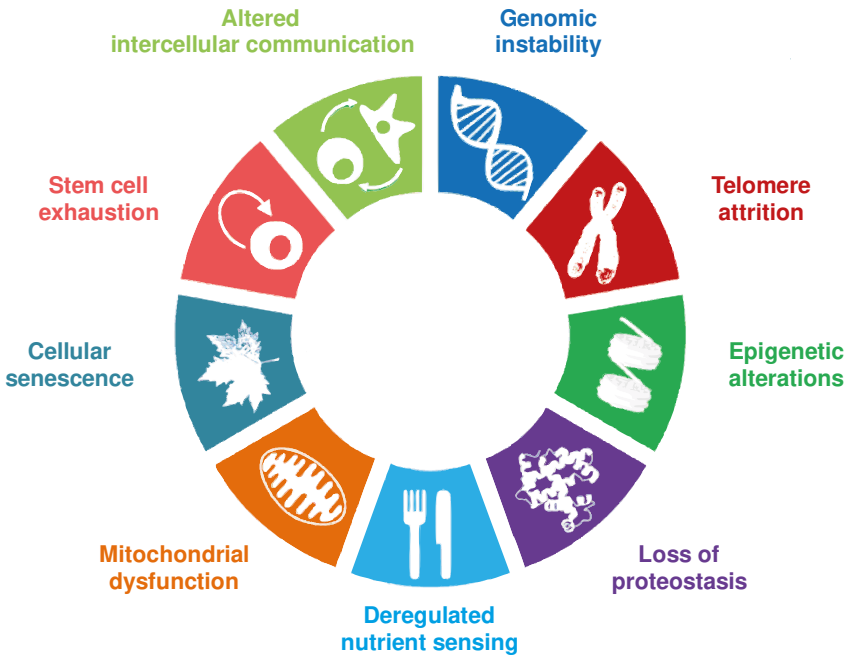

Figure 1. The Hallmarks of Aging. The diagram enumerates the proposed nine hallmarks of aging. In clockwise direction: genomic instability, telomere attrition, epigenetic alterations, loss of proteostasis, deregulated nutrient sensing, mitochondrial dysfunction, cellular senescence, stem cell exhaustion, and altered intercellular communication. Figure modified from (López-Otín et al., 2013).

Defining the hallmarks of aging may contribute to build a start point for future research on the molecular mechanisms of getting older and to design interventions for the new concept of "healthy aging" that has been defined by the World Health Organization (WHO) as "the process of developing and maintaining the functional ability that enables wellbeing in older age".

1.2. The history of aging theories

Despite the efforts of a number of researchers and the huge advances in molecular biology and genetics, the mechanisms underlying aging are still unknown (Davidovic et al., 2010). In order to increase human lifespan substantially, we first need to understand the primary cause of aging, which leads to the key questions of why and how we age. There are many theories trying to explain why we age; however each of them is focused on one particular aspect of the aging process and, for this reason, each theory is incomplete (Gladyshev, 2016). Aging theories mainly fall into three categories: **programmed theories,** that imply that aging follows a biological timetable; **evolutionary theories,** that try to explain the course of aging as an evolutionary mechanism; and, **damage or error theories,** that emphasize that aging could be a result of environmental action, that causes cumulative cellular damage at various levels (Jin, 2010; Park and Yeo, 2013).

The programmed and altruistic theory of aging considers that there is a genetic program that drives senescence and death, and this can be caused for two main altruistic reasons (Longo et al., 2005). Firstly, it benefits a small group of related organisms that acquire mutations to extend their lifespan; and, secondly, it must be necessary for the species as a group, as it could provide long-term benefits such as genetic diversity or acceleration of the pace of adaptation. In this context, the term "phenoptosis" (Skulachev, 1999) defines the death of an organism as a whole, alike to apoptosis (programmed cell death) which is a mechanism that has evolved to eliminate a portion of a multicellular organism. Similar phenomena are also already described at subcellular level, for example, the suicide of mitochondria is termed mitoptosis. Apoptosis is involved in many physiological processes such as cancer defence mechanism or immune response.

There are other sub-categories of programmed theories that view aging as a genetically regulated timetable. **The endocrine theory** postulates that the evolutionarily conserved insulin/IGF-1 signalling (IIS) pathway plays a key role in controlling the pace of aging (van Heemst, 2010). Also, **the immunological theory** states that the immune system is programmed to decline over time and that antibodies lose their effectiveness leading to an increased vulnerability to infectious disease and impaired immune function (Jin, 2010).

Almost 50 years ago, the evolutionary theorists proposed several arguments against these programmed theories, and a new series of evolutionary theories aroused, trying to explain how the aging process is a result of the evolution, as explained by Darwin in "The origin of species". The first argument postulated that the strength of natural selection declines with age, and, as a consequence, deleterious genetic mutations would accumulate and finally manifest at old age. This argument is known as **the mutation accumulation theory** and was proposed by Medawar in 1952 (Medawar, 1952). Few years later, in 1957, George Williams proposed another possibility: genetic trade-off alleles could cause harmful effects late in life but are selected because they are beneficial early in life. This proposal is known as the **antagonistic pleiotropy theory**. It suggests that aging evolves and does not act in any altruistic way for the species, but rather aging is adjusted by antagonistic pleiotropic genes. Another argument against programmed theories is introduced in the **disposable soma theory**, focused on metabolic trade-offs (Kirkwood, 1977). This theory stated that organisms have limited energy resources that have to be diverted between fertility and maintenance functions. The inability to allocate all resources makes repair functions less efficient over time and eventually it leads to damage accumulation.

Among the sub-category of damage and error theories, one of the most accepted is the **free radical theory** developed by Harman (Harman, 1956). This theory suggests that the ROS generated in cell metabolism randomly damage cellular components such as lipids, proteins, sugars and nucleic acids. Although several researchers have tried to prove this theory, the results have been mostly negative (Bokov et al., 2004). Reduction of ROS or increase of antioxidants is effective against oxidative stress but fail to increase longevity (Pérez et al., 2009). Furthermore, ROS species are also signalling molecules that can control gene

expression and other physiological processes, so total inhibition is detrimental (Sohal and Orr, 2012).

2. The muscle tissue

The muscle tissue is classified into three types according to its structure and function: skeletal, cardiac, and smooth muscle. Structurally, the skeletal muscle is attached to the bones and its function is to control voluntary movements. The cardiac muscle composes the contractile heart-wall and, thus, its function is to pump blood through the body. Finally, the smooth muscle recovers the internal organs and is responsible for their involuntary movement. The smooth muscle constitutes the contractile component of the digestive, urinary, and reproductive systems as well as the pulmonary airways and the arteries.

2.1. Skeletal muscle structure

Skeletal muscles are composed of bundles, termed fasciculus, of muscle cells or myofibers[1]. The muscle cell is tubular, multinucleated and no longer capable of division. Myofibers contain numerous tubular myofibrils, composed of repeating units of sarcomeres (**Fig. 2A**). Sarcomeres are composed of two types of contractile proteins, myosin and actin, that form thick and thin filaments, respectively. These filaments slide past each other when a muscle contracts or relaxes and, thus, their interaction is carefully regulated by the regulatory proteins called tropomyosin and troponin. Tropomyosin is a long, double-stranded, helical protein that wraps up the actin and serves to block its active site. Troponin is a small, globular protein complex composed of three subunits: troponin-C (TN-C) binds Ca^{2+} ions, troponin-T (TN-T) binds troponin to tropomyosin, and troponin-I (TN-I) inhibits the binding of actin to myosin in the resting state. The sarcomere is the basic contractile unit of skeletal muscles which is repeated between two Z-lines (**Fig. 2B**). The Z-line acts as an anchor of the actin filaments. Surrounding the Z-

[1] Both terms, muscle cell and myofiber, will be used as synonyms along the document.

line, it is located the region of the I-band, that is composed only by actin filaments. Following the I-band, it exists the A-band which contains both thick and thin filaments. Within the A-band is the M-line (in the middle of the sarcomere) formed of cross-connecting elements of the cytoskeleton (Henderson et al., 2017).

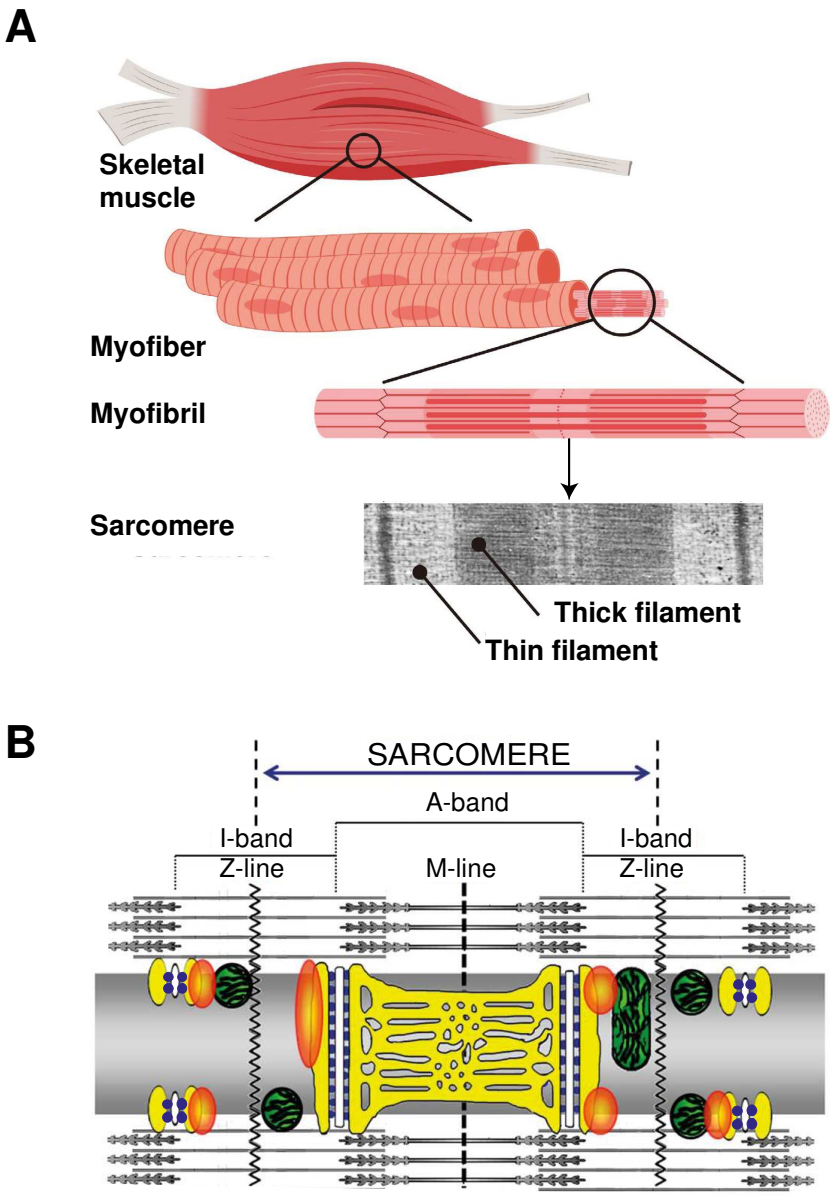

Figure 2. The skeletal muscle structure. A) Skeletal muscle tissue consists of bundles of myofibers, each one contains millions of myofibrils that are composed of repeating units of sarcomeres. The sarcomere is the minimum contractile unit, which consists of two types of contractile proteins, myosin and actin, that form thick and thin filaments, respectively. Figure modified from (Ojima, 2019). **B)** The picture represents the structure of the sarcomere. The sarcoplasmic reticulum is reproduced in yellow, while mitochondria (on both sides of the Z–lines) are illustrated in green. The white elongated structures display the plasma membrane T-tubules and the blue spots are the ryanodine receptors. Orange bubbles represent other sarcomere associated proteins. Figure modified from (Guarnieri et al., 2013).

The sarcoplasmic reticulum (SR) is a membrane-delimited intracellular organelle that spans the sarcomere and wraps up the contractile myofilaments in the skeletal muscle of almost all species and, thus, it is functionally involved in muscle contraction (Sorrentino, 2004). The SR is a specialized version of the endoplasmic reticulum (ER). The ER is a multifunctional organelle actively involved in Ca^{2+} signalling and other functions such as protein synthesis and correct folding, lipid metabolism and drug detoxification (Prins and Michalak, 2009). Morphologically, it appears as a continuous network with three distinct parts specialized in different functions (Pozzan et al., 1994; Friedman and Voeltz, 2011): the rough ER, the smooth ER and the nuclear envelope. The rough ER appears as flattened sacs and contains ribosomes for protein synthesis. Surrounding the nucleus is an extension of the ER called the nuclear envelope, also dotted with ribosomes, that acts as a discrete Ca^{2+} store in the perinuclear region, and supplies the nucleus with Ca^{2+} for gene transcription (Reddish et al., 2017). The smooth ER is an elongated, cylindrical network with three key functions in Ca^{2+} storage: Ca^{2+} uptake, mediated by pumps and exchangers; storage, enhanced by luminal Ca^{2+} binding proteins (CaBPs) that act as buffers; and, Ca^{2+} mobilization mediated by specific ion channels (Lam and Galione, 2013).

Morphologically, the SR consists on large tubes denominated terminal cisternae (TC) connected through elongated portions termed longitudinal SR. The Ryanodine receptor type 1 (RyR1) is located in TC whereas the sarco/endoplasmic reticulum Ca^{2+}-ATPase (SERCA) pump is found in the longitudinal SR, suggesting that the TC domain is in charge of Ca^{2+} release and the longitudinal SR of Ca^{2+} uptake (Rossi et al., 2008). In muscle cells, the TC domain is in close contact with the plasma membrane or sarcolemma, particularly with the tubule invaginations called transversal tubules or T-tubules. The dihydropyridine receptors (DHPRs), which are L-type voltage-dependent Ca^{2+} channels that activate upon muscle cell depolarization, are located in the T-tubules. In mammals DHPRs are physically in contact with the RyR type 1 of the TC to activate Ca^{2+} release when membrane depolarization occurs (Sorrentino, 2011). Skeletal muscle cells contain ER and SR regions, and the borders among them are not as obvious; the ER-SR compartment can be visualized as a patchwork of specialized domains (Rossi et al., 2008).

2.2. Skeletal muscle function

The muscle cells are functionally organized as motor units that consists on a single nerve (motoneuron) and all the muscle cells it innervates. In mammals, each skeletal myofiber is innervated by a single motoneuron; although the same motoneuron may also innervate other myofibers and, thus, the force of contraction of muscles is regulated by how many motor units are activated. Muscle contraction is initiated by the transmission of an impulse (action potential) from the motoneuron to the neuromuscular junction (NMJ), which is a chemical synapse between the motoneuron (presynaptic cell) and the muscle cell (postsynaptic cell). The motoneuron releases the neurotransmitter acetylcholine (ACh) to the synaptic cleft, which is the space between the pre- and post- synaptic cells, where it binds to its receptor in the muscle cell; which, in turn, leads to an action potential in the muscle. Skeletal muscle contraction (**Fig. 3**) is then activated by depolarization of cell membrane or sarcolemma. This signal spreads through the T-tubule system and activates DHPRs. The depolarization signal produces a conformational change in DHPRs that activates RyR1 channels. The opening of the RyR1 leads to a massive Ca^{2+} release from the SR towards the cytosol. Cytosolic Ca^{2+} binds to troponin-C (TN-C) which induces a conformational change in the regulatory complex such that troponin-I (TN-I) exposes a site on the actin molecule that is able to bind to the myosin ATPase located on the myosin head. This binding results in the adenosine triphosphate (ATP) hydrolysis that produces a conformational change in the actin-myosin complex. As a result, the actin and myosin filaments slide past each other, thereby shortening the sarcomere length (Allen et al., 2008; Zalk et al., 2007; Efremov et al., 2015). Ca^{2+} is sequestered to the SR by SERCA pump, thus, restoring the low-basal cytosolic Ca^{2+} concentration ($[Ca^{2+}]_C$) and removing Ca^{2+} from the TN-C. Unbinding of Ca^{2+} from TN-C induces a conformational change in the troponin complex leading, once again, to TN-I inhibition of the actin binding site. At the end of the cycle, a new ATP binds to the myosin head, displacing the adenosine diphosphate (ADP), and the initial sarcomere length is restored.

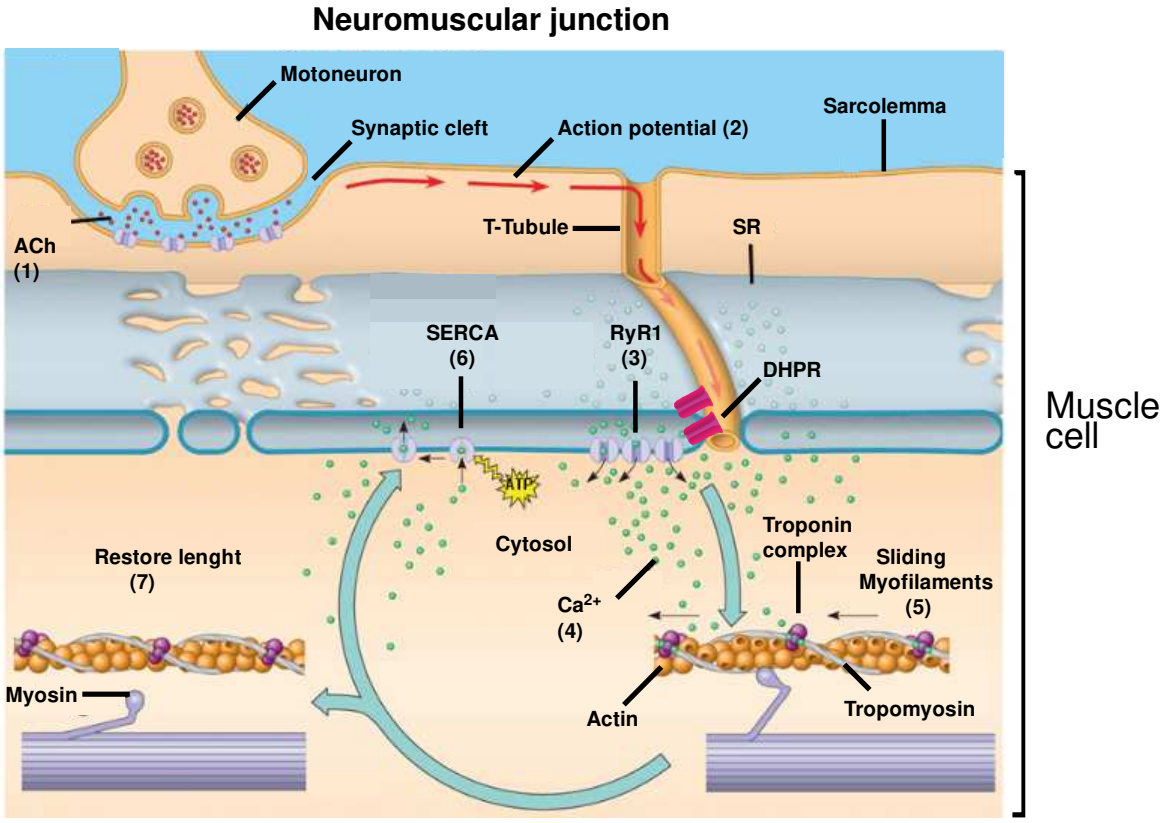

Figure 3. Skeletal muscle contraction. 1) An action potential arrives at the neuromuscular junction, and triggers acetylcholine release (ACh) that diffuses across the synaptic cleft and binds to its receptors on the plasma membrane. **2)** The action potential depolarizes the sarcolemma, and the signal spreads through the T-tubule system. **3)** The depolarization signal produces a conformational change in the dihydropyridine receptors (DHPR) that activates the Ryanodine receptor type 1 (RyR1). **4)** The opening of the RyR1 leads to an increase in cytosolic Ca^{2+} concentration. **5)** Cytosolic Ca^{2+} binds to the troponin complex, resulting in a conformational change such that the actin molecule exposes the active binding site and, binds to the myosin head. This shortens the sarcomeres length. **6)** The sarco/endoplasmic reticulum Ca^{2+}-ATPase (SERCA) pumps Ca^{2+} inside the sarcoplasmic reticulum (SR) and, therefore, refilling the SR store and restoring the low-basal cytosolic Ca^{2+} concentration. **7)** Unbinding of Ca^{2+} from troponin induces a conformational change in the troponin complex leading to inhibition of the actin binding site. The actin molecule is now unable to bind to the myosin head and, thus, the initial sarcomere length is restored. Modified from (Reece, 2011).

2.3. Skeletal muscle aging: sarcopenia

One of the tissues that mostly suffer in aging is skeletal muscle. The importance of age-related changes in muscle function is increasing in the last few years and there are multiple reasons to understand their underlying mechanism and to design specific treatments. First, due to an increase in lifespan, together with a decrease in fertility, the human population is aged. The prediction for 2050 is that the

percentage of people over sixty will double. This fact makes the proportion of elderly citizens with reduced motor ability and, thus, dependent, increasing; which, in turn, will give rise to social and economic consequences. Second, aging may be related to neuromuscular disorders such as amyotrophic lateral sclerosis (ALS), and muscular dystrophies such as Duchenne. Finally, the random mortality caused by infectious diseases has been replaced by the mortality caused by aging associated diseases or injuries (Larsson et al., 2019).

Loss of muscle mass and function in the elderly is clinically known as sarcopenia. At the structural and physiological level, the decline in muscle “quantity” or mass is mainly due to a reduction in the number and size of myofibers (Ansved and Larsson, 1990). By contrast, loss of muscle function or muscle “quality” is caused by the death of motoneurons. Moreover, this motoneuron loss is not properly compensated by an adequate re-innervation of the myofibers with the remaining motoneurons (Einsiedel and Luff, 1992). At the molecular level, the key players in skeletal muscle aging are the motor proteins involved in contractile function (e.g. myosin and actin) and the proteins involved in SR-Ca^{2+} handling (e.g. SERCA and RyR).

Muscle atrophy along aging is recognized by muscle weakness and slowing of movements, which represent phenotypic characteristics of impairment of function in sarcopenia. The latter is related to the motor unit function, and more specifically, the decreased speed of contraction that is the duration of the contraction-relaxation cycle. Many mechanisms may be involved in the contraction or the relaxation times: the transmission of the action potential, the SR-Ca^{2+} handling or the Ca^{2+} binding to the contractile proteins. It has been reported a strong correlation between SR-Ca^{2+} handling and the slowing of the contraction cycle in old individuals (Brody, 1976). It seems that a fast rate of Ca^{2+} pumping towards the SR lumen by SERCA will deprive the contractile proteins of Ca^{2+} and, thus, favour a fast relaxation and, in consequence reduce the contraction cycle time.

Sarcopenia is not only restricted to mammals, it also occurs in invertebrates such as the fruit fly *Drosophila melanogaster*. This phenomenon takes place at even a greater extent in these animals due to their relatively short lifespan (1-3 months). Furthermore, age-related changes are more dramatic in the invertebrate, at first

the main reason was thought to be the lack of muscle satellite stem cells, i.e. progenitor cells involved in the maintenance of the muscle mass and damage repair after injury (Biressi and Rando, 2010); however it has been recently shown that *Drosophila* does have a satellite stem cell population (Chaturvedi et al., 2017).

2.3.1. Factors involved in sarcopenia

Studies in model organisms have helped to elucidate that skeletal muscle changes with age are driven by extrinsic and intrinsic factors (Demontis et al., 2013). Extrinsic changes include: changes in the endocrine regulation; altered muscle regeneration by stem cells; and, defects in NMJs caused by loss of motoneurons. Organelle dysfunction (mitochondria, SR and lysosomes); sarcomere disorganization; stress response; or nuclear alterations; are the primary intrinsic causes. Sarcopenia seems to be also related to other more general changes such as accumulation of interstitial adipocytes (Stenholm et al., 2008) or decreased capillarization (Wandrag et al., 2017).

2.3.1.1. Extrinsic factors

a) **Changes in the endocrine regulation of the muscle.** Aged animals typically show lower nutrient intake, reduced physical activity and lower hormone levels of androgens, growth hormones or insulin-like growth factor (IGF1). Concretely in aged muscle, IGF1 and other anabolic cytokines are reduced (Goldspink and Harridge, 2004). Both insulin and exercise have been described to stimulate muscle protein synthesis (Stump et al., 2003) and this fact could explain decreases in many muscle proteins associated with age (Nair, 2005); such as myosin heavy chain (MHC) or mitochondrial proteins, e.g. enzymes involved in the oxidative energy production (Rooyackers et al., 1996). Another endocrine phenomenon that contributes to the progression of sarcopenia is “anabolic resistance”, a process defined as the lack of response in aged muscles to anabolic stimuli such as amino acid ingestion or exercise, that activate protein synthesis in young but fails to do so during age (Breen and Phillips, 2011). Moreover, aged

muscles are also less responsive to catabolic stimuli such as glucocorticoids, that fail to enhance protein breakdown in aged rats (Altun et al., 2010). The cellular basis for this altered sensitivity to anabolic or catabolic stimuli in aging remains unsolved.

b) **Altered muscle regeneration.** Muscle satellite cells are the adult stem cells responsible for skeletal muscle regeneration; they are located between the basal lamina and the myofiber membrane or sarcolemma. During the regeneration process, muscle satellite cells exit the quiescence state, and start to proliferate generating a population of myoblasts that finally differentiate in myofibers by fusing to each other or with damaged myofibers (Biressi and Rando, 2010). In mammals, it has been described that the number, the regenerative capacity (Shefer et al., 2010) and the response to endocrine stimuli that induces these cells activation (Kuang et al., 2008; Jones and Rando, 2011) decline during aging (**Fig. 4**).

c) **Defects in neuromuscular junctions.** The death of motoneurons can lead to denervation of myofibers in aged mammals (Delbono, 2003; Jang and Van Remmen, 2011). As a consequence, the neuromuscular system tends to reorganize the motor units by re-innervation. Skeletal myofibers can be broadly categorized into two types: slow-twitch (type I) and fast-twitch (type II) that are generally defined by the particular MHC isoforms that they express, but many other components contribute to the myofiber physiological characteristics. Type I myofibers are more efficient over long periods of time. They are mainly implicated in postural maintenance or endurance exercises. Type II myofibers are better for short bursts of speed than type I fibers, although they fatigue more quickly. There are many muscle disorders that preferentially affect specific skeletal myofiber types, and the reason for this remains unclear (Talbot and Maves, 2016). In sarcopenia, there is a reduced size and greater atrophy of type II fibers (Nilwik et al., 2013). Given that the type of fiber is determined by the type of motoneuron that innervates it, when type II fast-twitch fibers are re-innervated by nerves that innervate adjacent type I slow-twitch fibers, there is a fiber type transition (**Fig. 4**), and consequently, as the muscle ages, there is a fast-to-slow myosin isoform switch (Ansved and Larsson, 1990; Einsiedel and Luff, 1992). The presence of this denervation-reinnervation process is also well established in aged muscles,

although the extent of this event is dependent on the species or the strain of animal studied, and differs even between different types of muscles (Larsson and Ansved, 1995). Age-related alterations in NMJ have also been described in *Drosophila* (**Fig. 4**): the size of the axon terminal (also called synaptic bouton) increases in parallel with the decrease of the nerve diameter (Beramendi et al., 2007); synaptic vesicles density increases and there is a gradual expansion of the electron-dense membrane apposition of the pre- and post- synaptic membranes of the motoneuron and the muscle cell, respectively (Wagner et al., 2015). Furthermore, *Drosophila* flight muscles do not respond to electrical stimuli with age, indicating that the dorsal longitudinal muscle (DLM) synapse is altered and loses its function (Martinez et al., 2007).

2.3.1.2. Intrinsic factors

a) **Mitochondrial dysfunction.** Several defects have been observed in mitochondria isolated from aged muscles from mammals, including: decreased mitochondrial protein synthesis (Rooyackers et al., 1996); mitochondrial morphology changes like enlargement (**Fig. 5**) that could indicate increased mitochondrial fusion (Seo et al., 2008); and, increased generation of ROS (Mansouri et al., 2006), among many others. A number of mitochondrial functional and metabolic changes have also been described in aged flies. For instance, decline in the respiration rates and in the activities of the electron transport complexes (Ferguson et al., 2005); downregulation of a number of mitochondrial genes and other nuclear genes encoding enzymes that participate in oxidative phosphorylation and tricarboxylic acid cycle (Girardot et al., 2006); mitochondrial enlargement (Webb and Tribe, 1974); accumulation of deletions in the mitochondrial DNA (Yui et al., 2003); carbonylation of mitochondrial proteins in *Drosophila* flight muscles as an indicator of oxidative damage (Toroser et al., 2007); defects in lipid peroxidation (Magwere et al., 2006); and, finally, increases in ROS production (Cochemé et al., 2011).

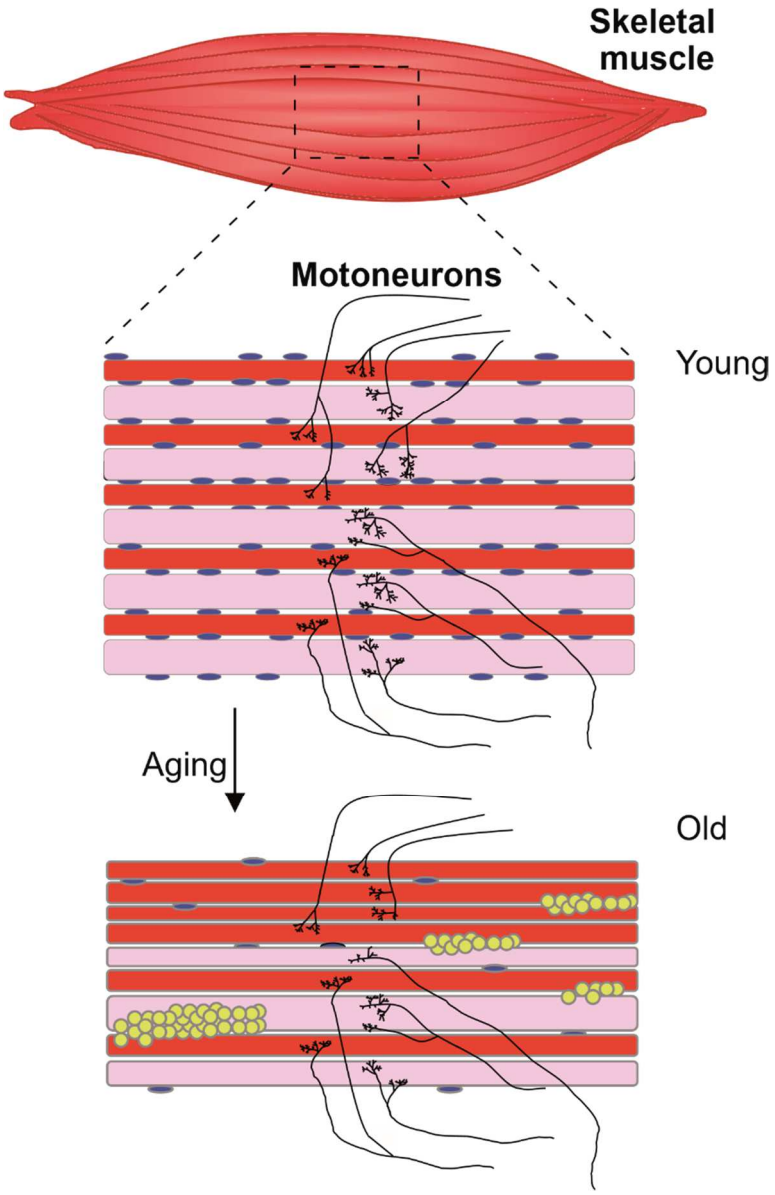

Figure 4. Extrinsic factors involved in sarcopenia. Aged muscles display death of motoneurons (black) and reduced number of satellite stem cells (represented in blue), which is directly related to a decrease in the regeneration capacity of the tissue. There is a fast-to-slow myosin isoform switch, observed as a decrease in type II fibers (pink) and, to a lesser extent, type I fibers (red). Sarcopenia seems to be also related to other wider changes such as accumulation of interstitial adipocytes (yellow). Modified from (Demontis et al., 2013).

b) **Sarcoplasmic reticulum changes and loss of Ca^{2+} homeostasis.** It has been reported that murine aged muscles suffer SR morphological changes (**Fig. 5**), such as aggregation of tubular SR membranes (Schiaffino, 2012), which leads to disruption in Ca^{2+} uptake and release (Jiménez-Moreno et al., 2008). Also, the DHPRs suffer functional changes with age that would implicate that myofibers from

old mice are dependent on extracellular Ca^{2+} to maintain maximal tetanic force whereas young fibers are not (Payne et al., 2004). In addition, a decrease in $[Ca^{2+}]_{SR}$ has been reported in isolated mice skeletal fibers after application of electrical stimulation (Jiménez-Moreno et al., 2010). Moreover, one of the most convincing theories of skeletal muscle aging postulates that RyR1 channels are damaged in aged muscles, due to modifications (oxidation, nitrosylation) of the cysteine residues and depletion of the subunit calstabin1 which stabilizes the closed conformation of the channel. These complex remodelling of the RyR1 would lead to "leaky" channels, with increased open probability (Andersson et al., 2011). This hypothesis has also been tested in *Drosophila* calstabin mutant flies, where the rescue of the mutant phenotype restores the sensitivity of motor function to age (Kreko-Pierce et al., 2016).

c) **Sarcomere disorganization.** In mammals, muscle weakness of typically old muscles can be partially explained by structural and functional variations in the sarcomeric proteins, actin and myosin (Prochniewicz et al., 2007). In *Drosophila*, it has been described that sarcomeres exhibit reduced length (**Fig. 5**) and disorganization (Webb and Tribe, 1974); as well as changes in the myofibril components with age, concretely in the connecting filaments that anchor the thick filaments to the Z-line (Miller et al., 2008).

d) **Stress response in aged muscles.** The ER is the largest Ca^{2+} storage organelle in eukaryotic cells and, the resting ER Ca^{2+} levels are not only key for amplifying and maintaining intracellular Ca^{2+} signals; but they are also necessary for the proper function of CaBPs that serve as Ca^{2+} buffers as well as chaperons or folding enzymes. It has been described that a reduction of the ER Ca^{2+} content triggered the unfolded protein response (UPR) with induction of several ER stress markers, e.g. the chaperone GRP78 or BiP (immunoglobulin protein) (Gallego-Sandín et al., 2011). BiP and other UPR markers have been reported to be upregulated during muscle aging in mice (Hwee et al., 2014). However, it has been described that BiP levels can vary between different types of muscles from aged mice (Chalil et al., 2015): i.e. BiP levels were reported decreased in tibialis anterioris; increased in extensor digitorum longus; and, remained without changes in gastrocnemius and soleus muscles. Furthermore, BiP protein levels remain

unchanged in skeletal muscle from aged rats (Baehr et al., 2016) and in human aged muscle (Ogborn et al., 2014).

e) **Defects in the autophagy-lysosome system.** Mammalian aged muscles show accumulation of lipofuscin or age pigment (**Fig. 5**), which is a recognized hallmark of aging (Hütter et al., 2007). Lipofuscin is a polymeric protein located in the lumen of the lysosome that has been demonstrated to accumulate under oxidative stress (Brunk and Terman, 2002). Lipofuscin accumulation may also interfere with the cell autophagocytotic capacity by acting as a sink for newly produced lysosomal enzymes and, therefore, result in improper turnover of cellular components and organelles. In *Drosophila*, defects in the autophagy-lysosome system are exemplified by an accumulation of poly-ubiquitinated protein aggregates during aging. This suggests that there is a progressive protein damage that, together with a decrease in the turnover of muscle proteins, may result in the age-related decline of muscle strength. FOXO (Forkhead box; class O) transcription factors are key players in muscle protein homeostasis, given their ability to activate multiple systems of protein disposal, among them the autophagy-lysosome proteolytic system. Overexpression of wild-type (WT) FOXO in muscles of adult flies is protective because it prevents the age-related decline in protein homeostasis and, therefore, it preserves muscle function. Conversely, during aging, FOXO null flies accumulate more protein aggregates in skeletal muscles than WT flies (Demontis and Perrimon, 2010).

f) **Alterations in the nuclear and plasma membrane integrity.** Below the plasma membrane there is a protein network known as the dystrophin glycoprotein complex (DGC) that helps to maintain membrane integrity and protects muscle cells from the damage produced by mechanical muscle contraction (Doherty and McNally, 2003). Mutations in dystrophin gene cause Duchenne muscular dystrophy (DMD) in mammals and mutations in the DGC homologs in *Drosophila* cause mobility defects and shortening of lifespan (Shcherbata et al., 2007). Nuclear membranes also show age-related deterioration. Both mice and *Drosophila* display nuclei with aberrant shape (**Fig. 5**), condensed chromatin and spatial disorganization with age (Brandt et al., 2008; Cristea et al., 2010). The nuclear lamina, as the DGC complex, maintains nuclear shape and stability. It is composed

by fibrous proteins from the nuclear intermediate filaments family called lamins. In addition to their structural roles, they are implicated in basic nuclear functions such as chromatin organization, DNA replication, DNA transcription, DNA repair, and cell cycle progression. Mutations in lamins produce diseases named laminopathies, among them the Hutchinson–Gilford progeria syndrome (HGPS). The most frequent mutation in HGPS patients is a *de novo* mutation in the lamin A gene which produces a truncated protein with a 50 amino acid deletion termed progerin and its phenotype is characterized by accelerated aging and muscle degeneration (Prochniewicz et al., 2007). Flies carrying lamin mutations also show locomotor defects (Muñoz-Alarcón et al., 2007).

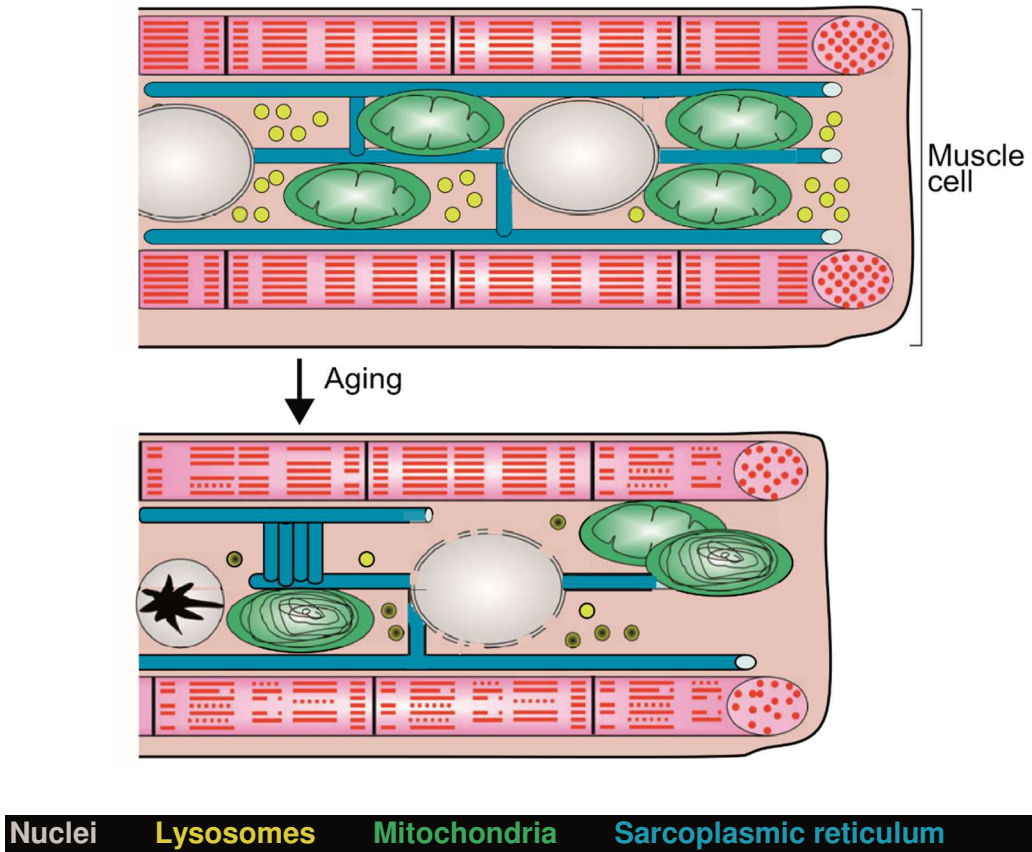

Figure 5. Intrinsic factors involved in sarcopenia. During aging, muscle cells progressively accumulate damaged proteins. Sarcomeres (red), exhibit disorganization and reduced length (myofibrils are shown in pink). Lysosomes (yellow) accumulate lipofuscin deposits and have decreased capability for degradation. Mitochondria (green) show functional and morphological abnormalities. Aggregation of membrane proteins of the sarcoplasmic reticulum (light blue) can result in tubular aggregates and improper Ca^{2+} handling in old age. Nuclei (grey) present altered shape, spatial disorganization (black star) and loss of nuclear membrane integrity (shown as the discontinuous line). Taken from (Demontis et al., 2013).

3. Ca^{2+} signalling mechanisms

Ca^{2+} signalling relies on the capacity of the cells to maintain the gradient between intracellular and extracellular Ca^{2+} concentrations (Clapham, 2007). Under resting conditions, $[Ca^{2+}]_C$ is around 100 nM whereas extracellular $[Ca^{2+}]$ is 1-2 mM. The ER is the major Ca^{2+} storage organelle of the cell and the $[Ca^{2+}]_{ER}$ is similar to the extracellular, between 0.2 and 1 mM (Alonso et al., 1998; de la Fuente et al., 2013). Other organelles such as the Golgi apparatus (GO), the lysosome, the endosome or the peroxisome can also serve as Ca^{2+} reservoirs (Prins and Michalak, 2009; Lam and Galione, 2013). When cells are activated, Ca^{2+} entry and/or Ca^{2+} release from the stores produces a rise in the $[Ca^{2+}]_C$ that controls numerous cellular functions, such as cell proliferation, neurotransmitter release, muscular contraction or gene expression (Berridge et al., 2003; Berridge, 2016).

Upon the arrival of a stimulus, Ca^{2+} can enter from the extracellular medium through a variety of channels located in the plasma membrane and named according to their activation or deactivation properties. Ca^{2+} can also be released from the intracellular stores through two receptor families, the Inositol 1,4,5-triphosphate receptors (IP_3Rs) and the Ryanodine receptors (RyRs), both located in the ER and the GO membranes. These channels are closed under resting conditions and they open upon stimulation, generating a rise in $[Ca^{2+}]_C$, and, then they rapidly close after stimulation. The transient increase in $[Ca^{2+}]_C$ triggers a cellular response that can vary in a window time from milliseconds in muscular contraction, to days in cell proliferation. This Ca^{2+} transient is shaped by calcium-binding proteins (CaBPs) and by intracellular organelles such as the mitochondria that can uptake Ca^{2+} through the Mitochondrial Calcium Uniporter (MCU). Both of them act as Ca^{2+} buffering systems. Given that a sustained increase in $[Ca^{2+}]_C$ is toxic for the cells, restoring of Ca^{2+} to basal levels is necessary. The cytosolic Ca^{2+} clearance mechanisms include the Ca^{2+}-ATPases, which pump Ca^{2+} against the concentration gradient outside the cells or inside the stores, and the exchangers that collaborate with the pumps to restore the basal Ca^{2+} levels. This allows the cell to return to a resting state where it is able to respond to another stimuli (Berridge, 1997).

3.1. The Ca^{2+} signalling toolkit

In order to generate Ca^{2+} signals, cells contain a number of Ca^{2+} channels in the plasma membrane and in the intracellular organelles. The channels, pumps, exchangers and the buffering systems that participate in Ca^{2+} mobilization form the Ca^{2+} signalling toolkit (**Fig. 6**).

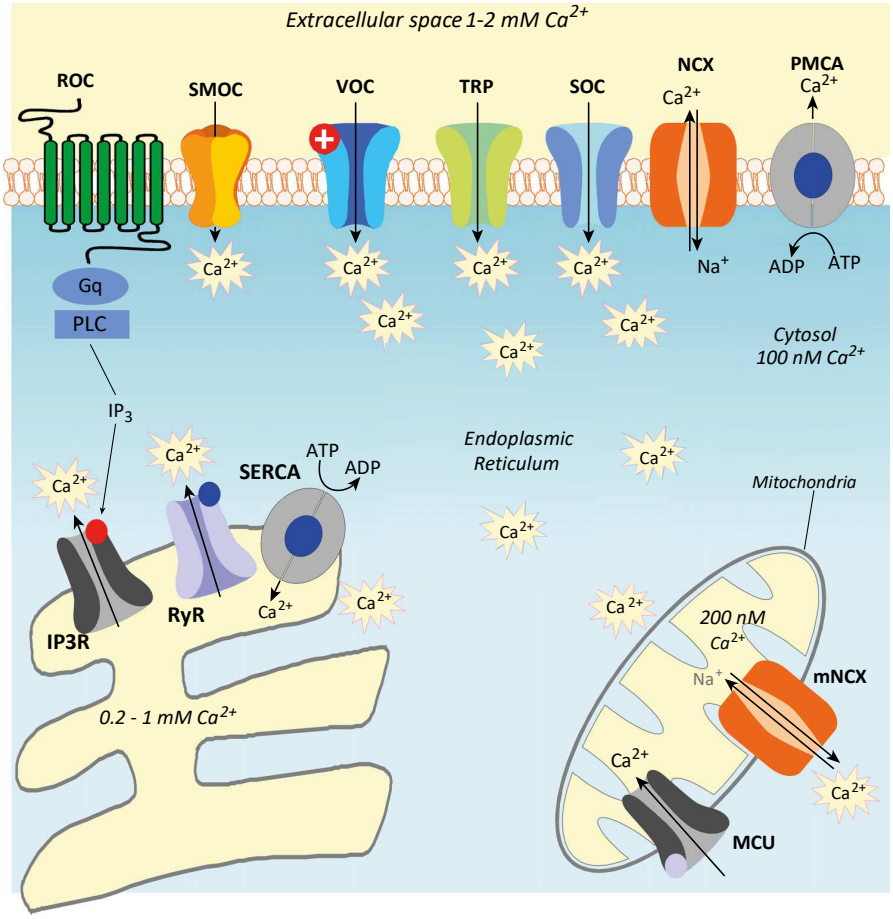

Figure 6. The Ca^{2+} signalling toolkit. Increases in cytosolic Ca^{2+} concentration trigger many physiological processes. They are due to Ca^{2+} entry through the numerous Ca^{2+} channels in the plasma membrane and to Ca^{2+} release from the intracellular stores. The plasma membrane Ca^{2+} channels are classified according to the stimulus that produce their opening in: Receptor-Operated Calcium Channels (ROCCs), Second-Messenger-Operated Calcium Channels (SMOCCs), Voltage-Operated Calcium Channels (VOCCs), Transient Receptor Potential channels (TRPCs), and Store-Operated Calcium Channels (SOCCs). Ca^{2+} release from the endoplasmic reticulum is mediated by two main families: the Inositol 1,4,5-triphosphate receptors (IP_3Rs) and the Ryanodine receptors (RyRs); whereas the sarco/endoplasmic reticulum Ca^{2+}-ATPase (SERCA) pump is in charge of refilling after stimulation. Moreover, upon cell stimulation, mitochondria can sequester Ca^{2+} rapidly through the Mitochondrial Calcium Uniporter (MCU) and then release it slowly through the Na^+/Ca^{2+} exchanger (mNCX). Finally, the plasma membrane contains two main mechanisms that regulate Ca^{2+} extrusion: pumps (Plasma Membrane Ca^{2+}-ATPase; PMCA) and Ca^{2+} exchangers (NCX). Modified from (Shigetomi et al., 2016).

3.1.1. Ca^{2+} entry from the extracellular medium

Ca^{2+} signalling capacity is driven by the large electrochemical gradient that exists across the plasma membrane. The membrane potential is -60 mV (negative inside) and [Ca^{2+}] is four orders of magnitude higher in the extracellular medium than in the cytosol. Cells are remarkably impermeable to Ca^{2+} under resting conditions; however, when a signal arrives to the cell, a variety of Ca^{2+} channels with different properties are activated, allowing Ca^{2+} entry.

Ca^{2+} channels are classified according to their gating properties in: Receptor-Operated Calcium Channels (ROCCs), Second-Messenger-Operated Calcium Channels (SMOCCs), Voltage-Operated Calcium Channels (VOCCs), Transient Receptor Potential Channels (TRPCs), and Store-Operated Calcium Channels (SOCCs) (**Fig. 6**).

The **ROCCs** are plasma membrane channels opened as a result of the binding of an agonist to its receptor, being the agonist a neurotransmitter, a hormone or even a nucleotide (Barritt, 1999). ROCCs are non-selective cation channels that are permeable to Ca^{2+}, but can also admit Na^{+} and K^{+}. ROCCs can be classified in two main types, ionotropic or metabotropic. Ionotropic receptors, also called ligand-gated ion channels, combine transmitter-binding and channel functions into a single molecular entity and, thus, the receptor is itself a channel. Examples of this type of channels include: the α-amino-3-hydroxy-5-methyl-4-isoxazolepropionic acid (AMPA) receptor, widely distributed in the central nervous system (CNS); the glutamate N-methyl-D-aspartate (NMDA) found at the excitatory synapses; the gamma-aminobutyric acid (GABA) receptor, located in the limbic area of the brain that deals with memories and emotions; and the nicotinic acetylcholine (nACh) receptor, abundant in the neuromuscular junctions. The metabotropic receptors do not have ion channels as part of their structure; they are proteins physically separated from the channel and, so, the mechanism of channel opening implies one or more metabolic steps. Metabotropic receptors are either G protein-coupled receptors (GPCRs) that activate second messengers such as cyclic adenosine monophosphate (cAMP) and cyclic guanosine monophosphate (cGMP) indirectly gating the ion channel, or receptor tyrosine kinases that open the channels directly or indirectly by phosphorylation. Examples of metabotropic receptors include the

metabotropic glutamate receptors (mGluRs) that exist primarily in the CNS; or the muscarinic acetylcholine receptors (mAChRs), of which there are five subtypes (M_1-M_5) that play important roles, such as the smooth muscle contraction that recovers the blood vessels and the pulmonary airways.

The **SMOCCs** are activated by second messengers such as cyclic nucleotides (cAMP or cGMP), that activate cyclic nucleotide-gated (CNG) channels, whose function has been established in retinal photoreceptors and olfactory sensory neurons (Kaupp and Seifert, 2002); or arachidonic acid that induces activation of arachidonate-regulated Ca^{2+} channels (ARCs), implicated in modulating the frequency of oscillatory Ca^{2+} signals in various cell types (Shuttleworth, 2009).

The **VOCCs** are activated by membrane depolarization and, thus, are key transducers of the electrical signal of the action potential into intracellular Ca^{2+} transients that initiate many physiological events (Catterall, 2011). These channels close when the plasma membrane repolarizes and they can be activated during *in vitro* experiments with high extracellular K^+ concentration. There are ten members of the VOCC family in mammals, classified in three subfamilies (Ca_V1, Ca_V2 and Ca_V3) according to the different central pore forming α1 subunits that define the types of Ca^{2+} currents. Ca^{2+} currents are classified according to their activation properties in Low or High Voltage for Activation (LVA or HVA); and, according to their kinetics of inactivation in three subtypes: long-lasting (L-type), no long-lasting (no-L) and transient (T-type). The LVA currents are T-type, and the HVA are either L-type currents or no-L that include N, P/Q and R currents. L-type Ca^{2+} currents are mediated by the Ca_V1 type of α1 subunit. Ca_V1 channels can trigger an array of cellular responses: excitation-contraction (EC) coupling in skeletal, cardiac, and smooth muscle; excitation-secretion coupling in endocrine cells and at ribbon synapses in specialized sensory cells; and excitation-transcription coupling or gene expression in nerve and muscle. Ca_V1 channels are sensitive to dihydropyridine (DHP) molecules, that act as antagonist blocking the channel and, thus, these channels are also called dihydropyridine receptors (DHPRs). The Ca_V2 subfamily conducts N, P/Q and R currents and is primarily responsible for the initiation of synaptic transmission at fast synapses. These channels are blocked by spider, snake or scorpion toxins. The Ca_V3 subfamily is important for repetitive firing of action potentials (T-type currents) in rhythmically firing cells such as

cardiac myocytes and thalamic neurons. They are insensible to DHP or the toxins that block the Ca_V2 channels. The classification of the VOCC family is summarized in **Table 1**.

α1 subunit	Ca^{2+} Current	Specific Blocker	Physiological function
Ca_V1	HVA. L-type	DHP	Excitation-contraction, Excitation-secretion, and Excitation-transcription coupling
Ca_V2	HVA. N, P/Q and R type	Toxins	Synaptic transmission at fast synapses
Ca_V3	LVA. T-type	Insensible	Rhythmically firing cells

Table 1. The voltage operated Ca^{2+} channels.

The **TRPCs** constitute a large superfamily of cation channels forming proteins which exhibit a large variety of functional properties and play diverse cellular and physiological roles (Gees et al., 2012). In mammals, 28 different genes have been identified, subdivided into multiple subfamilies; and, all related to the gene product of the *trp* locus, originally discovered in *Drosophila* (Montell and Rubin, 1989). In terms of gating mechanisms, there is a huge variation within the TRP superfamily, being many of them polimodal and some of them constitutively active channels. They can be activated by a variety of factors including depolarization, temperature, ligands, osmolarity or mechanical stimuli. Originally these channels were found in the plasma membrane, although an increasing number of them are being described in intracellular organelles, such as the ER, the Golgi apparatus or the endo-lysosome (Zhang et al., 2018).

The **SOCCs** are plasma membrane channels that mediate Ca^{2+} influx from the extracellular medium upon emptying of the intracellular stores (Prakriya and Lewis, 2015). Before the genes codifying for these channels were identified, they were referred to, in general, as Calcium Release-Activated Channels (CRACs) but nowadays the channels are known as Orai1-3 proteins (Feske et al., 2006). Ca^{2+} release from the ER lowers $[Ca^{2+}]_{ER}$, this reduces the Ca^{2+} affinity from the EF-

hands (Ca^{2+}-binding domain) of STIM (stromal interaction molecule) proteins that act as ER Ca^{2+} sensors (Liou et al., 2005). In turn, activated STIM monomers oligomerize and translocate to the plasma membrane to form punctate structures at the existent ER/PM junctions, where the endoplasmic reticulum (ER) and the plasma membrane (PM) are kept in close appositions. Orai channels are also redistributed from diffusely distributed clusters along the plasma membrane into the punctate structures forming complexes with STIM. Oligomerized STIM directly activates Orai channels, which, in turn, lead to selective Ca^{2+} influx and refilling of the ER-stores through the sarco/endoplasmic reticulum Ca^{2+}-ATPase (SERCA) pump. This phenomenon has been termed as capacitive entry or Store-Operated Ca^{2+} Entry (SOCE) (Putney, 1986; Ambudkar et al., 2017).

Regardless of its nature and gating properties, the opening of the plasma membrane channels generate a high [Ca^{2+}] at its mouth, on the inner side of the plasma membrane, termed subplasma membrane Ca^{2+} microdomains (Rizzuto and Pozzan, 2006). These Ca^{2+} microdomains control a number of cellular functions, such as secretion of neurotransmitters at the presynaptic membrane or modulation of mitochondria Ca^{2+} uptake capacity. Mitochondria have been shown to sense Ca^{2+} gradients near Orai channels and, therefore, modulate their Ca^{2+}-dependent inactivation (Gilabert and Parekh, 2000).

3.1.2. Cytosolic Ca^{2+} exit to the extracellular medium

The plasma membrane contains two main mechanisms that regulate Ca^{2+} extrusion, the Ca^{2+}-pumps or Ca^{2+}-ATPases and the ionic exchangers (**Fig. 6**), which operate to pump Ca^{2+} out of the cytoplasm against the electrochemical gradient (Brini and Carafoli, 2011). Ca^{2+}-ATPases are primary active transport pumps that need to be phosphorylated to transport Ca^{2+}, whereas the exchangers accomplish Ca^{2+} extrusion by using the electrochemical gradient of Na^{+}, so there is no direct coupling of ATP. This type of transport is known as secondary active transport or co-transport.

The **Plasma Membrane Ca^{2+}-ATPase (PMCA)** has a low transport capacity (turnover frequency of 150 s^{-1}) and a high Ca^{2+} affinity (K_D of 10-30 µM in resting

state), so it can operate at low $[Ca^{2+}]_C$ and contribute to maintain the resting $[Ca^{2+}]_C$. The PMCA was originally discovered in erythrocytes (Schatzmann, 1966) and, then, it was described and characterized in other numerous cell types. There are four basic PMCA isoforms (the PMCA is the product of four separate genes) that differ in tissue distribution. PMCA1 and 4 are ubiquitous whereas PMCA2 and PMCA3 expression is restricted to some tissues: PMCA2 is expressed in the nervous system and in the mammary gland and PMCA3 in the nervous system (Brini and Carafoli, 2009). The PMCA pump belongs to the family of P-type ATPases, it operates transporting Ca^{2+} upon ATP hydrolysis with a 1:1 stoichiometry (Hao et al., 1994) and, hence, it is electrogenic (1 Ca^{2+} in exchange for 1H^+). The activity of the pump is highly regulated: it is activated by acidic phospholipids and calmodulin (Carafoli et al., 1996); and also inhibited by many agents such as vanadate, lanthanum or caloxin. Structurally, it consists of ten transmembrane domains, two large intracellular loops, and the amino- and the carboxy-terminal cytoplasmic tails.

In contrast to Ca^{2+}-ATPases, **Ca^{2+} exchangers** have a low Ca^{2+} affinity (K_D of 0.1-0.3 µM) and a high transport capacity (turnover frequency up to 5000 s^{-1}) and, thus, are able to remove high amounts of Ca^{2+} from the cytosol in a short time. The Na^+/Ca^{2+} exchanger (NCX) and the $Na^+/Ca^{2+}/K^+$ exchanger (NCKX) are the two main classes of Na^+/Ca^{2+} antiporters found in animals that play a critical role in Ca^{2+} exit from the cytosol (Sharma and O'Halloran, 2014). The NCX includes three proteins (NCX1, 2 and 3) encoded by three separate genes (DiPolo and Beaugé, 2006): NCX1 is practically ubiquitous although it is highly expressed in the heart, in the brain and in the kidney; NCX2 is selectively expressed in the brain; and, NCX3 expression is restricted to the brain and the skeletal muscle. NCX accomplishes the exit of 1Ca^{2+} ion in exchange for 3Na^+ ions that enter the cell. The NCKX comprises five members: NCKX1 is expressed in retinal rod photoreceptors; NCKX2 is expressed in cone photoreceptors; NCKX3 and NCKX4 are abundant in the brain, but also in other tissues; and, NCKX5 is expressed in skin, retinal epithelium and brain (Schnetkamp, 2004; Lytton, 2007). NCKX transports 1K^+ together with 1Ca^{2+} in exchange for 4Na^+ ions. The operation of the exchangers is fully reversible, and the direction of the movement of the transported ions depends on the electrochemical gradients of Na^+ and Ca^{2+}.

3.1.3. Ca^{2+} buffering systems

The level of intracellular Ca^{2+} is determined by a balance between the 'on' reactions that introduce Ca^{2+} into the cytoplasm and the 'off' reactions through which Ca^{2+} is removed by the combined action of pumps, exchangers and buffers. During the 'on' reactions, most of the Ca^{2+} gets bound to the buffers that shape the amplitude, the duration, and the extent of the cytosolic Ca^{2+} transient, whereas a small proportion of the Ca^{2+} binds to the sensors or effectors that are responsible for stimulating numerous Ca^{2+}-dependent processes. Both of them, buffers and sensors are CaBPs. During the 'off' reactions, Ca^{2+} unbinds the sensors and buffers (Berridge et al., 2003).

There are many protein families among the **CaBPs**, some of them are extracellular, like the Ca^{2+} binding epidermal growth factor like proteins (cbEGF), but most of them are intracellular. Within the intracellular class, all of them contain negatively charged groups arranged for chemical Ca^{2+} coordination, although they differ in the evolutionary conserved motifs or domains capable of binding Ca^{2+} ions. Among them, the annexins; the C2-domain proteins; or the EF-hand proteins. The majority of the EF-hand protein family belongs to the group of Ca^{2+} sensors; these proteins, upon binding of Ca^{2+} ions, undergo a conformational change which allows them to act as regulators of specific targets (Schwaller, 2010). The prototypical example of Ca^{2+} sensor is the calmodulin protein (Chin and Means, 2000). However, some of these EF-hand proteins act as Ca^{2+} buffers, including parvalbumin, calbindin or calretinin. The "EF-hand" domain (**Fig. 7**) was first described by Kretsinger in 1973 as a Ca^{2+}-binding variant of a helix-loop-helix motif in the structure of parvalbumin (Kretsinger and Nockolds, 1973). The name EF-hand was termed given the resemblance of the spatial distribution of the α-helixes E and F of the parvalbumin, to the letter "L" that forms the spread thumb and forefinger of a human hand. The loop of the EF-hands is composed by 12 amino acid residues. Amino acids in positions 1, 3, 5, 7, 9 and 12 (denoted by X, Y, Z, -Y, -X and –Z) are involved in Ca^{2+} coordination and, thus, are acidic and highly conserved. The glutamate residue in the last position (12) of the loop serves as a bidentate ligand and, thus, contributes two oxygen atoms of its γ-carboxyl group, and the central residue (7) binds Ca^{2+} with the main-chain carbonyl oxygen atom. Next to this central residue,

there is a hydrophobic amino acid (most frequently isoleucine, valine or leucine) that makes two hydrogen bonds to the equivalent residue of the paired EF-hand and there is a bridged water (via position 9) that contributes another two oxygen atoms (**Fig. 7**). Therefore, Ca^{2+} is linked to seven oxygen atoms arranged in a pentagonal bipyramid (Grabarek, 2006). The EF-hand motifs always occur in pairs, which has some important functional consequences: it increases protein stability and Ca^{2+} affinity; and, it produces positive cooperativity that minimizes the Ca^{2+} signal required to reach protein saturation. Furthermore, the structure connecting the Ca^{2+}-binding loops plays the key role in the Ca^{2+}-induced conformation change involved in the interactive properties with target proteins such as kinases, phosphatases, metabolic enzymes, ion channels, ion pumps or transcription factors (Marshall et al., 2015).

The ER is the major source of Ca^{2+} within the cell and, hence, it possesses its own **ER-CaBPs**. These proteins are diverse in terms of structure, oligomerization, affinity and capacity for Ca^{2+}, but they have in common that they also serve other roles within the cell; furthermore most of them are chaperones that assist protein folding. Although some Ca^{2+} exists as free ions within the ER, much of it is buffered by these proteins in a polymerized state (Guerrero-Hernandez et al., 2010). The most important of these proteins are calreticulin (CR) in non-muscle cells, and calsequestrin (CSQ) in cardiac and skeletal muscle cells. CR is responsible for buffering up to 50% of the ER Ca^{2+}. Structurally, the N-terminal domain is implicated in chaperone function and the C-terminal domain is enriched in acidic amino acids that bind Ca^{2+} (Nakamura et al., 2001). CSQ is the most abundant Ca^{2+} buffer protein in the SR. In addition to its buffering role, there is evidence that it functions as a modulator of the RyR channels (Royer and Ríos, 2009). Other important Ca^{2+} buffer protein in the ER is BiP, responsible for buffering approximately 25% of the total ER Ca^{2+} load and with an ATPase domain through which it obtains energy to fold its client proteins (Prins and Michalak, 2011).

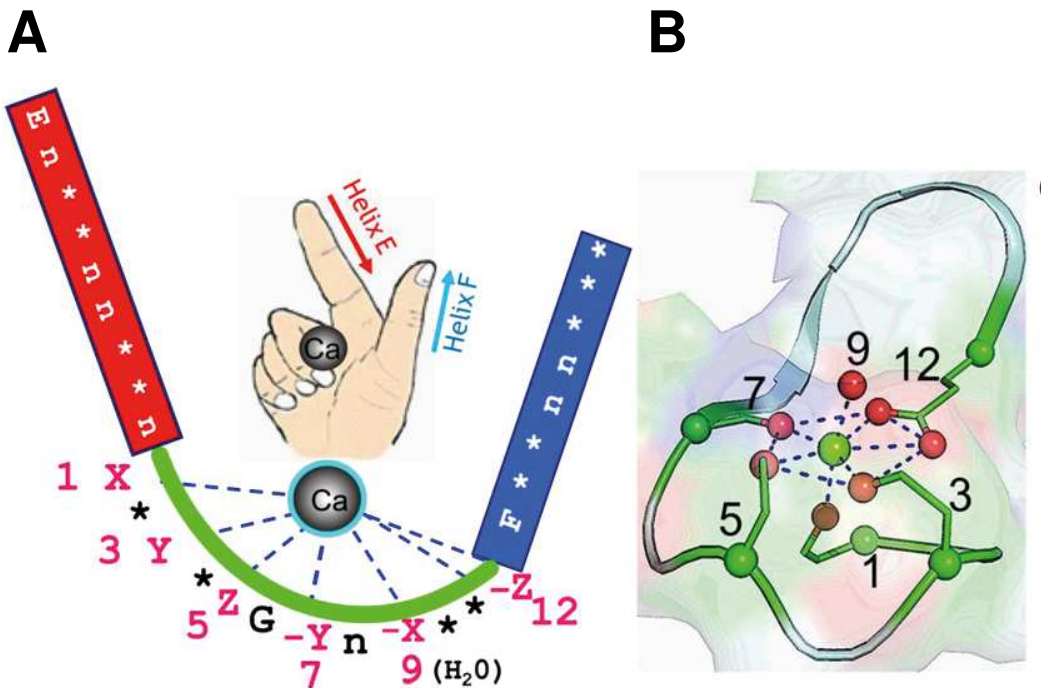

Figure 7. The EF-hand Ca^{2+}-binding motif. A) Figure illustration of the EF-hand Ca^{2+}-binding motif that resembles the spread thumb and forefinger of the human hand. Ca^{2+} is coordinated by ligands within the 12-residue loop, including seven oxygen atoms from the side chain carboxyl or hydroxyl groups (loop sequence positions 1, 3, 5, 12), a main chain carbonyl group (position 7), and a bridged water (via position 9). Residue at position 12 serves as a bidentate ligand. **B)** The Ca^{2+}-binding pocket adopts a pentagonal bipyramid geometry. Modified from (Zhou et al., 2009).

Mitochondria can also accumulate Ca^{2+} at an optimal uptake rate of µM Ca^{2+} concentrations. During the 'on' reactions, mitochondria sequester Ca^{2+} rapidly through the MCU (Baughman et al., 2011; De Stefani et al., 2011) and, then, it is released more slowly back into the cytosol by the mitochondrial H^+/Ca^{2+} (mHCX) and Na^+/Ca^{2+} (mNCX) exchangers (Crompton et al., 1977) during the 'off' reactions. In this way, mitochondria control various processes which involve high Ca^{2+} microdomains (Rizzuto and Pozzan, 2006; Patron et al., 2013): mitochondria can cluster together acting as "firewall", transiently blocking the Ca^{2+} waves and, thus, modulating its expansion (Tinel et al., 1999); they can also regulate neurotransmitter secretion, as in chromaffin cells (Montero et al., 2000); or they can prevent the inactivation of channels that are inhibited by high $[Ca^{2+}]$ in its inner mouth, such as the Orai channel involved in SOCE (Gilabert and Parekh, 2000). Mitochondria are dynamic organelles that can cluster in high energy demand locations or they can also move through the microtubules in response to

physiological changes. Ca^{2+} regulates mitochondrial motility (Jeyaraju et al., 2009) and also activates mitochondrial metabolism (Rizzuto et al., 2012). The main mechanism by which Ca^{2+} modules mitochondrial function is through activation of the three mitochondrial matrix dehydrogenases of the Krebs cycle, and the ATP synthase. This leads to mitochondrial energization by increasing the ratio NADH / NAD^+ and, therefore, the flow of electrons in the respiratory chain (Hansford, 1994). Increases in mitochondrial Ca^{2+} concentration along with the accumulation of ROS can trigger the release of mitochondrial factors to the cytosol such as cytochrome c and apoptosis inducing factor (AIF). Together with the effector caspases, these factors form a macromolecular machinery termed apoptosome that leads to cell death (Liu et al., 1996).

3.1.4. Sarco/endoplasmic mediated Ca^{2+} signalling

The SR is a morphologically distinct version of the ER specialized for muscle contraction, and, therefore, it is only found in excitable cells such as cardiac and skeletal muscle cells. The ER is found in all cell types, excitable and non-excitable. The distribution of the receptors and pumps implicated in Ca^{2+} uptake and release is different between the ER and the SR. In the ER, the IP_3R and the RyR (types1-3) that release Ca^{2+} from the organelle; and, the Ca^{2+}-ATPase SERCA, that pumps the ion inside the lumen; are uniformly distributed within the whole organelle (**Fig. 8A**). This does not include some cell types like astrocytes where a heterogeneous distribution of Ca^{2+} sources and sinks has been proposed (Volterra et al., 2014). In contrast, in the SR of muscle cells, these three proteins are distributed strategically according to their specialized function (**Fig. 8B**). RyR, type 1 in the skeletal muscle and type 2 in the cardiac muscle, is highly expressed and concentrated in the terminal cisternae (TC) region, and the SERCA pump is located on the longitudinal region.

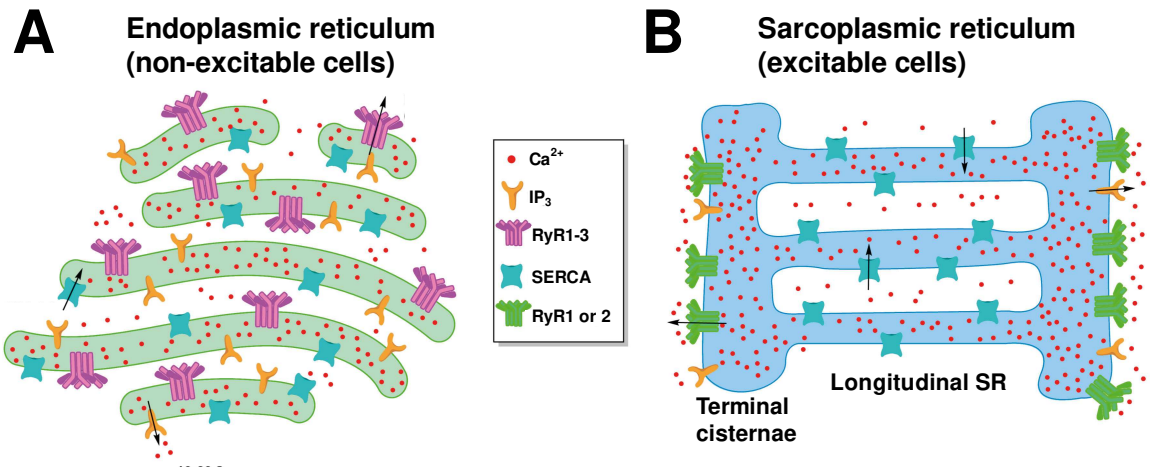

Figure 8. Distribution of the endoplasmic and the sarcoplasmic reticulum Ca^{2+} channels and pumps. A) The endoplasmic reticulum (ER) is found in non-excitable cells. The sarco/endoplasmic reticulum Ca^{2+}-ATPase (SERCA), implicated in Ca^{2+} uptake, and the Inositol 1,4,5-triphosphate receptors (IP_3Rs) and the Ryanodine receptors (RyR1-3) that mediate Ca^{2+} release, are evenly distributed in the organelle. **B)** The sarcoplasmic reticulum (SR) is only found in excitable cells; and receptors and pumps are localized in strategical positions according to their function. The RyR (type 1 in the skeletal muscle or type 2 in the cardiac muscle) is mainly concentrated in the terminal cisternae (TC) region, whereas the SERCA pump is located on the longitudinal SR. The black arrows indicate the direction in which Ca^{2+} flows through the corresponding receptor or pump. Taken from (Reddish et al., 2017).

3.1.4.1. Ca^{2+} release channels

The IP_3R and the RyR are the two main families of Ca^{2+} release channels situated on the ER and SR membrane (Berridge, 2009; Seo et al., 2015). **The IP_3R** is present on the ER membrane of non-excitable cells although it is also present in excitable cells (**Fig. 8**), where it serves to amplify the Ca^{2+} signal generated from depolarization (Zhu et al., 2011). The IP_3R was first identified in 1989 as the cerebellar P400 protein in mice lacking cerebellar Purkinje cells (Furuichi et al., 1989). The purified protein was, then, proved to function as a Ca^{2+} release channel when incorporated to lipid bilayers (Miyawaki et al., 1990). In mammals, there are three isoforms of the IP_3R, each of them encoded by a different gene. IP_3R1 is the most studied one and it is expressed in neurons; IP_3R2 is present in cardiomyocytes and astrocytes; and, IP_3R3 is expressed in all tissues. IP_3R is a tetrameric protein complex of 1000 kDa, with two distinct parts: a large cytosolic domain resembling a mushroom, which contains the IP_3-binding domain and the

modulatory domain with phosphorylation sites; and, a transmembrane domain, composed by six transmembrane segments conforming the pore with the Ca^{2+} binding domain (Mikoshiba, 2007). It is a non-selective cation channel that also permeates K^+ and other mono/divalent ions. Channel activity is regulated by both Ca^{2+} and IP_3 as co-agonists and, the activation of the channel requires the binding of both (Foskett, 2010; Taylor and Tovey, 2010). First, IP_3 binds to each of the four IP_3-binding sites of the tetrameric IP_3R, which initiate the conformational changes necessary for channel opening; and, then, Ca^{2+} binding causes the channel to open completely. IP_3 molecule is generated through the activation of metabotropic G protein-coupled receptors or GPCRs (Patterson et al., 2004). For example, the purinergic receptor P2YR is activated by binding of nucleotides such as ATP (Dubyak and el-Moatassim, 1993). Binding of an agonist to the GPCR results in a conformational change in the receptor that ultimately activates the phospholipase C (PLC), that produces the breakdown of phosphoinositol-4,5-bisphosphate (PIP_2) in the plasma membrane, into diacylglycerol (DAG) and IP_3, both of them are second messengers. On the other hand, cytosolic Ca^{2+} has a biphasic effect: it activates the channel at low concentrations, in the range of submicromolar, and it inhibits it at higher concentrations (Bezprozvanny et al., 1991). Additionally, IP_3R can be activated through phosphorylation of the modulatory domain by protein kinase A (PKA), protein kinase B (PKB), cyclin-dependent kinase 1 (CDK1), or Mitogen-Activated Protein kinases (MAPK) (Shah et al., 2015).

The RyR was first identified as the skeletal/cardiac SR Ca^{2+} release channel and named after the neutral plant alkaloid ryanodine that showed high affinity binding to the channel (Lai et al., 1988). The RyR exists in three isoforms in mammals: RyR1-3 (Zalk et al., 2007). Each isoform is predominately found in a specific cell type: RyR1 is the dominant isoform in the skeletal muscle although it can be expressed at lower concentrations in other tissues like the smooth muscle or the cerebellum; RyR2 is the cardiac muscle isoform, also expressed in the brain; and RyR3 is expressed in the thalamus, the hippocampus, the corpus striatum, and the smooth muscle. Their specific location on the SR/ER membrane also varies among the isoforms, the RyR isoforms 1 and 2 are more predominately found in the SR than isoform 3 (**Fig. 8**). RyRs form tetrameric channels of ~2000 kDa that interact with a variety of small molecules, proteins or ions that regulate the channel. Each

subunit contains 4–10 transmembrane α-helixes at the C-terminus conforming the pore of the channel and a huge N-terminal cytosolic domain that forms a bulbous head. The pore contains an intracellular loop domain for the binding of: cytosolic ligands (**Fig. 9**) that can act as activators such as ATP or as inhibitors like Mg^{2+} (Xu et al., 1996); and, luminal proteins including junctin, triadin and calsequestrin (CSQ) (Fill and Copello, 2002; Lanner et al., 2010). The N-terminal cytosolic domain functions as a scaffold to bind a large number of regulatory components (**Fig. 9**): e.g. calmodulin (CaM), DHPRs, S100A proteins and FK506 binding proteins (FKBPs). FKBPs have attracted considerable interest, as removal of these proteins from the RyR complex has been shown to destabilize the channels (Brillantes et al., 1994; Marx et al., 2000). The action of Ca^{2+} on the RyR channel is complex as it activates, it inhibits, and it conducts through this channel. RyRs are activated by cytosolic Ca^{2+} in the range of 1–10 μM $[Ca^{2+}]_C$, this process is known as Calcium Induced Calcium Release (CICR) and contributes to potentiate cytosolic Ca^{2+} signal and generate Ca^{2+} waves (Fabiato, 1983); and inhibited in the range of 1–10 mM $[Ca^{2+}]_C$. In addition, the RyRs are sensitive to regulation by luminal Ca^{2+} in the range of 0.1–10 mM either by interacting with the luminal binding sites, or with the associated luminal proteins (Kong et al., 2007). Furthermore, RyRs are also sensitive to chemical compounds such as caffeine (Friel and Tsien, 1992) or ruthenium red (Meissner, 1986).

The charge translocation associated with SR Ca^{2+} release through IP_3R and RyR channels is compensated by a simultaneous SR K^+ influx mediated by K^+-selective cation channels abundant in the SR membrane (Miller, 1978). This influx is essential because, with no countercurrent, the SR membrane potential would reach the Ca^{2+} equilibrium potential in less than 1 ms and, thus, SR Ca^{2+} release would cease. Like the plasma membrane, the resting potential of the SR/ER is governed by electrochemical mechanisms. The SR membrane is mainly permeable to K^+ and, thus, the SR membrane potential is clamped at the Nernst potential of K^+, which is 0 mV, as the $[K^+]$ in the SR lumen is not significantly different from the adjacent cytoplasmic concentration (Somlyo et al., 1981). The SR membrane is also known to be permeable to Cl^- and H^+ although their physiological significance is relatively less well understood (Meissner and McKinley, 1982). Cell signalling requires efficient Ca^{2+} mobilization from

intracellular stores through Ca^{2+} release channels as well as predicted counter-movement of ions across the SR membrane to balance the transient negative potential generated by Ca^{2+} release. The transmembrane protein named Trimeric Intracellular Cation (TRIC) channels (TRICA and B), formerly known as mitsugumin which is the Japanese for junction, is A SR-K^+ channel thought to provide counter-ion currents that facilitate the active release of Ca^{2+} from intracellular stores (Yazawa et al., 2007). However, it has been shown that RyR and likely IP_3R channels might mediate its own countercurrent given its ionic non-selectivity and high permeability to monovalent ions (Gillespie and Fill, 2008).

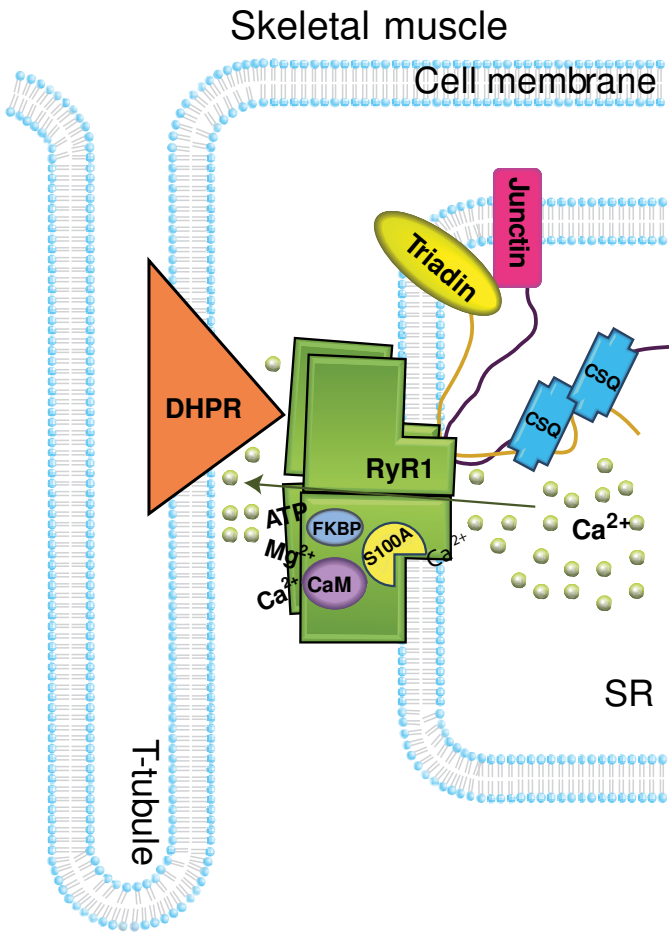

Figure 9. Structure of the ryanodine receptor type 1. Schematic of the Ryanodine receptor type 1 (RyR1) and its modulators. RyR1 (in green) is localized in the tubular cisternae region of the sarcoplasmic reticulum where it physically interacts with the dihydropyridine receptors (DHPR; in orange) to activate Ca^{2+} release when membrane is depolarized. RyRs are activated by cytosolic Ca^{2+} or ATP; and inhibited by Mg^{2+}. A number of binding partners that regulate the channel has been described: e.g. calmodulin (CaM; purple), S100A proteins (yellow), or FK506 binding proteins (FKBP; blue), from the cytosolic side; and junctin (pink), triadin (yellow) or calsequestrin (CSQ; blue), from the luminal side. Modified from (Lanner et al., 2010).

3.1.4.2. The sarco/endoplasmic reticulum Ca^{2+}-ATPase

The Ca^{2+}-ATPase found on the membrane of the SR/ER is **the SERCA** pump that contributes, along with PMCA and the Ca^{2+} exchangers in the plasma membrane, to restore $[Ca^{2+}]_C$ to 100 nM after cell stimulation by actively pumping the Ca^{2+} ion into the SR/ER lumen and, thus, refilling the intracellular stores (Brini and Carafoli, 2009; Berridge, 2012). The Golgi apparatus also contributes in this task with two pumps: the SERCA located in the cis-Golgi region (cGO) and the Secretory Pathway Ca^{2+}-ATPase (SPCA) in the trans-Golgi apparatus (tGO) (Vandecaetsbeek et al., 2011; Aulestia et al., 2015). Like PMCA, SERCA pump is a P-type ATPase pump, powered by ATP hydrolysis to move Ca^{2+} ions against the concentration gradient. The SERCA pump, as PMCA, has low transport capacity (turnover frequency of 200 s^{-1}) and high Ca^{2+} affinity, with a K_D for Ca^{2+} of 0.2 μM under resting conditions and 1 μM under conditions of maximal activation (Strehler and Treiman, 2004). However, SERCA is more efficient than PMCA, as it transports two Ca^{2+} ions into the ER lumen for each hydrolyzed ATP molecule instead of one (Toyoshima, 2009), and it is electrogenic (it exchanges $2Ca^{2+}$ for $2H^+$). There are three genes, each of them encode one protein isoform (SERCA1-3) that display tissue-specific expression: SERCA1 is primarily distributed in fast-twitch (type II) skeletal muscle; SERCA2 is found in fast and slow-twitch (type I) muscle, in cardiac and smooth muscle, and also in non-muscle cells; and, SERCA3 is expressed in non-muscle cells (Periasamy and Kalyanasundaram, 2007). Structurally (**Fig. 10**), SERCA is a monomer of 110 kDa molecular weight, consisting on a large cytosolic domain that includes the phosphorylation site (domain P), the nucleotide-binding site (domain N), and the anchor (domain A); and, a transmembrane domain of 10 α-helixes that contain two Ca^{2+} binding sites (Toyoshima et al., 2003). SERCA activity is highly regulated by phosphorylation and protein interactions. For example, increases in $[Ca^{2+}]_C$ activate calmodulin that, in turn, activates Ca^{2+}/calmodulin kinase II (CaMKII), which phosphorylates and activates SERCA pump (Vangheluwe et al., 2005). Furthermore, it is well established that the transmembrane proteins phospholamban and sarcolipin regulate the activity of the pump (MacLennan et al., 2003). Moreover, SERCA is inhibited by three specific inhibitors: the irreversible inhibitor thapsigargin, isolated from *Thapsia garganica* (Thastrup et al., 1989); and, the reversible inhibitors

cyclopiazonic acid (CPA) isolated from fungi such as *Aspergillus* and *Penicillum* (Demaurex et al., 1992), and 2,5-di(tert-butyl)-1,4-benzohydroquinone (TBH) (Moore et al., 1987).

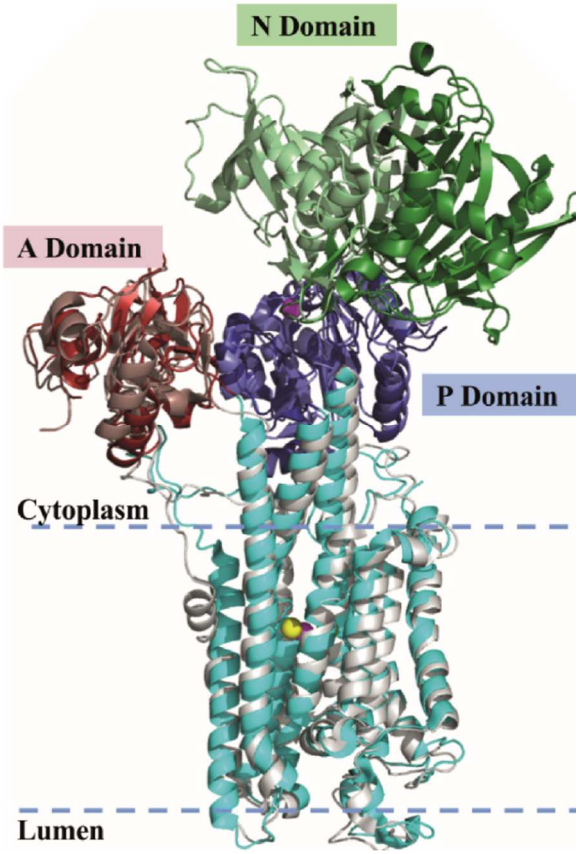

Figure 10. Structure of the sarco/endoplasmic reticulum Ca^{2+}-ATPase. The Sarco/Endoplasmic Reticulum Ca^{2+}-ATPase (SERCA) crystal structure**.** SERCA protein contains a large cytosolic domain and a transmembrane domain. The cytosolic part of the protein consists on the phosphorylation site (domain P, shown in dark blue), the nucleotide-binding site (domain N, shown in green), and the anchor (domain A, in red). The transmembrane domain (in cyan) is composed of 10 α-helices that contain two Ca^{2+} binding sites (Ca^{2+} ion is shown in yellow). Taken from (Sun et al., 2019).

3.1.4.3. Ca^{2+} leak channels

In addition to regulated Ca^{2+} release pathways, there are also leak pathways that can be revealed by Ca^{2+} loss from ER Ca^{2+} stores when SERCA pump is inhibited (Camello et al., 2002). Therefore, the resting free Ca^{2+} concentration maintained inside the ER is the result of a pump/leak steady state between the SERCA pump which mediates Ca^{2+} entry and the ER Ca^{2+} leak, whose molecular nature is still

controversial. Two types of Ca^{2+} release pathways have been proposed: novel, still non-identified proteins; or known Ca^{2+} release channels (such as RyRs and IP_3Rs) that are deregulated. A number of channel proteins have been implicated in basal Ca^{2+} leak pathways and. therefore, proposed to be the leak channel. These include: the translocon or Sec61 complex, the major entry site of newly synthesized proteins in the ER (Lang et al., 2011); the presenilins, whose mutations are linked to Alzheimer's disease, have been associated with decreased Ca^{2+} leak from the ER (Tu et al., 2006); the pannexins or protein pores, associated with ribosomes in rough ER (Abeele et al., 2006); the anti-apoptotic protein B-cell lymphoma-extra-large (Bcl-x_L), which interacts with IP_3Rs to enhance the opening of the channel (Li et al., 2007); Bax inhibitor-1 (BI-1), that protects against apoptosis and ER stress (Bultynck et al., 2012); FKBP proteins, whose dissociation from RyR destabilizes the channel and render it leaky (Brillantes et al., 1994); or proteins involved in RyR channel complex remodelling, including PKA phosphorylation and S-nitrosylation (Bellinger et al., 2009, 2008). FKBP12 and FKBP12.6 also known as calstabin1-2 (calcium channel stabilizing binding protein) are peptidyl-propyl-cis-transisomerases that associate with RyR1-2, respectively, via amphiphilic β-sheet structures. In order to regulate the channel gating through protein-protein interactions (Brillantes et al., 1994) and prevent pathological intracellular Ca^{2+} leak (Santulli and Marks, 2015), one calstabin molecule binds to each RyR monomer (Timerman et al., 1993; Xin et al., 1995). This association helps to stabilize the closed state of the channel (Efremov et al., 2015); and, is crucial for EC coupling in both skeletal and cardiac muscles (Lanner et al., 2010); as well as in the brain where the RyR-mediated leakiness hypothesis was also recently proposed as an underlying mechanism in Alzheimer's disease (Lacampagne et al., 2017). FKBPs are a highly conserved protein family, existing eight FKBP proteins in *Drosophila* which share its homology with the human FKBP12 protein (Ghartey-Kwansah et al., 2018). Finally, a new ER transmembrane membrane protein named Transmembrane and coiled-coil domains 1 (TMCO1) was recently discovered (Wang et al., 2016). TMCO1 has been proposed to have a role in preventing Ca^{2+} stores from overfilling; in such a way that, upon Ca^{2+} overloading, the protein forms homotetramers that would open and, thus, trigger Ca^{2+} release from the ER. Then, the complex undergoes disassembly upon Ca^{2+} depletion.

3.1.4.4. Endoplasmic reticulum junctions with other organelles

In the last decades, the contact sites between the ER membrane and other organelles have gained increased attention (Phillips and Voeltz, 2016). Plasma membrane-ER contact sites, such as the punctate structures involved in SOCE (Smyth et al., 2010), or ER-lysosome contact sites (Venkatachalam et al., 2015), have been linked to the regulation of Ca^{2+} homeostasis. Besides their role in Ca^{2+} homeostasis, MAMs are also involved in mitochondrial functions such as the transport of phospholipids or direct Ca^{2+} transmission to mitochondria that activates the enzymes implicated in the tricarboxylic acid cycle; and, in other physiological functions such as: inflammation, autophagy, and apoptosis. Moreover, the ER and the mitochondria are tightly associated with very dynamic structures termed mitochondria-associated membranes (MAMs) that are approximately 10 nm distance at the smooth ER and 25 nm at the rough ER (Csordás et al., 2006). MAMs provide a platform that allow rapid exchange of biological molecules and, thus, is fundamental for several cellular functions, such as: Ca^{2+} homeostasis, autophagy, lipid metabolism, and apoptosis. To the date, numerous MAM-specific proteins have been identified (Hayashi et al., 2009). Most of these proteins are ER proteins (ion channels, metabolic enzymes or molecular chaperones), with only a few belonging to mitochondria (electron transport chain proteins or mitochondrial fusion proteins). In fact, alterations in the composition of MAMs or in the crosstalk between the two organelles lead to different pathological conditions such as cancer or neurodegenerative diseases (Bravo et al., 2011).

3.2. The "Ca^{2+} hypothesis" of aging

The "Ca^{2+} hypothesis" of aging was proposed by Khachaturian in 1994 (Khachaturian, 1994) to explain the neurophysiological mechanisms involving Ca^{2+} signalling related to aging and neurodegeneration. Several changes in the components of the Ca^{2+} signalling (channels, pumps, exchangers or mitochondria) have been described to be altered in aging (Toescu and Vreugdenhil, 2010). For instance it has been reported: an increased in Ca^{2+} influx through VOCCs

(Campbell et al., 1996); an increased ER Ca^{2+} release mediated mostly by RyR, proposing this channel as a biomarker of aging in neurons (Gant et al., 2006; Thibault et al., 2007); an altered mitochondrial buffering capacity (Xiong et al., 2002); and more recently, a decrease in SOCE (Calvo-Rodríguez et al., 2016). However, different models trying to verify the "Ca^{2+} hypothesis" of neuronal aging yielded a set of rather inconsistent results. Indeed, the increased plasma membrane Ca^{2+} entry reported in hippocampal neurons of brain slices (Thibault and Landfield, 1996) was not observed in other neuronal types like dorsal-root ganglia neurons (Kostyuk et al., 1993) or cerebellar neurons (Kirischuk and Verkhratsky, 1996), indicating that aging might have affect differentially the various types of neurons in the brain or even tissues in the body. At present, the reason for these differential effects in each neuronal type is not known (Toescu and Verkhratsky, 2003).

Considering the association between Ca^{2+} dyshomeostasis and brain aging or neurodegenerative diseases, the development of novel drugs against target molecules of the Ca^{2+} signalling toolkit, such as ER leak channels or the Mitochondrial Calcium Uniporter (MCU), could be promising (Chandran et al., 2019).

3.3. The Ca^{2+} sensors

Ca^{2+} ion is the most ubiquitous intracellular second messenger, involved in almost every physiological process, from gene expression to muscle contraction or neurotransmitter release (Berridge et al., 2003). Unlike other molecules that serve as transduction elements, Ca^{2+} is neither synthesized nor metabolized. Instead, the ion storage and circulation is controlled by the Ca^{2+} signalling toolkit. Under normal conditions, only transient increases of $[Ca^{2+}]_C$ occur, and Ca^{2+} overload compromises cell viability and is a signal for apoptosis. Alterations in Ca^{2+} homeostasis have been proposed as possible sources of many pathological conditions such as cancer or neurodegenerative diseases (Berridge, 2016). Therefore, it is important to accurately measure the $[Ca^{2+}]$ to fully understand physiological and pathological processes. For this reason, a number of Ca^{2+}

sensors or indicators[2] with different nature and properties have been developed that can be divided in two main classes: synthetic Ca^{2+} indicators (also known as chemical) and genetically encoded Ca^{2+} indicators (GECI).

3.3.1. Synthetic Ca^{2+} indicators

Synthetic Ca^{2+} indicators are small molecules that can chelate Ca^{2+} ions due to the presence of carboxylic acid groups in their structure. These molecules are based on the BAPTA (1,2-bis(o-aminophenoxy)ethane-N,N,N′,N′-tetraacetic acid) molecule. Synthetic Ca^{2+} indicators are unable to cross lipid membranes due to their hydrophilic nature, making necessary the use of physical or chemical methods to load them inside the cell. The protection of the carboxylic groups as acetoxymethyl (AM) esters makes the dye[3] hydrophobic, so it can cross the cell membrane by simple diffusion (Tsien, 1981). Once inside the cell, the esterases cleave the AM groups, and the hydrophobic indicator becomes hydrophilic and, thus, trapped inside the cell.

Indicators can be classified into either ratiometric or single wavelength dyes. Ratiometric indicators shift the peak wavelength of either their excitation or emission spectra upon binding of Ca^{2+} ions. Based on this fact, this group can be subdivided in dual excitation or dual emission dyes. Fura-2 is a dual excitation dye, widely considered the standard for quantitative intracellular Ca^{2+} measurements (Grynkiewicz et al., 1985). The excitation peak shifts from 340 nm in the Ca^{2+}-bound state to 380 nm in the Ca^{2+}-free state; with fluorescence emission at 500 nm for either excitation wavelength (**Fig. 11A**). Indo-1 is a dual emission dye, with a single excitation peak at 350 nm and a dual peak emission that occurs at 405 nm and 485 nm in the Ca^{2+}-bound and Ca^{2+}-free states, respectively (**Fig. 11B**). This enables ratiometric measurements that provide a more accurate quantification of the [Ca^{2+}] and are less prone to artefacts such as uneven dye loading, dye leakage, photo bleaching or changes in cell volume. On the contrary, single wavelength

[2] Both terms, Ca^{2+} sensor and Ca^{2+} indicator, will be used along the document as synonyms.
[3] A dye is a coloured substance that chemically binds to the substrate to which it is being applied and, thus, changes its colour. The term will be used to refer to different types of dyes: synthetic Ca^{2+} indicators (mainly Fluo-4); Hoescht that stains nuclei in blue; and, Brilliant Blue G dye used to determine protein concentration in the Bradford assay.

indicators exhibit significant Ca^{2+} dependent changes in fluorescence intensity without shifting their excitation or emission wavelengths and, thus, they are also called intensiometric. This sensors normally yield higher dynamic ranges, which is the ratio of maximum and minimum fluorescence intensity (F_{max}/F_{min}). Within this group, the indicators based on the rhodamine (e.g. Rhod-2) or the fluorescein chromophores (e.g. Fluo-3; **Fig. 11C and D**) (Minta et al., 1989).

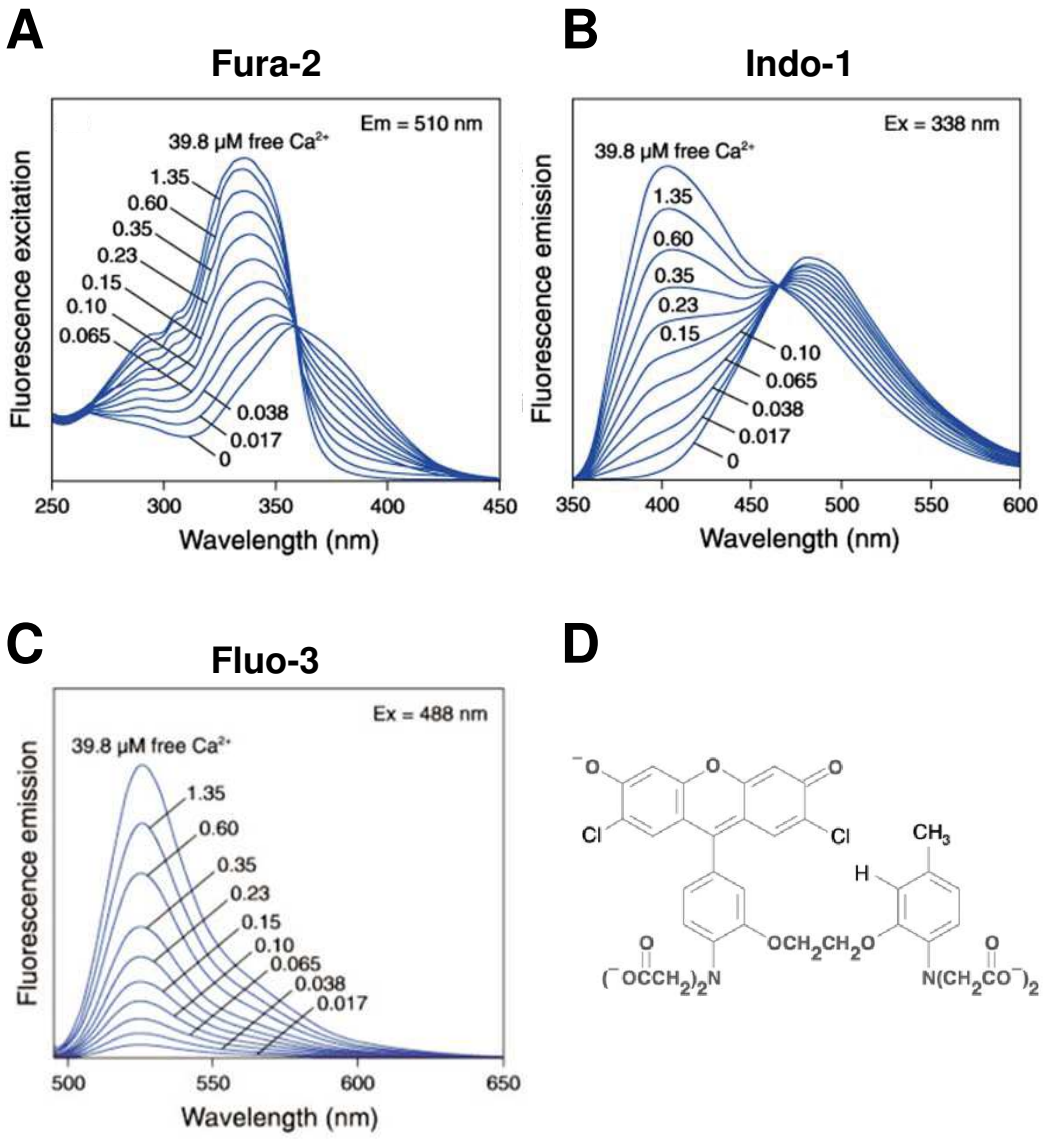

Figure 11. Fluorescence spectra and structure of the main synthetic Ca^{2+} indicators. The figures represent fluorescent spectra with Ca^{2+} concentration ranging from 0 to 39.8 µM Ca^{2+}. **A)** Excitation spectra of Fura-2. **B)** Emission spectra of Indo-1. **C)** Emission spectra of Fluo-3. **D)** Chemical structure of Fluo-3. (Modified from "The Molecular Probes Handbook, a guide to fluorescent probes and labeling technologies"; chapter 19, "Indicators for Ca^{2+}, Mg^{2+}, Zn^{2+} and other metal ions").

In this thesis we used a fluorescent Ca^{2+}-dye based on the fluorescein chromophore, Fluo-4 AM, to measure cytosolic Ca^{2+} *in vitro*. Fluo-4 is a single wavelength Ca^{2+} indicator with an excitation wavelength of 494 nm and emission wavelength of 516 nm. Ca^{2+} binding to the dye produces increases of 100 times in fluorescence. The high affinity of the synthetic dye to Ca^{2+} (K_D = 335 nM) makes it appropriate for cytosolic Ca^{2+} measurements.

A major advantage of synthetic indicators is the broad range of Ca^{2+} affinities that are commercially available for the user (from <50 nM to >50 µM). Higher affinity indicators can be used to quantify Ca^{2+} levels in the cytosol while lower affinity indicators can be optimized for measuring Ca^{2+} in subcellular compartments with higher Ca^{2+} concentrations. Also, they do not have to be transfected or expressed in cells, as cell loading protocols have been very well established (Takahashi et al., 1999). A major disadvantage is that the cellular localization of Ca^{2+} indicators cannot be specifically targeted to a particular organelle. In addition, synthetic indicators tend to compartmentalize and are eventually extruded from the cell during long recording experiments.

3.3.2. Genetically encoded Ca^{2+} indicators (GECIs)

Genetically encoded Ca^{2+} indicators (GECIs) are proteins composed by at least one light emitting protein and one Ca^{2+}-responsive element, so that Ca^{2+} binding changes its optical properties. The main advantages of GECIs over synthetic Ca^{2+} indicators is their precise targeting to organelles by the fusion with signal peptide sequences; and, the generation of transgenic animals, which makes them inheritable. GECIs can be classified in three main groups: bioluminescent, based on the aequorin photoprotein; fluorescent, composed by a single fluorescent protein and a Ca^{2+}-responsive element, e.g. camgaroos, pericams, GCaMPs and GECOs; and fluorescence resonance energy transfer (FRET) based, composed by two fluorescent proteins between a Ca^{2+}-responsive element, e.g. camaleons and troponin-based Ca^{2+} sensors. However, in our laboratory, we have generated the GAP (GFP-Aequorin Protein) family of GECIs (Rodriguez-Garcia et al., 2014). GAP is a unique dual-mode Ca^{2+} indicator, able to function either as a fluorescent

or a luminescent sensor, depending on whether the photoprotein aequorin is in its apo-state or reconstituted with its cofactor coelenterazine (Rodríguez-Prados et al., 2015). In this thesis we used GAP in the fluorescent mode and other fluorescent (non-FRET based) GECIs to measure [Ca^{2+}].

3.3.2.1. GAP (GFP-Aequorin Protein)

To measure endoplasmic reticulum Ca^{2+} we used the GAP indicator, composed by the fusion of the two proteins from the jellyfish *Aequorea victoria*: Green Fluorescent Protein (GFP) and aequorin.

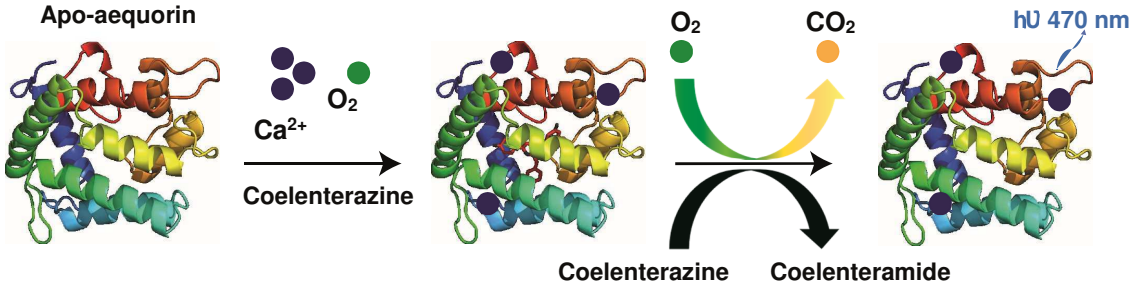

Figure 12. Bioluminescence reaction catalysed by aequorin. Apo-aequorin is reconstituted with the cofactor coelenterazine, and in the presence of O_2 (represented in green) it binds three Ca^{2+} ions (blue). Aequorin undergoes a conformational change, oxides coelenterazine into coelenteramide and emits blue light (470 nm), being also the product of this reaction CO_2 (yellow).

Aequorin is a Ca^{2+} sensitive photoprotein that emits blue light when binding to Ca^{2+} ions and in the presence of O_2 and its prosthetic group, the cofactor coelenterazine (Shimomura et al., 1962; Shimomura and Johnson, 1972). In the bioluminescence reaction (**Fig. 12**), aequorin undergoes a conformational change and oxides coelenterazine into coelenteramide, being also the products of this reaction CO_2 and blue light (470 nm). At a structural level, aequorin is a globular protein containing a hydrophobic core cavity that accommodates the ligand coelenterazine. With a molecular weight of 21.5 kDa, aequorin contains four helix-loop-helix 'EF-hand' domains (I, II, III and IV) or Ca^{2+} binding sites arranged in pairs, of which the second domain is not functional. Mutations in these 'EF-hand' domains can reduce the aequorin affinity for Ca^{2+}. For example, the mutation D119A, located

in the third domain, reduces 20 times the Ca^{2+} affinity of aequorin (Kendall et al., 1992), and the D119A mutation combined with low-affinity variants of coelenterazine, such as coelenterazine n, can reduce the aequorin affinity for Ca^{2+} by 1000 times compared to the wild type (WT) aequorin (Barrero et al., 1997).

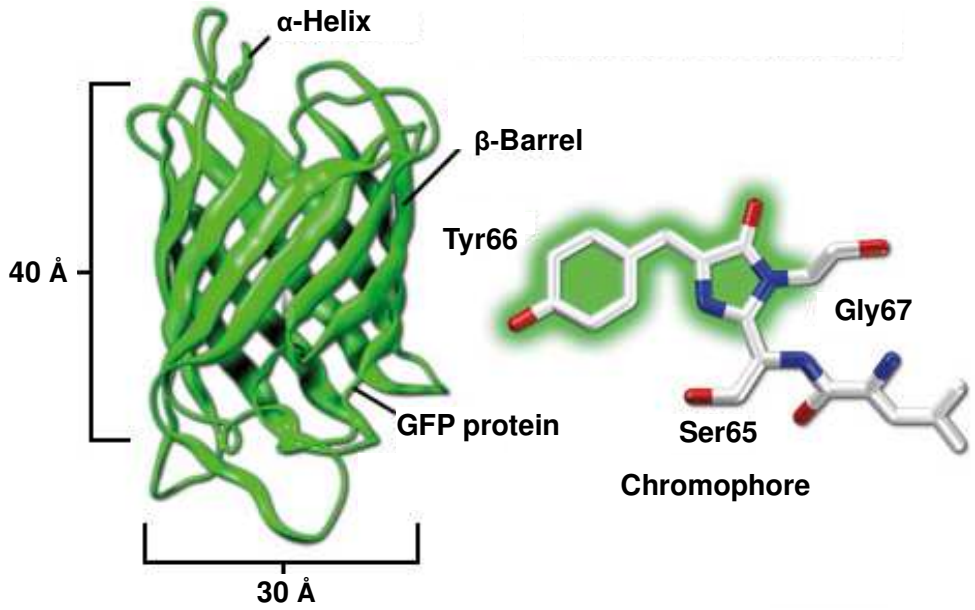

Figure 13. GFP structure. The protein is composed by eleven β-strands that form a barrel (40 Å long and 30 Å wide) and a α-helix that runs through it. The chromophore, responsible for the green light emission, is the tripeptide Ser65-Tyr55-Gly67 and is positioned in the middle of the β-barrel structure. (Figure modified from http://zeiss-campus.magnet.fsu.edu/print/probes/fpintroduction-print.html).

GFP is a 31 kDa protein with a β-barrel structure, composed by eleven antiparallel β-strands and a α-helix that runs through the barrel. The chromophore is the tripeptide Ser65-Tyr55-Gly67, located in the middle of the β-barrel, and is responsible for the green light emission (**Fig. 13**). The GFP protein used to generate the GAP protein was a GFP variant (GFPuv), optimized for maximal fluorescence obtained by molecular evolution using DNA shuffling (Crameri et al., 1996). This method allows the recombination of DNA sequences from different genes. The technique consists on the generation of gene libraries by random fragmentation of one gene or a pool of related genes, followed by the reassembly of the fragments in a self-priming PCR reaction. The excitation spectrum of the

GFPuv shows the same two excitation peaks as the WT GFP, one at 405 and a second one at 470 nm.

In the light organ of the jellyfish *Aequorea victoria*, aequorin interacts with GFP by a bioluminescence resonance energy transfer (BRET) reaction: the blue light emitted by aequorin upon Ca^{2+} binding excites the GFP molecule, which, in turn, emits green light (510 nm). In the GAP sensor, the two proteins are fused together by a peptide of 18 residues. There are different GAP variants, with different Ca^{2+} affinities. In this thesis, we used the low-affinity variant GAP3 (**Fig. 14A**) that has two mutations (D24N and D119A), in the first and in the third aequorin EF-hands, respectively. These mutations decrease the affinity of GAP for Ca^{2+} (GAP3, K_D =489 µM) and, hence, makes it adequate for measuring Ca^{2+} in high Ca^{2+} content organelles, such as the ER or the Golgi apparatus (Navas-Navarro et al., 2016; Alonso et al., 2017b). The indicator is targeted to the ER with the calreticulin (CR)/KDEL strategy, i.e. the *CR* signal peptide sequence is fused to the amino-terminus of the GAP protein and the ER retention signal *KDEL*, the tetrapeptide sequence, to the carboxy-terminus of the protein. This construct is named erGAP3. This variant has also mutations in several residues of the GFP moiety (L15Q, I167V, S175G and D180Y), in order to increase its fluorescence intensity. Furthermore, its sequence has been changed to optimize the codon usage for mammalian expression. GAP3 protein conserves the two excitation peaks (at 405 and 470 nm) of the WT GFP spectrum but shows a Ca^{2+}-dependent fluorescence, in an Ca^{2+}-free medium it exhibits a maximum excitation peak at 405 and a minor one at 470 nm, and upon Ca^{2+} binding, the fluorescence excited at 470 nm increases with a parallel decrease of the fluorescence excited at 405 nm (**Fig. 14B**).

It should be noted that the apo-aequorin cofactor coelenterazine is not required for emitting fluorescence, indicating that the mechanism is not based on a BRET reaction as it occurs in the light organ of the jellyfish. The Ca^{2+}-dependent fluorescence exhibited by the GAP sensor may be due to the interaction between the two moieties. Importantly, GAP indicator can be used in combination with Ca^{2+} synthetic dyes such as Fura-2 for simultaneous Ca^{2+} measurements in in the ER and in the cytosol.

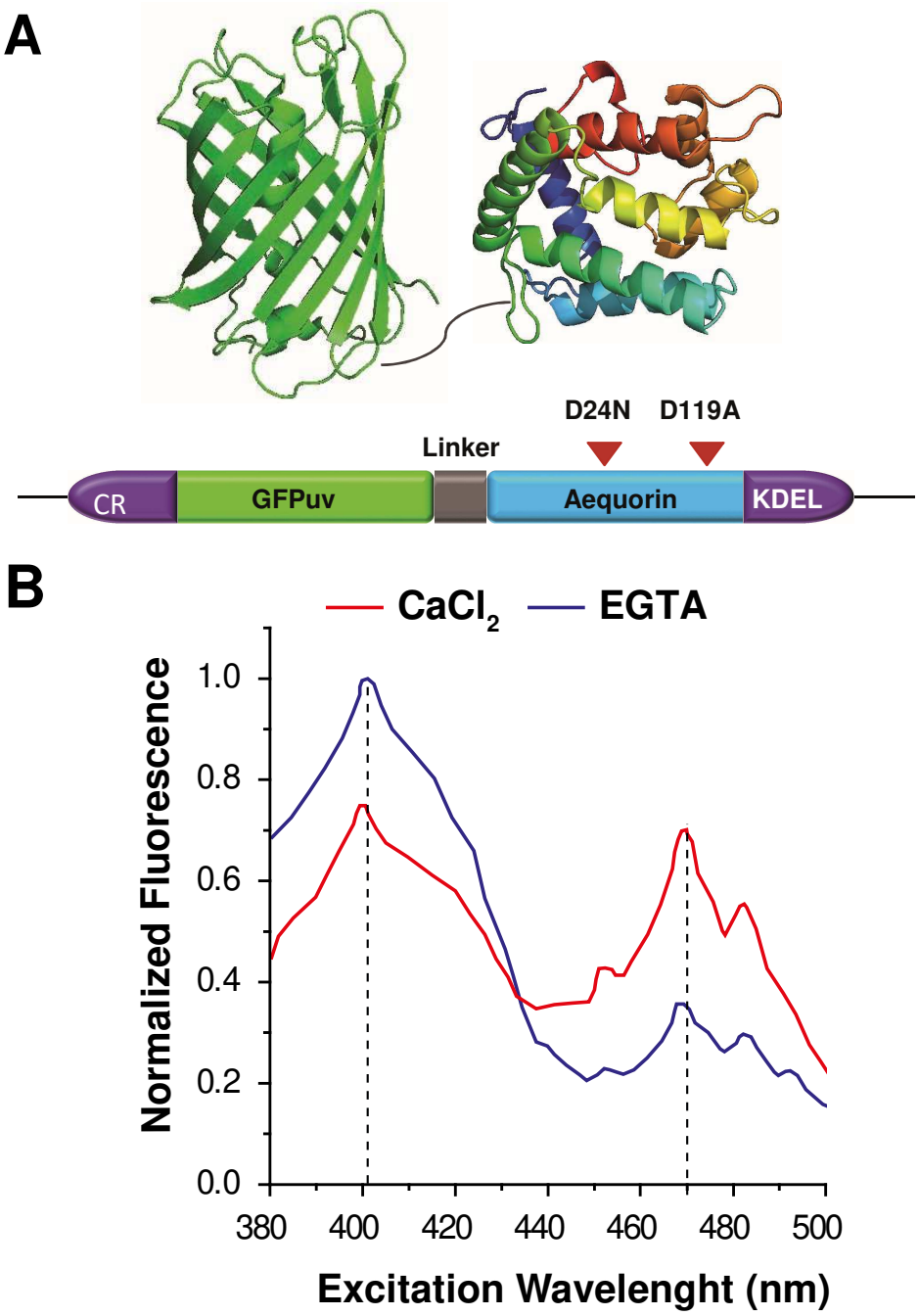

Figure 14. The erGAP3 Ca^{2+} sensor. A) The low-affinity variant GAP3 is a result of the fusion of two proteins: GFPuv (variant optimized for maximal fluorescence) and apo-aequorin (mutations D119A and D24N in the aequorin EF-hands) linked by a peptide of 18 residues. The sensor is targeted to the endoplasmic reticulum (ER) with the calreticulin (*CR*) signal peptide sequence fused to the amino-terminus of the GAP protein and the ER retention signal *KDEL*, the tetrapeptide sequence, to the carboxy-terminus. GAP3 has a K_D for Ca^{2+} of ~489 µM which is adequate for measuring in the ER. **B)** Excitation spectra of GAP3, 8.5 µg of protein in phosphate saline buffer (PBS) and in the absence (0.1 mM EGTA; blue line) or in the presence (1 mM $CaCl_2$; red line) of Ca^{2+}. The characteristic Ca^{2+}-dependent peaks at 405 and 470 nm are indicated with the black dashed line.

3.3.2.2. GCaMPs

To measure cytosolic Ca^{2+} *in vivo* we used another GECI: GCaMP3 indicator. **GCaMP** (Green fluorescent protein-CalModulin Protein) is a family of Ca^{2+} sensors result of the fusion of three proteins: the cpEGFP, which is a GFP variant with enhanced GFP fluorescence (EGFP) and also, circularly permutated (cp), where the amino and carboxyl portions of the protein had been interchanged; the calmodulin, fused to the carboxy-terminus of cpEGFP; and the M13 peptide, which is the calmodulin-binding domain from the myosin light chain kinase, fused to the amino-terminus of the pEGFP (**Fig. 15**). The fluorescent spectra of GCaMP proteins display a single excitation peak at 489 nm and an emission peak at 509 nm. GCaMP protein increases its fluorescence intensity upon binding to Ca^{2+} ions due to changes in the chromophore environment (Nakai et al., 2001). The variant used in this thesis, GCaMP3, has a DR of 12 and a K_D of 660 nM (Tian et al., 2009). The high affinity for Ca^{2+} is appropriate to measure Ca^{2+} in the cytosol. More recently, new variants have been developed with improved Ca^{2+} signal detectability, termed GCaMP6 and GCaMP8 (Ohkura et al., 2012); and, for combination with optogenetics, variants of different colours derived from GFP such as blue, cyan, and yellow variants ("BCaMP," "CyCaMP," and "YCaMP," respectively) and from circularly permuted mRuby the red variant "RCaMP" (Akerboom et al., 2013).

Based on GCaMP proteins, a new family of low affinity GECIs were generated named Calcium-measuring organelle-Entrapped Protein IndicAtors (**CEPIA**). GCaMP2 variant was engineered to reduce its Ca^{2+} binding affinity by a factor of ~1,000, by site-directed mutagenesis in the calmodulin EF-hands. It was targeted to the ER (CEPIA1er) and then, they generated colour variants: the R-CEPIA1er (K_D =565 µM, DR= 8.8); the G-CEPIA1er ((K_D =672 µM, DR= 4.7); and the GEMCEPIA1er ((K_D = 558 µM, DR= 21.7). The first ones being intensiometric and the last one is ratiometric and therefore adequate for calibration (Suzuki et al., 2014).

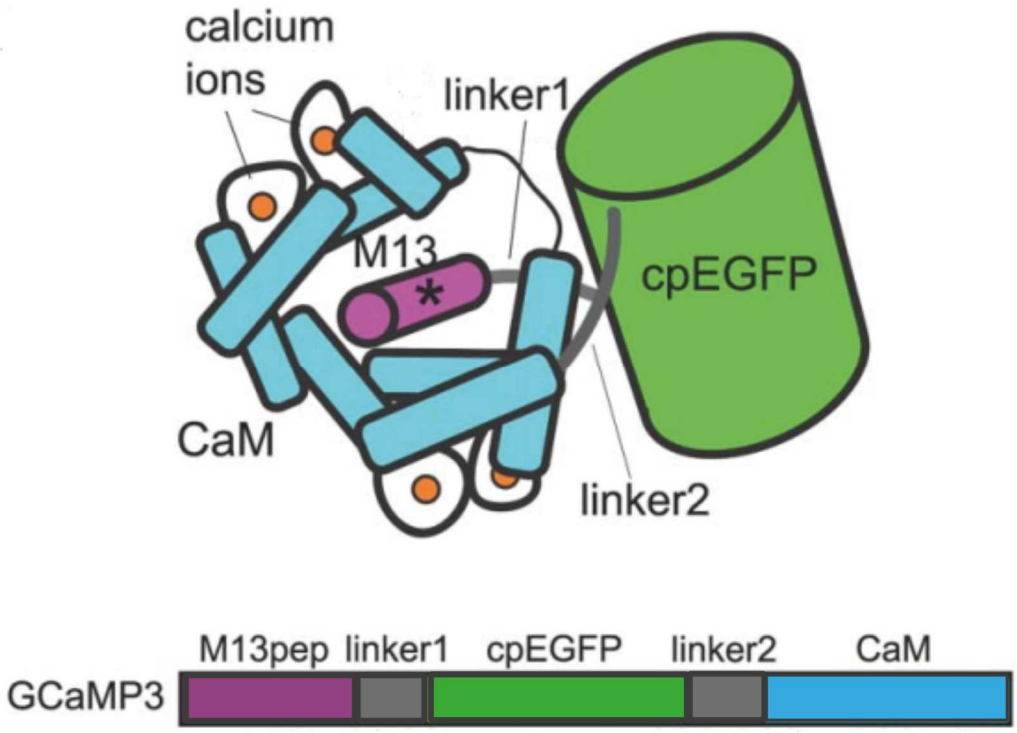

Figure 15. The GCaMP Ca^{2+} sensor. Schematic representation of GCaMP sensors: the circularly permutated enhanced GFP (cpEGFP) is shown in green, the peptide M13 (in purple) is fused to the amino-terminus of the cpEGFP by linker 1 (grey) and the calmodulin protein (in blue) is fused to the carboxy-terminus of cpEGFP by linker 2 (grey). Calcium ions are illustrated as orange spheres. Modified from (Akerboom et al., 2012).

4. *Drosophila melanogaster*

Drosophila melanogaster is a small fly classified in the taxonomic order Diptera and family Drosophilidae. The species is commonly known as fruit fly or vinegar fly, as they are often found on rotting fruit (Powell, 1997). *Drosophila melanogaster* became known as a model system at the beginning of the 20th century, when Thomas Hunt Morgan at Columbia University confirmed the chromosome theory of inheritance (Morgan, 1910). Since then, *Drosophila* has been widely used in science. To date, eight Nobel prizes had been awarded for research using *Drosophila*, being the last one in 2017, in Physiology and Medicine to American researchers for their pioneering work with *Drosophila* in elucidating molecular mechanisms' responsible for circadian rhythms. Flies are easily maintained in the laboratory and, there are few ethical or safety regulations that have to be taken into account for their laboratory use.

4.1. Life cycle

A major advantage of using the fruit fly as animal model is their particularly short life cycle (**Fig. 16**), which allows a rapid generation of large populations to use in genetic crosses. In *Drosophila*, the generation time between embryo and adult requires on average 9–10 days at 25°C; however, the speed of the process can be temperature-regulated, for example flies cultured at a lower temperature of 18 °C will require longer periods, approximately 19 days from egg to adult.

Upon fertilization, embryogenesis is completed in 24 h, followed by three larval stages, termed first (1 day), second (1 day) and third instar (3 days) (**Fig. 16**). Thus, 5 days after fertilization, larval development is complete and the animals metamorphose within a hard, protective chitin-based pupal case or puparium. The animal remains in the pupal stage for 3–4 days, during which adult structures develop from the imaginal discs or progenitor cells present in the larvae. Adult flies eclose from the pupal case and become sexually mature in 8–12 h, allowing the life cycle to repeat (Hales et al., 2015). *Drosophila* lifespan is affected by environmental conditions, such as temperature and diet. Fly life shortens as temperature is increased: the maximal survival time is 40 days at 29 °C, 80 days at 25 °C and 160 days at 18 °C (Linford et al., 2013).

Drosophila exhibits sexual dimorphism: males and females are distinguished primarily by size, being females about 2.5 mm longer than males. Also, the two genders display differential abdominal pigmentation patterns and different genitals. Furthermore, males present secondary specific structures such as: “sex combs”, located on the front legs, they are modified bristles that males use to grasp the female; and, the clasper, which is a cluster of spiky hairs surrounding the reproduction organs used to attach to the female during mating.

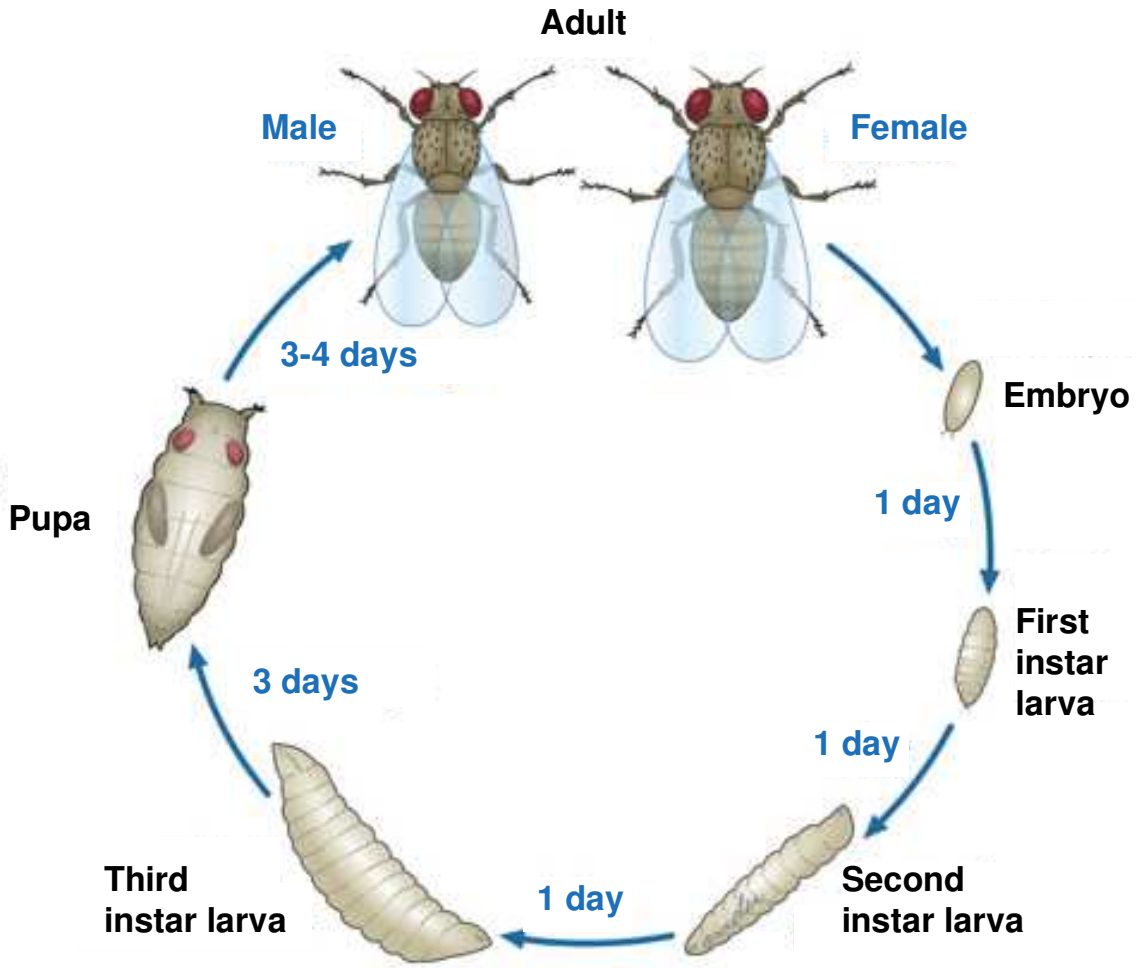

Figure 16. *Drosophila* life cycle. The whole life cycle of *Drosophila* takes around 10–12 days at 25 °C. The *Drosophila* development is divided into various stages: embryo (1 day), larva (first, second and third instars; 5 days), pupa (3-4 days) and adult. Taken from (Ong et al., 2015).

4.2. Genetics

Another advantage of the fly as an animal model is that they have a compact genome, mostly because intergenic and intronic sequences are reduced in size compared to other vertebrate genomes, which makes it easier to manipulate genetically. Also, they have many orthologous genes associated with human diseases. The genome of *Drosophila* contains four pairs of chromosomes, an X/Y pair and three autosomes, labelled 2, 3 and 4. The first pair or the sex chromosomes are composed by an acrocentric X chromosome and a submetacentric Y chromosome, that is almost entirely composed of heterochromatin (highly compacted, transcriptionally silent DNA and dense in

repeats). The remaining three pairs are autosomes. Chromosomes 2 and 3 are large metacentric autosomes, and chromosome 4 (the dot chromosome) is very small and often ignored, apart from the genetic markers *yellow* and *white*, affecting body and eye colour, respectively. Other classic examples of these genetic markers are: *Curly* (*Cy*), on the second chromosome (affecting wing shape); and *Stubble* (*Sb*), on the third chromosome (affecting bristle length) (Greenspan, 1997). Genetic markers are commonly used in *Drosophila* to identify a phenotype and, thus, accurately track genetic crosses by selection of offspring that inherited one version or the other of a chromosome. For example, a geneticist may collect non-*Cy* winged flies to obtain those that inherited the parent's other copy of the second chromosome with a mutation of interest. However, recombination of the mutation of interest onto the *Cy* chromosome could occur during meiosis in the parent. To prevent this, the chromosomes with genetic markers also contain multiple inversions to prevent viable recombinant offspring; thus, the only viable offspring are those with one or the other of the parent's two intact chromosomes (either with the mutation of interest or with the genetic marker). These engineered chromosomes are named "balancer chromosomes." Besides genetic markers and multiple inversions, balancer chromosomes have a third feature, recessive lethal mutations, which prevent the mutations of interest from being selected out of an inbred population.

A turning point of genetic technology that made the fruit fly such a powerful animal model system was the identification and the development of the *P-element* as a germ-line transformation vector. The *P-element* is a classic transposable DNA that contains the gene encoding the transposase enzyme, flanked by inverted repeats, which allows movement within the genome. First, Rubin and Spradling replaced the transposase gene with a gene of interest and co-injected the construct into *Drosophila* embryos with an intact *P-element* that supplies the transposase enzyme, finding an excellent system for inserting DNA into the fly (Rubin and Spradling, 1982). Then, Brand and Perrimon took the *P-element* transformation vector and used it to create a gene expression system that would eventually allow for the expression of any gene of interest in any particular tissue within the fly (Brand and Perrimon, 1993). They cloned the yeast transcription factor GAL4 (galactose-induced gene 4) into a *P-element* vector and showed that a defined

promoter could be cloned upstream of GAL4. To drive the gene expression, they created a corresponding *P-element* vector, *pUAST*, containing the upstream activating sequences (UAS), to which GAL4 protein can bind. These *UAS* sequences were connected to a general promoter and a cloning site to allow for the insertion of any gene of interest. However, the system had some pitfalls such as lack of control over the final resting place of the transposable element, the risk of disruption of an endogenous gene, or the possibility of gene insertion in a locus that may reduce or switch-off the expression. For these reasons, the GAL4-UAS system has been modified and improved over the years (Duffy, 2002). Nowadays, a new transformation system is routinely used derived from the ϕC31 bacteriophage: the *pUAST* vector containing the *UAS* sequence and the gene of interest is co-injected in *Drosophila* embryos along with the integrase *ϕC31* mRNA. The integrase ϕC31 is a serine recombinase protein from the bacteriophage that recombines sequences using the *attB* and *attP* sequences integration sites in a site specific manner (Groth et al., 2004). For recombination to occur, one of this integration sites is in the *pUAST* vector and the other is located in the fly genome.

4.3. *Drosophila* anatomy and physiology

The body of the fly is divided into three segments: head (A); thorax (B); and abdomen (C) represented in **Figure 17**. Firstly, in the head region (A) it can be distinguished: the antennae, which are sensory elements used to detect sound (Matsuo and Kamikouchi, 2013); the compound eye, which is composed by thousands of cells with distinct functions, from photoreception to non-neuronal cells (Cagan, 2009); and the ocellar triangle, housing the ocelli, which are another type of photoreceptor. The organ termed proboscis is a tubular part of the head with various functions: feeding; detection of toxic compounds and of non-volatile pheromones; and, egg laying. The thoracic region (B) is subdivided in three segments, each of them with a pair of legs located on the ventral side. The wings are on the dorsal side of the second thoracic segment; and, a pair of rudimentary halteres, are placed on the next posterior segment (**Fig. 17**). The halteres are modified hind wings used for balancing during flight (Mureli and Fox, 2015). Specifically, the halteres are mechanosensory organs that provide rapid feedback

to the wing-steering muscles, as well as to the muscles responsible for stabilizing the head. The bristles are also sensory organs placed across the whole surface of the adult fly body. Finally, the abdomen is subdivided in 8 abdominal segments, of which the last four are compressed and modified for reproductive functions.

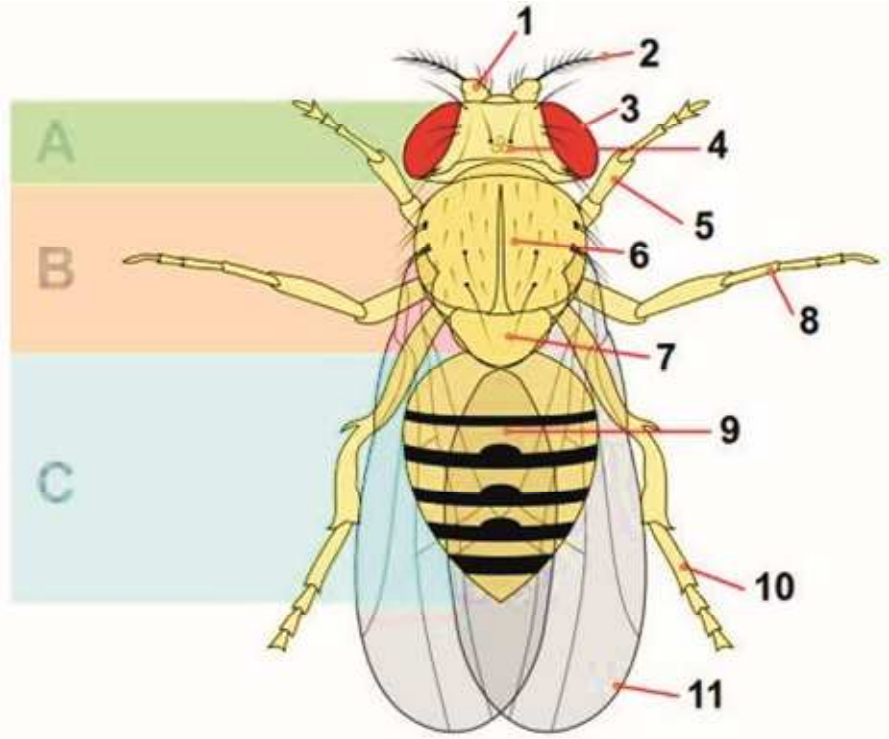

Figure 17. *Drosophila* external anatomy. The body of the fly follows a segmented pattern and is subdivided into three parts: **A,** head; **B**, thorax; and **C**, abdomen. The head contains the antennae (**1**, first; and **2**, second antennal segment), the compound eye (**3**) and the ocelli (**4**). The thoracic region (**7**) is where the main muscle groups are located and also where the three pairs of legs (**5, 8,** and **10**) and the wings (**11**) are inserted. The sensory bristles (**6**) are located through all the body. The abdomen (**9**) is also segmented and modified for reproductive functions. (Retrieved from https://www.cherrybiotech.com/scientific-note/drosophila-life-cycle-and-fly-anatomy).

4.3.1. *Drosophila* musculature

The three vertebrate muscle types (skeletal, cardiac and smooth) have their anatomical counterparts in *Drosophila* (skeletal, cardiac and visceral). The skeletal muscle system is the largest organ in motile animals, constituting around 40% of the human body mass and up to 75% of the body mass in *Drosophila*, of which 65% is comprised by the flight musculature. The skeletal muscle is in charge of the

precision of motor commands and, thus, is highly relevant in many common behaviours, including stabilization of body posture, heading control and directed escape responses. The skeletal muscles of humans and flies are very similar at the molecular and the structural level (Taylor, 2013). Both are composed of tandem arrays of sarcomeres containing the thin and thick filaments, which, in a typical muscle twitch, slide past each other in response to Ca^{2+} release from the SR and, eventually, result in force generation. Furthermore, muscle metabolism in humans is also similar to those in the fruit fly with myofibers divided in type I (slow-twitch) and type II (fast-twitch). In both cases, mammals and *Drosophila*, it has been shown that the muscle is an adaptive tissue that responds to exercise, nutrient supply, and endocrine factors with alterations in myofiber composition and size (Taylor, 2013; Piccirillo et al., 2014). However, motor units are organized slightly differently in invertebrates; all myofibers within a single muscle are simultaneously driven by the same motoneuron (Chakraborty et al., 2015). In vertebrates, each myofiber is innervated by a single motoneuron and, thus, a single muscle is innervated by numerous motoneurons whose synergistic activity controls muscular precision (Fuglevand, 2011).

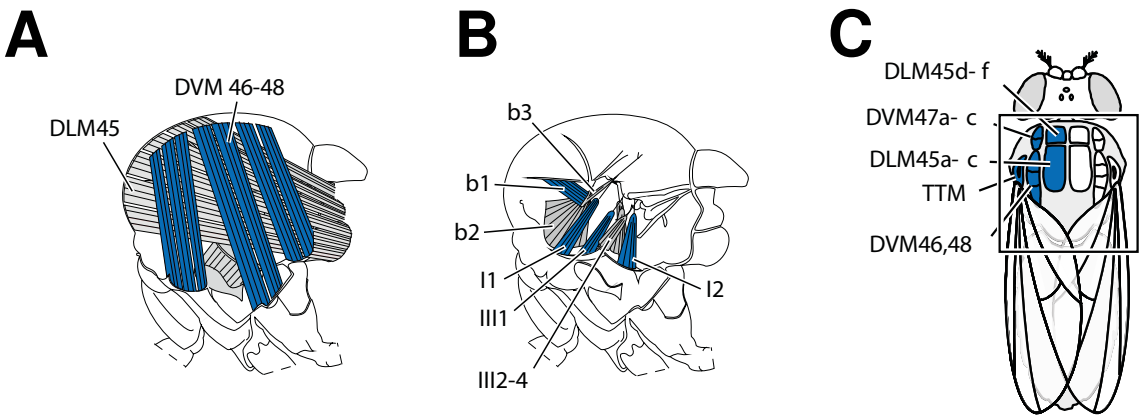

Figure 18. The flight musculature of *Drosophila.* The flight muscles consist of two groups: the asynchronous indirect flight muscles (A-IFMs) and the synchronous direct flight muscles (DFMs). **A)** Side view of the A-IFMs located inside the fly thorax. A-IFMs are subdivided into dorsal longitudinal muscles (DLMs; represented in grey) and dorsal ventral muscles (DVMs; dark blue). Structurally, they are arranged in an antagonistic manner. **B)** Side view of the DFMs located at the fly's wing hinge and classified according to their insertion site into basalars (b1-3; in grey) and axillaries (I1-2 and III2–4; in dark blue). **C)** Top view of the location of A-IFMs in the thorax. The numbers (45-48) indicate the number of the shown myofiber. The tergotrochanter muscles (TTM, tergotrochanter) are located in the base of the wing; and functionally they are involved in the jumping and the walking locomotion. Modified from (Lehmann and Bartussek, 2017).

The flight musculature of flies consists of two anatomically, physiologically, and functionally distinct groups: **the asynchronous indirect flight muscles** (A-IFMs) and the synchronous direct flight muscles (DFMs). The main muscle group is the A-IFMs, located in the thoracic region and subdivided into dorsal longitudinal muscles (DLMs) and dorsal ventral muscles (DVMs) (**Fig. 18A**). The A-IFMs of insects are characterized by the asynchrony between muscle electrical and mechanical activity, so that their contractions are not triggered by motoneuron spikes in the conventional one-for-one mode (i.e. one impulse-one contraction) like synchronous muscles (Josephson et al., 2000). When these muscles are stimulated by action potentials, they contract in an oscillatory manner and, thus, individual contractions are, instead, activated mechanically by stretch. In this way, A-IFMs are not activated and deactivated in concert with neurogenically controlled cycling of $[Ca^{2+}]_C$ but rather are stretching and shortening at a constant level of activating $[Ca^{2+}]_C$ (Gordon and Dickinson, 2006; Lehmann et al., 2013). This oscillatory mechanism is possible due to the antagonistic arrangement of DLMs and DVMs that operates as a semi-autonomous oscillator. The elevated power required for flight is, thus, delivered by the A-IFMs that generate wing flapping by the mechanical linkage between the muscles and the wings (Dickinson and Lighton, 1995; Lehmann and Dickinson, 1997).

The second minor group **is the DFMs**, responsible for the subtle changes in wing motion required for rapid manoeuvres and flight stability. These muscles are a set of tiny, highly specialized muscles that insert directly on the wing hinge (Lindsay et al., 2017). The DFMs are classified according to the insertion site into (**Fig. 18B**): the basalars (b1, b2, and b3) and the axillaries (I1-2 and III2–4). In addition, there are three other sets of thoracic muscles that do not insert directly on the wing hinge: tergopleurals, pleurosternals, and tergotrochanter. The first two sets are situated on the base of the wing and their function is poorly understood. However, they are thought to influence wing motion by altering the mechanics of the thorax. The third set, the tergotrochanter muscles (**Fig. 18C;** TTM, tergotrochanter), are located just behind the base of the wing and, they are involved in the jumping and the walking locomotion. Finally, there are also other muscles in the legs and others attached to the body wall.

4.3.2. *Drosophila* nervous system

Drosophila **central nervous system (CNS)** is composed of the brain and the ventral nerve cord (equivalent to the spinal cord in vertebrates) which is a fusion of thoracic and abdominal ganglia (**Fig. 19A**). Ganglia are often composed of multiple, fused units termed neuromeres. The adult *Drosophila* CNS contains over 100,000 neurons (Lovick et al., 2013) and 15,000 glial cells of various types (Kremer et al., 2017), these cells provide neurotransmitter and ionic homeostasis to neurons and serve as immune cells. Although flies and humans show the same subdivision of the CNS, the structure of the fly neurons is different, being unipolar while most mammalian CNS neurons are multipolar (Martin and Krantz, 2014). However, in terms of electrophysiological properties they are similar to mammalian neurons. They fire proper Na^+/K^+-based action potentials and, they use neurotransmitters for synaptic vesicle release. Also, although *Drosophila* brain is comprised by a lower number of neurons, compared to humans, their activity regulates similar behavioural functions such as: motor activity, reward and aversion, memory formation, feeding or sexual appetite. The neurons involved in negative geotaxis behaviour are dopaminergic neurons located in the protocerebral anterior medial region (Kasture et al., 2018). The CNS can be subdivided into two histological regions: the cortex regions, where neuronal cell bodies are located; and, the neuropiles areas to which axons and dendrites project and form synaptic connections (Pyza and Meinertzhagen, 1993). The dense synaptic neuropil areas are covered by astrocytes and glia.

The peripheral nervous system includes all of the nerves that branch out from the CNS and connect with the sensory organs and the fly musculature (**Fig. 19B**). Given the semitransparent nature of *Drosophila* wing, one of the most studied peripheral nerves are the wing sensory neurons that can be used as models of axon injury (Soares et al., 2014). Each wing neuron extends a long axonal projection that merge to form a thick nerve track that connects to the CNS by projecting into the thoracic ganglion located in the ventral nerve cord (Fang and Bonini, 2015). Structurally, the wing is a thin and simple structure. The most easily visible features of the wing are the veins. These are not veins in the vertebrate sense but ectodermal tubes that serve as structural supports for the wing and as

vessels for haemolymph (analogue to blood in vertebrates), and the peripheral nerves. In the nomenclature most commonly used in *Drosophila* studies (**Fig. 19C**), there are five main longitudinal veins (L1–5) that run proximodistally; two smaller abbreviated veins (L0 and L6); and three cross veins, the anterior and posterior crossveins, which bridge L3–L4 and L4–L5, respectively, and the humeral cross vein, which runs between the anterior wing margin and L0. The neurons are mainly located in the anterior wing margin (along L1 and the coastal vein) and, in less number, in the L3 vein (**Fig. 19C**).

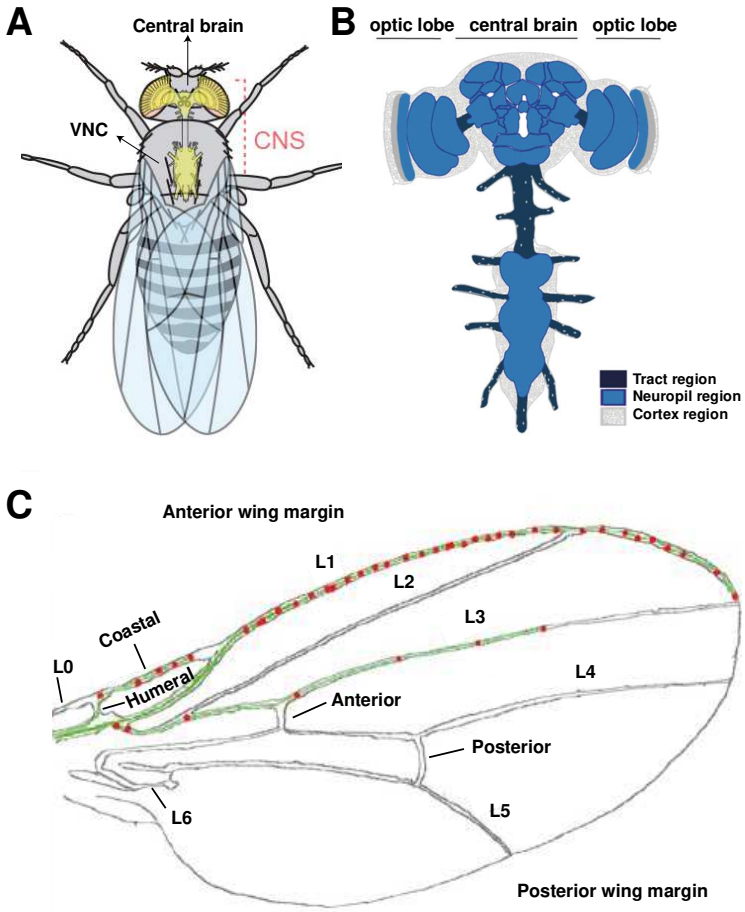

Figure 19. *Drosophila* nervous system. A) The fly central nervous system (CNS; shown in yellow) includes the central brain, located in the head, and a ventral nerve cord (VNC), located in the thoracic cavity. Figure modified from (Namiki et al., 2018). **B)** Histological regions of the CNS. The brain is flanked by the optic lobes. The cortex regions (grey areas) contain the neuronal and most of the glial cell bodies; the neuropils (light blue) harbor synaptic connections; and the small and large axon tracts (dark blue) connect the different neuropiles. Figure modified from (Batelli et al., 2017). **C)** An illustration of the peripheral nervous system in the *Drosophila* wing. There are five main longitudinal veins (L1–5) and two smaller abbreviated veins (L0 and L6); and three crossveins: the anterior, the posterior and, the humeral. The neurons (cell bodies are represented in red; and their projections in green) are located in the anterior wing margin (along L1 and the coastal vein) and, in less number, in the L3 vein. Modified from (Fang and Bonini, 2015).

4.4. Ca^{2+} signalling toolkit in *Drosophila*

Drosophila genome sequencing was completed in 2000 (Adams et al., 2000). This enabled the identification of genes encoding the Ca^{2+} signalling toolkit, represented by vertebrate homologs, and most of them single genes. Thus, studying Ca^{2+} signalling in *Drosophila* is considerably simplified (Chorna and Hasan, 2012). The research approach for this study was the generation of *Drosophila* mutants in Ca^{2+} signalling genes. However, given the importance of Ca^{2+} signalling in embryogenesis, mutations in genes affecting Ca^{2+} signalling proteins were frequently homozygous lethal. In this regard, the use of genetic methods for spatial-temporal expression of mutant genes, such as the GAL4-UAS system, has been of vital importance (Brand and Perrimon, 1993).

Ca^{2+} entry from the extracellular medium is also mediated by numerous channels located in the plasma membrane and named according to their gating properties. Among Receptor-Operated Calcium Channels **(ROCCs)**, glutamate-gated ionotropic receptors (iGluRs) are represented in *Drosophila* by 15 genes encoding different subunits. As in other animal species, *Drosophila* uses glutamate as a fast neurotransmitter in NMJs, and highly Ca^{2+} permeable iGluRs are clustered in active zones in postsynaptic motoneuron terminals (DiAntonio, 2006). As mentioned before, vertebrate Voltage-Operated Calcium Channels **(VOCCs)** are classified in three families (Ca_V1, Ca_V2 and Ca_V3) according to the pore forming subunit α1 (Catterall, 2011). The *Drosophila* genome also encodes three α1 subunits (Dmca1D, Dmca1A, and Ca-α1T), which can be classified as Ca_V1, Ca_V2 and Ca_V3 channels, respectively. Channels formed by Dmca1D are dihydropyridine (DHP) sensitive, similar to L-type channels of vertebrates, and are expressed in the adult muscles (Eberl et al., 1998). The Dmca1A channel is encoded by the cacophony (*cac*) gene, it is insensitive to DHP and widely expressed in the embryonic nervous system (Smith et al., 1996). The transient receptor potential **(TRP)** superfamily includes 28 mammalian members, which are subdivided into multiple subfamilies. Each of these subfamilies is represented by at least one of the 13 members found in *Drosophila*, suggesting common evolutionary relationships. Importantly, about the Store-Operated Ca^{2+} Entry (SOCE) players, *Drosophila* genome contains single **STIM** (*dSTIM*) and **Orai**

(*dOrai*) genes, whereas mammals have two and three copies, respectively (Venkiteswaran and Hasan, 2009).

Cytosolic Ca^{2+} exit to the extracellular medium is mediated by pumps and exchangers. In contrast to humans and other mammals, where there are four **PMCA** isoforms (PMCA1, 2, 3 and 4) encoded by distinct genes, the *Drosophila* genome contains a single gene (*CG2165*) encoding a plasma membrane Ca^{2+}-ATPase, which is expressed in all tissues, including the muscle (Bai et al., 2008). The *Drosophila* **Na^+/Ca^{2+} exchanger**, CALX, shares 55% identity with the three mammalian isoforms (NCX1, NCX2 and NCX3) and is mainly expressed in the fly adult brain and in the eye (Ruknudin et al., 1997). *Drosophila* also has a homolog for the vertebrate **Na^+/Ca^{2+}/K^+ exchanger**, NCKX30C, which is expressed in the adult brain, in larval imaginal discs and during embryonic development (Haug-Collet et al., 1999).

In regard to the **Ca^{2+} buffering systems**, a Mitochondrial Calcium Uniporter (**MCU**) homologue has been identified and characterized in *Drosophila*, the gene *CG18769* (Walkinshaw et al., 2015; Drago and Davis, 2016). A homolog of the mammalian **chaperone** BiP has also been identified in *Drosophila,* known as heat shock cognate 70 (HSC70-3) (Rubin et al., 1993). Importantly, there is no protein similar to calsequestrin (CSQ), abundant in the muscle and with Ca^{2+} binding properties, in *Drosophila*. However, the CaBP characteristic of the ER of non-muscle cells, calreticulin (CR), is encoded in the fly by the *Calr* gene (Smith, 1992).

Finally, regarding the **intracellular Ca^{2+} transport systems**, a single gene dubbed *Ca-P60A*, that encodes **SERCA** protein was identified (Magyar and Váradi, 1990). It displays a higher homology with mammalian SERCA1 and SERCA2 (71–73%) than with SERCA3 (67–69%). It is expressed at high levels in the central nervous system and in the muscles (Magyar et al., 1995). A dominant temperature-sensitive loss-of-function allele of the *Ca-P60A* gene (*Ca-P60AKum170*) was isolated in a screen for temperature sensitive paralytic mutants and has been very valuable for understanding the physiological role of SERCA in *Drosophila* (Sanyal et al., 2005, 2006). The homologous gene of mammalian Secretory Pathway Ca^{2+}-ATPase (**SPCA**) in *Drosophila* is known as *SPoCk* or *CG32451*, that produces three isoforms (SPoCk-A-C) each localized in different cellular compartments: SPoCk-A

is found in the Golgi apparatus; SPoCk-B in the ER; and SPoCk-C in the peroxisome (Southall et al., 2006). As for the SR/ER Ca^{2+} release channels, **the RyRs and IP_3Rs**, in vertebrates each of these proteins are represented by three different isoforms whose expression is tissue specific. In contrast, the *Drosophila* genome contains unique IP_3R and RyR genes. The RyR gene, ryanodine receptor 44F (*ryr* or *ryr-44F*), encodes a protein showing approximately 45% identity with the three vertebrate family members (Hasan and Rosbash, 1992; Takeshima et al., 1994). The IP_3R gene (itpr) in *Drosophila* is represented by two splice variants, referred to as the embryonic and the adult head isoforms (Sinha and Hasan, 1999). *Drosophila* IP_3R shares 68% similarity with the mouse IP_3R1 (Patel et al., 1999) and its functional properties are also similar to those of the vertebrate isoform (Srikanth et al., 2004).

4.4.1. Ca^{2+} imaging in *Drosophila*

A critical aspect of Ca^{2+} signalling is the kinetics and spatial localization of cellular Ca^{2+} changes upon cell activation. The development of genetically encoded Ca^{2+} indicators (GECIs) has allowed these measurements in flies *in vivo* in animals (Palmer et al., 2011). GECIs allow monitoring of Ca^{2+}, not only in the cytosol, but also in organelles thanks to the addition of specific targeting sequences. However, this type of measurements are still poorly exploited in living animals and few examples are available in *Drosophila* (Vajente et al., 2020). Among them, Drago and Davis generated a transgenic line for a mitochondria-targeted GCaMP (named 4mtGCaMP3) that was expressed in mushroom body neurons (Drago and Davis, 2016); and the GAP (GFP-Aequorin-Protein) sensor (see materials and methods) targeted to the SR (Navas-Navarro et al., 2016).

4.5. *Drosophila* as a model of aging

Drosophila has emerged as an excellent model to study the complexity of the aging process, and this is due to several reasons (Partridge and Barton, 1993). First, the fruit fly has a relatively short lifespan of 40 days at 29 °C and a generation time of

9 days at 25 °C. Second, the genome has been fully sequenced and annotated (Adams et al., 2000), and there are available tools for genetic manipulation (e.g. *P-element*, GAL4-UAS system) and phenotypic markers for analysis (e.g. eye colour, balancer chromosomes). Moreover, compared to vertebrate models, *Drosophila* has considerably less genetic redundancy, making the characterization of protein function less complicated. Third, relevant genes and cellular processes are conserved between flies and mammals (Yoshihara et al., 2001) and, remarkably, over 60% of known human disease-causing genes have a fly orthologue (Wangler et al., 2015). Finally, flies exhibit complex behaviours and, like in humans, many of these behaviours, including learning, memory and motor ability, deteriorate with age (Simon et al., 2006).

Studies in flies have identified single gene mutations that affect lifespan, the most studied ones are reduction in the activity of the nutrient-sensing insulin/IGF-1 signalling (IIS) pathway and the associated Target of Rapamycin (TOR) pathway (Clancy et al., 2002; Evans et al., 2011). However, the rate of aging is also determined by environmental conditions, such as diet, oxidative stress or inflammation (He and Jasper, 2014).

Recent studies have focused on the effects of aging on specific tissues, such as skeletal muscle. Specific genetic perturbations in the muscle include the accumulation of protein aggregates (Demontis and Perrimon, 2010). Moreover, functional, metabolic, and structural deterioration of the skeletal muscle have also been associated to aging, but the underlying mechanisms are only beginning to be understood (Augustin and Partridge, 2009; Demontis et al., 2013). A quantitative non-invasive assay for skeletal muscle function has been developed based on the natural negative geotactic behaviour of flies, or startle-induced vertical movement. This movement is basically a climbing function, as it has been shown that jumping or flying has little impact on the distance moved and, furthermore, the removal of the hind legs, but not the wings, impairs climbing (Rhodenizer et al., 2008). Moreover, the decrease on the climbing speed strongly correlates with age, suggesting negative geotaxis is an universal feature of aging in *Drosophila* and a reliable measure of locomotor function across age in flies (Grotewiel et al., 2005). For this reason, the climbing assay is a frequently used index of locomotor behaviour in flies (Arking and Wells, 1990; Chavous et al., 2001; Gargano et al.,

2005; Goddeeris et al., 2003; Kang et al., 2002; Miquel et al., 1976; Mockett et al., 2001; Ruan et al., 2002; Simon et al., 2006). Regarding the aging brain, morphological characterization of changes during aging has focused on the presence and number of dopaminergic neurons. It is known that dopaminergic neurons control locomotor behaviour, and while locomotion declines with age, no significant changes in the number of dopaminergic neurons have been observed in aging flies (White et al., 2010).

Aims and hypothesis

The Ca^{2+} hypothesis of aging proposed in the 1980s that alterations in Ca^{2+} homeostasis could modulate brain aging and increase susceptibility to neurodegenerative diseases. Moreover, a hallmark of aging is the progressive decline in skeletal muscle function known as sarcopenia which suggests that the Ca^{2+} dependent excitation-contraction (EC) process may be impaired in aging. Recent studies in this area suggests that Ryanodine receptor type 1 (RyR1), the skeletal muscle sarcoplasmic reticulum (SR) Ca^{2+} release channel required for muscle contraction, suffers complex remodelling during aging (oxidation, nitrosylation and depletion of calstabin1) leading to "leaky" channels with increased open probability. This fact will result in decrease $[Ca^{2+}]_{SR}$ in the skeletal muscle.

General objective

- Determine whether alterations within the Ca^{2+} content of the SR are at the origin of the loss of Ca^{2+} homeostasis observed in sarcopenia; and if they are related with the loss of muscle function.

Specific objectives

- Generation and characterization of transgenic flies that express the ratiometric low affinity Ca^{2+} indicator GAP3 targeted to muscle sarcoplasmic reticulum or the endoplasmic reticulum (ER) in neurons.
- Development of a method that allows quantitative and calibrated measurements of SR/ER Ca^{2+} content *in vivo*.
- Determine the SR Ca^{2+} levels in aged flies and correlate it with muscle function.
- Monitor cytosolic Ca^{2+} dynamics during muscle contraction in aging.
- Measure the ER Ca^{2+} content in other aging tissues, such as different types of neurons, and determine if the results can be extrapolated to those obtained in aged muscles.
- Explore the molecular mechanisms involved in the maintenance of the $[Ca^{2+}]_{SR/ER,}$ by analysing the expression levels of the proteins directly implicated in this process.

Methods

1. Gene construction

The fusion gene encoding GAP3 targeted to the ER (erGAP3) was cloned into a *pUASTattB* vector to generate *pUASTattB-erGAP3*. erGAP3 protein contains the calreticulin (CR) signal peptide sequence fused to the amino-terminus of the GAP protein and the ER retention signal *KDEL*, the tetrapeptide sequence, in the carboxy-terminus of the protein (Navas-Navarro et al., 2016). The fusion gene *erGAP3* was expressed under the control of the upstream activating sequence (*UAS*) promoter in the *pUASTattB* plasmid. This vector is designed to integrate a sequence of interest into the fly genome and contains the following genetic elements: the *white* selectable marker that increases pigment levels in the eye, conferring red colour[4]; the *loxP* recombination site; the *UAS-erGAP3-SV40* expression cassette; and an *attB* integration site (**Fig. 20**).

Basic molecular biology techniques were used in the cloning: isolation of plasmid DNA by miniprep (PureYield™ Plasmid Miniprep; Promega, A1222) and maxiprep (Quiagen, 12163) protocols; bacterial transformation by heat shock method (DH5α™ Competent Cells; ThermoFisher, 18258012); DNA agarose gel electrophoresis; DNA gel purification (Wizard® SV Gel and PCR Clean-Up System; Promega, A9282); the Polymerase Chain Reaction (PCR); restriction enzyme digests; DNA ligation reaction; primer design; and, DNA quantification by NanoDrop™ spectrophotometer. The resulting DNA plasmid was sequenced by the Sanger method (Secugen S.L) to verify the construct integrity. The SnapGene® software version 5.0 was used to plan, visualize, and document molecular biology procedures.

2. Generation of transgenic flies

To generate transgenic flies, the *pUASTattB-erGAP3* vector above described was microinjected into *Drosophila* embryos "*y1 M{vas-int.Dm}ZH-2A w*; M{3xP3-RFP.attP} ZH86Fb*" (BL24749 strain; BestGene® Inc.), containing the locus *86F* in the third chromosome which includes an *attP* integration sequence and it lacks the

[4] Mutations on the white gene produce viable flies with white eyes, and hence, its name.

white marker that affects eye colour (**Fig. 20**). This locus is also composed by the artificial *3xP3* promoter followed by a *Red Fluorescent Protein (RFP)* marker flanked by *loxP* recombination sequences. The *pUASTattB-erGAP3* vector was microinjected along with the integrase *ϕC31* mRNA, which is required to integrate the *UAS-erGAP3-SV40* expression cassette into the fly genome (Bischof et al., 2007). After the integration has occurred, the *Cre* recombinase mRNA was microinjected to eliminate the *RFP* and the *white* markers (Chen et al., 2013).

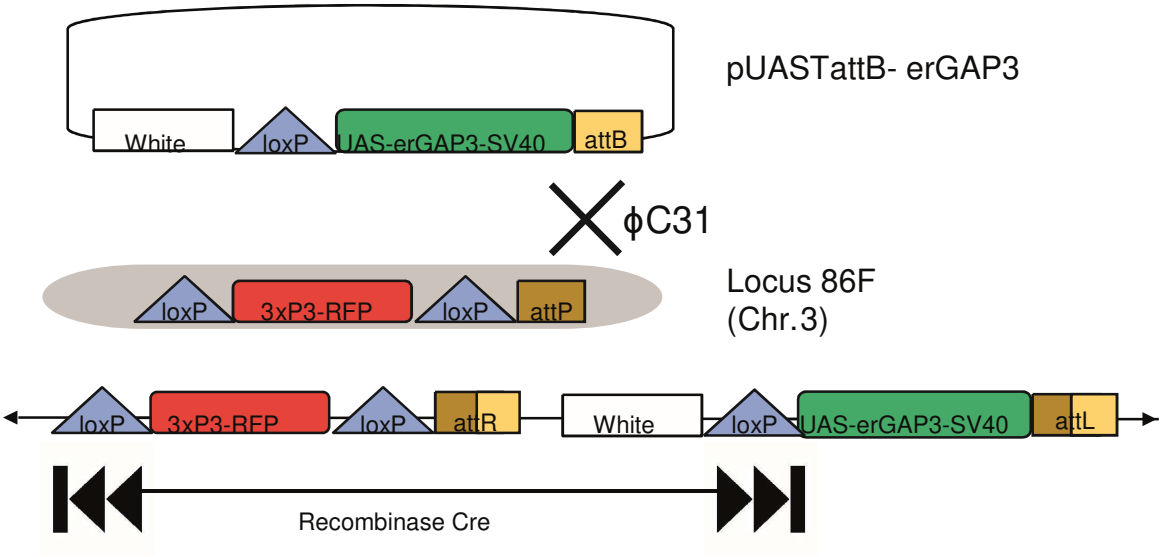

Figure 20. Generation of UAS-erGAP3 transgenic flies. The integrase ϕC31 catalyses the integration of *pUASTattB-erGAP3* vector in locus *86F* located in the third chromosome (Chr.3) of the fly genome by *attB* and *attP* recombination and, thus, generating the *attR* and *attL* sites. Next, Cre recombinase deletes the *Red Fluorescent Protein (RFP)* and the *white* markers flanked by the two more distant *loxP* sites.

In order to express erGAP3 in muscle or neuronal tissues, we used the GAL4-UAS system (Brand and Perrimon, 1993; Hampel et al., 2011). This system consists of the GAL4 (galactose-induced gene 4) transcription factor that specifically binds the *UAS* sequence (**Fig. 21**). The UAS-erGAP3 flies (Navas-Navarro et al., 2016), generated by the ϕC31 system, were crossed with flies expressing the transcription factor GAL4 under the control of the muscle specific myosin heavy chain (*Mhc*) promoter (Mitra et al., 1996) or the nervous system specific embryonic lethal abnormal visual system (*elav*) promoter (Yao et al., 1993). The *elav* gene is expressed in most or all types of neurons and, thus, is referred to as pan-neuronal. In addition, the cytosolic Ca^{2+} indicator GCaMP3 was expressed in the muscle, by

crossing the UAS-GCaMP3 flies (Tian et al., 2009) with the Mhc-GAL4 flies. We assigned each line a specific code[5], summarized in the table below (**Table 2**). The wild type flies, used as control, were from the *w*^{1118} strain; as the transgenic flies were constructed in this *white* genetic background.

Fly line	Genotype	GECI	Targeted tissue	Targeted organelle
DM006	*Mhc-GAL4 // erGAP3*	erGAP3	muscle	SR
DN005	*Elav-GAL4 // erGAP3*	erGAP3	nervous system	ER
DM010	*Mhc-GAL4 // GCaMP3*	GCaMP3	muscle	Cytosol
Wild type	*w*^{1118}	-	-	-

Table 2. Fly lines used in this thesis.

3. Lifespan assay

Fly stocks were maintained in an incubator (Ibercex, M-17004) at 29 °C, constant 12 h[6] light/dark cycles, and 60% humidity. Flies hatched in the same day were collected and sorted by gender. So that flies can be sexed and scored, they were anaesthetised with CO_2 for 1-10 min using a square CO_2 station. The station is composed by a holed base covered with white felt, which is a porous material designed to permit CO_2 to flow through, while preventing *Drosophila* from falling through the holes beneath. The station is fed by a CO_2 tank and the gas flow is regulated by a valve system. After sorting, groups of 20 flies were placed into food vials. The food was prepared with: 1 packet (177.67g) of Nutri-Fly® Molasses Formulation (Genesee Scientific, 66-112); 0.9% (v/v) propionic acid (Sigma-Aldrich, 81910); and, 0.6% (w/v) Agar type I (iNtron Biotechnology, 25999); diluted in 1 L of bottled water. Changes onto new vials with fresh food were made every two or three days in order to avoid larvae disrupting food. In each change of food,

[5] DM= *Drosophila* muscles; DN= *Drosophila* neurons.
[6] Please note that, along the document, the most common units of: time, concentration, mass, distance, voltage, revolutions, frequency, and others; are written in symbols, according to the metric system.

we counted the dead flies in the old vial and, also, the dead flies carried onto the new vial in order not to double-count the same dead flies. Flies that escaped or were dead by accident, immediately left the experiment. The assay ended when the last survivor was dead. The data were represented as the percentages of survival at the day indicated.

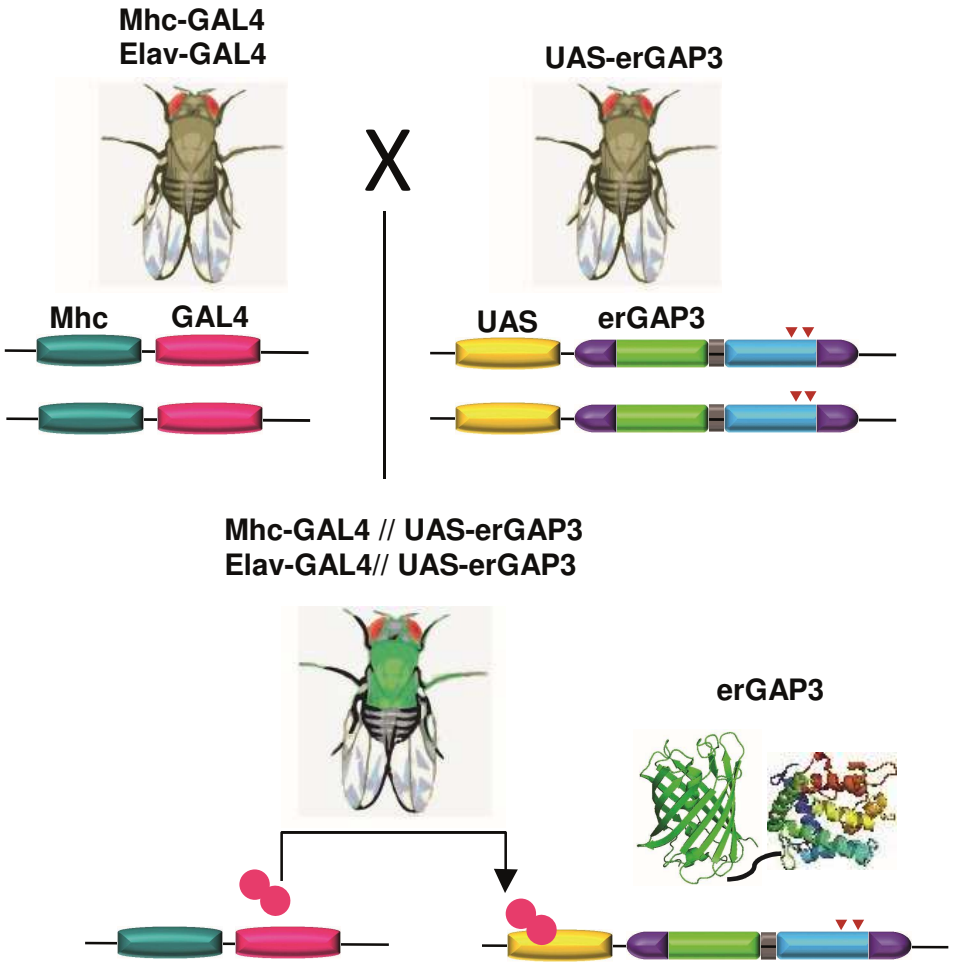

Figure 21. Generation of erGAP3 transgenic muscle and neuronal lines. The GAL4-UAS system allowed tissue-specific expression of erGAP3 sensor. Flies expressing the GAL4 transcription factor (pink) downstream the tissue specific promoter myosin heavy chain (*Mhc*; represented in blue) were crossed with UAS-erGAP3 flies. As a result, in the first generation, GAL4 transcription factor is only expressed in the skeletal muscle tissue where it binds to the *UAS* sequence (yellow) allowing the expression of erGAP3 protein. The same procedure was followed to generate the neuronal transgenic line with the pan neuronal tissue specific promoter embryonic lethal abnormal visual system (*elav*).

4. Climbing assay

The climbing assay is a well standardized procedure based on *Drosophila* negative geotaxis (their tendency to go up) that can be used as an indicator of motor function across age in flies. The aim is to measure a known distance climbed in a certain time, in this case we used 5 cm in 18 s. The day prior to the experiment, we changed the flies of a known age onto vials with fresh food. The day of the experiment, groups of ten flies were transferred onto vials without food and previously labelled with the known height mark of 5 cm. The experiment was always performed at the same time of the day, early in the morning, to avoid bias due to changes in the circadian rhythms of the flies. We let them acclimate to the new environment for a few min and, then, the experiment was started. The vials were tapped vigorously onto the table surface making sure that all the flies were placed onto the bottom of the tube. After three taps we counted simultaneously the number of flies able to climb 5 cm in 18 s, and the time in which 50% of the flies surpassed the 5 cm mark. We let the flies rest for 15 min and, then, the assay was repeated another 3 times with the same group of flies. The climbing assays were performed on days 7 (i.e., when the flies were 7 days old), 14, 21, 28 and 35.

5. Protein induction and extraction

First, the gene encoding GAP3 was cloned into the bacterial expression vector *pET28a* and transformed in *E. coli* BL21 strain (Stratagene). Second, bacteria were grown in 3 ml of Luria-Bertani Broth medium (LB Broth; Sigma-Aldrich, L3022) containing 40 µg/ml of kanamycin (Sigma-Aldrich, K4000), at 37°C and 250 rpm for 12-15 h. The next day, the bacterial cultures were diluted 50 times in the same medium containing LB and kanamycin, and grown until the optical density of the sample, measured at a wavelength of 600 nm, was between 0.6 and 1 (OD>0.6); which was usually 2 h. The optical density was measured in the UV-visible spectrophotometer (Thermo^{TM} electro corporation uv1). Then, protein expression was induced by the addition of 0.01 mM isopropyl β-D-thiogalactoside (IPTG; Sigma-Aldrich, I5502) for 6 h at 30°C and 250 rpm. The cells were, then, pelleted by centrifugation at 6.000 g for 10 min; and, resuspended in a buffer containing:

150 mM NaCl (Merck; 106406); 0.5 mM DTT (Dithiothreitol; Sigma-Aldrich, D9760); 20 mM Tris-HCl (Trizma® base; Sigma-Aldrich, T1503); pH 8.8; diluted in Milli-Q® ultrapure water; and, a cocktail of protease inhibitors with EDTA (Roche, 11836153001) diluted 10 times in the buffer. Next, the cells were lysed by sonication (Vibra cell 75115, Biolock Scientific). The sonication protocol was performed on ice and consisted on 5 cycles, 15 s ON/ 1 min OFF, at 30% vibration amplitude. Finally, the bacterial lysate was centrifuged at 30.000 g for 10 min, and the supernatant was used as a source of GAP protein. The supernatant was aliquoted, frozen in liquid nitrogen, and stored at -80°C.

6. Protein quantification

Total protein extracts were quantified by the Bradford assay. The procedure is based on the formation of a complex between the dye, Brilliant Blue G, and the proteins in the solution. The protein-dye complex causes a shift in the absorption maximum of the dye from 465 to 595 nm, measured in the UV-visible spectrophotometer. The Bradford Reagent concentrate (Bio-Rad, 500-006) is prepared by diluting 1 part of reagent in 4 parts of water. Then, we mix 1 part of the protein sample with 30 parts of the Bradford Reagent. Protein concentrations were determined by comparison to a standard curve. The standard curve was performed with bovine serum albumin (BSA; Sigma-Aldrich, A2153) diluted in 50 mM Tris-HCl, pH 8.8; in a concentration range between 0 and 2 mg/ml.

7. Fluorescence spectra

Fluorescence spectra for GAP3 protein were performed in fluorescence spectrophotometer (HITACHI 650-150) equipped with a xenon lamp. The excitation spectra were recorded between 380 and 500 nm wavelengths with the emission set at 520 nm. First, the spectrophotometer cuvette was filled with 1 ml of extracellular medium (without Ca^{2+}) composed of: 145 mM NaCl; 5 mM KCl (Merck; 104938); 1 mM $MgCl_2$ (Merck; 102367); 10 mM glucose (Merck; 108342); and, 10 mM Na-HEPES (Sigma-Aldrich, H3375); pH 7.4; diluted in Milli-Q®

ultrapure water; and 8.5 µg of the protein extract containing GAP3[7]. Second, the same recording was performed with the addition of 1 mM $CaCl_2$ (Merck; 102382) to the extracellular medium. Then, a new sample was prepared with another 8.5 µg of the same protein extract in extracellular medium; and, immediately heated for 10 min in an Eppendorf tube® at 50°C in the thermal bath. After heating, another spectrum was recorded under the same conditions, i.e. in the absence and in the presence of Ca^{2+}.

8. Immunofluorescence

Larvae were dissected under the Stereo Microscope (ZEISS Stemi DV4) in HL3 buffer containing: 70 mM NaCl; 5 mM KCl; 10 mM $NaHCO_3$ (Merck, 106329); 5 mM Na-HEPES; 5 mM trehalose (Merck, 108216); 115 mM sucrose (Merck; 107651); 1.5 mM $CaCl_2$; and, 20 mM $MgCl_2$; pH 7.2 in Milli-Q® ultrapure water. First, larvae were dorsally immobilized in the dissection plate with two pins, one placed in the anterior part of the animal and the other in the posterior part; second, larvae were opened through the mid-dorsal line with micro-scissors; third, the cuticle was opened and fixed very straight with four pins (two anterior and two posterior), making visible all the internal organs; finally, the internal organs were removed with the tweezers, leaving intact the CNS and the muscle wall. This larvae preparations were fixed for 10 min in 4% (v/v) paraformaldehyde (PFA; Sigma-Aldrich, 76240) diluted in phosphate-buffered saline 1X (PBS; ThermoFisher, Gibco™, 10010023) pH 7.4. PFA was removed by washing with PBS 1X for three times, then, tissues were permeabilized for 1 h with the permeabilization solution: 0.15% (v/v) Triton X-100 (TX-100; Merck, 108603); 5% (v/v) goat serum (GS; ThermoFisher, Gibco™, 16210064) and 2% (w/v) BSA; diluted in PBS 1X. After three washes with PBS 1X, larvae were incubated overnight with the SERCA primary antibody (1:500; Sanyal et al., 2005) diluted in the permeabilization solution without TX-100 detergent. The next day, after removing the primary antibody, the samples were washed with PBS 1X and revealed with the corresponding Alexa Fluor 568-conjugated secondary antibody (1:100; ThermoFisher, A11031), by incubation for 1 h at room

[7] Obtained as described in section **5.Protein induction and extraction.**

temperature (RT). Larvae were washed with PBS 1X for three times and, once with Milli-Q® ultrapure water to eliminate salts. Finally, nuclei were labelled with cell permeant Hoescht 33322 (3 µM; ThermoFisher, H3570) for 10 min. Tissues were mounted on glass slides with Vectashield® antifade mounting medium (Vector Laboratories, H-1000).

Whole adult flies were embedded and cryopreserved in Tissue-Tek® (Sakura Finetek, 4583), frozen in dry ice and subsequently stored at -80°C. Tissue slices (10-15 µm) were performed in a HM550 Thermo Scientific™ Cryostat Microtome. The protocol described above for larvae was applied for immunostaining adult tissue.

GAP3 was detected as green fluorescence (excited at 470/40 nm and emitted at 540/50 nm) in a Zeiss Axioplan 2 upright microscope[8] equipped with a 63X/1.2w Korr objective and an AxioCam MRm camera (12 bits) connected through the software interface Axiovision Rel 4.6.3 (Zeiss). The red fluorescence was recorded with excitation at 560/40 and emission at 605/50 nm. The nuclei, stained with Hoescht, were detected exciting at 340/80 nm and emitting at 435/85 nm. The Zeiss ApoTome^{R} system was used for optical sectioning.

9. Western blotting

The flies were anesthetized with CO_2, and their tissues (thorax[9] or head) were dissected with micro-scissors. Single thoraxes or heads were placed in an Eppendorf tube® and homogenised with a Kontes™ Pellet Pestle made of blue polypropylene (5 to 10 times) in radio immunoprecipitation assay (RIPA) buffer: 150 mM NaCl; 50 mM Tris-HCl; 0.1% (v/v) sodium dodecyl sulphate (SDS; Sigma-Aldrich, L3771); 0.5% (v/v) sodium deoxycholate (SDC; Sigma-Aldrich, D6750); and 1% (v/v) TX-100; pH 7.4; diluted in distilled water. Total protein extracts were quantified by the Bradford assay and, then, diluted in buffer Laemmli 5X: 0.3 M Tris-HCl; 50% (v/v) glycerol (Sigma-Aldrich; G5516); 10% (w/v) bromophenol blue

[8] The same microscope was used for the Ca^{2+} imaging experiments *in vitro*.
[9] The legs and the wings were removed from the thoracic part of the fly.

(Sigma-Aldrich, B0126); 100 mM DTT; and, 10% (w/v) SDS; pH 6.8 in distilled water.

The thorax or head protein extracts from individual flies (10-20 µg) were loaded per lane on a polyacrylamide gel (Bio-Rad, 161-0158), along with the molecular weight marker (Precision Plus Protein All Blue Standards, Bio-Rad; 161-0373). The gel is divided into stacking (5% (v/v) polyacrylamide; 0.1% (v/v) SDS; 0.1% (v/v) ammonium persulfate (APS; Sigma-Aldrich; A3678); 0.2% (v/v) tetramethylethylenediamine (TEMED; ThermoFisher; 17919) 0.4 M Tris-HCl; pH 8.8; diluted in Milli-Q® ultrapure water) and separating gel (6% (v/v) polyacrylamide, 0.1% (v/v) SDS; 0.1% (v/v) APS; 0.2% (v/v) TEMED; 60 mM Tris-HCl; pH 6.8; diluted in Milli-Q® ultrapure water). Polyacrylamide gel electrophoresis (PAGE) separates the proteins according to their electrophoretic mobility (size, charge and conformation) and was performed in running buffer 1X: 25 mM Tris; 192 mM glycine (Sigma-Aldrich, G8898), and, 0.1% (v/v) SDS; pH 8.3; diluted in distilled water.

After electrophoresis (SDS-PAGE) is complete (50 mA, 200 V, 1 h), proteins were transferred onto nitrocellulose membranes (0.45 µm pore-size; Bio-Rad, 1620115) by wet electroblotting (400 mA, 100 V, 1 h). The gel is placed in the “transfer sandwich” (from cathode to anode: sponge pad - filter paper – gel – membrane - filter paper - sponge pad) pressed together by a support grid. The supported gel sandwich is placed vertically in a tank filled with transfer buffer 1X: 25 mM Tris; 192 mM glycine; 20% (v/v) methanol (Merck, 106009) and 0.3% (v/v) SDS; pH 8.3; diluted in distilled water. Then, in order to prevent antibodies from binding non-specifically, the membrane is blocked for 2 h with blocking solution or TBST (Tris buffer saline, Tween) buffer: 20 mM Tris; 150 mM NaCl; and, 0.05% (v/v) TWEEN® 20 (Sigma-Aldrich, P1379); pH 7.5; diluted in distilled water; containing 2% (w/v) defatted dry milk (Nestlé Sveltesse). Membranes were sequentially incubated overnight with the primary antibodies (**Table 3**) in blocking solution at 4°C. After three washes with TBST, membranes were incubated for 1 h with the corresponding secondary antibodies labelled with horseradish peroxidase (HRP) enzyme (**Table 4**), at RT. After another three washes, protein was detected by incubating for 1 min with enhanced chemiluminescence solution (ECL): 2.9 mM p-Coumaric acid (Sigma-Aldrich, C90008); 1.25 mM luminol (Sigma-Aldrich, A8511);

0.1 M Tris-HCl; pH 8.8; and, 0.1% (v/v) hydrogen peroxide (H_2O_2; Sigma-Aldrich, H1009); diluted in distilled water; or the commercial solution ECL Western Blotting Substrate (ThermoFisher, 34577) and visualized in the dark room with hyperfilms (GE Healthcare Amersham™ Hyperfilm™ ECL; ThermoFisher, 28906837).

Primary antibody	Dilution	Target	Host species	MW (kDa)	Source
SERCA *Drosophila*	1:10.000	ER Ca^{2+}-ATPase	Rabbit	100	Dr.Ramaswami
BiP/GRP78	1:5.000	ER chaperone	Rabbit	78	Sigma-Aldrich; G9043
RyR *Drosophila*	1:2.500	ER Ca^{2+} release channel	Guinea Pig	565	Robert Scott
Tubulin	1:10.000	Cytosolic protein	Mouse	50	Sigma-Aldrich; T6074

Table 3. Primary antibodies for Western blotting.

Secondary antibody	Dilution	Target	Source
Goat anti Mouse IgG (H/L):HRP	1:2.000	Mouse	Bio-Rad 1706516
Goat anti Rabbit IgG (H/L):HRP	1:2.000	Rabbit	Bio-Rad 1706515
Goat anti Guinea Pig IgG (H/L):HRP	1:2.000	Guinea pig	Bio-Rad AHP863P

Table 4. Secondary antibodies for Western blotting.

Hyperfilms were scanned with the GS-800™ Calibrated Imaging Densitometer (Bio-Rad) and analysed with the Image J software. First, background was subtracted. Second, a rectangular region of interest (ROI) was drawn horizontally enclosing all the bands within the same height (molecular weight). Third, in the analyse menu, select the tool gels, select first line and plot lanes. A new window appears with the lane profile plots drawn as peaks. Fourth, we used the straight line selection tool to draw base lines and/or drop lines so that each peak of interest

defines a closed area. Finally, the area inside each peak, that represents a single band, is measured with the wand tool. It should be noted that the western blot was performed blinded to the distribution of the samples during the experiment and during the analysis.

10. Cell culture and transfection

The immortal HeLa cell line (human cervical cancer of patient Henrietta Lacks, ATCC: CCL-2) stably-expressing erGAP3 has been previously described (Navas-Navarro et al., 2016). Clones were generated by Lipofectamine® 2000 transfection (ThermoFisher, Invitrogen™, 11668-019) of *pcDNA3-crERGAP3kdel* vector (Addgene, 78118) followed by 0.8 mg/ml G-418 (Geneticin; ThermoFisher, Gibco™, 11811-023) selection. The population of GFP-positive cells was enriched by cell sorting FACSAria™ (BD Bioscience). Single-cell clones were selected by limited dilution. Other immortal cell lines used were the human embryonic kidney cells 293T (HEK293T), and the mouse myoblast cell line C2C12 as a model of muscle cell.

Cells were maintained in DMEM (Dulbecco's modified Eagle's medium, high glucose, GlutaMAX™-I supplement; ThermoFisher, Gibco™, 10566-016) supplemented with: 10.000 U/ml penicillin-streptomycin (ThermoFisher, Gibco™, 15140163); 10% (v/v) foetal bovine serum (FBS; Lonza, DE14-801F); and 0.2 mg/ml G418 (only the stable clones); at 37°C under 5% CO_2 saturation in an incubator (Heraeus® HERACell® 150). Cells were maintained in 100 mm culture plates (ThermoFisher; Nunc™, 150350) and sub-cultured every three days under the following protocol: DMEM culture medium was removed and cells were washed with PBS 1X. Next, cells were detached by treatment for 1-3 min with 0.25% (v/v) trypsin-EDTA (Ethylenediamine tetraacetic acid; ThermoFisher, Gibco™, 25200-056) and finally trypsin was inactivated by adding DMEM medium with serum. Then, cells were centrifuged at 1000 rpm for 4 min and pellet was re-suspended in 1 ml DMEM. Cells were counted using *Neubauer* chamber, and 1:3 diluted cells were seeded in 100 mm plates for maintenance. For Ca^{2+} experiments, erGAP3 expressing HeLa cells were seeded on 12 mm-diameter round coverslips,

previously treated with 0.1 mg/ml poly-L-lysine (Sigma-Aldrich, P1274), each placed in 4-well plates (ThermoFisher; Nunc™, 167063) at a density of 4 x 10^4 cells per well.

For transient transfection experiments, HEK293T cells and C2C12 were transfected with *pcDNA3-crERGAP3kdel* vector; and HeLa cells[10] with *pCMV-G-CEPIA1er* (Addgene, 58215); all of them at 1 µg using Lipofectamine® 2000 following manufacturer's instructions. Briefly, DMEM medium of the cell culture was substituted with OPTI-MEM™-I (ThermoFisher, Gibco™, 11524456) medium. In an Eppendorf tube®, 1 µg of DNA was mixed with 2 µl Lipofectamine (per well) in 100 µl OPTI-MEM medium. After 20 min, the mixture was added drop by drop on the well and incubated for 5-6 h. Finally, transfection medium was removed and replaced by DMEM. Cells were imaged 24-48 h after transfection.

11. Cortical astrocytes cultures

Brain cortices were isolated from P2-3 C57BL/6JCrl (Charles Rivers) erGAP3 (L1 or L10) transgenic mice lines (Navas-Navarro et al., 2016). Cortices were dissected under the ZEISS Stemi DV4 Stereo Microscope, in cold Hank's balanced salt solution (HBSS; no phenol red, Ca^{2+} and Mg^{2+} free, ThermoFisher, Gibco™, 14175-053) supplemented with 10 mM glucose and 0.05% (w/v) BSA. Tissues were removed free of meninges and rapidly cut into small pieces. Next, tissues were enzymatically digested for 20 min at 37°C with 0.5 mg/ml papain (Worthington Biochemical Corporation, LS003119) and 0.04 mg/ml DNase (Roche, 10104159001) dissolved in HBSS. When the tissue fragments were settled at the bottom of the tube, they were washed 3 times with cold HBSS; resuspended in Neurobasal™ medium (ThermoFisher, Gibco™, 21103049) supplemented with 0.04 mg/ml DNase and 10% (v/v) FBS to inactivate papain; and, then, mechanically dissociated with glass pipettes of three different pore size (10 times with each size). Finally, cells were resuspended in Neurobasal™ medium, supplemented with: 1% GlutaMAX™-I (ThermoFisher, Gibco™, 35050-038); 2 % (v/v) B27™ (ThermoFisher, Gibco™, 17504-044); 10.000 U/mL penicillin-streptomycin; and

[10] Not the stable clone for erGAP3, but the human wild type HeLa cells.

10% (v/v) horse serum (HS; ThermoFisher, Gibco™, 16050122); and plated on a poly-L-lysine-coated 75 cm^2 flask. After 2 and 5 days flasks were slapped to remove neurons and other loosely attached cells such as microglia and oligodendrocytes. After 1 week, cells were trypsinized and seeded in the same medium onto poly-L-lysine-coated 12 mm diameter glass coverslips at a density of 2.5 x 10^4 cells/coverslip. The cultures were used for imaging experiments within 1–2 weeks.

12. The Ca^{2+} measurements

12.1. Measuring sarcoplasmic/endoplasmic reticulum Ca^{2+} concentration in *Drosophila*

The flies were anaesthetized with ice for 1-5 min, by laying them on a glass petri dish placed inside a box full of ice. Once they started to awake, they were tethered ventrally in a small drop of warm 2% (w/v) low-gelling temperature agarose (Sigma-Aldrich, A6560) diluted in distilled water; and, then, quickly transferred to a Leica M205FA fluorescence stereo microscope stage (**Fig. 22**). Five fluorescence images at each GAP3 wavelength (405 and 470 nm) were collected at 5 s intervals. Line DM006 and DM010 were used to image thorax muscles and line DN005 for brain or wing neurons (**Table 2**). A Plan Apo 1.0X objective (NA = 0.30) and a 100 W mercury lamp were used, with either a 470/40 nm or a 405/40 excitation filter and, in both cases with a 525/50 nm emission filter. Images were acquired at 16 bits, with binning of 4x4 and a zoom of 6.5X. To determine R_{min} (for Ca^{2+} calibration), at the end of each measurement, each fly was carefully heated in the bath for 10 min at 50 °C and, then, imaged using the same settings. Images were analysed with the Image J software (https://imagej.nih.gov/ij/): first, the average fluorescence intensity projection (Image J; Z Project function) of the five time-lapse image sequence was generated for each channel; second, a threshold was set to divide the images into two classes of pixels termed foreground and background; and, finally the pixel-by-pixel 470/405 ratio was calculated by dividing the two individual wavelengths with the Image Calculator plugin, that performs arithmetic and logical operations between two images. The measurements were performed

with the “Limit to Threshold” checked in the “analyse” menu, so that only thresholded pixels were included in the measurement calculations.

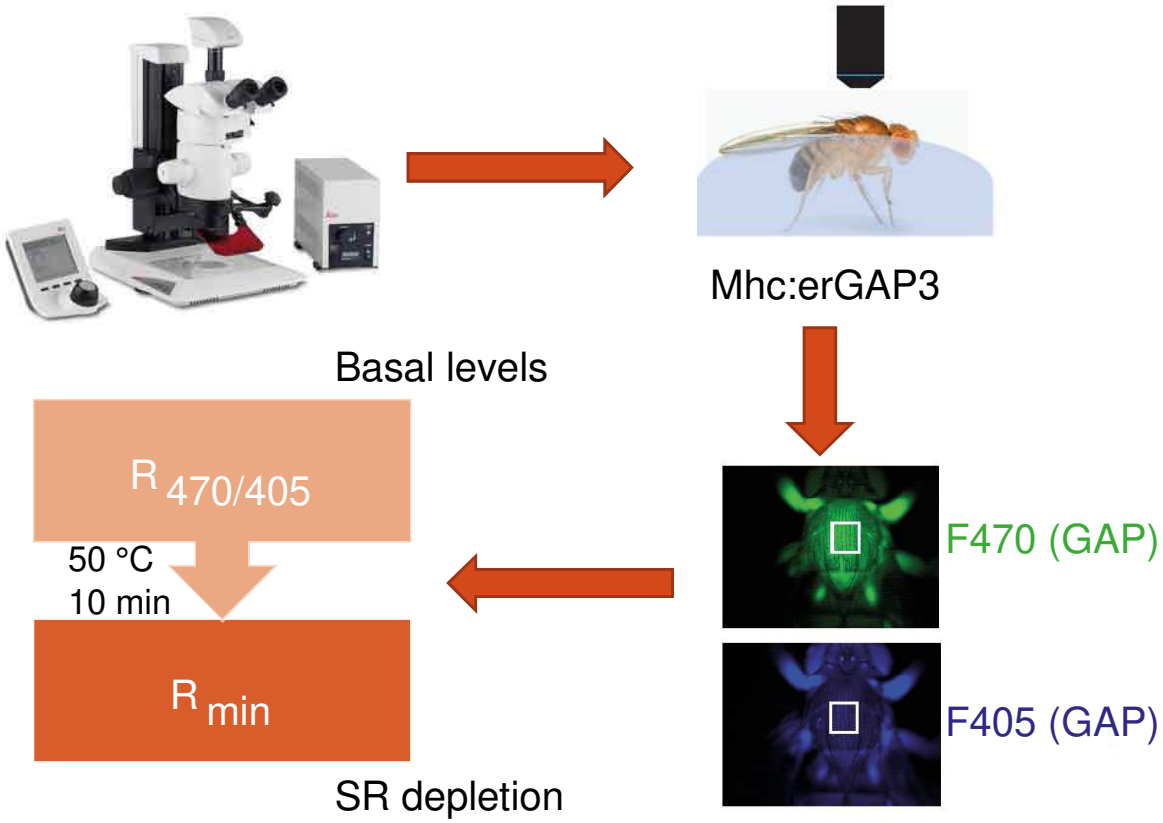

Figure 22. Sarcoplasmic reticulum Ca^{2+} imaging *in vivo* in *Drosophila.* Flies were immobilized in a small drop of agar and two fluorescence images at each GAP3 wavelength (405 and 470 nm) were acquired in the muscles of the fly thorax under resting conditions (basal levels). Then, to determine R_{min} (sarcoplasmic reticulum depletion), each fly was carefully heated in the thermal bath for 10 min at 50 °C and, then, imaged using the same settings. Fluorescence images were acquired with a fluorescence stereo microscope (M205FA, Leica) using either 470/40 nm or 405/40 excitation filters and a 525/50 nm emission filter, 16 bits, 4X4 binning and 6.5X zoom. Images were analysed with the Image J software and the measurements were performed in the region of interest (ROI, represented by a white square in the fly image) in the thorax of each fly.

12.2. Measuring cytosolic Ca^{2+} in *Drosophila*

Flies of the DM010 line (**Table 2**) were anesthetized and immobilized in agarose as previously described. Recordings of the dorsal longitudinal muscles in the fly thorax were obtained by stimulation with CS-20 stimulator (Cibertec) of the giant fiber system (GFS) through two tungsten electrodes impaled into the fly eyes (Allen and Godenschwege, 2010). The *Drosophila* GFS is a well-characterized neuronal

circuit that mediates the escaping behaviour in the fly (**Fig. 23**). It is named after the two largest interneurons in the fly, the giant fibers (GFs), which pass along the signal from the brain to the mesothoracic ganglion, located in the ventral nerve cord. In the mesothoracic ganglion each giant fiber makes two synapses: one to a large motoneuron (TTMn) that drives the tergotrochanter "jump" muscle (TTM); and another to the peripherally synapsing interneuron (PSI), which, in turn, synapses the dorsal longitudinal motoneurons (DLMns) of the dorsal longitudinal (flight) muscles (DLMs). These muscles are, along with the dorsoventral muscles (DVMs), the main muscle group located in the thoracic region, the A-IFMs[11]. By stimulating the giant fiber neurons directly in the brain of the adult fly we can obtain recordings from the flight muscles.

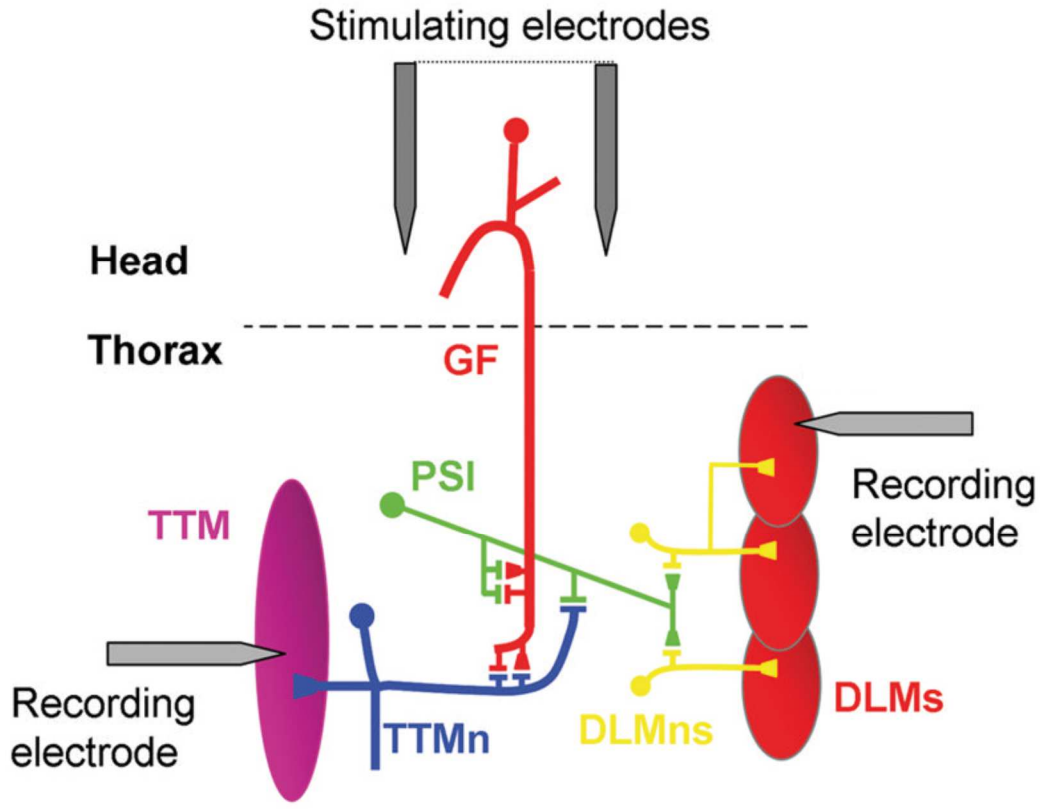

Figure 23. Electrical stimulation protocol in *Drosophila.* Flies were immobilized in agarose, and two tungsten electrodes (stimulating electrodes) were impaled into the fly eyes in order to stimulate the two giant fibers (GFs; in red). The GFs pass along the signal from the brain to the mesothoracic ganglion, where each giant fiber makes two synapses: one to a large motoneuron (TTMn; in purple), that drives the tergotrochanter "jump" muscle (TTM; in blue); and another to the peripherally synapsing interneuron (PSI; in green), which, in turn, synapses the dorsal longitudinal motoneurons (DLMns; in yellow) that drive the flight muscles (DLMs; in red). Taken from (Allen and Godenschwege, 2010).

[11] See **Figure 12** of the introduction, in section 6.3.2. *Drosophila* Muscles.

The stimulation protocol consisted of repetitive stimulation with 5 V/50 ms stimuli at different frequencies (0.5 or 10 Hz), and was performed during 5 s. Each experiment started with a visual check of twitches in the wing after stimulation to assure that the electrodes were correctly positioned. For these experiments, fluorescence images were acquired every 100 ms only at the 470 nm wavelength[12], using the 470/40 nm excitation filter and the 525/50 nm emission filter. Images were acquired and analysed[13] as mentioned previously. To normalize the results obtained in different experiments fluorescence (F) was divided by the average of the F values obtained during the first 5–10 frames (F_0), resulting in F/F_0.

12.3. Ca^{2+} measurements in cells

Cell imaging was performed in a Zeiss Axioplan 2 upright microscope equipped with a 20X water-immersion objective (W-Achroplan, Zeiss; NA = 0.5) and a Zeiss AxioCam camera MRm (12 bit) connected through a software interface (Axiovision Rel 4.6.3, Zeiss) to a 75 W Xenon fluorescent excitation source (Osram, XBO75) and a filter wheel. GAP3 was excited sequentially at 405 and 470 nm using the dichroic mirror 505DRPL (XF2031) and the 405IL25 (Comar, T-GQD) and 470DF35 (Omega, XF1013) excitation filters, coupled in the filter wheel. Fluorescence emission was registered between 517-552 nm with 535DF35 (Omega, XF3007) emission filter. Images were acquired with 5x5 binning sequentially at each wavelength every 10 s. All experiments were recorded at 25 °C. Neutral density filters (DN 1.0 and DN 0.5, Omega Optical 142588 and 164526, respectively) were also used to prevent bleaching.

Briefly, 12 mm-diameter round coverslips were placed in the aluminium chamber and carefully adjusted in the center with a silicone piece that contains two grooves, one for the perfusion and the other for the vacuum. The chamber is placed in a specific platform that is then set in the microscope and connected to the valves-

[12] The fluorescent spectra of GCaMP proteins display a single excitation peak at 489 nm and an emission peak at 509 nm.
[13] GCaMP3 is intensiometric, the protein increases its fluorescence intensity upon binding to Ca^{2+} ions. Therefore, the analysis is performed only in the F_{470} wavelength. With the acquisition of only one wavelength, the calculation of the ratio is not possible; and, thus, these measurements are not calibrated into $[Ca^{2+}]$.

perfusion system. This is a gravity, bath perfusion system composed by eight channels, each of them can contain a different solution. These channels are controlled by the valve controller which allows quick switching of the solutions flowing into the perfusion chamber. First, cells were perfused at 5 ml/min with extracellular medium (145 mM NaCl; 5 mM KCl; 1 mM $CaCl_2$; 1 mM $MgCl_2$; 10 mM glucose; and 10 mM Na-HEPES; pH 7.4) for 4-6 min. Then, cells were stimulated with either ATP (100 µM; Sigma-Aldrich, A3377), an agonist of ionotropic (P2X) and metabotropic (P2Y) purinergic receptors; or carbachol (CCh, 100 µM; Sigma-Aldrich, C4382) as an agonist of the acetylcholine receptors (AChR; both muscarinic and nicotinic); for 30 s. All the agonists were diluted in extracellular medium. Finally, at the end of each recording, the ER was depleted by stimulating with Ca^{2+}-free extracellular medium (145 mM NaCl; 5 mM KCl; 1 mM $MgCl_2$; 10 mM glucose; 0.5 mM EGTA (Ethylene Glycol Tetraacetic Acid; Sigma-Aldrich, E4378); and 10 mM Na-HEPES; pH 7.4) containing ATP (100 µM), and the SERCA reversible inhibitor TBH (10 µM; Sigma-Aldrich, 112976), for 6-8 min. For the heating experiments, immediately after the recording, the coverslips were placed in extracellular medium at 50 °C for 10 min. Then, the same protocol was applied and fluorescence images were captured using the same settings. The output images were analysed using the ImageJ software: first background was subtracted; second, a threshold was set for each image stack, which correspond to the individual recording for the two GAP3 wavelengths; finally, pixel-by-pixel ratios were calculated by dividing the two individual wavelengths with the Image Calculator plugin. The regions of interest (ROIs) were carefully drawn for each individual cell and, the measurements were performed with the “Limit to Threshold” checked in the “analyse” menu, so that only thresholded pixels were included in the measurement calculations. For GAP3, the ratio ($R=F_{470}/F_{405}$) was used as an index of $[Ca^{2+}]_{ER}$ and in order to normalize the results obtained in different experiments this ratio was divided by the average of the R values obtained during the first 5–10 frames (R_0), resulting in R/R_0.

To measure cytosolic Ca^{2+} *in vitro* we used the fluorescent Ca^{2+}-dye Fluo-4 AM (ThermoFisher, F14201). Cells were loaded with 2 µM of the dye diluted in extracellular medium. The incubation time was of 45 min, during which cells were maintained at RT and in dark conditions. Cell imaging was performed in the same

microscope, and the acquisition conditions were the same as for the GAP3 470 nm wavelength. Briefly, Fluo-4 loaded cells were excited at 470 nm using the 470DF35 (Omega, XF1013) excitation filter, and fluorescence emission was acquired every 5 s between 517-552 nm with 535DF35. The protocol was as follows: first, cells were challenged with ATP (100 uM) diluted in extracellular medium for 30 s. Then, the same cells were heated as explained previously and the ATP response was checked with another 30 s pulse. Finally, cells were permeabilized with digitonin (50 µM; Sigma-Aldrich, D141) for 5 min diluted in Ca^{2+}-free extracellular medium. For cytosolic measurements with Fluo-4[14], the image analysis was performed only in the F_{470} wavelength image stack. The results were also normalized by the average of the F values obtained during the first 5-10 frames (F_0) of each experiment, resulting, in this case, in F/F_0.

12.4. Calibration of Ca^{2+} measurements

The transformation of GAP3 fluorescence data into $[Ca^{2+}]_{ER}$ is based on the following equation (1):

$$\mathbf{Y = \frac{R - R_{min}}{R_{max} - R_{min}}} \qquad \textbf{(Equation 1)}$$

Being "Y" the normalized fluorescence with values between 0 and 1; "R" the ratio (F_{470}/F_{405}) at a given time point of the experiment; "R_{min}" is the "R" when GAP sensor is not bound to Ca^{2+}, which is obtained at the end of each experiment by depleting the ER with EGTA, IP_3-producing agonists and SERCA inhibitors (*in vitro*) or by heating[15] (*in vivo*); and "R_{max}" is a calculated by multiplying "R_{min}" by the dynamic range (DR) of the sensor, in this case 3.

After calculating "Y", $[Ca^{2+}]_{ER}$ can be calculated with the Hill equation (2):

$$\mathbf{Y = \frac{V_{max} \cdot [Ca^{2+}]^n}{K_D^n \cdot [Ca^{2+}]^n}} \qquad \textbf{(Equation 2)}$$

[14] Fluo-4 is intensiometric, as the indicator GCaMP3 used for cytosolic Ca^{2+} measurements in flies. Therefore, the analysis is performed only in the F_{470} wavelength, and, these measurements are not calibrated into $[Ca^{2+}]$.

[15] This calibration method was developed in this thesis for *in vivo* measurements, but it also proved to be valuable *in vitro*. See results section **2**.

Equalizing the equations number (1) and (2), and, assuming V_{max} is 1, we can solve for $[Ca^{2+}]_{ER}$ (3):

$$[\mathbf{Ca^{2+}}] = \frac{\mathbf{K_D}}{(\frac{\mathbf{R_{max}-R}}{\mathbf{R-R_{min}}})^{1/\mathbf{n}}} \qquad \textbf{(Equation 3)}$$

It has been determined, both *in vitro* and *in situ* (Navas-Navarro et al., 2016), that the coefficient Hill value (n) for the binding of GAP3 to Ca^{2+} is 1. Substituting this value (n=1) in equation number (3) will lead us to the same equation (4) that has been previously described to calibrate Fura-2 measurements (Grynkiewicz et al., 1985):

$$[\mathbf{Ca^{2+}}] = \frac{\mathbf{K_D \cdot (R-R_{min})}}{\mathbf{R_{max}-R}} \qquad \textbf{(Equation 4)}$$

Knowing the DR of GAP3 (R_{max}/R_{min}) is 3.0, and the K_D (Ca^{2+}-GAP3 dissociation constant) is 489 µM (Alonso et al., 2017b) an approximate calibration of the $[Ca^{2+}]$ signals can be performed using R/R_{min} values according to the equation (5):

$$\frac{\mathbf{R}}{\mathbf{R_{min}}} = \mathbf{1} + (\mathbf{DR} - \mathbf{1})(\frac{[\mathbf{Ca^{2+}}]}{\mathbf{K_D} + [\mathbf{Ca^{2+}}]}) \qquad \textbf{(Equation 5)}$$

13. Statistical analysis

The software OriginLab® (version 7 or Pro 8) was used to graph, analyse and interpret data. Results are expressed as mean ± SD (standard deviation) or mean ± SEM (standard error of the mean), as indicated. The statistical significance was evaluated using Student's t-test or One-way ANOVA with GraphPad InStat® software version 3.0. The significance level is shown as * for $p<0.05$; ** for $p<0.01$; and, *** for $p<0.005$. The vector graphics software Adobe Illustrator® version CS5 was used to create the final figures.

14. Reagents and resources

Reagent	Source	Identifier
Antibodies		
SERCA *Drosophila*	(Sanyal et al., 2005)	Dr.Ramaswami
Ryanodine receptor *Drosophila*	(Gao et al., 2013)	Robert Scott
GRP78/BiP	Sigma-Aldrich	G9043
Tubulin	Sigma-Aldrich	T6074
Goat anti Mouse IgG (H/L):HRP	Bio-Rad	170-6516
Goat anti Rabbit IgG (H/L):HRP	Bio-Rad	170-6515
Goat anti Guinea Pig IgG (H/L):HRP	Bio-Rad	AHP863P
Alexa Fluor 568 goat anti-rabbit	ThermoFisher	A-11031
Bacterial strains		
MAX Efficiency™ DH5α™ Competent Cells	ThermoFisher	18258012
BL21(DE3) Epicurian Coli Competent Cells	Stratagene	N/A
Chemicals		
Tissue-Tek®	Sakura Finetek	25608-930
Paraformaldehyde (PFA)	ThermoFisher	76240
Phosphate saline buffer (PBS)	Sigma-Aldrich	P5119
TritonX-100	Merck	1086031000
Goat serum (GS)	ThermoFisher	16210064
Bovine serum albumin (BSA)	Sigma-Aldrich	A2153
Hoescht 33322 cell permeant	ThermoFisher	H3570
Vectashield®	Vector laboratories	H-1000
Propionic acid	Sigma-Aldrich	81910
Nutri-Fly®	Genesee Scientific	66-112
Agar type I	iNtron Biotechnology	25999
Agarose low gelling temperature	Sigma-Aldrich	A6560
Lipofectamine® 2000	ThermoFisher	1668-019
Geneticin® (G-418)	ThermoFisher	11811-023
Dulbecco's modified Eagle's medium	ThermoFisher	10566-016
Penicillin Streptomycin	Lonza	DE17-602-E
Foetal bovine serum (FBS)	Lonza	DE-14-801F
Trypsin-EDTA	ThermoFisher	25200-056
Poly-L-lysine	Sigma-Aldrich	P1274
OPTI-MEM™-I	ThermoFisher	11524456
Hank's balanced salt solution	ThermoFisher	14175-053
Papain	Worthington Biochemical Corporation	LS003119
DNase	Roche	10104159001
Neurobasal medium	ThermoFisher	17504-044
glutaMAX™-I	ThermoFisher	35050-038

B27	ThermoFisher	177504-044
Horse serum (HS)	ThermoFisher	16050122
Isopropyl b-D-thiogalactoside (IPTG)	Sigma-Aldrich	I5502
DTT (Dithiothreitol)	Sigma-Aldrich	D9760
Digitonin	Sigma-Aldrich	D141
Fluo-4, AM, cell permeant	ThermoFisher	F14201
ATP	Sigma-Aldrich	A3377
Carbachol (CCh)	Sigma-Aldrich	C4382
EGTA (Ethylene Glycol Tetraacetic Acid)	ThermoFisher	E1219
Tert-Butylhydroquinone (TBH)	Sigma-Aldrich	112976
Sodium dodecyl sulphate (SDS)	Sigma-Aldrich	L3771
Sodium deoxycholate	Sigma-Aldrich	D6750
Trizma® base	Sigma-Aldrich	T1503
Glycerol	Sigma-Aldrich	G5516
Bromophenol blue	Sigma-Aldrich	B0126
Glycine	Sigma-Aldrich	G8898
Methanol	Merck	106009
Protein Assay Dye Reagent Concentrate	Bio-Rad	500-006
Acrylamide	Bio-Rad	161-0158
Precision Plus Protein All Blue Standards	Bio-Rad	161-0373
TWEEN® 20	Sigma-Aldrich	P1379
Defatted dry milk	Nestle Sveltesse	Nestlé España, S.A
p-Coumaric acid	Sigma-Aldrich	C-90008
Luminol	Sigma-Aldrich	A-8511
Hydrogen peroxide (H_2O_2)	Sigma-Aldrich	H-1009
Sodium chloride (NaCl)	Merck	1064060500
Potassium chloride (KCl)	Merck	1049380500
Calcium chloride ($CaCl_2$)	Merck	10035-04-8
Magnesium chloride ($MgCl_2$)	Merck	7791-18-6
Glucose	Sigma-Aldrich	G7021
Sucrose	Merck	107651
Trehalose	Sigma-Aldrich	T0167
Sodium bicarbonate ($NaHCO_3$)	Merck	106329
Na-HEPES	Sigma-Aldrich	75277-39-3
LBroth	Sigma-Aldrich	L3152
LB-Agar	Sigma-Aldrich	L3027
Ampicillin	ThermoFisher	11593027
Kanamycin	Sigma-Aldrich	K4000
Critical Commercial Assays		
SuperSignal™ West Pico PLUS Chemiluminescent Substrate	ThermoFisher	34577
Plasmid Maxi Kit	QIAGEN	12163
Wizard® SV Gel and PCR Clean-Up System	Promega	A9282

PureYield™ Plasmid Miniprep	Promega	A1222
Experimental Models: Organisms/strains		
w[1118]; [+]; [+]	Lola Ganfornina (IBGM)	N/A
*y[1] w[*]; M{**UAS-erGAP3**}ZH-86Fb*	Bloomington Drosophila Stock Center	80904
*w[*]; P{w[+mC]=**Mhc-GAL4**.K}2/TM3, Sb[1]*	Bloomington Drosophila Stock Center	55133
*y[1] w[*];P{w[+mC]=**Mhc-GAL4**.K}2/TM3, Sb[1] M{**UAS-erGAP3**}ZH-86Fb*	(Navas-Navarro et al., 2016)	N/A
*P{w[+mW.hs]=GawB}**elav-GAL4**; w[*];Gal80^{TS} / TM3^{Ser}*	A. Ferrús (Instituto Cajal, Madrid, Spain)	N/A
*P{w[+mW.hs]=GawB}**elav-GAL4**; w[*]; M{**UAS-erGAP3**}ZH-86Fb*	This thesis	N/A
erGAP3 transgenic mice C57BL/6JCrl (Charles Rivers)	(Navas-Navarro et al., 2016)	N/A
Experimental Models: Cell Lines		
Human: HeLa cells	ATTC	CCL-2
HeLa stably-expressing erGAP3	(Navas-Navarro et al., 2016)	N/A
HEK293T	ATTC	CRL-3216
C2C12	ATTC	CRL-1772
Recombinant DNA		
Plasmid: *pUASTattB-erGAP3*	(Navas-Navarro et al., 2016)	N/A
Plasmid: *pcDNA3-erGAP3*	Addgene	78118
Plasmid: *pCMV-G-CEPIA1er*	Addgene	58215
Software and Algorithms		
Axiovision Rel	Version 4.6.3	Zeiss
Image J	Version 1.52a	NIH, USA
Graphpad InStat®	Version 3.0	Graphpad
Leica Application suite X	Version LasX	Leica
SnapGene®	Version 5.0	SnapGene
OriginLab®	7 or Pro 8	OriginLab

Table 5. Reagents and resources used in this thesis.

Results

1. Characterization of erGAP3 transgenic flies

In order to measure $[Ca^{2+}]_{ER}$ we chose the fluorescent Ca^{2+} sensor GAP3. GAP3 is a low affinity Ca^{2+} indicator of the GAP family with a K_D of 489 µM, suitable for measuring Ca^{2+} concentrations between 0.05 and 2 mM (Navas-Navarro et al., 2016; Alonso et al., 2017b). This concentration range covers the wide span of SR/ER lumen concentrations previously found in the conventional cell lines (HeLa, HEK293T, CHO cells) and in specialised primary cells such as astrocytes or cortical hippocampal neurons, among others (Suzuki et al., 2014; Rodríguez-Prados et al., 2015). The GAP3 sensor was targeted to the ER by the CR/KDEL strategy and termed erGAP3.

Combining the ϕC31 (Bischof et al., 2007) and the GAL4-UAS systems (Brand and Perrimon, 1993) we achieved the generation of transgenic flies. Specific expression of erGAP3 in muscle cells (line DM006, **Table 2**; Navas-Navarro et al., 2016) or in neurons (line DN005, **Table 2**) is driven by the muscle specific promoter, *Mhc* (Mitra et al., 1996); or the nervous system specific promoter, *elav* (Yao et al., 1993), respectively.

1.1. Tissue specific expression of erGAP3

First, in order to confirm that erGAP3 sensor was indeed expressed in the fly and that this expression was tissue-specific, erGAP3 expression was monitored as GFP green fluorescence (**Fig. 24**). In the DM006 line, GFP fluorescence is mainly localized in the muscle mass of the fly thorax (**Fig. 24A**), which includes the asynchronous indirect flight muscles (A-IFMs), the small synchronous muscles on the wing hinge and the jumping muscles. In the lateral view of the fly (**Fig. 24B**) it can be observed that expression is not restricted to the fly thorax, as there is also expression in the legs, and in other muscles attached to the body wall. These results are expected as *Drosophila* has a single *Mhc* gene, expressed in all the muscles.

In the DN005 line, GFP expression is mainly localized in the brain (**Fig. 24C**), but there is also GFP expression in peripheral nervous system; observed in the wing margin, the leg and the halter sensory neurons (**Fig 24D**). The erGAP3 expression pattern in the DN005 line confirmed the expected location of the pan-neuronal *elav* driver.

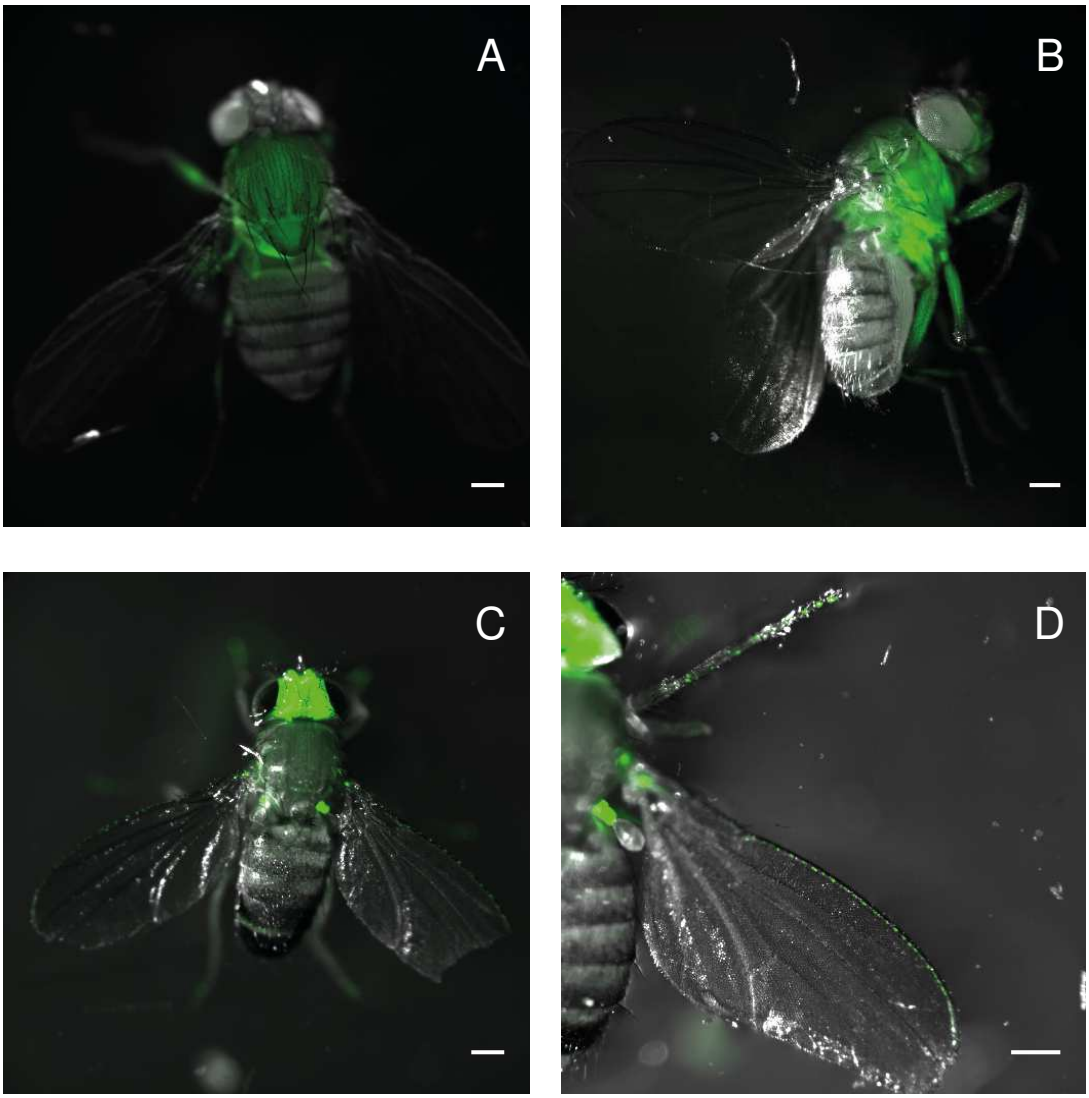

Figure 24. Tissue-specific expression in erGAP3 transgenic flies. Images show merged bright field and fluorescent images recorded at 470 nm of erGAP3 transgenic flies that express the Ca^{2+} indicator in the skeletal muscle (line DM006) or in neurons (line DN005). **A)** Dorsal view of the DM006 skeletal muscle line, where GFP expression is mainly localized in the fly thorax. **B)** Lateral view of the DM006 line. GFP expression is localized in the muscle legs and in the muscles attached to the body wall, as well as in the thorax. **C)** Dorsal view of DN005 neuronal line, where GFP expression is mainly restricted to the fly brain. **D)** Dorsal view of DN005 line. The fly is shown at higher magnification in order to notice the expression of the sensor in the peripheral nervous system (wing margin, leg and halter sensory neurons). In both lines, GFP expression is highly localized in the targeted tissue and clearly excluded in others. Calibration bars: 200 µm.

In both lines it is remarkable that GFP expression was highly localized in the targeted tissue and clearly excluded in others. The expression was very robust, as the levels were constant in all animals analysed from the same line; although expression in females tend to be higher, given that they are bigger in size than males. Furthermore, expression is maintained during the whole fly life and, also, across generations. In our hands, after more than 60 passages, the fly lines maintained the initial levels of expression and without signs of mislocalization.

1.2. Subcellular localization of erGAP3

We next checked the subcellular localization of the erGAP3 protein in the SR by staining the organelle with a resident protein such as SERCA. This was performed by immunofluorescence, using a specific antibody against *Drosophila* SERCA protein. The immunostaining was performed in larvae (**Fig. 25A-C**) and adult (**Fig. 25D-F**) tissue from the DM006 line, and showed a high degree of colocalization of the erGAP3 sensor with the SERCA protein. erGAP3 expression was recorded as green GFP fluorescence (**Fig. 25A and D**) whereas SERCA protein was labelled in red with Alexa-Fluor 568 (**Fig. 25B and E**) and the nuclei were stained in blue with Hoechst dye (**Fig. 25C**). erGAP3 and SERCA protein exhibited the same striated pattern shown by dark and light bands, typical of the sarcomere repeated organization. As expected from SR location, erGAP3 expression and immunostaining with the anti-SERCA antibody showed staining extension through the entire multinucleated muscle cell (**Fig. 25A and B**). Nuclear exclusion is also evident in the larvae preparation, where nuclei are apparent (**Fig. 25C**). In conclusion, erGAP3 protein is properly located in the SR, as immunostaining with anti-SERCA antibody showed overlapping expression of the sensor and the resident SR marker protein in the thorax muscles of larvae and adult flies (**Fig. 25C and F**).

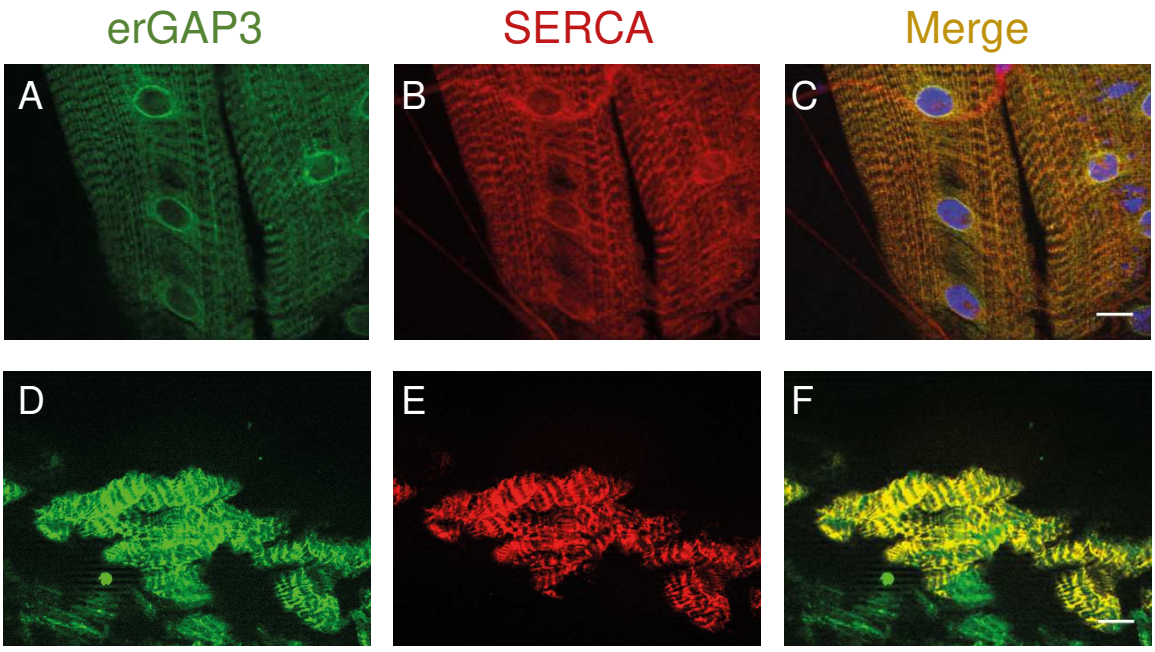

Figure 25. Subcellular localization of erGAP3 sensor in the skeletal muscle. Confocal microscopy images of the skeletal muscles of DM006 flies (erGAP3 transgenic muscle line). **A, B and C** (upper row) correspond to larvae muscles; and **D, E and F** (lower row) to adult myofibers. **A and D)** erGAP3 expression was recorded as GFP fluorescence, at 470 nm. The sensor shows the typical muscle striated pattern of dark and light bands and also, the sarcoplasmic reticulum (SR) expression pattern along the whole cell with exclusion of the nuclei. **B and E)** Images show the immunostaining of the SR resident protein SERCA, labelled with Alexa Fluor 568 in red. The expression pattern corresponds to the expression of erGAP3 sensor. **C and F)** Merged images of both proteins, with nuclei stained with Hoescht (in blue; **C**), show high colocalization (in yellow) of erGAP3 and SERCA protein. Calibration bars: 5 µm.

1.3. Survivorship of the erGAP3 transgenic lines

To study aging in the *Drosophila* model, we first assessed the mean and maximal longevity of the wild type (WT) flies from the w^{1118} strain and these of the newly generated erGAP3 transgenic lines. The mean longevity was defined as the mean in the life expectancy of all the individuals of the cohort, and the maximal longevity was established as the longest lifespan recorded among all the individuals of the cohort (Viña et al., 2007; Linford et al., 2013). We performed the lifespan assay obtaining a survival curve that represents survival (in percentage) over age (in days). Results are shown in **Fig. 26** that compares the lifespan data obtained in WT flies (**Fig. 26A;** 80 females and 80 males), with the two transgenic fly lines: the muscle line DM006 (**Fig. 26B;** 58 females and 59 males) and, the neuronal line DN005 (**Fig. 26C;** 78 females and 78 males).

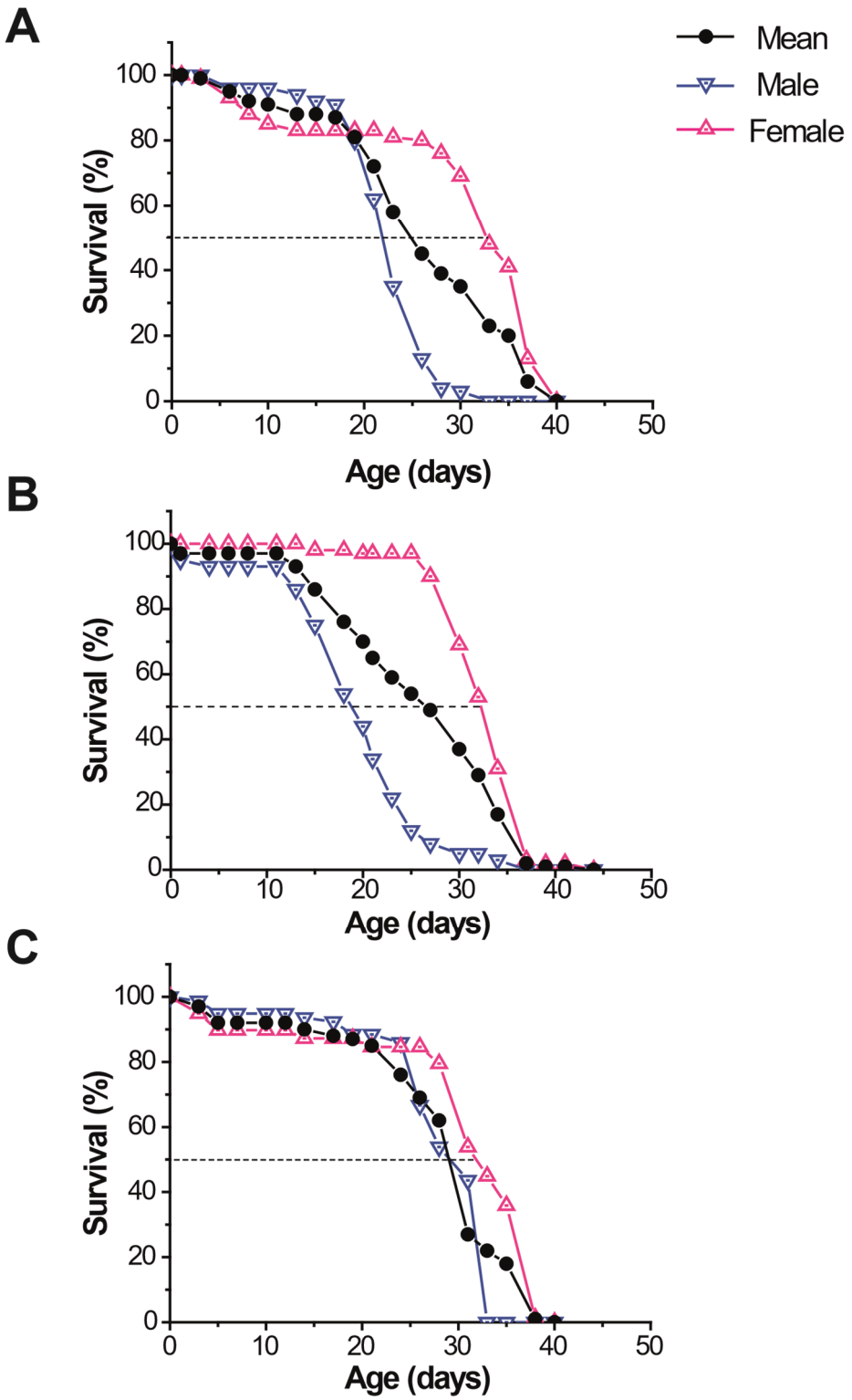

Figure 26. Survival curves of *Drosophila* wild type and erGAP3 transgenic lines. Plots representing survival (in percentage) over age (in days) of: **A)** Wild type (WT) fly line, 160 flies (80 of each gender); **B)** erGAP3 transgenic muscle line (DM006), 117 flies (58 females and 59 males; and **C)** erGAP3 transgenic neuronal line (DN005), 156 flies (78 of each gender). The pink triangles represent the females, the inverted blue triangles represent the males and the black circles represent the mean of both genders. The mean (discontinuous line; 50% survival) and the maximal longevity (last data point) values were similar when comparing the three lines and, in all cases, females live longer than males.

WT flies had a mean lifespan (50% survival) of 25 days (**Fig. 26A**), with the survival of the females being longer than that of the males: for example, at day 33, the survival is 0% for male flies whereas it is still 45% for female flies. Regarding the muscle line (**Fig. 26B**), the mean lifespan is 26 days, very similar to that of the WT line, whereas for the neuronal line (**Fig. 26C**), the mean lifespan is slightly higher, 30 days. In both transgenic lines, female flies also lived longer than male flies. For example, in the muscle line, at 19 days the survival of the males is 50% whereas that of the females is of 97%. In the neuronal line, at the same time point, the survival is 88% for both genders, however at day 28 it is 79% for females and 54% for males. The maximal lifespan reached values of 33-37 for male flies and 40-44 in female flies. In the three lines, survival slowly declines until day 12-25 and, then, between 25-32 days the survival is around 50%. At that time point, flies started to die abruptly until there are no individuals alive at day 33-40. From this point onwards, we divided the cohort into five age groups: 7, 14, 21, 28 (males and females) and 35 (only for females) days. The mean and the maximal longevity values are summarized in **Table 6**. To conclude, the expression of the erGAP3 indicator did not alter the fly survival, as no significant changes in these parameters are observed when transgenic lines were compared with WT flies from the w^{1118} strain (**Table 6**).

	Wild type	DM006 line	DN005 line
Mean lifespan (days)	25	26	30
Maximal lifespan (days)	40	44	40

Table 6. Mean and maximal longevity values obtained from the survival curves shown in Fig. 26.

1.4. Monitoring muscle function over age with the climbing assay

Being the progressive loss of muscle function, known as sarcopenia, a hallmark of aging, we decided to characterize the loss of function of the skeletal muscle in DM006 transgenic flies by the well-characterized climbing assay (**Fig. 27**).

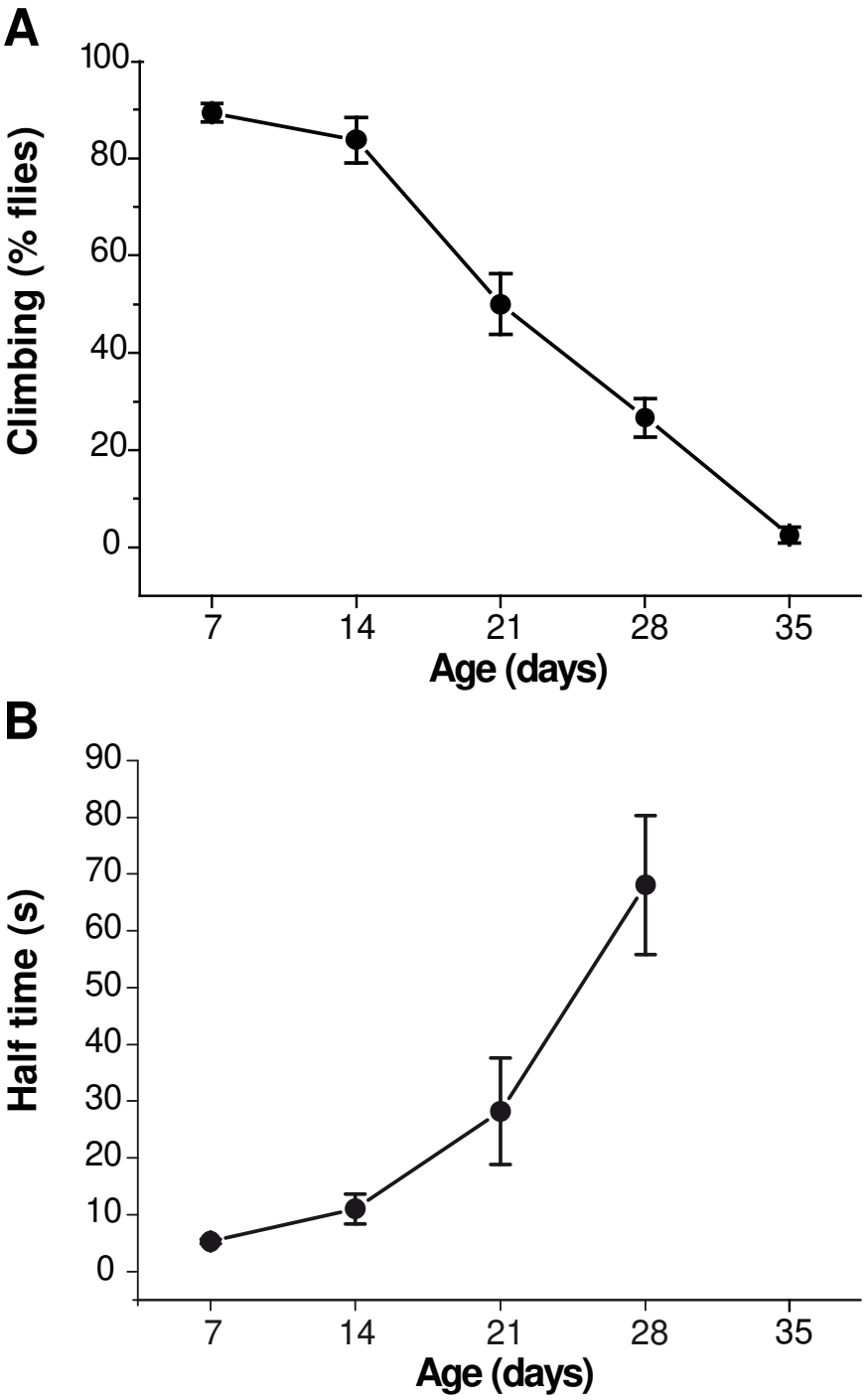

Figure 27. Climbing ability over age in the erGAP3 transgenic muscle fly line. The figure shows the climbing assay, that measures the muscle function, performed in DM006 flies (erGAP3 transgenic muscle line) over age (7, 14, 21, 28 and 35 days). The data are represented in mean ± SEM of groups of 20 flies, being 10 flies used for each individual experiment. **A)** The plot represents the number of flies (in percentage) able to climb 5 cm height in 18 s over age (in days). This number significantly declines over age. The last four points fit a linear correlation, with a coefficient of 0.997 ($p<0.005$). **B)** The plot represents the time (in seconds) in which 50% of the flies performing a given experiment surpass the 5 cm mark over age (in days). The differences between the means of consecutive age groups were statistically significant for all the three pairs ($p<0.05$ to $p<0.001$, One-way ANOVA, Bonferroni multiple comparisons tests).

This test consists on counting the number of flies able to climb 5 cm height in 18 s (**Fig. 27A**), and was performed in males and females separately (results not shown). The data are represented in mean ± SEM of groups (7, 14, 21, 28 and 35 days) of 20 flies, being 10 flies used for each individual experiment. We found a slight non-significant decrease between the young flies of 7 and 14 days-old, where 89 and 84% of the flies, respectively, performed the task; but from that age onwards, flies progressively lost their ability to climb, till the oldest age group measured, 35 days where only 3% of the flies were able to climb within the limits set in the assay. The data of the last four points fits a straight line (linear correlation coefficient, $r=0.997$, $p<0.005$). In a different climbing test, we also monitored the time in which 50% of the flies performing the test[16] reached the 5 cm height mark (**Fig. 27B**), and observed a gradual increment over age, from (mean ± SEM) 5 ± 0.4 s for young flies (7-day old), up to 68 ± 12 s for old flies (28-day old). The differences between the means of consecutive age groups were statistically significant for all the three pairs ($p<0.05$ to $p<0.001$, One-way ANOVA, Bonferroni multiple comparisons tests).

1.5. Sarcoplasmic reticulum Ca^{2+} measurements in the thorax muscles of aging flies

One of the most convincing theories of skeletal muscle aging, postulates there is a disruption in Ca^{2+} uptake and release with age that leads to an impairment of the excitation-contraction (EC) coupling. Whereas the cytosolic Ca^{2+} has been widely studied, little is known about the role of Ca^{2+} dynamics within the SR in muscle excitation. In order to study the effects of aging on the $[Ca^{2+}]_{SR,}$ DM006 transgenic flies were maintained at 29 °C and divided into five age groups (7, 14, 21, 28 and 35 days). This allows to measure $[Ca^{2+}]_{SR}$ along the whole fly life, according to the survival curve of the line, previously shown in **Fig. 26B**. Each age group contained 20 flies, 10 of each sex. For the experiment, flies were immobilized in agar and fluorescent images[17] were acquired at the two excitation wavelengths of erGAP3

[16] Usually 10 flies performed an individual experiment and, thus, we counted the time in which 5 of them surpass the height mark.
[17] Five fluorescence images at each GAP3 wavelength (405 and 470 nm) were collected at 5 s intervals.

sensor in the thorax muscles. The erGAP3 fluorescence ratio ($R=F_{470}/F_{405}$) was, then, calculated by dividing, pixel-by-pixel, the individual wavelengths acquisitions, so that erGAP3 ratio is proportional to $[Ca^{2+}]_{SR/ER}$ (Alonso et al., 2017b; Navas-Navarro et al., 2016). Therefore, this ratiometric measurement in the thoracic muscle mass of the DM006 fly should give a quantification of the $[Ca^{2+}]_{SR}$. The erGAP3 fluorescence ratio was measured for all five age groups. As this value can vary if the experimental settings change, the same settings were maintained for all the measurements (e.g., gain or integration period).

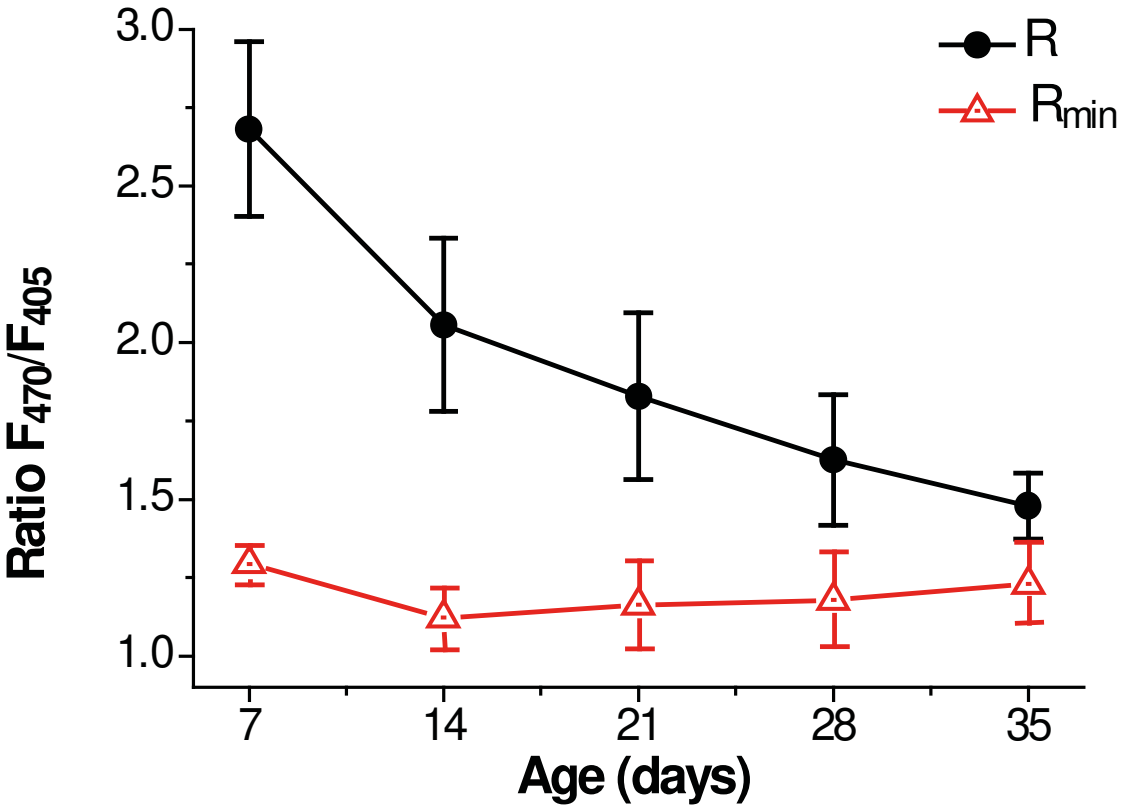

Figure 28. Sarcoplasmic reticulum Ca^{2+} measurements *in vivo* in the erGAP3 transgenic muscle fly line. DM006 flies (erGAP3 transgenic muscle line) from different ages (7, 14, 21, 28 and 35 days) were imaged at the two individual wavelengths of erGAP3 sensor (405 and 470 nm) in the thorax muscles. erGAP3 ratios ($R= F_{470}/F_{405}$) were calculated pixel-by-pixel from the individual wavelengths. Recordings for each fly were performed before (black circles; baseline values expressed as R) and, after 10 min-heating at 50 °C (red triangles; empty store, R_{min}). Each value is the mean ± DS of 20 flies, one half females and one half males, except for flies aged 35 days groups, which contained only 10 female flies. The results show that erGAP3 ratio (R) decreased progressively and significantly over age ($p<0.001$, One-way ANOVA; Bonferroni test). Note that R_{min} values were constant during the whole fly life.

The results are shown in **Fig. 28,** which represents the erGAP3 fluorescence ratios in the DM006 transgenic line over age. In the thorax muscles of the DM006 flies *in vivo*, erGAP3 ratio (**Fig. 28;** black circles) decreased progressively over age from 2.68 ± 0.28 (mean ± SD; n=20) in the young flies (7-day old) down to 1.48 ± 0.10 (mean ± SD; n=10) in the old flies (35-day old). There is a two-fold difference in the erGAP3 ratio between young and old flies, considered statistically significant ($p<0.001$, One-way ANOVA; Bonferroni multiple comparisons test).

2. Calibration of erGAP3 fluorescent signal into $[Ca^{2+}]_{ER}$ or $[Ca^{2+}]_{SR}$

The data shown in **Fig. 28** demonstrates an age-dependent decrease in the SR Ca^{2+} content, although the calibration of the fluorescent signal into $[Ca^{2+}]$ was not possible. Knowing that the dynamic range (DR) of GAP3 (R_{max}/R_{min}) is about 3, and the K_D is 489 µM, it is possible to calibrate the fluorescent signal into $[Ca^{2+}]_{SR/ER}$ with the following equation:

$$\frac{\mathbf{R}}{\mathbf{R_{min}}} = \mathbf{1} + (\mathbf{DR} - \mathbf{1})\left(\frac{[\mathbf{Ca^{2+}}]}{\mathbf{K_D} + [\mathbf{Ca^{2+}}]}\right) \qquad \textbf{(Equation 5)}$$

Where "R" is a given GAP3 fluorescence ratio ($R= F_{470}/F_{405}$), "R_{min}" is the minimal fluorescence ratio obtained when the ER store is completely empty, "DR" is the dynamic range of GAP3, "K_D" is the Ca^{2+}-GAP3 dissociation constant (489 µM) and "$[Ca^{2+}]$" is the Ca^{2+} concentration. The resulting values of R/R_{min} should range between 1 at $[Ca^{2+}]= 0$ and 3 at $[Ca^{2+}]=$ infinite. The calibration curve for DR = 3 and $K_D=$ 489 µM allows the transformation of the fluorescent signal into Ca^{2+} concentration (**Fig. 29**); however a method to obtain the R_{min} value is necessary for $[Ca^{2+}]$ computation. In the *in vitro* experiments, perfusion allows the addition of agonists and inhibitors that act to deplete the ER. However, this manipulations are not feasible during *in vivo* measurements due to the inaccessibility of the Ca^{2+} indicator.

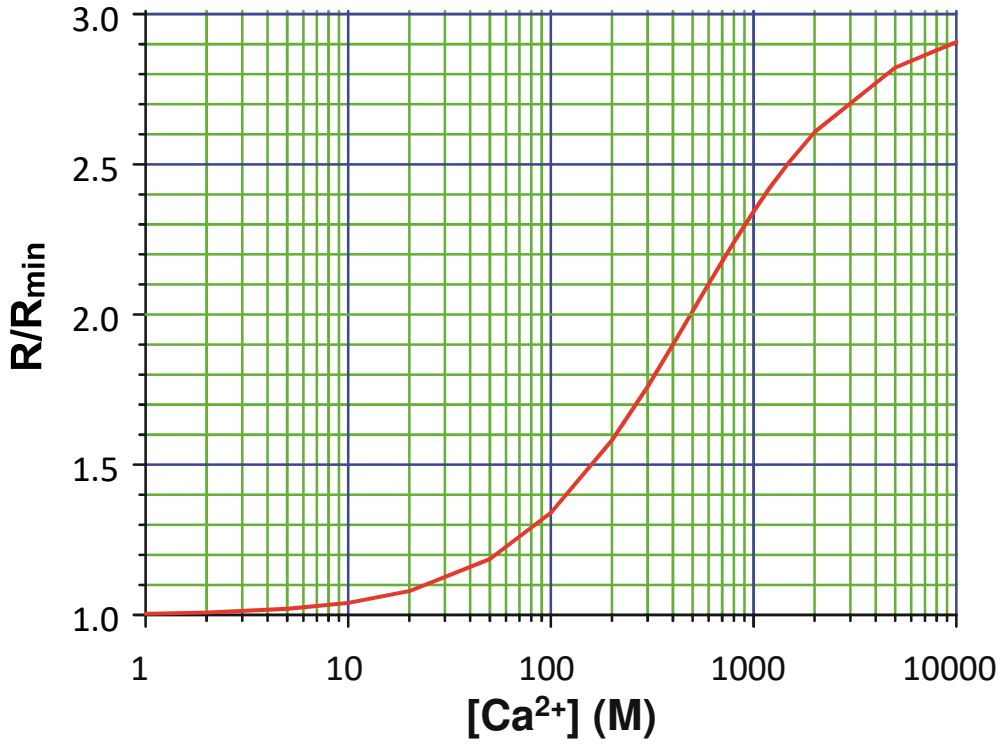

Figure 29. Ca^{2+} calibration curve of GAP3. GAP3 protein isolated from *E.coli* was titrated for Ca^{2+}. The curve was drawn using the following parameters: dynamic range (DR) = 3; Ca^{2+}-GAP3 dissociation constant (K_D) = 489 µM; Hill number (n) = 1. On the left axis, R/R_{min} that ranges between 1.0 at $[Ca^{2+}]$ = 0 and 3.0 at $[Ca^{2+}]$ = infinite. On the abscissa, $[Ca^{2+}]$ in log scale. The red line corresponds to the following equation:
$R/R_{min} = 1 + (DR - 1)*([Ca^{2+}] / (K_D + [Ca^{2+}]))$ (Equation 5).

2.1. Calibration procedure for the *in vitro* experiments

Calibration of the fluorescent signal into Ca^{2+} concentration during *in vitro* experiments in HeLa cells stably-expressing erGAP3 is performed by completely emptying the ER at the end of each experiment. In this way, the minimal value of fluorescence (F_{min}) is obtained and computation of $[Ca^{2+}]$ from the ratio ($R=F_{470}/F_{405}$) is possible. A representative experiment of ER Ca^{2+} measurements in Hela cells is shown in **Figure 30**. Panel A shows the two individual excitation fluorescent wavelengths of the erGAP3 sensor (F_{470} and F_{405}). They display, the typical reciprocal responses of a ratiometric Ca^{2+}-sensitive sensor; upon Ca^{2+} dissociation, one wavelength (470 nm, in green) decreases in parallel with an increase of the other wavelength (405 nm, in blue). Panel B shows the ratio (R) of the two individual fluorescences.

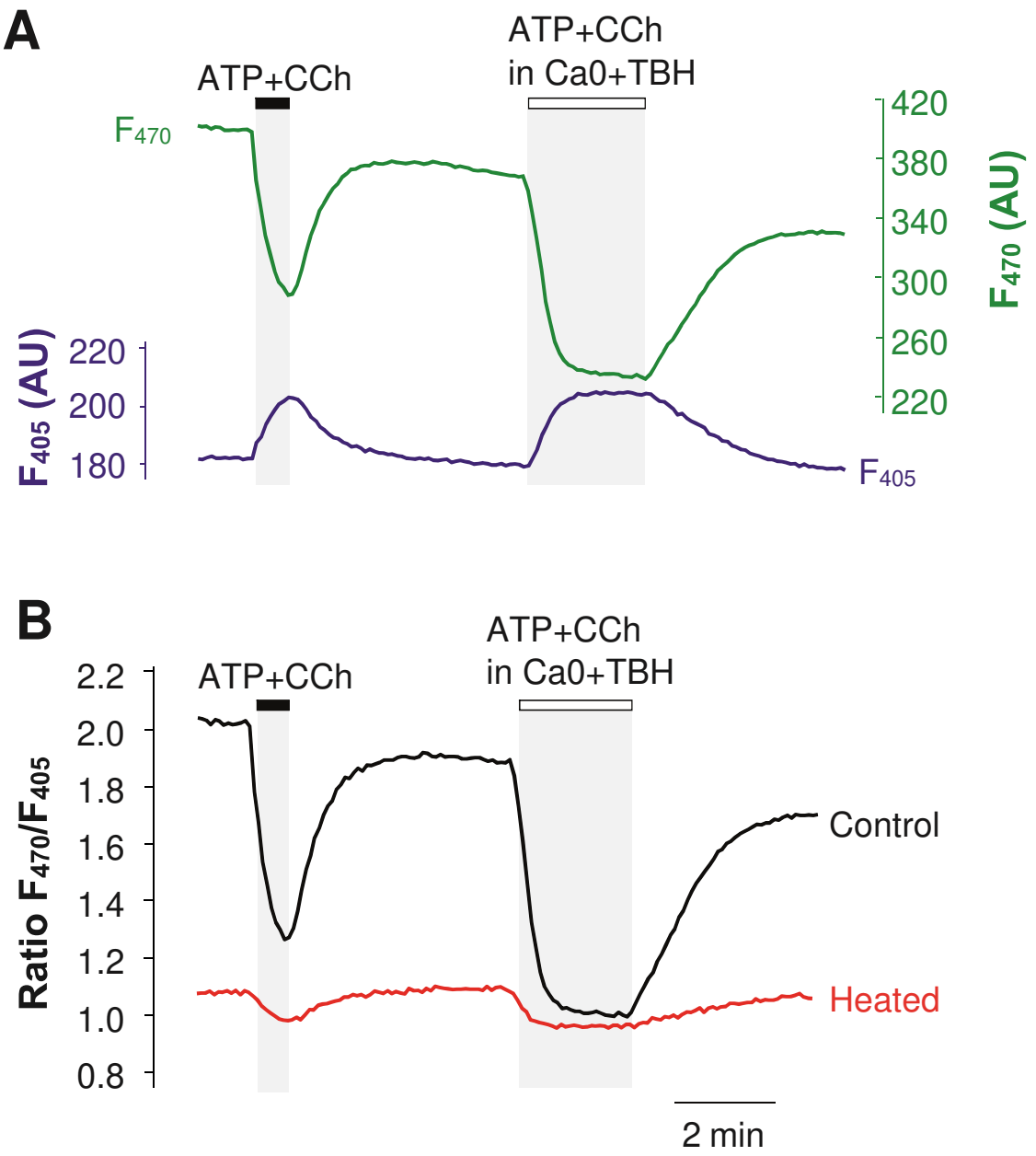

Figure 30. Calibration of erGAP3 fluorescence signal into endoplasmic reticulum Ca^{2+} concentration *in vitro*. A) Endoplasmic reticulum (ER) Ca^{2+} measurements in HeLa cells stably-expressing erGAP3 sensor. Traces show partial (first challenge) and complete (second challenge) ER Ca^{2+} emptying by perfusion with inositol 1,4,5-triphosphate (IP_3)-producing agonists (ATP+CCh (carbachol); 100 µM each) or the ER "depletion cocktail" (ATP+CCh in Ca0+TBH) that contains the same stimulus in Ca^{2+}-free solution and with the sarco/endoplasmic reticulum Ca^{2+}-ATPase (SERCA) reversible inhibitor 2,5-di(tert-butyl)-1,4-benzohydroquinone (TBH; 10 µM), respectively. Both stimulus are highlighted in grey shading. The traces show one representative experiment, average of 100 cells from the same microscopic field. The individual GAP fluorescence, F_{405} in blue (scale at the left) and F_{470} in green (scale at the right), in the control cells is shown. **B)** The same cells were heated at 50 °C for 10 min and immediately subjected to the same protocol. The panel shows erGAP3 ratio (R= F_{470}/F_{405}) with the traces before (Control, black trace) and after heating (Heated, red trace). Note that erGAP3 ratio after heating remains stable during the whole experiment, with no significant changes upon neither of the challenges.

The protocol is as illustrated in **Figure 30**. In order to check that cells were physiologically responsive, they were stimulated during a pulse of 30 s with a mixture of ATP+CCh, at maximal stimulation concentrations, and this stimulus produces a large but partial depletion of the ER (**Fig. 30B,** "control" black trace). Next, the ER stores were refilled by perfusion with extracellular medium containing 1 mM Ca^{2+} for 5 min and, then, the cells were challenged again with an ER "depletion cocktail" containing the same stimulus, in Ca^{2+}-free solution and with the SERCA reversible inhibitor TBH (10 µM). This challenge produces a complete ER discharge and, thus, the F_{min} value can be obtained at the end of the experiment (**Fig. 30B,** "control" black trace). After washing the ER "depletion cocktail" by perfusion with extracellular medium containing 1 mM Ca^{2+}, the ER trace recovered its basal value, a sign of ER Ca^{2+} refilling. Finally, the same cells were heated at 50 °C for 10 min in 1 mM Ca^{2+} extracellular medium, and immediately subjected to the same protocol (**Fig. 30B,** "heated", red trace). Note that erGAP3 ratio remains stable during the whole experiment, with minimal changes during the challenge with ATP+CCh or the ER "depletion cocktail" (ATP+CCh in Ca^{2+} free solution with TBH).

The application of agonists or inhibitors is not possible during the *in vivo* experiments performed with flies, given the impermeable nature of the chitin compound of the fly cuticle that prevents medium exchange. However, the fluorescence value obtained by heating at 50 °C for 10 min HeLa cells stably-expressing erGAP3, was the same as that produced by the complete ER "depletion cocktail" as shown in **Figure 30B** (compare traces, "control" and "heated"). Results are highly reproducible, as shown in **Figure 31A,** where mean values ± SEM of 6 different experiments are represented. The ratios (R) were normalized to the initial fluorescence values (R_0) in order to homogenize the baseline among different cell batches. The R/R_0 value obtained by heating is not significantly different from the one obtained by depletion with Ca^{2+}-free solution containing 10 µM TBH and IP_3-producing agonists (**Fig. 31A**). The conclusion is that the heating treatment could be used for calibration, even during *in vivo* experiments with *Drosophila*. Importantly, the morphology of the cells (observed as green GFP expression) was not modified by the heating treatment, and there were no signs of GAP3 aggregation (compare panels, "control" and "heated", in **Fig. 31B**). Moreover, the

changes in fluorescence were similar in the different cells and also among different ER regions within the same cell, as demonstrated by the homogeneous intensity of all the pixels in the ratio image (right panel in **Fig. 31B**).

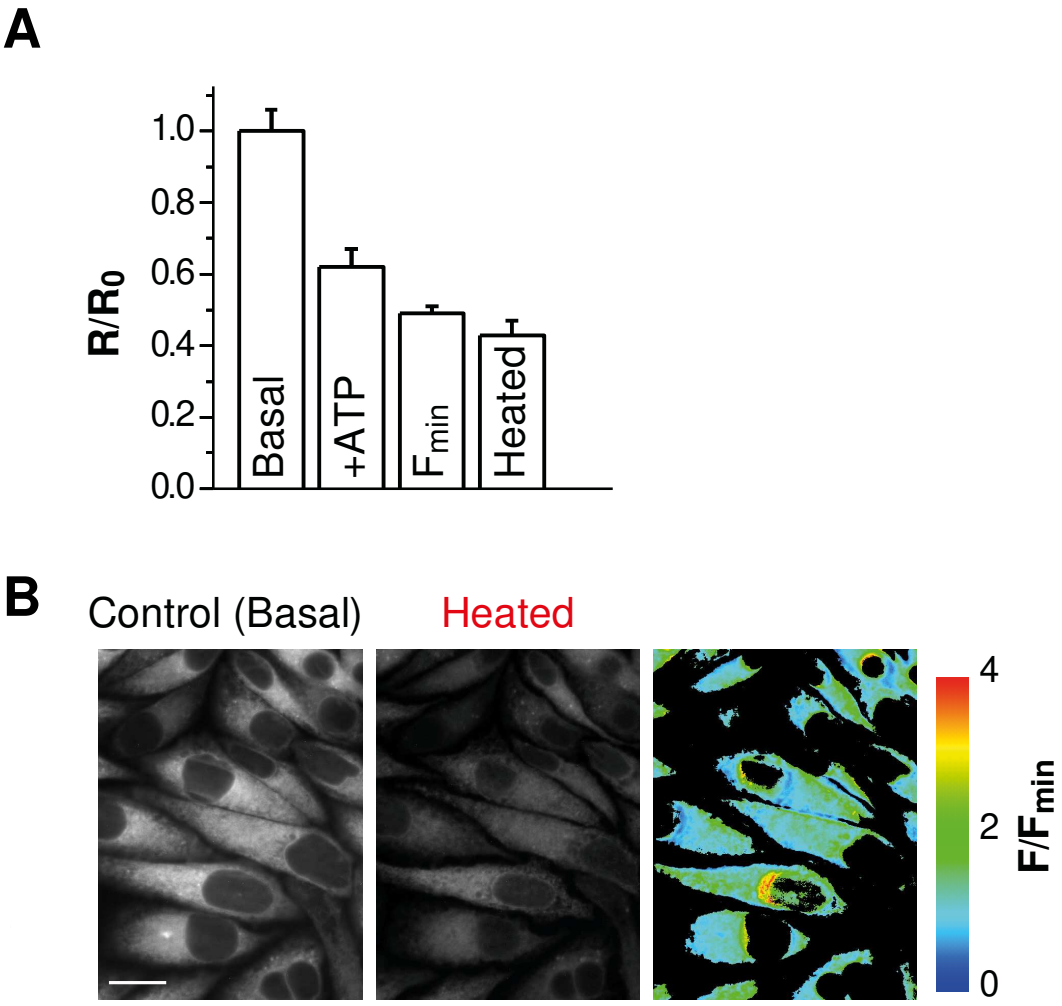

Figure 31. Calibration of erGAP3 fluorescence signal into endoplasmic reticulum Ca^{2+} concentration *in vitro*. The Ca^{2+} levels in control and heated cells. A) The figure shows the mean ± SEM values of 6 independent experiments as the one presented in **Figure 30.** erGAP3 ratios ($R= F_{470}/F_{405}$) were normalized to the initial fluorescence values (R_0) in order to homogenize the baseline among different cell batches. The histogram shows the endoplasmic reticulum (ER) Ca^{2+} levels, expressed as R/R_0, at: baseline (Basal); after stimulation with the agonists alone (+ATP); after stimulation with the ER "depletion cocktail" (F_{min}); or after the heating treatment (Heated); according to the protocol illustrated in **Figure 30**. All the values were significantly smaller than the baseline value ($p<0.001$; One-way ANOVA, Bonferroni test), whereas the "F_{min}" and the "Heated" bars did not differ significantly. **B)** erGAP3 fluorescence images recorded at 470 nm excitation before (Control) and after heating (Heated), both in the baseline condition. The right image shows the pixel-by-pixel ratio of both images (F/F_{min}) coded in pseudocolour (scale on the right) where warm colours (such as red or yellow) represent high ER Ca^{2+} concentration ($[Ca^{2+}]_{ER}$) and the cold colours (blue or cyan) represent low high $[Ca^{2+}]_{ER}$. Calibration bar, 10 µm.

The same set of experiments was also performed in other cell types, such as transiently-expressing erGAP3 HEK293T cells or primary hippocampal cortical astrocytes obtained from erGAP3 transgenic mice. In both cases the results obtained were similar to those obtained in HeLa cells. A summary of these results of 4-6 individual experiments, with 100-150 individual cells per experiment, are shown in **Table 7**, where the values of F_{min} obtained by perfusion with the ER "depletion cocktail" and by heating the cells were very similar. The conclusion is that the heating treatment can be used as a general method for calibrating fluorescent signals into $[Ca^{2+}]_{SR/ER}$ in different cell types.

	R/R$_0$ (mean ± SEM)		
	HeLa	**HEK 293T**	**Astrocytes**
Basal	1.00	1.00	1.00
ATP	0.62 ± 0.02	0.91 ± 0.02	0.79 ± 0.01
F_{min}	0.49 ± 0.05	0.62 ± 0.01	0.65 ±0.01
Heated	0.43 ± 0.04	0.45 ± 0.01	0.54 ± 0.01

Table 7. Calibration of erGAP3 fluorescent signal into $[Ca^{2+}]_{SR/ER}$ in different cell types. Table comparing the ER Ca^{2+} levels, expressed as R/R_0, at baseline (Basal), after stimulation with IP_3-producing agonists alone (ATP), together with TBH (F_{min}) and after the heating treatment ("heated") in three different cell types: stably-expressing erGAP3 HeLa cells, transiently-expressing erGAP3 HEK293T and cortical astrocytes obtained from erGAP3 transgenic mice. The mean ± SEM values of 4-6 independent experiments, with 100-150 individual cells per experiment, are shown. Note that, for each cell type, "F_{min}" and "Heated" values were very similar.

As we have generated the DM006 transgenic fly line expressing erGAP3 in muscle cells, and the calibration heating protocol was intended to be used in the DM006 flies *in vivo*; we next investigated whether erGAP3 was appropriate for measuring $[Ca^{2+}]_{SR}$ in this muscle cell type in mammals. For this purpose, mouse myoblast cells (C2C12) were transiently transfected with the erGAP3 gene cloned in the mammalian expression vector pcDNA3. The protocol is represented in **Fig. 32** as the ratio of the two individual erGAP3 fluorescence wavelengths ($R=F_{470}/F_{405}$). First, the ER stores are kept filled by perfusion with extracellular medium containing 1 mM Ca^{2+} to obtain the resting $[Ca^{2+}]_{ER}$ levels. Then, the dynamic range of erGAP3 in C2C12 myoblasts was tested by complete depletion of the ER achieved by perfusion with the "depletion cocktail" composed by ATP (100 µM) and the SERCA

inhibitor TBH (10 µM) in a Ca^{2+} free-medium containing EGTA (0.5 mM). There was a two-fold difference in the erGAP3 ratio between the filled and the empty store (**Fig. 32**), which is similar to the values obtained with erGAP3 in HeLa cells, in HEK cells and in brain astrocytes (**Table 7**) suggesting that erGAP3 behaves normally also in the muscle cell line.

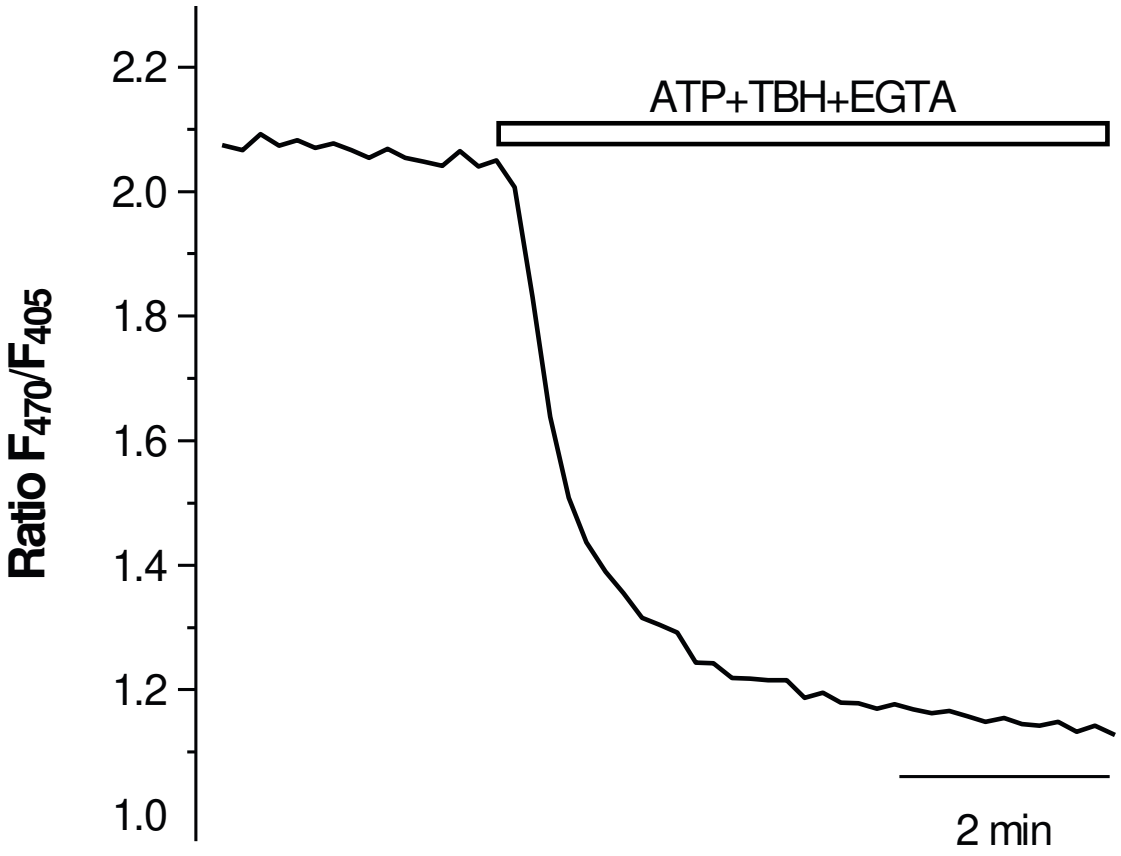

Figure 32. Dynamic range of erGAP3 in muscle cells. Endoplasmic reticulum (ER) Ca^{2+} measurements in mouse myoblast cells (C2C12) transiently transfected with erGAP3 gene cloned in the mammalian expression vector pcDNA3. The trace is the average of 35 cells in the same microscope field and represents the ratio of the two individual erGAP3 fluorescence wavelengths ($R= F_{470}/F_{405}$). The protocol is as illustrated in the figure: cells were perfused with extracellular medium containing 1 mM Ca^{2+} to obtain the baseline and, then, the dynamic was tested by applying the ER "depletion cocktail" (ATP+TBH+EGTA) that contains an IP_3 producing agonist (ATP; 100 µM) in Ca^{2+}-free solution (EGTA; 0.5 mM) and with the sarco/endoplasmic reticulum Ca^{2+}-ATPase (SERCA) reversible inhibitor 2,5-di(tert-butyl)-1,4-benzohydroquinone (TBH; 10 µM). There was a two-fold difference in the erGAP3 ratio between the filled and the empty store, which is similar to the values obtained with erGAP3 in other cell types. The experiment is representative of 3 similar ones.

2.2. Calibration procedure for the *in vivo* experiments

We next applied the heating calibration method described above to the *in vivo* measurements in *Drosophila* in order to obtain the R_{min} fluorescence value for each fly at the end of each experiment.

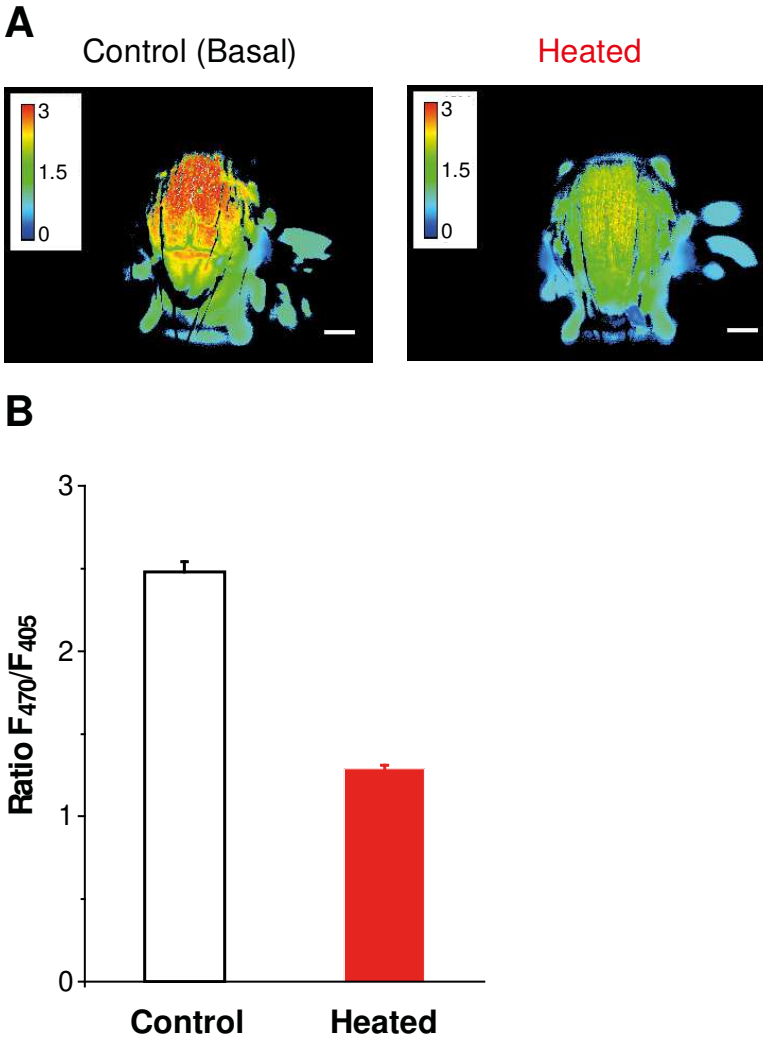

Figure 33. Calibration of erGAP3 fluorescence signal into sarcoplasmic reticulum Ca^{2+} concentration *in vivo*. A) The images show erGAP3 ratio ($R= F_{470}/F_{405}$) coded in a pseudocolour scale in pixels, where warm colours (such as red or yellow) indicate high sarcoplasmic reticulum Ca^{2+} concentrations ($[Ca^{2+}]_{SR}$) and cold colours (blue or cyan) indicate low $[Ca^{2+}]_{SR}$. In the experiment, fluorescent images at the two individual wavelengths of erGAP3 sensor (405 and 470 nm) were acquired in the thorax muscles of individual flies (DM006; erGAP3 transgenic muscle line), before (Control, left panel) and after heating 10 min at 50 °C (Heated, right panel). erGAP3 ratios were, then, calculated pixel-by-pixel from the individual GAP wavelengths. The difference in erGAP3 ratio of the fly before (R) and after heating (R_{min}) is noticeable. Calibration bar 200 µm. **B)** Histogram shows the mean ± SEM of 10 individual experiments (5 female flies and 5 male flies). The heating protocol reduced erGAP3 ratio by 50% in the thoracic muscles of DM006 flies. Importantly, R_{min} values are reproducible among individual flies.

First, the experiment was performed by measuring the erGAP3 ratio value (R) in the living fly; in this case, in the thorax muscles of the DM006 transgenic line. The fluorescence images at the two excitation wavelengths of the sensor were acquired and, the pixel-by-pixel ratio between them was calculated (**Fig. 33A,** left panel). Second, at the end of the experiment, we applied the 10 min-heating treatment at 50 °C to the studied fly, and immediately afterwards we measured the new erGAP3 ratio value. Note that the decrease of the ratio is now equivalent to the R_{min}, the minimal fluorescence value obtained when the SR Ca^{2+} store is empty (**Fig. 33A,** right panel). **Figure 33A** shows an individual experiment with erGAP3 ratio values coded in a pseudocolour scale, where warm colours (such as red or yellow) represent high $[Ca^{2+}]_{SR}$ and cold colours (blue or cyan) represent low $[Ca^{2+}]_{SR}$. The difference in the erGAP3 ratio of the fly before and after heating is noticeable: in the basal (resting) condition warm colours prevailed indicating a filled SR Ca^{2+} store; whereas, after the heating treatment the image is composed of cold colours that represent low $[Ca^{2+}]$. The changes in the ratio are homogeneous in all the thorax, suggesting that they affect all the thoracic muscles. Similarly to the *in vitro* experiments, the heating protocol reduced the erGAP3 ratio by 50%, from 2.5 ± 0.06 ("control"; mean ± SEM, n=10) to 1.3 ± 0.02 ("heated"; mean ± SEM, n=10) in the thoracic muscles of DM006 flies. The results are shown in **Figure 33B** as the mean ± SEM of 10 individual flies (5 from each gender). Note that the R_{min} values were constant among the experiments. Note also that the resting erGAP3 ratio (R) values decrease along the whole fly life until reaching values that are very similar to those of the "heated" flies in the old flies (35-day old) (**Fig. 28**). Furthermore, the R_{min} values were also constant during the whole fly life, as shown in **Figure 28**.

In most of the studies conducted with *Drosophila*, flies are maintained at 25 °C. In our case we maintained the flies at 29 °C, which shortens the fly life. In order to exclude that this protocol may have affected the results obtained with erGAP3 and, thus, check that the decrease observed in the erGAP3 ratio is independent of the lifespan; we repeated the aging experiment in the same DM006 transgenic line but maintaining the flies at a lower temperature of 25 °C. The fly life is extended as the temperature is decreased and at 25 °C the maximal longevity is of 80 days and the mean lifespan is 60 days (Linford et al., 2013). The results obtained at 25 °C (**Fig. 34**) were qualitatively and quantitatively very similar to those at 29 °C (**Fig. 28**).

The erGAP3 ratio values (R) decreased progressively over age from 2.8 ± 0.19 (mean ± SD; n=6) in the young flies (7 day-old) down to 1.44 ± 0.07 (mean ± SD; n=11) in the old flies (60 day-old). This difference, up to two-fold as that obtained at 29 °C, was considered significant ($p<0.001$, One-way ANOVA; Bonferroni multiple comparisons test). The R_{min} values were also independent of the age of the flies and the differences between the age groups were not significant (One-way ANOVA; Bonferroni multiple comparisons test). To conclude, the erGAP3 ratio values (R) values obtained in individual flies and in different experiments can be normalized by dividing by the R_{min} value.

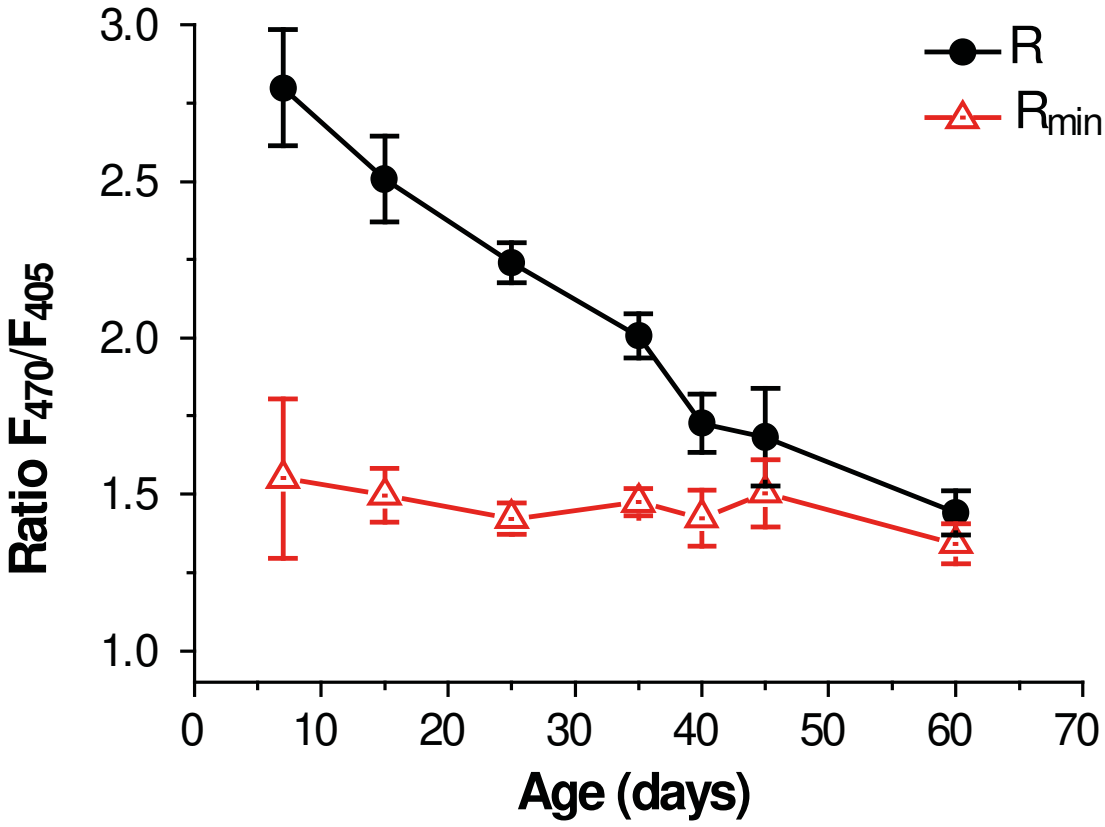

Figure 34. Sarcoplasmic reticulum Ca^{2+} measurements *in vivo* in the erGAP3 transgenic muscle fly line extending lifespan. The aging experiment shown in **Figure 28** in DM006 flies (erGAP3 transgenic muscle line) was repeated but maintaining the flies at a lower temperature of 25 °C, to check that the results obtained were independent of the flies lifespan. Flies from different ages (7, 15, 25, 35, 40, 45 and 60 days) were imaged at the two individual wavelengths of erGAP3 sensor (405 and 470 nm) in the thorax muscles. erGAP3 ratios ($R= F_{470}/F_{405}$) were calculated pixel-by-pixel from the individual wavelengths. Recordings for each fly were performed before (black circles; baseline values expressed as R) and after 10 min-heating at 50 °C (red triangles; empty store, R_{min}). Each value is the mean ± DS of 3-6 flies. The results are similar as the ones obtained at 29 °C (**Fig. 28**) and show that erGAP3 ratio (R) decreased progressively and significantly over age ($p<0.001$, One-way ANOVA; Bonferroni test). The R_{min} values were homogenous and independent of the age of the flies.

2.3. Effects of the heating treatment on the integrity of the cell

We hypothesized that the heating treatment results in Ca^{2+} depletion of ER by Ca^{2+} leak to the cytosol, with collapse of the ER/cytosol gradient. This leak requires, therefore, maintenance of the low $[Ca^{2+}]_C$ (~100 nM). Since $[Ca^{2+}]$ in the extracellular medium is ~1 mM, maintenance of the low $[Ca^{2+}]_C$ requires the barrier action of the plasma membrane to avoid entry of Ca^{2+} from the extracellular medium to the cytosol. To test this hypothesis, we loaded HeLa cells with the cytosolic dye Fluo-4 and compared "control" (non-heated) and "heated" values. Fluo-4 was recorded as green fluorescence at 470 nm excitation wavelength. The results are shown in **Figure 35**, where the trace is the time course of the experiment and represents the average of the 100 cells shown in the green fluorescence images above. The images (**Fig. 35A; i–v**) correspond to the time points marked in the trace (**Fig. 35B**). (**i**) Under resting conditions, cells loaded with Fluo-4 display dim green fluorescence. (**ii**) Upon a 30 s stimulation pulse with ATP (100 µM), an IP_3-producing agonist, Ca^{2+} is released from the ER to the cytosol, which is reflected by a transient increase in the $[Ca^{2+}]_C$ in the "control" group (compare changes in fluorescence in panels (**i**) and (**ii**) in **Fig. 35A**). (**iii**) After heating the cells at 50 °C for 10 min, the fluorescence image is very similar in intensity to "control" cells under resting conditions (compare panels (**i**) and (**iii**) in **Fig. 35A**), indicating that the plasma membrane is intact and, thus, Fluo-4 remains in the cytosol of the "heated" cells. (**iv**) The ATP response was, then, checked in the "heated" cells with another 30 s pulse. Cells did not respond to ATP, as there was an absence in the $[Ca^{2+}]_C$ peak, that would be reflected as an increment in fluorescence. This could be due to a complete discharge of the stored Ca^{2+} in the ER induced by the heating treatment. (**v**) However, the fact that Fluo-4 remains in the cytosol after heating was also confirmed by the addition of digitonin (Dig; 50 µM), that permeabilizes the cell membrane and, thus, the dye exits the cells. This results in a total loss of green fluorescence (**Fig. 35A,** panel **v**).

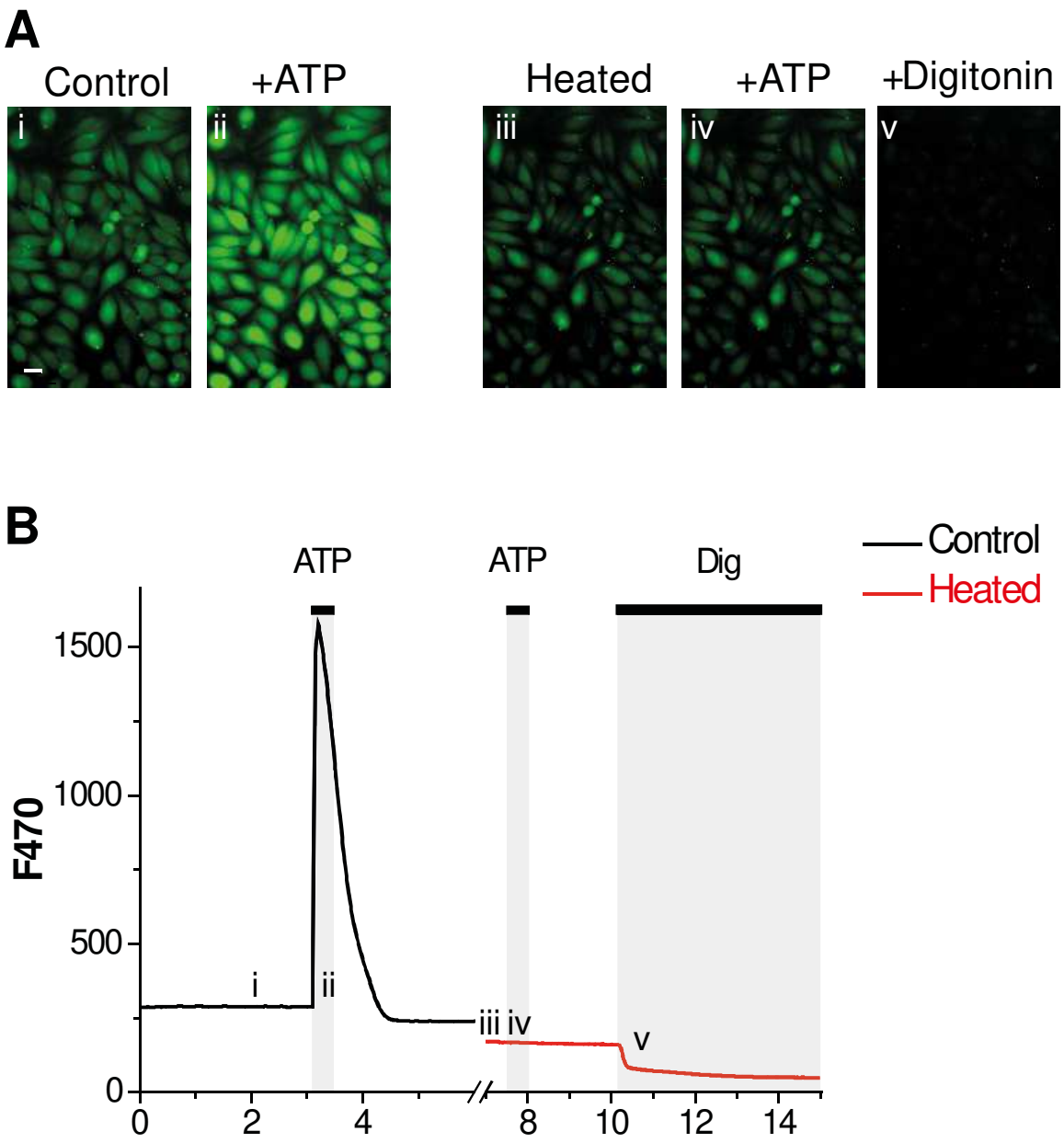

Figure 35. Effects of heating on cytosolic Ca^{2+}. A) Fluorescence images recorded at 470 nm of HeLa cells loaded with the cytosolic dye Fluo-4. From left to right: (**Ai**) image shows the characteristic green fluorescence of Fluo-4 that reflects resting cytosolic Ca^{2+} concentration ($[Ca^{2+}]_C$) in the cells; (**Aii**) after stimulation with ATP (100 µM), Fluo-4 fluorescence increases; (**Aiii**) same cells after heating 10 min at 50 °C. Fluo-4 is maintained in the cytoplasm and $[Ca^{2+}]_C$ continues low; (**Aiv**) the fluorescent signal becomes insensitive to cell stimulation with ATP; (**Av**) plasma membrane permeabilization with digitonin (Dig, 50 µM) releases Fluo-4 and reduces fluorescence. Calibration bar, 20 µm. **B)** Cytosolic Ca^{2+} measurements (green fluorescence measured at 470 nm excitation) showing the experiment time course with "non-heated" cells shown in the black trace (Control) and the same cells after the heating treatment in the red trace (Heated). The stimulus (ATP) and membrane permeabilization (Dig) are highlighted in grey shading. The traces represent the average of 100 cells shown in the green fluorescence images above. The images (**i–v**) correspond to the time points marked in the trace (**i–v**).

2.4. GAP3 remains functional after heating

In order to use the heating method for calibration of $[Ca^{2+}]_{SR/ER}$, functionality of GAP3 after heating must be demonstrated. Therefore, we checked whether GAP3 sensor remained Ca^{2+}-sensitive and maintained the structure after heating. For this purpose, we isolated the recombinant GAP3 protein produced in bacteria. Firstly, we checked if GAP3 remained Ca^{2+}-sensitive with the heating treatment: the protein was heated at 50 °C and a fluorescence excitation spectrum, in a Ca^{2+}-free or in a Ca^{2+}-containing medium, was obtained in the fluorescence spectrophotometer. The excitation spectrum of the "heated" GAP3 protein continued to be Ca^{2+}-sensitive and, thus, changed upon Ca^{2+} binding to the sensor, so that the fluorescence excited at 470 nm increases with a parallel decrease of the fluorescence excited at 405 nm (**Fig. 36**).

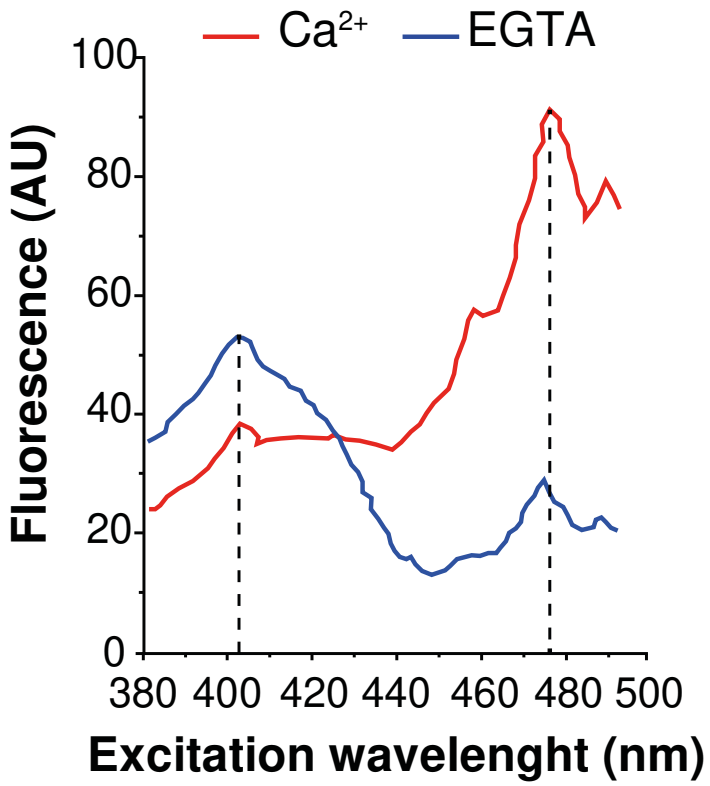

Figure 36. GAP3 remains functional after the heating treatment. Excitation spectra of 50 °C heated GAP3 protein produced in bacteria. The spectrophotometer cuvette was filled with extracellular-like medium containing 8.5 µg of the heated protein and excitation spectra were performed (between 380 and 500 nm with the emission set at 520 nm) in the absence (0.1 mM EGTA; blue line) or in the presence (1 mM $CaCl_2$; red line) of Ca^{2+}. Characteristic Ca^{2+}-dependent peaks at 405 and 470 nm (black dashed line) are preserved and, thus, the protein is functional after heating.

Secondly, to characterize protein stability, we performed a denaturation assay that quantifies the thermal stability of a protein under different denaturation conditions such as basic pH of 8.8, the reducing agent DTT, or the Ca^{2+} chelating agent EGTA. The outcome is the transition unfolding temperature (T_m) where the concentrations of folded and unfolded protein are equal. According to the GAP3 thermal denaturation assay, the concentration of folded protein at 50 °C temperature is almost 1 and the T_m is of 79 °C (**Fig. 37**), almost 20 °C above the temperature used for the heating treatment. The conclusion is that, after 50 °C heating, GAP3 protein remains functional and, also, the structure is maintained.

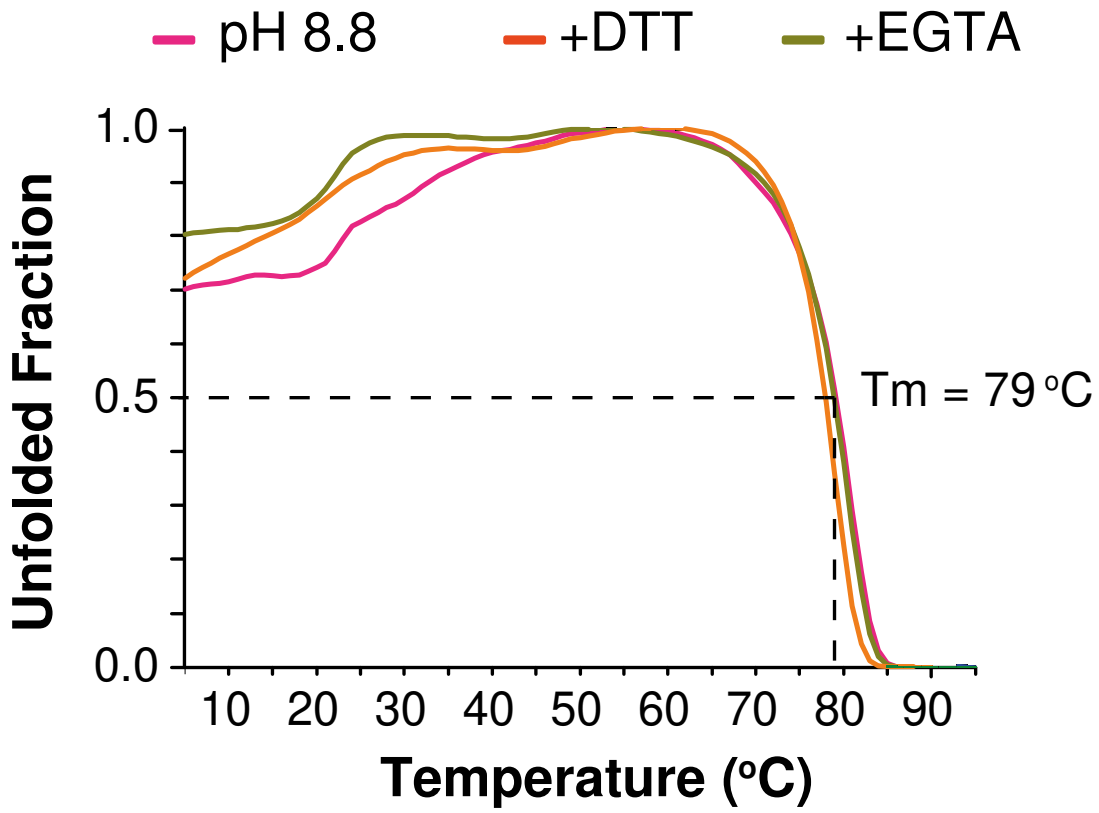

Figure 37. Thermal stability of GAP3. Denaturation assay of GAP3 protein under different denaturation conditions such as basic pH (pH= 8.8; pink trace), the reducing agent DTT (Dithiothreitol; orange trace), or the Ca^{2+} chelating agent EGTA (Ethylene Glycol Tetraacetic Acid; green trace). GAP3 remained folded at 50 °C and the transition unfolding temperature (T_m; black dashed line) is of 79 °C. Performed at the EMBL Sample Preparation and Characterization Facility, Hamburg, Germany.

2.5. Calibration procedure for other low affinity Ca^{2+} indicators

We next asked whether the erGAP3 calibration protocol was also valid for other Ca^{2+} indicators. We chose one of the CEPIA family members with low Ca^{2+} affinity, the G-CEPIA1er. This a green Ca^{2+} indicator, with a K_D of 672 µM and a DR of 4.7, also adequate to measure [Ca^{2+}] in the lumen of the ER.

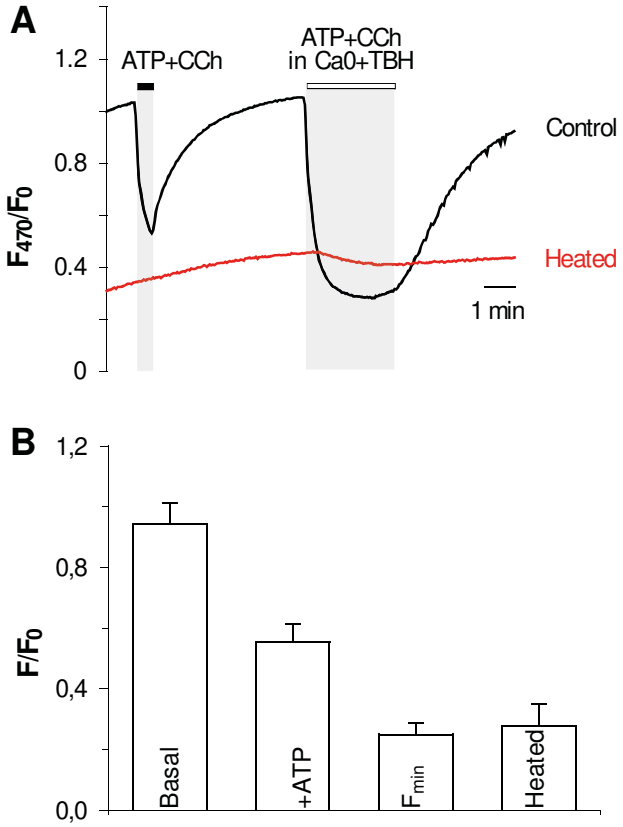

Figure 38. Calibration of the fluorescence signal into endoplasmic reticulum Ca^{2+} concentration *in vitro* for other low affinity Ca^{2+} indicators. A) Endoplasmic reticulum (ER) Ca^{2+} measurements in G-CEPIA1er transiently transfected HeLa cells recorded at 470 nm. The fluorescence values were normalized by the initial fluorescence (F_0) and expressed as F_{470}/F_0. Traces show one representative experiment, average of 100 cells from the same microscopic field, before (Control, black trace) and after heating (Heated, red trace). The protocol was identical to the one described for erGAP3 (**Figure 30**). Traces show partial (first challenge, ATP+CCh) and complete ER Ca^{2+} emptying (second challenge, ATP+CCh in Ca0+TBH). Both stimulus are highlighted in grey shading. **B)** Histogram representing the normalized values by the initial fluorescence (F/F_0), expressed: at baseline (Basal); after stimulation with IP_3-producing agonists alone (+ATP, first challenge); the agonists together with the SERCA inhibitor TBH ($F_{min,}$ second challenge); or after heating the cells at 50 °C for 10 min (Heated). The mean ± SEM values of 4 independent experiments are shown.

To search whether the calibration method could be used for CEPIA, we tested the protocol described above for erGAP3 in G-CEPIA1er transiently transfected HeLa cells and imaged the cells 24 h after transfection (**Fig. 38A**). G-CEPIA1er is an intensiometric Ca^{2+} indicator and, therefore, we measured fluorescence at 470 nm and normalized the data by dividing by the initial fluorescence (F_0). We compared the F_{min} value (mean ± SEM of 4 individual experiments) obtained by perfusion with the ER "depletion cocktail" (0.25 ± 0.03) with the F_{min} value obtained after heating (0.28 ± 0.07), and conclude that they did not differ significantly (**Fig. 38B**). These results indicate that the heating treatment may be a general method that can be applied to different low affinity Ca^{2+} sensors.

3. Calibrated Ca^{2+} measurements *in vivo*

3.1. Sarcoplasmic reticulum Ca^{2+} concentration decreases progressively with age

Given that the calibration method had proved to be valuable for *in vitro* and *in vivo* experiments, we next applied the calibration procedure to the erGAP3 measurements previously obtained in the SR of the DM006 transgenic line *in vivo* (**Fig. 28**). Thus, the obtained erGAP3 ratio values (**Fig. 28**, black circles) for each fly were normalized by dividing by its corresponding R_{min} value (**Fig. 28**, red triangles), measured in the same fly after heating at the end of the experiment (R/R_{min}). This treatment of the data homogenized the outcomes from different experiments. For example, the coefficients of variation estimated for five sets of flies of different ages were 11.70 ± 3.17 (%, mean ± SD; n=5) for the erGAP3 ratio (R) values and 8.06 ± 1.54 (%, mean ± SD; n=5) for R/R_{min}; the difference was significant ($p<0.05$; paired t-test). Note that complete Ca^{2+} emptying of the SR would be reflected by a decrease of R/R_{min} to 1, whereas saturation with Ca^{2+} inside the SR would produce, according to the estimated dynamic range, a R/R_{min} value of 3. The normalized data are shown in **Fig. 39**. Each value is the mean ± SEM of 10-20 flies, half females and half males, except for the group of flies aged 35 days, which contained only 10 female flies. The SR Ca^{2+} content (R/R_{min}) in the skeletal muscle decreased monotonically with age from a value of 2.22 ± 0.02 (mean ±

SEM; n=20) in the young (7-day old) flies to 1.03 ± 0.03 (mean ± SEM; n=10) in the old flies (35-day old), which makes a two-fold difference (**Fig. 39,** left axis). All the values of the following groups were significantly smaller than the value at 7 days ($p<0.001$; One-way ANOVA; Bonferroni multiple comparisons test). Finally, the calibration procedure can be applied to calculate the real $[Ca^{2+}]_{SR}$ for each age group (**Fig. 39,** right axis). The approximate value of $[Ca^{2+}]_{SR}$ was near 600 µM in young flies (7-day old) and dropped dramatically, to one tenth of this concentration, 50 µM, in the old flies (35-day old). As a conclusion of these results, there was a gradual and significant decrease of R/R_{min} that reflects the progressive emptying of the SR Ca^{2+} store with age.

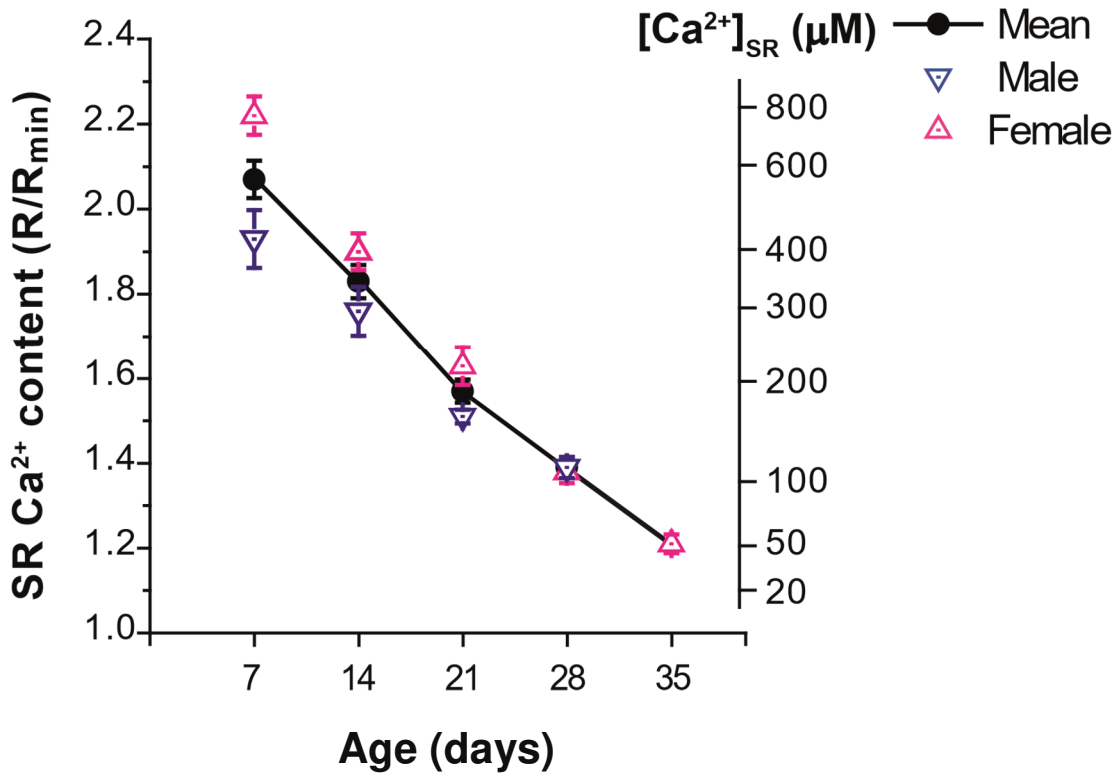

Figure 39. Decrease of the resting sarcoplasmic reticulum Ca^{2+} concentration in aging flies. The previously obtained erGAP3 ratios ($R= F_{470}/F_{405}$) in the DM006 flies (erGAP3 transgenic muscle line) were normalized by dividing by the erGAP3 ratio obtained in the same fly after heating (R_{min}), that correspond to a completely empty sarcoplasmic reticulum (SR) store. The normalized data (R/R_{min}; left axis) represent a quantification of the SR Ca^{2+} content that range between 1 at $[Ca^{2+}]= 0$ and 3 at $[Ca^{2+}]=$ infinite. Then, the calibration into sarcoplasmic reticulum Ca^{2+} concentration ($[Ca^{2+}]_{SR}$) was calculated with the normalized values (R/R_{min}), the Ca^{2+}-GAP3 dissociation constant ($K_D= 489$ µM) and the dynamic range (DR= 3). The approximate $[Ca^{2+}]_{SR}$ is given on the right axis. All the values were significantly smaller than the value at 7 days ($p<0.001$; One-way ANOVA; Bonferroni test). The values correspond to the females flies (pink triangles, n= 10), the male flies (blue inverted triangles, n= 10) or the mean of both genders (solid black circles, males and females n= 20).

3.2. The muscle function correlates with $[Ca^{2+}]_{SR}$

We next studied the relationship between the decrease in $[Ca^{2+}]_{SR}$ and the loss of muscle function with age in the DM006 line. The results are shown in **Fig. 40**.

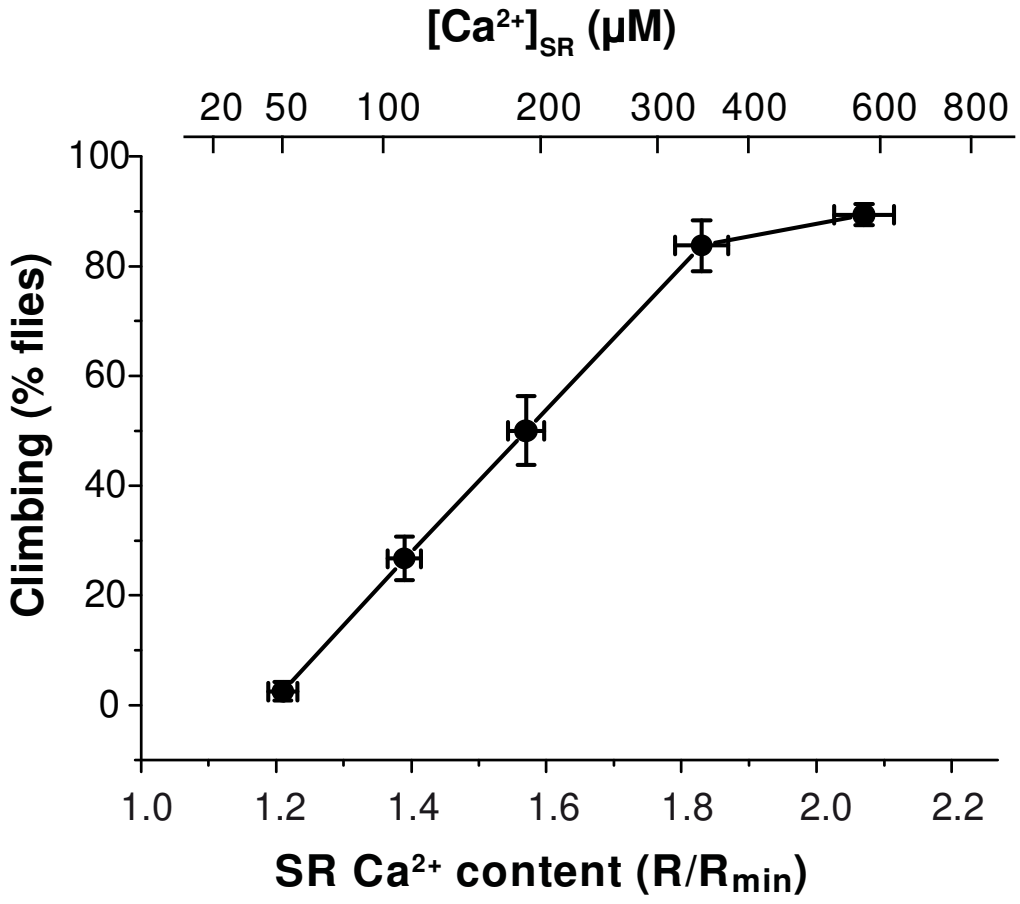

Figure 40. Correlation between the resting sarcoplasmic reticulum Ca^{2+} concentration and fly climbing ability with age. The sarcoplasmic reticulum (SR) Ca^{2+} content is measured as R/R_{min} on the lower axis and ranges between 1 at $[Ca^{2+}]$= 0 and 3 at $[Ca^{2+}]$= infinite; calibration of erGAP3 signal into sarcoplasmic reticulum Ca^{2+} concentration ($[Ca^{2+}]_{SR}$) is represented on the upper abscissa axis and ranges between 50 μM and 600 μM; and, the climbing ability is represented as percentage of the number of flies that surpassed 5 cm height in 18 s over the total of flies in each experiment on the left ordinate axis. There was close correlation between the motor function and the $[Ca^{2+}]_{SR}$. Values represent mean ± SEM of groups of 10-20 flies.

According to our calibration, the $[Ca^{2+}]_{SR}$ was near 600 μM in young flies (7-day old) and 89% of these flies were able to perform the climbing assay. Then, we observed that there is a threshold around 400 μM that corresponds to the fly age of 14 days, above this value the motor function was maintained, but below this

value both $[Ca^{2+}]_{SR}$ and climbing ability collapsed with very similar time courses. In the middle age group (21 day-old) 50% of the flies can perform the climbing test, and the $[Ca^{2+}]_{SR}$ was about 200 µM and, thus, has decreased three times compared to the youngest flies (7-day old). The oldest flies (35-day old) showed a $[Ca^{2+}]_{SR}$ of 50 µM, about one tenth of the $[Ca^{2+}]_{SR}$ value found in the youngest flies. This dramatic decrease of $[Ca^{2+}]_{SR}$ was associated to an almost absolute inability to climb, as only 3% of the flies were able to perform the climbing test. As a conclusion, we found an excellent correlation between SR Ca^{2+} concentration and muscle function, measured in the climbing assay.

3.3. Cytosolic Ca^{2+} dynamics is altered with age

We next checked whether the variations in resting $[Ca^{2+}]_{SR}$ observed with age were associated to the dynamics of cytosolic Ca^{2+}. For this purpose, we studied the $[Ca^{2+}]_C$ responses to muscle stimulation through motoneurons in DM010 transgenic flies that express the cytosolic Ca^{2+} sensor GCaMP3. This indicator does not have any basal fluorescence in the muscle and is not ratiometric, so quantitative measurements of resting cytosolic Ca^{2+} were not feasible. Instead we measured the cytosolic Ca^{2+} response in the dorsal longitudinal (flight) muscles located in the fly thorax by stimulation of the giant fiber system (GFS). Flies were immobilized in agarose and the giant fibers were stimulated through two tungsten electrodes impaled into the fly eyes. After checking the correct positioning of the electrodes by observing twitches in the wing after stimulation, a protocol of repetitive stimulation with 5 V/50 ms stimuli at a frequency of 0.5 or 10 Hz was performed during 5 s. Fluorescent measurements were recorded as green GFP fluorescence, acquired every 100 ms, and normalized to the values obtained during the first 5-10 frames (F/F_0). The protocol is illustrated in **Fig. 41A,** where the mean ± SEM of 6 -11 individual recordings of young (7-day old) and old (21-day old) flies is shown. In both age groups, we can observe that at 0.5 Hz, there are small repetitive increases in $[Ca^{2+}]_C$. However, at 10 Hz stimulation, there is one individual event fused and peaked resulting in a much larger cytosolic Ca^{2+} increase. It seems clear that, at both frequencies, the increase of $[Ca^{2+}]_C$ is larger

in the younger (7-day old) flies. This output is consistent with the higher resting $[Ca^{2+}]_{SR}$ found in the younger flies.

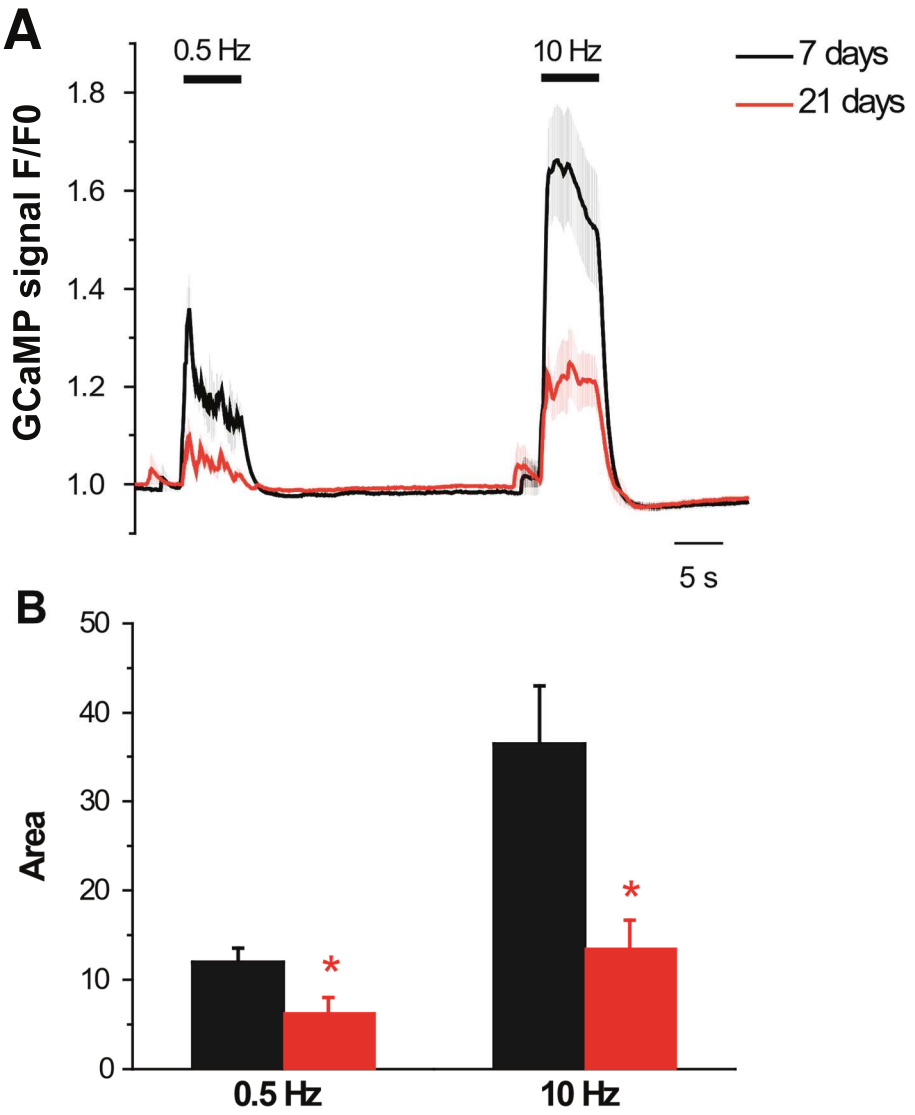

Figure 41. Effect of age on cytosolic Ca^{2+} dynamics upon muscle stimulation in *Drosophila.* A) Recordings of the cytosolic Ca^{2+} response in the flight muscles of young (7 days) and old (21 days) flies from the DM010 line, expressing the GCaMP3 cytosolic Ca^{2+} indicator in the thorax muscles. Flies were immobilized in agarose and impaled through two tungsten electrodes in the eyes. Recordings were obtained by stimulation of the giant fibers which synapse the motoneurons that drive the flight muscles. The stimulation protocol consisted of repetitive stimuli of 5 V/50 ms and 5 s duration at low (0.5 Hz) and high (10 Hz) frequencies. Fluorescent measurements were acquired at 470 nm excitation every 100 ms, normalized to the values obtained during the first 5-10 frames (F_0) and represented as F_{470}/F_0. The black trace represents the mean ± SEM of 6 young flies and the red trace the mean ± SEM of 11 old flies. **B)** Histogram comparing the area under the curve of the cytosolic Ca^{2+} transients shown in (A) at low (0.5 Hz) and high (10 Hz) frequencies and in young (7 days old) and old flies (21 days old). The reduction of the cytosolic Ca^{2+} transients in the old flies was statistically significant (red *; $p<0.05$; unpaired t-test).

The Ca^{2+} transients were quantified by measuring the area under the curve, and the results expressed as the mean ± SEM of 6-11 flies are shown in **Fig. 41B**. Comparing age groups, at low frequencies, the area showed a reduction of 50% in the old flies. At high frequencies the reduction was of 65%. Both of these values were statistically significant ($p<0.05$; unpaired t-test). This outcome validated the results obtained with erGAP3 in the DM006 muscle line and confirmed that the old flies had a lower SR Ca^{2+} levels and, thus, release less Ca^{2+} to the cytosol, in comparison to young flies.

3.4. Endoplasmic reticulum Ca^{2+} concentration does not change with age in brain neurons

In order to investigate whether the reduction of SR Ca^{2+} content in the aged flies was a general phenomenon occurring in all tissues, we studied the changes of $[Ca^{2+}]_{ER}$ with age in the brain neurons, using the DN005 transgenic fly line. We measured $[Ca^{2+}]_{ER}$ in the whole brain (**Fig. 24C and D**). The experimental procedure was the same as in the muscle. First, flies were divided by age and fluorescent images were acquired in the brain before and after heating, to calculate R and R_{min}, respectively. Then, values were normalized to obtain ER Ca^{2+} content (R/R_{min}) and finally $[Ca^{2+}]_{ER}$ was calculated for each age group. The ER Ca^{2+} content in the brain (**Fig. 42**, left scale) had a value of 1.75 ± 0.05 (mean ± SEM; n=20) in the young flies (7-day old) and did not change over age, yielding a value of 1.70 ± 0.05 (mean ± SEM; n=12) in the old flies (35-day old). Finally, we calibrated the measurements into $[Ca^{2+}]_{ER}$ (**Fig. 42**, right ordinate scale) and, unlike the aged muscle, the $[Ca^{2+}]_{ER}$ of the brain neurons remained stable at about 300 µM along the whole fly life. Results show that the variation among the means of the different age groups (12-22 flies) was not significantly greater than those expected by chance ($p=0.995$; One-way ANOVA; Bonferroni multiple comparisons test).

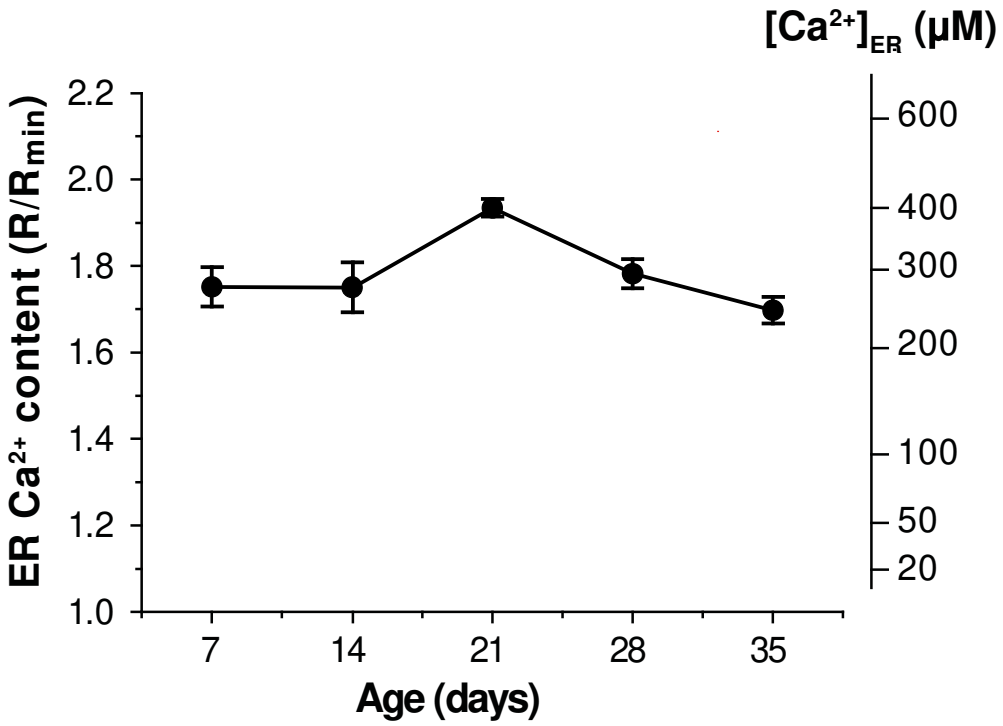

Figure 42. The resting endoplasmic reticulum Ca^{2+} concentration does not change with age in brain neurons. erGAP3 fluorescence (F_{405} and F_{470} nm) was measured in the whole brain of DN005 flies (erGAP3 transgenic neuronal line) from different ages. erGAP3 ratios were calculated before ($R= F_{470}/F_{405}$) and after (R_{min}) heating for each fly. Normalized data (R/R_{min}), which are proportional to endoplasmic reticulum (ER) Ca^{2+} content, are shown on the left axis. An approximate calibration of erGAP3 fluorescence into endoplasmic reticulum ER Ca^{2+} concentration ($[Ca^{2+}]_{ER}$) is given on the right axis. Each value is the mean ± SEM of 12-22 flies, one half females and one half males, except for flies aged 35 days groups, which contained only 12 female flies. Results show that the variation among the means of the different age groups is not significantly greater than expected by chance (One-way ANOVA; Bonferroni Multiple Comparisons Test).

3.5. Endoplasmic reticulum Ca^{2+} concentration decreases with age in wing sensory neurons

In the DN005 fly line, erGAP3 expression is controlled by the pan-neuronal promoter *elav* and, thus, the indicator is expressed in all neurons (**Fig. 24C and D**). As we have observed that $[Ca^{2+}]_{ER}$ does not change with age in brain neurons, we decided to test whether the behaviour was similar in other neuronal types such as the peripheral sensory wing neurons. We measured $[Ca^{2+}]_{ER}$ in the wing margin of the DN005 fly line following the same procedure used with the whole brain.

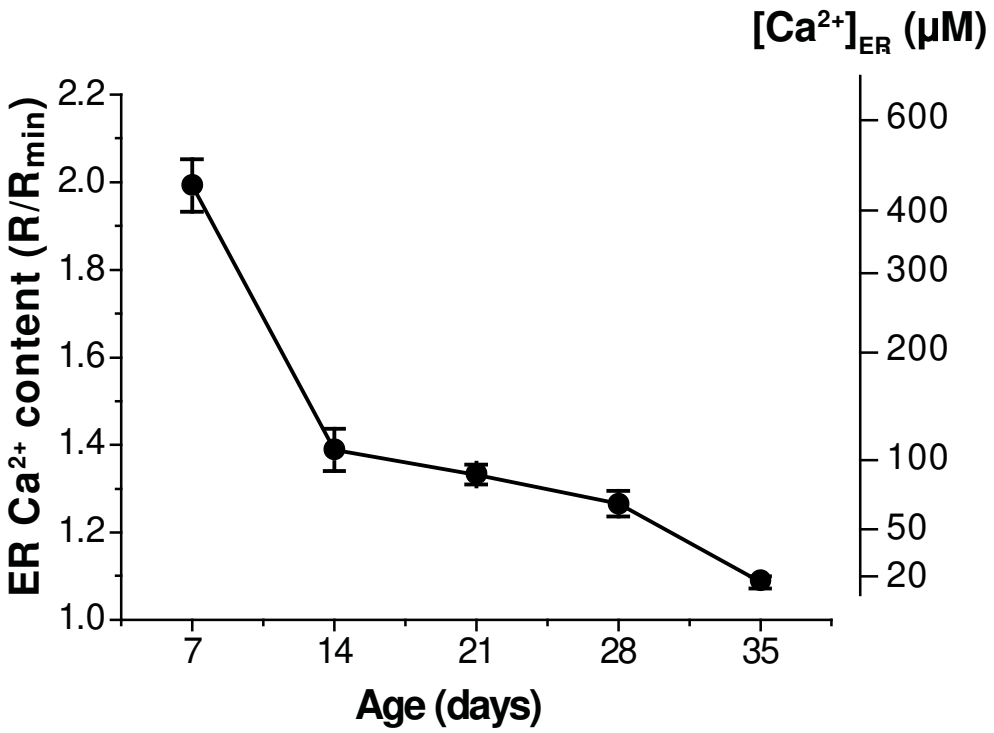

Figure 43. The resting endoplasmic reticulum Ca^{2+} concentration decreases with age in the wing sensory neurons. erGAP3 fluorescence (F_{405} and F_{470} nm) was measured in the peripheral sensory neurons located in the anterior wing margin of DN005 flies (erGAP3 transgenic neuronal line) from different ages. erGAP3 ratios were calculated before ($R= F_{470}/F_{405}$) and after (R_{min}) heating for each fly. Normalized data (R/R_{min}), which are proportional to endoplasmic reticulum (ER) Ca^{2+} content, are shown on the left axis. An approximate calibration of erGAP3 fluorescence into endoplasmic reticulum ER Ca^{2+} concentration ($[Ca^{2+}]_{ER}$) is given on the right axis. Each value is the mean ± SEM of 10-28 flies, one half females and one half males, except for flies aged 35 days groups, which contained only 10 female flies. All the values were significantly smaller than the value at 7 days ($p<0.001$; One-way ANOVA; Bonferroni test).

The results of the sensory wing neurons are summarized in **Fig. 43**. Each value is the mean ± SEM of 10-28 flies, half females and half males, except for flies aged 35 days groups, which contained 10 female flies. The ER Ca^{2+} content of the wing neurons of young flies (7-day old) is of 1.99 ± 0.06 (mean ± SEM; n=28), similar to the SR Ca^{2+} content value of the skeletal muscle of DM006 flies (**Fig. 39**) of the same age of 2.22 ± 0.02 (mean ± SEM; n=20), which calibrated gave a $[Ca^{2+}]_{ER}$ value of around 600 µM in both cases. However, in the following group of age (14-day old) the value in the wing neurons dropped dramatically to about 100 µM (R/R_{min} = 1.39 ± 0.04; mean ± SEM; n=13), and decreased in the following 3 weeks until it reached very low values of 20 µM at 35 days (R/R_{min} = 1.08 ± 0.06; mean ± SEM; n=10). To conclude, we found that in the wing sensory neurons the tendency

is very similar to that in the muscle and, ER Ca^{2+} resting levels decrease progressively and significantly with age ($p<0.001$; One-way ANOVA; Bonferroni multiple comparisons test). However, $[Ca^{2+}]_{ER}$ resting levels in the brain remain stable during the whole fly life indicating that aging might affect differentially the various types of neurons or tissues.

4. Sarco/endoplasmic reticulum Ca^{2+} homeostasis

In order to explore the mechanisms involved in the maintenance of the $[Ca^{2+}]_{ER,}$ we analysed the expression levels of an array of three classes of proteins directly implicated in this process. The Ca^{2+} concentration maintained inside the ER is the result of a pump/leak steady state between the sarco/endoplasmic reticulum Ca^{2+}-ATPase (SERCA)-mediated Ca^{2+} entry and the ER leak (Stein, 1967), whose molecular nature is still controversial. However, a number of channel proteins have been implicated in basal Ca^{2+} leak, among them the ryanodine receptor (RyR) channels. The RyR channels are the main SR Ca^{2+} channels in muscle cells and they have been proposed to undergo modifications with age (e.g. oxidation, nitrosylation and calstabin depletion) that would render them leaky. Therefore, we choose to study the SERCA and the RyR channel as direct key players. On the other hand, although some Ca^{2+} exists as free ions within the ER, most of it is buffered by calcium-binding proteins (CaBPs) in a polymerized state. The most abundant CaBP within the SR is calsequestrin (CSQ). However, as there is no homolog of CSQ in *Drosophila*, we also included in the analysis a ubiquitous and highly conserved ER-CaBP, the immunoglobulin protein (BiP), also known as GRP78. This protein is a molecular chaperon and, thus, it plays a crucial role in maintaining skeletal muscle proteostasis.

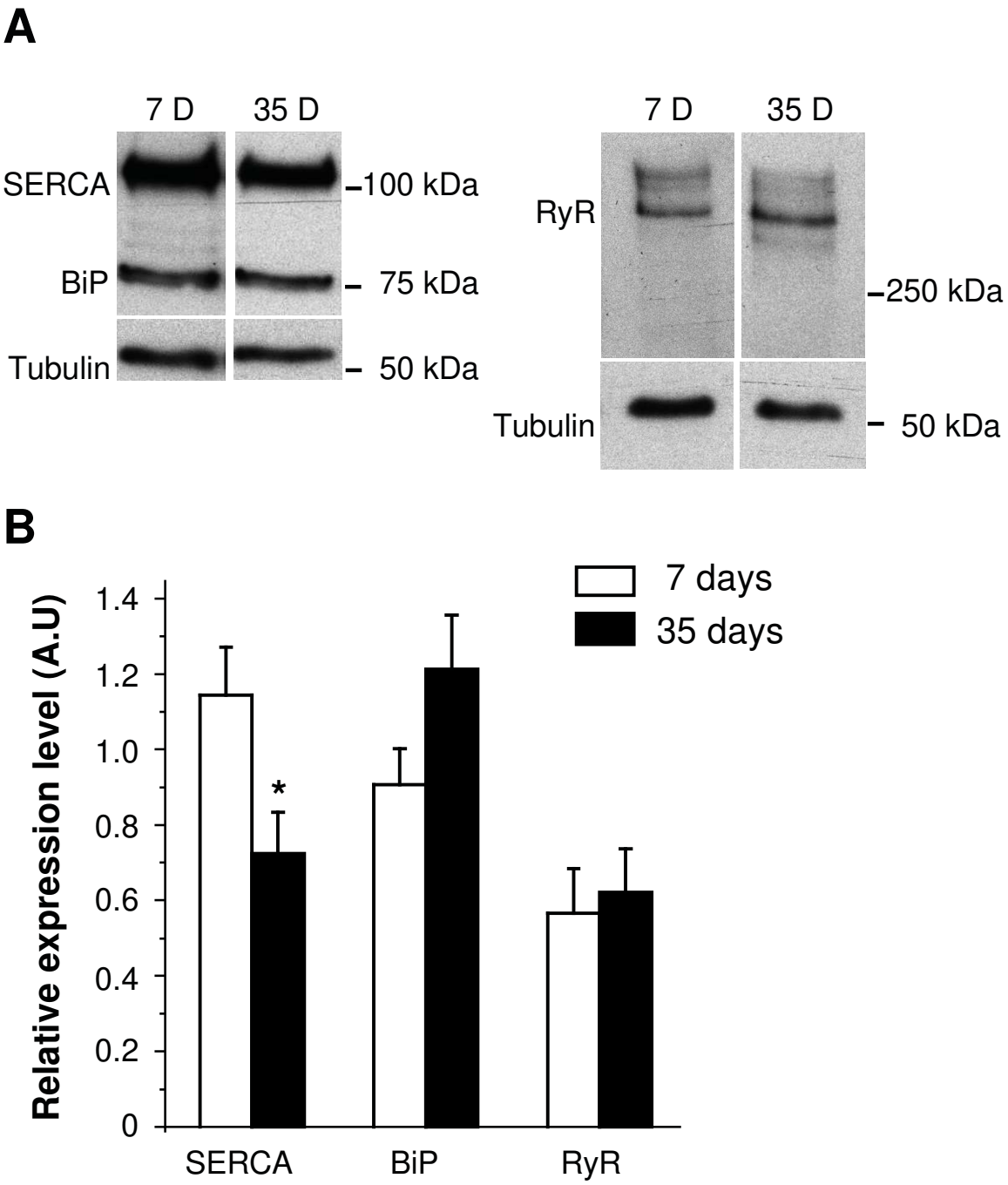

Figure 44. Protein expression levels of SERCA, RyR and BiP in *Drosophila* skeletal muscle with age. A) Representative blots of the sarco/endoplasmic reticulum Ca^{2+}-ATPase (SERCA), the ryanodine receptor (RyR) and the immunoglobulin protein (BiP) expression in young (7 days) and old (35 days) DM006 flies (erGAP3 transgenic muscle line). The whole thorax protein extract from one individual fly was loaded per lane, subjected to SDS-PAGE, and revealed with the specific antibodies for SERCA, RyR and BiP. Tubulin was used as the protein loading control. **B)** Quantification of multiple data similar to that shown in panel **A**. The results were, in all the cases, normalized to tubulin expression levels. Each value is the mean ± SEM of 16-32 flies. The reduction in SERCA protein levels observed in the old flies (35%) was statistically significant (*; $p<0.05$, unpaired t-test), whereas the differences in the expression levels observed for RyR or BiP were not statistically significant.

The protein expression analysis was performed by western blotting. Total protein from individual thoraxes was extracted from young (7-day old) and old flies (35-day old) of the DM006 line. The samples were subjected to 6% SDS/PAGE, electrotransferred onto nitrocellulose membranes and sequentially incubated with the array of primary antibodies. Total protein expression was normalized to the tubulin expression and the changes in expression were calculated in percentage. The data obtained are shown in **Fig. 44A**, were representative blots from young and old flies are shown for the three selected proteins (SERCA, RyR and BiP) and the housekeeping tubulin. The quantification analysis (**Fig. 44B**) revealed a small (35%) but significant reduction of SERCA protein levels with age ($p<0.01$; unpaired t-test). This decline in the expression of the SERCA pump could partially explain the reduced $[Ca^{2+}]_{SR}$ observed in old flies. However, it is noticeable that SERCA expression was reduced by only 35% whereas the $[Ca^{2+}]_{SR}$ is reduced by 600% when comparing the 7- and the 35-day old flies. Therefore, other mechanisms besides SERCA expression must be implicated. The quantification also showed a non-significant increase of 10% in the RyR expression levels with age (**Fig. 44B**), which could be in agreement with the hypothesis of increased RyR leakiness with age, but, again such a small increase could not explain the huge decrease of $[Ca^{2+}]_{SR}$. Finally, we found that BiP levels increased 28% between young and old flies (**Fig. 44B**), which could indicate that unfolding protein response (UPR) players are upregulated in the aging muscle.

Then, we analysed the same selected array of proteins in the brain of young (7-day old) and old flies (28-day old). The protein was extracted from individual heads from the DN005 fly line and the same blotting protocol was applied (**Fig. 45A**). In contrast to the thorax muscles, the expression levels of SERCA protein did not vary significantly in the brain of old flies; we found a slight change (14% decrease) with age (**Fig. 45B**). However, in parallel to the muscle, we found that BiP levels were significantly increased in the brain by 40% comparing young and old flies ($p<0.05$; unpaired t-test). The quantification also showed that RyR protein levels were increased in the brain of the old flies; reaching a value of 25% which was not statistically significant (**Fig. 45B**).

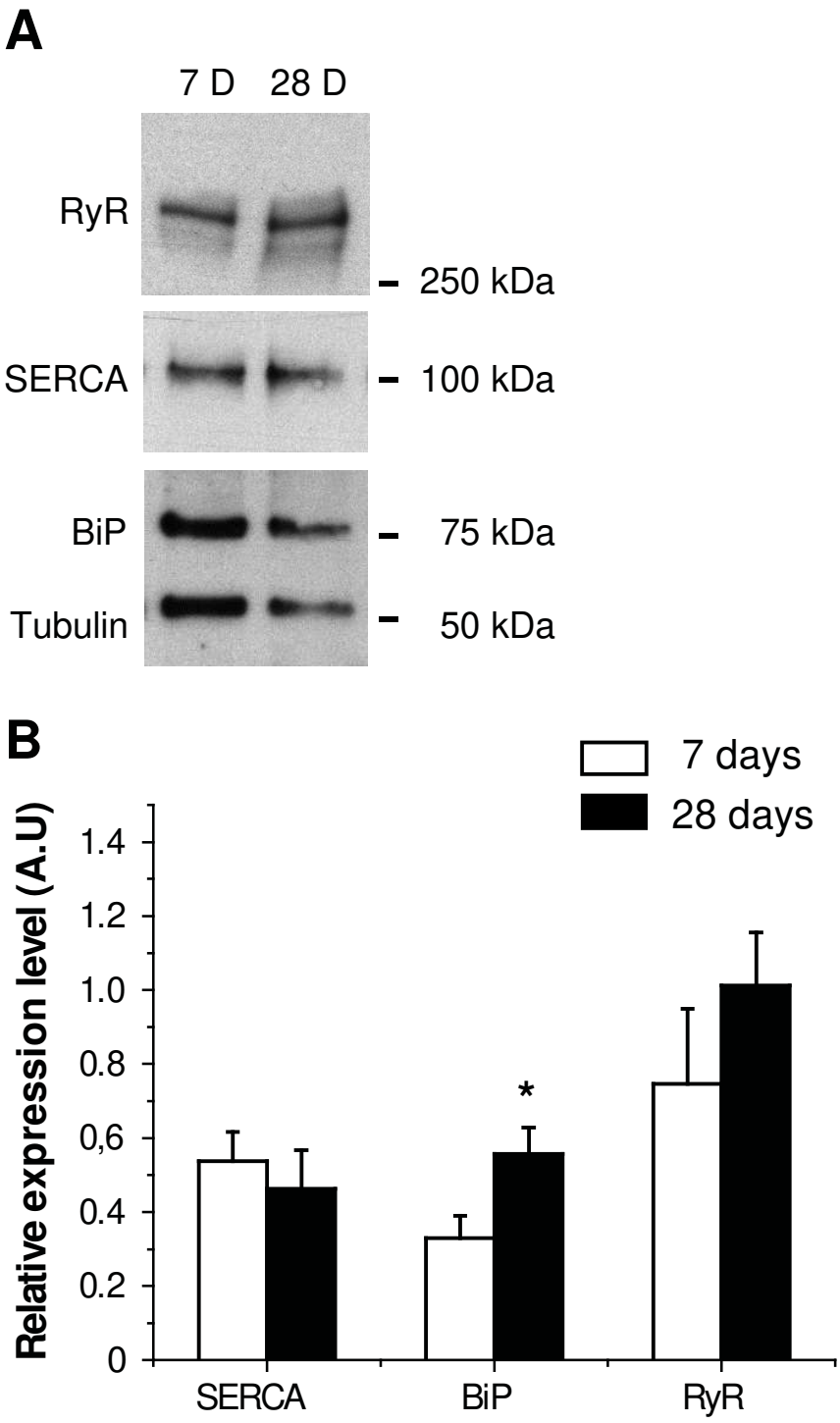

Figure 45. Protein expression levels of SERCA, RyR and BiP in *Drosophila* brain with age. A) Representative blots of the sarco/endoplasmic reticulum Ca^{2+}-ATPase (SERCA), the ryanodine receptor (RyR) and the immunoglobulin protein (BiP) expression in young (7 days) and old (28 days) DN005 flies (erGAP3 transgenic neuronal line). The whole head protein extract from one individual fly was loaded per lane, subjected to SDS-PAGE, and revealed with the specific antibodies for SERCA, RyR and BiP. Tubulin was used as the protein loading control. **B)** Quantification of multiple data similar to that shown in panel **A**. The results were normalized to tubulin expression levels. Each value is the mean ± SEM of 16-32 flies. The increase in the expression of BiP in the old flies (40%) was statistically significant (*; $p<0.05$, unpaired t-test), whereas the differences in the expression levels observed for SERCA or RyR were not statistically significant.

Discussion

Aging is associated with a decline in physiological functions, which includes loss of muscle mass and strength (sarcopenia) as one of the most prominent landmarks (Vijg and Campisi, 2008). The increase in $[Ca^{2+}]_C$ is the trigger for muscle contraction, and therefore the proposal that a loss of Ca^{2+} homeostasis might be involved in the genesis of sarcopenia, could be considered a reasonable working hypothesis. As the increase in muscle $[Ca^{2+}]_C$ is due to the sudden release of Ca^{2+} from the SR, measurement of $[Ca^{2+}]_{SR}$ seems essential to trace the mechanisms of muscle dysfunction. However, it is difficult to limit the $[Ca^{2+}]$ measurements to just the SR/ER compartment and to avoid contamination by signals from cytosol, nucleus, mitochondria or other intracellular compartments. In order to circumvent this problem, we generated a transgenic fly that expressed a genetically encoded Ca^{2+} indicator specifically targeted to the SR lumen, erGAP3. This sensor is a low affinity GAP variant that was engineered to allow accurate measurements in high $[Ca^{2+}]$ compartments without saturation (Alonso et al., 2017b). The requirement to perform these $[Ca^{2+}]_{SR}$ measurements *in vivo* made the experimental approach even more challenging. By using tools specifically developed for this project, we have attempted to check the following working hypothesis: is the age-induced sarcopenia due to a loss of Ca^{2+} homeostasis that prevents Ca^{2+} accumulation in SR? What are the mechanisms? Are these mechanisms responsible for additional features of aging?

1. *Drosophila* as a model of aging

The fruit fly *Drosophila melanogaster* has emerged as an advantageous model to study aging. The fly short lifespan is certainly a great advantage, but the availability of a large array of genetic tools to modify the fly genome is even more important. In our case, the GAL4:UAS system enabled to generate transgenic flies that express erGAP3 sensor specifically in the muscle and in the nervous system (Brand and Perrimon, 1993). The sensor also showed a correct subcellular location in the SR/ER, as verified by colocalization of erGAP3 and the SERCA immunofluorescence (**Fig. 25C, D and F**). It is worth noting that the new ϕC31 transformation system allows site specific integration in the fly genome, which improves and normalizes expression. Another advantage of this system is that the

transgenic line can be easily reproduced, which saves long periods of maintenance of the fly stocks (Bischof et al., 2007).

The survival data indicate that the expression of the sensor erGAP3 did not modify survival compared to wild type flies, as no significant differences, neither in the mean nor in the maximal longevity were observed (**Fig. 26**). However, there are many environmental factors that could alter longevity, including: diet (Bass et al., 2007), larval and pupal density (Joshi and Mueller, 1997; Sørensen and Loeschcke, 2001), temperature (Miquel et al., 1976; Linford et al., 2013), humidity and lightning (Pittendrigh and Minis, 1972). In order to avoid the possible bias introduced in the experiments by these factors, special care was taken so that these conditions were uniform along the whole lifespan studies. It has been reported that the use of CO_2 as anaesthetic may affect physiological functions under long exposure times (Bartholomew et al., 2015). To avoid this bias, the use of CO_2 as anaesthetic in the longevity studies was restricted to the selection of animals by gender after eclosion, and always limiting the exposure time to a maximum of 10 min.

Our results indicate that female flies live longer than males. In the fruit fly aging depends, among other factors, on the genotype or the mating status. For instance, it has been described that mating decreases longevity in both sexes (Malick and Kidwell, 1966). Furthermore, in most strains, virgin females live longer than virgin males, although in some minor strains it occurs the opposite (Arya et al., 2010). In order to control for this potential source of bias, female and male virgins were collected separately in the survival experiments, as they were sorted the same day of pupal eclosion. As it has been previously described in *Drosophila* (Linford et al., 2013), females live longer than males which is also the general pattern in mammals; yet these differences have not been studied extensively. There are three main hypotheses that try to explain this phenomenon (Austad and Fischer, 2016). First, the evolutionary hypothesis, that presumes that the differences in longevity patterns are due to differential vulnerability to environmental hazards. This is due to intrinsic characteristics of both sexes, for example the body size. The second is the mechanistic hypothesis that focuses on sexual hormones. These molecules may influence physiological mechanisms such as immunological responses that affect lifespan. The last theory proposes that the differences are

due to the asymmetric inheritance of sex chromosomes. This hypothesis postulates that males live less because they have only one X chromosome. Specifically, the logic of this hypothesis is that because the females possess two X chromosome copies, the phenotypic effect of sex-linked deleterious alleles can be masked by the normal alleles on the other X, whereas males have no second X chromosome to compensate for a single bad allele. In our case, $[Ca^{2+}]_{SR}$ decreased with age in both sexes in a similar manner and the differences between males and females were very small (**Fig. 39**).

Age-related sarcopenia in flies most likely reflects a decrease in muscle function rather than a loss of muscle mass. There is a lack of studies on loss of muscle mass in fruit flies with age, probably because of the difficulty to detect changes of mass in such a small organism (Piccirillo et al., 2014). However, age-related functional impairment of the muscles that causes defects in flight, climbing and locomotion ability are quite evident (Grotewiel et al., 2005; Martinez et al., 2007; Miller et al., 2008) and they can be easily measured by performing simple behavioural assays such as the climbing assay, which is a representative index of global muscle activity (Gargano et al., 2005). This assay is frequently used to measure the locomotor function in flies, and it has been reported that the decrease on climbing speed correlates negatively with age (Grotewiel et al., 2005). Loss of muscle function has also been related to inadequate innervation of motoneurons in the aging mice (Einsiedel and Luff, 1992), and a number of studies have focused on studying the neuromuscular junction in aging *Drosophila* (Beramendi et al., 2007; Martinez et al., 2007; Wagner et al., 2015). Without excluding this possibility, our results have been focussed on a muscular origin of aging associated sarcopenia. Our data showed a linear decrease of the climbing activity with age from 14 to 35 days. The climbing ability maintained quite well during the first two weeks of age, whereas it practically ceased at 35 days (**Fig. 27A**). Another parameter obtained in the climbing test was the time required for a given climbing height and this result confirmed a slower activity for the aged flies (**Fig. 27B**). The age-dependent loss of motor function that we observed correlated quite well with the age-dependent decrease of $[Ca^{2+}]_{SR}$. We propose a threshold in $[Ca^{2+}]_{SR}$ around 400 µM, below which muscle function begins to be compromised (**Fig. 40**).

2. GAP3 as a tool to measure Ca^{2+} concentration inside the sarco/endoplasmic reticulum

Our working hypothesis stated that age associated-sarcopenia is related to a decrease in the Ca^{2+} stored inside the SR. This would lead to a diminished Ca^{2+} release and the concomitant reduced $[Ca^{2+}]_C$ peak that triggers skeletal muscle contraction. The first challenge we addressed was to perform $[Ca^{2+}]_{ER}$ measurements in the living fly in a reliable manner. In previous work in our laboratory, we had engineered a Ca^{2+} sensor GAP (GFP-Aequorin Protein) to have an appropriate Ca^{2+} affinity, adequate to accurately measure $[Ca^{2+}]$ in high $[Ca^{2+}]$ organelles, such as the ER (Alonso et al., 2017b). This low affinity GAP variant was dubbed GAP3 and displays a K_D for Ca^{2+} of 489 µM. In most mammalian cell types $[Ca^{2+}]_{ER}$ has been estimated to lie between 200 and 1000 µM (Suzuki et al., 2014; Rodríguez-Prados et al., 2015). The K_D value is in the expected range of $[Ca^{2+}]_{ER}$, which means that the indicator would be far away from saturation and, hence, it would allow accurate measuring of resting $[Ca^{2+}]_{ER}$. On the other hand, the background in our model, the fly thorax, is low, and this increases the signal to noise ratio of the GAP3 indicator. Notably, the sensor exhibits a Ca^{2+}-dependent fluorescence, with two excitation peaks at 405 and 470 nm, at low and high $[Ca^{2+}]$, respectively. This enables ratiometric measurements, essential for a reliable quantification and less prone to imaging artefacts, such as those produced by movement or quenching. These artefactual changes would, in principle, affect both individual wavelengths in a similar manner and, thus, these changes would be largely cancelled out by the ratio between the two wavelengths ($R=F_{470}/F_{405}$).

The Ca^{2+}-dependent fluorescence of GAP3 follows the Hill equation, and the Hill coefficient value is 1, probably because its structure contains only one functional EF-hand. This facilitates the Ca^{2+} calibration. Moreover, this indicator is insensitive to Mg^{2+}, and to H^+ in the 6.5–8.5 pH range (Alonso et al., 2017a). The measured pH of the ER lumen is around 7.2 (Kim et al., 1998), so it is not so problematic for the fluorescence emission of GAP3 as it would be in the Golgi apparatus or the mitochondria. Finally, another advantageous property of the sensor, especially for the *in vivo* measurements, as it is the aim of this project, is its orthogonality: GFP and aequorin are both genes from the jellyfish *Aequorea victoria* and, thus, they do

not have mammalian or fly homologues. Therefore, the possibility of interaction between GAP3 and endogenous proteins in such a way as calmodulin binds to a plethora of target proteins is not expected. On the other hand, GAP3 was targeted to the lumen of the SR/ER (erGAP3), that has a specific Ca^{2+}-binding proteins and none of them is known to interact with aequorin.

Since erGAP3 is a ratiometric indicator, changes in $[Ca^{2+}]_{ER}$ should be indicated by proportional changes in the ratio ($R=F_{470}/F_{405}$). Indeed, this ER-Ca^{2+} ratio decreased significantly with age (**Fig. 28**), indicating a decrease of $[Ca^{2+}]_{SR}$, although we had to know the minimal fluorescence ratio value (R_{min}) and the dynamic range (R_{max}/R_{min}) to calculate the $[Ca^{2+}]$. The dynamic range of GAP3 measured with the purified protein *in vitro* or in permeabilized HeLa cells is 3 (Navas-Navarro et al., 2016). This value, along with K_D and the R_{min}, are necessary for calibration of the fluorescence signal into $[Ca^{2+}]$, and we shall discuss this topic below. Importantly, GAP3 itself is thermostable (T_m= 79 °C, **Fig. 37**) and preserves the ability for ratiometric measurement of $[Ca^{2+}]$ after the 10 min-heating at 50 ˚C (**Fig. 36**). As a result of the combination of these properties, the R_{min} value can be approximated by the R measurements when heating (**Fig. 31A; Fig. 33**).

3. Calibration of erGAP3 fluorescence signal into $[Ca^{2+}]_{ER}$ *in vivo*

Although changes of Ca^{2+} content of the SR/ER (increase or decrease) can be monitored from the ratio ($R= F_{470}/F_{405}$) and, therefore, the normalized data (R/R_{min}) represent a quantification of the SR Ca^{2+} content, it is important to accurately know the $[Ca^{2+}]$ to fully understand the physiological and pathological processes. However, $[Ca^{2+}]$ values are barely found in the published literature. We report in this study that $[Ca^{2+}]_{SR}$ decreases progressively with age in *Drosophila*. In order to accurately measure the $[Ca^{2+}]_{SR}$ in the flies, we developed a novel protocol to calibrate erGAP3 fluorescent signal into $[Ca^{2+}]_{SR}$ *in vivo*.

As stated above, because of the ratiometric nature of the erGAP3 measurements, computation of the Ca^{2+} concentration is feasible if R_{min}, the dynamic range (R_{max}/R_{min}), and K_D are known (Alonso et al., 2017b). Calibration of the fluorescent

signal into Ca^{2+} concentration during *in vitro* experiments is performed by completely emptying the ER at the end of each experiment and, therefore, obtaining the minimal value of fluorescence, R_{min}. The ER is completely emptied by perfusion with a "depletion cocktail" containing IP_3-producing agonists (such as ATP) in Ca^{2+}-free medium (with EGTA chelating agent) containing the SERCA inhibitor TBH. This strategy has proved to be reproducible and valid in a variety of cells and tissues *in vitro* (Navas-Navarro et al., 2016). Similar protocols based on perfusion with extracellular-like medium containing EGTA, SERCA inhibitors and/or ionophores, for obtaining the minimal fluorescence value (R_{min}) are used for calibration when measuring Ca^{2+} with either synthetic dyes or GECIs (Palmer and Tsien, 2006; Fernandez-Sanz et al., 2019). This approach is not feasible *in vivo* because the impermeable fly exoskeleton composed of chitin (poly-N-acetylglucosamine) hinders the accessibility of the Ca^{2+} indicator to the perfused extracellular-like solutions. We discovered that heating cultured cells to 50 °C provided the R_{min} value of Ca^{2+}, and this method *in vitro* was valid for different cells such as HeLa cells (**Fig. 30** and **31**), HEK cells, cortical astrocytes (**Table 7**) and myoblast C2C12 cells (**Fig. 32**). In addition, it is to be noticed that this calibration method can serve for general use for other low affinity Ca^{2+} indicators. For example, another GFP-based Ca^{2+} indicator for ER Ca^{2+} measurements (CEPIA) (Suzuki et al., 2014) could be calibrated in a similar way (**Fig. 38**). In parallel with the *in vitro* studies, the heating method proved to be valid for calibration *in vivo*. The protocol allowed to obtain the minimal value of fluorescence in the thoracic muscles, with values that were highly reproducible among individuals (**Fig. 33**). Furthermore, the depletion of the SR/ER by 50 °C-heating in different *Drosophila* tissues, such as muscle, brain or sensory wing neurons was not altered by age or gender. Altogether, the heating procedure allowed normalization of the erGAP3 fluorescent signal and provided an approximate calibration of $[Ca^{2+}]_{ER}$ *in vivo*.

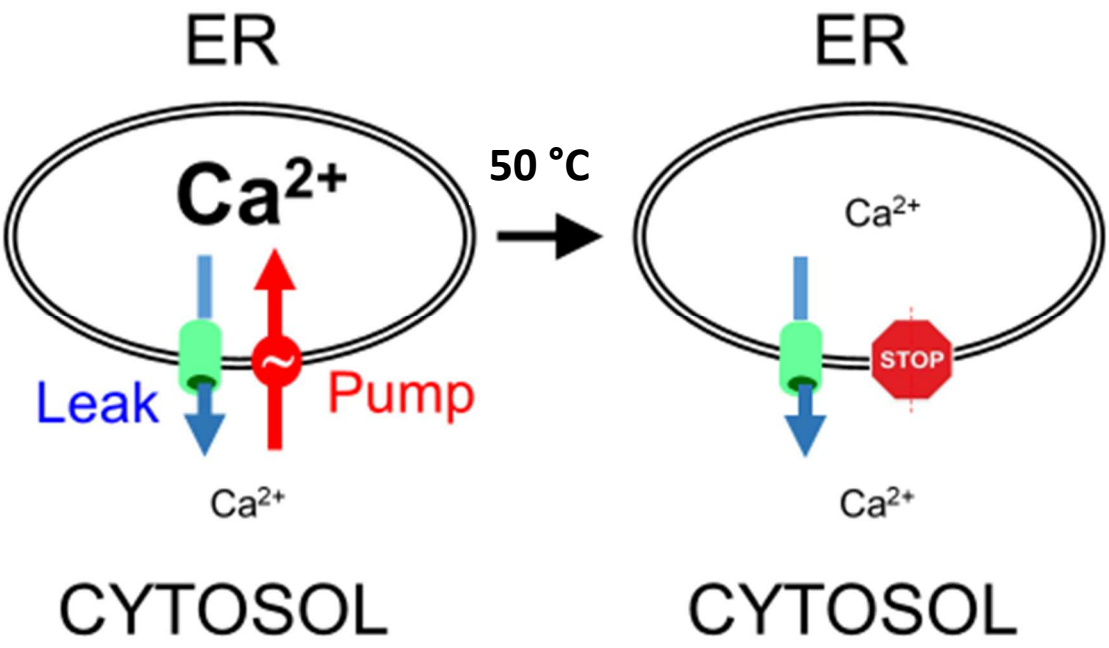

Figure 46. Mechanism for the heating effect. Illustration of the proposed heating-treatment effect on cell Ca^{2+} homeostasis. The Ca^{2+} concentration maintained inside the endoplasmic reticulum (ER) is the result of a pump/leak steady state between the sarco/endoplasmic reticulum Ca^{2+}-ATPase (SERCA)-pump (represented in red), that mediates Ca^{2+} entry; and, the ER leak (represented as a blue arrow) whose molecular nature is still unknown. SERCA has been reported to denature at 49 °C and, therefore, Ca^{2+} pumping inside the ER is abolished after heating at 50 °C (stop sign); in consequence, Ca^{2+} leaks out from the ER until the Ca^{2+} concentration gradient between ER and cytosol collapses. Surprisingly, the plasma membrane barrier seems to remain functional enough to preserve a substantial Ca^{2+} electrochemical gradient between the extracellular medium and the cytosol after heating at 50 °C.

The proposed mechanism underlying the heating effect is as follows: the $[Ca^{2+}]_{SR/ER}$ depends of the pump/leak steady state reached at the SR/ER membrane when leak (**Fig. 46**, leak shown in blue) equals pumping through SERCA (**Fig. 46**, pump shown in red). Under resting conditions, in the muscle of the young flies, at the steady-state the $[Ca^{2+}]_{ER}$ equals $3\text{-}6x10^{-4}$ (**Fig. 29**) and $[Ca^{2+}]_C$ is around 10^{-7} M, a $[Ca^{2+}]$ gradient of 3000-6000 times. SERCA has been reported to denature at 49 ˚C and, therefore, Ca^{2+} pumping inside the SR/ER is abolished after heating (Lepock et al., 1990). In this way, when the SERCA pump is blocked, $[Ca^{2+}]_{SR/ER}$ would dramatically fall to coincide with $[Ca^{2+}]_C$. In this moment, GAP3 (which is thermostable) would be completely free of Ca^{2+} and, therefore, yield the F_{min} value (**Fig. 31**). On the other hand, the expected resting $[Ca^{2+}]_C$ result of the steady-state between the PMCA and the plasma membrane

leak-in (Ca^{2+} entry from the extracellular medium), would be a low $[Ca^{2+}]_C$. This seems to be the case, as the barrier function of the plasma membrane seems to be largely preserved. As evidence for this statement, we found: 1) that the cytosolic dye Fluo-4 is retained in the cytosol after the 50 ˚C-heating (compare **Fig. 35Ai and 35Aiii**); and 2) Ca^{2+} is not entering massively into the cytosol through the plasma membrane as, otherwise it would have saturated of Fluo-4 (K_D= 335 nM; at 3000 nM $[Ca^{2+}]_C$, Fluo-4, would be 88% saturated with Ca^{2+}). Also, the resting $[Ca^{2+}]_C$ was well below F_{max}, as demonstrated by the increase of Fluo-4 signal more than 3 fold upon cell stimulation with ATP (**Fig. 35Ai and 35Aii**). On the other hand, this is consistent with the low thermic sensitivity reported for PMCA (Chambers et al., 1987). As a consequence of the treatment, $[Ca^{2+}]_C$ remains low (even below 10^{-5} M, which would be less than 1% F_{max}, **Fig. 29**). This procedure allows normalization of the GAP3 signal and approximate calibration into $[Ca^{2+}]_{ER}$.

4. The sarcoplasmic reticulum Ca^{2+} content decreases with age

The main objective of the generation of a transgenic animal expressing a Ca^{2+} sensor is to be able to perform reliable Ca^{2+} measurements *in vivo*. Given that the necessary Ca^{2+} for contraction comes from the SR, the decrease in $[Ca^{2+}]_{SR}$ observed in old animals could lead to a disruption in the excitation-contraction coupling and, thus, be implicated in the loss of muscle function characteristic of sarcopenia. For this reason, it is a challenge to measure Ca^{2+} dynamics in the SR in this physiological process. Furthermore, one of the intrinsic factors postulated in sarcopenia is a disrupted SR-Ca^{2+} handling, and our results here provided support this theory.

There are very few studies on SR Ca^{2+} content, and those existent monitored SR-Ca^{2+} only in isolated myofibers, not in the whole animal *in vivo*. Direct monitoring of SR Ca^{2+} was first performed *ex vivo* in isolated mouse skeletal myofibers using an SR-targeted ratiometric cameleon (D1ER) and two-photon confocal microscopy (Rudolf et al., 2006). The authors reported values of resting $[Ca^{2+}]_{SR}$ between 100-300 µM in adult mice and a decrease of 50 µM after electric stimulation. It should

be noted that the D1ER sensor has a dynamic range of 2 and two binding sites for Ca^{2+}, each with a different K_D value which complicates the calibration that was, in this case, extrapolated from *in situ* measurements in cultured cells. A second work also using the D1ER sensor, described a decrease in SR Ca^{2+} content in isolated mice skeletal myofibers after stimulation with the RyR agonist 4-chloro-*m*-cresol (Jiménez-Moreno et al., 2010). These authors claimed that the calibration *in vivo* was technically difficult and they did not provide any data on resting $[Ca^{2+}]_{SR}$. To obtain R_{min} they tried treating the muscle fiber with cyclopiazonic acid but the protocol did not yield a maximal SR Ca^{2+} depletion.

Regarding SR-Ca^{2+} data in the context of aging studies, it was reported that SR Ca^{2+} release declines in myofibers from aging mice (Jiménez-Moreno et al., 2008). This study was performed with Oregon Green BAPTA, a low affinity Ca^{2+} synthetic dye, injected into the cytosol via patch-clamp and, so, it did not measure the $[Ca^{2+}]_{SR.}$ In another study of the same group, now measuring resting $[Ca^{2+}]_{SR}$ in dissociated mouse myofibers, the authors did not find any variations with age, being around 500 µM, both in young and old mice (Tang et al., 2011). These measurements were performed with the low affinity Ca^{2+} indicator CatchER, an intensiometric single wavelength Ca^{2+} indicator, hence, not optimal for accurate measuring resting $[Ca^{2+}]$, and subjected to putative artefacts. The conclusion of this work was that Ca^{2+} release diminishes significantly in old mice without a decrease in resting $[Ca^{2+}]_{SR}$ These results are in clear contrast with our actual data in fly thorax muscles, which demonstrate that resting $[Ca^{2+}]_{SR}$ levels decreased progressively with age, reaching very low levels in the oldest flies, around one tenth of the baseline levels obtained in the youngest animals (**Fig. 39**).

The resting $[Ca^{2+}]_{SR}$ values we report here in the thorax muscles of young flies (7 and 14 day-old) are in the range 300-700 µM. These values are in the range (between 400 and 700 µM) of those measured with the same erGAP3 indicator in various cells types, e.g., HeLa, HEK293T and CHO cells, hippocampal neurons or astrocytes (Rodríguez-Prados et al., 2015). Furthermore, these values are also in agreement with $[Ca^{2+}]_{ER}$ values measured with other low affinity Ca^{2+} indicators. The CatchER sensor reported in HeLa, HEK-293 and C2C12 cells resting $[Ca^{2+}]_{ER}$ values of 396 ± 13 µM, 742 ± 134 µM, and 813 ± 89 µM, respectively (Tang et al., 2011); and cameleon-based ER sensors reported $[Ca^{2+}]_{ER}$ concentrations of 100–

900 µM (Palmer et al., 2004). To our knowledge this is the first report of calibrated $[Ca^{2+}]_{SR}$ measurements in the muscle *in vivo* although a recent work in *Drosophila* has demonstrated *in vivo* light-induced ER-Ca^{2+} release in fly photoreceptors using ER-GCaMP6-150 (Liu et al., 2020).

The cytosolic Ca^{2+} peaks are often used as a $[Ca^{2+}]_{ER}$ readout. From our $[Ca^{2+}]_{SR}$ data in aging muscle, it seemed likely that the rise in cytosolic Ca^{2+} would be reduced in aged muscle. For this purpose, we performed cytosolic Ca^{2+} measurements in muscles of flies expressing the Ca^{2+} indicator GCaMP, often used to measure $[Ca^{2+}]_C$ in *Drosophila* in: adult sensory neurons (Akerboom et al., 2012), the neuromuscular junction (Vonhoff and Keshishian, 2017) and, the indirect flight muscles (IFMs) (Lehmann et al., 2013; Weitkunat et al., 2017). Indeed, electrical activation of the flight muscles via the giant fiber produced a $[Ca^{2+}]_C$ transient that was significantly reduced in the old flies compared to the young (**Fig. 41**). These results validate the SR calibration method here developed and also the results obtained.

5. Mechanisms involved in the sarcoplasmic reticulum Ca^{2+} content decrease with age

The free Ca^{2+} concentration maintained inside the ER is the result of a pump/leak steady state between the SERCA pump, which mediates Ca^{2+} entry in the ER lumen, and the ER Ca^{2+} leak. Although the ultimate molecular identity of the Ca^{2+} leak remains unknown, the ER Ca^{2+} channel RyR can play a leak function in the SR membrane of the skeletal myofibers. Other key players in the maintenance of the free SR/ER Ca^{2+} concentration are the SR/ER resident calcium-binding proteins (e.g. calreticulin or calsequestrin) that act as luminal Ca^{2+} buffers. It is known that calsequestrin polymerizes into large filaments within the SR lumen, and it has been proposed that this filaments act as buffers hiding a Ca^{2+} source much larger than the free Ca^{2+} ions inside the SR/ER lumen (Wang et al., 1998; Royer and Ríos, 2009). The ER Ca^{2+} release channels can induce depolymerization of calsequestrin filaments and produce a massive release of this Ca^{2+} source (Guerrero-Hernandez et al., 2010). However, *Drosophila* lacks calsequestrin or

any homologue of it; that is, with Ca^{2+} binding properties and abundant in the muscle tissue.

We provide evidence for a small but statistically significant decrease of SERCA expression in the thorax muscles of aged flies. This decline of 35% of the SERCA protein would tend to drop $[Ca^{2+}]_{SR}$ (**Fig. 44**). However, we found that the decrease in $[Ca^{2+}]_{SR}$ with age is much larger (one tenth), so the reduced expression of SERCA cannot be the only mechanism involved. We also found a small, non-significant increase of RyR expression in aged flies, which could increase the ER leak and, therefore, decrease $[Ca^{2+}]_{SR;}$ but again, it cannot account for the ten-fold $[Ca^{2+}]_{SR}$ decrease either. Thus, we conclude that the reduction in $[Ca^{2+}]_{SR}$ must be due to an increase of the activity, the leakiness, of the leak pathway. Recent research in mammalian skeletal muscle show that, RyR1 could be the physical substrate of the increased leak, especially in the aged mice (Bellinger et al., 2008; Jiménez-Moreno et al., 2008; Andersson et al., 2011). These studies demonstrated that RyR1 suffers posttranslational modifications, such as oxidation or nitrosylation, and/or dissociation of the stabilizing protein calstabin1 (FKBP12). All these modifications increase the RyR resting conductance and, thus, render it leaky (Mei et al., 2013). However, these studies reported no decrease in RyR protein levels in aged mice, pointing out again that the parameter affected is the leakiness of the RyR rather than the expression level. A similar mechanism has been proposed in human B-lymphocytes (Kushnir et al., 2018). This hypothesis has also been tested in *Drosophila*, where defective calstabin mutant flies do not live longer but they have reduced sensitivity to the effects of age and also to oxidative stress on motor function assays (Kreko-Pierce et al., 2016).

Calsequestrin is absent in *Drosophila* muscles, therefore, we studied another CaBP resident in the ER lumen, the immunoglobulin protein BiP, also named GRP78. The BiP expression was found slightly increased in the thorax muscles of aged flies, but not significantly (**Fig. 44**). This result could indicate that UPR players are upregulated in the aging muscle of flies similarly as it has been found in mice (Hwee et al., 2014; Carreras-Sureda et al., 2018).

6. Endoplasmic reticulum Ca^{2+} concentration does not change with age in brain neurons

Ca^{2+} alterations reported in neural tissues have been studied mainly in mice, and focused on $[Ca^{2+}]_C$ alterations rather than in the ER Ca^{2+} dynamics (Thibault et al., 2007; Alzheimer's Association Calcium Hypothesis Workgroup, 2017). The "Ca^{2+} hypothesis" of aging was proposed by Khachaturian in 1994 (Khachaturian, 1994) to explain the neurophysiological mechanisms involving Ca^{2+} signalling related to aging and neurodegeneration. Several changes in channels, pumps, exchangers or mitochondria buffering capacity have been described to be altered in aging (Toescu and Vreugdenhil, 2010). However, most of these reports have used an *in vitro* system based on dissociated cultured neurons, very often isolated of new-born mice. Obviously, this model is not the optimal one to draw conclusions and to extrapolate them to an aging animal. In our study in the intact fly *in vivo*, we report that the $[Ca^{2+}]_{ER}$ measured in brain neurons remained invariable at 300-400 µM along the whole fly lifespan (**Fig. 42**) and so did SERCA levels (**Fig. 45**). There are few studies examining the effects of aging on dynamics of $[Ca^{2+}]_{ER}$, or on RyR expression. It has been proposed an increased ER Ca^{2+} release by RyR channels in aged neurons (Gant et al., 2006; Thibault et al., 2007), but RyR expression did not reveal a clear pattern (Stutzmann et al., 2006; Vanterpool et al., 2006). We found RyR levels to be increased, although not significantly, in the *Drosophila* brain with age. Dysregulated RyR expression and/or activity of RyRs may be involved in brain senescence associated with aging (Abu-Omar et al., 2018) and may also play important roles in the development of a number of neurodegenerative diseases (Vervliet, 2018). Furthermore, the RyR-mediated leakiness hypothesis was also recently proposed as an underlying mechanism in Alzheimer's disease (AD) (Lacampagne et al., 2017). As it occurs with the RyR1 in the muscle, it seems that neuronal RyR2 channels in brains of AD patients and in murine models of AD also undergo post-translational remodelling and depletion of, in this case, calstabin2 (or FBP12.6) resulting in ER Ca^{2+} leak.

The different effects of aging on skeletal muscle and brain neurons with regards to Ca^{2+} homeostasis and Ca^{2+} signalling may reflect a variation of Ca^{2+} handling among tissues. For example, amplification of the cytosolic Ca^{2+} signal by Ca^{2+}

release from the ER, a process known as Calcium Induced Calcium Release (CICR), has been reported only in some types of neurons. In general, $[Ca^{2+}]_C$ peaks in neurons are mainly due to Ca^{2+} entry from the extracellular medium through VOCCs rather than to Ca^{2+} release from the ER, whereas in the muscle the SR is the source of Ca^{2+} during muscle contraction.

A further difference between muscle cells and neurons may arise from the presence of CaBPs that can shape the Ca^{2+} transients, as demonstrated in mammalian muscle (Sztretye et al., 2011; Manno et al., 2017; Ríos, 2018). However, we found that the behaviour can vary in various types of neurons, as we can also appreciate a decrease in the $[Ca^{2+}]_{ER}$ of the sensory wing neurons (**Fig. 45**), similar to what is happening in the skeletal muscle. This may be due to differential Ca^{2+} channel toolkit among neurons, that in turn, can also be triggered either by changes of membrane potential or by extracellular or intracellular messengers. It has also been shown that $[Ca^{2+}]_{ER}$ and $[Ca^{2+}]_{GO}$ are reduced in Alzheimer's disease in fibroblast from patients, cell lines and rat primary neurons (Zatti et al., 2006) and in *Drosophila* cholinergic neurons expressing mutant presenilin (Michno et al., 2009). Furthermore, as in mammals, the flies mechanisms for regulation of intracellular Ca^{2+} peaks can differ in different regions of the nervous system (Chorna and Hasan, 2012).

Conclusions

1. We have designed and generated two transgenic lines of *Drosophila melanogaster* that express the ratiometric low affinity Ca^{2+} indicator erGAP3 in muscle cells or neurons. erGAP3 expression was specifically localized in the endoplasmic reticulum of each targeted tissue. The expression was robust, as the erGAP3 protein levels remained constant in each fly line, along the fly life and, also, across generations, with no signs of mislocalization. Importantly, erGAP3 expression did not alter longevity parameters compared to wild type flies.

2. We have designed and developed a new method for measuring endoplasmic reticulum Ca^{2+} concentration in different fly tissues *in vivo* for erGAP3 sensor. The calibration of erGAP3 fluorescent signal into endoplasmic reticulum Ca^{2+} concentration is achieved by complete Ca^{2+} depletion of the endoplasmic reticulum when heating at 50 °C and, thus, reaching the minimal fluorescence value (F_{min}). The measurements were reproducible from cell to cell, from batch to batch, and among tissues. Importantly, GAP3 protein maintained its structure and functionality after heating. This method can also be used for other low affinity Ca^{2+} indicators.

3. We have demonstrated that *in vivo* resting sarcoplasmic reticulum Ca^{2+} concentration decreases progressive and significantly along fly aging in skeletal muscle. The resting value of the sarcoplasmic reticulum Ca^{2+} concentration was about 600 µM in young flies and dropped dramatically, to one tenth of this concentration, 50 µM, in the old flies. There is a strong correlation between sarcoplasmic reticulum Ca^{2+} concentration decrease and loss of muscle function. We observed that there is a threshold around 400 µM, below which both sarcoplasmic reticulum Ca^{2+} concentration and muscle function collapsed with very similar time courses.

4. The reduction in sarcoplasmic reticulum Ca^{2+} concentration in the old flies correlated with a large reduction in the cytosolic Ca^{2+} transients, triggered by activation of the muscles via the giant fiber system and reported by the cytosolic Ca^{2+} indicator GCaMP.

5. SERCA protein levels were significantly reduced in the old fly skeletal muscle, although the drop, of only 35%, cannot account for the sarcoplasmic reticulum Ca^{2+} concentration decrease of more than 600%. The expression levels of RyR protein were 10% increased with aging but, again, such a small increase could not explain the huge decrease of the sarcoplasmic reticulum Ca^{2+} concentration. Our data are compatible with an increase of the activity, the leakiness, of the leak pathway in the old flies.

6. The underlying mechanism of sarcopenia in the old skeletal muscle is consistent with the following: first, the increase in the leakiness of the RyR causes the decrease in the sarcoplasmic reticulum Ca^{2+} concentration; second, Ca^{2+} leaks out from the sarcoplasmic reticulum until the Ca^{2+} concentration gradient between sarcoplasmic reticulum and cytosol collapses; third, the decrease in the sarcoplasmic reticulum Ca^{2+} concentration reduces sarcoplasmic reticulum Ca^{2+} release during muscle activation and, thus, decreases the Ca^{2+} cytosolic peak; and, forth, the reduced Ca^{2+} cytosolic peak compromises the strength of the muscle twitch. These findings suggest that sarcopenia would benefit from clinical treatments that reduce RyR leakiness at resting conditions.

7. Resting endoplasmic reticulum Ca^{2+} concentration does not change in aging brain neurons, suggesting that the mechanism described for skeletal muscle aging is tissue-specific. However, in the wing sensory neurons the tendency is very similar to that in the muscle and, endoplasmic reticulum Ca^{2+} concentration resting levels decrease progressively with age, indicating that the mechanisms for regulation of Ca^{2+} homeostasis can vary in different regions of the nervous system.

Bibliography

Abeele, F.V., Bidaux, G., Gordienko, D., Beck, B., Panchin, Y.V., Baranova, A.V., Ivanov, D.V., Skryma, R., Prevarskaya, N., 2006. Functional implications of calcium permeability of the channel formed by pannexin 1. J Cell Biol 174, 535–546.

Abu-Omar, N., Das, J., Szeto, V., Feng, Z.-P., 2018. Neuronal Ryanodine Receptors in Development and Aging. Mol. Neurobiol. 55, 1183–1192.

Adams, M.D., Celniker, S.E., Holt, R.A., Evans, C.A., Gocayne, J.D., Amanatides, P.G., Scherer, S.E., Li, P.W., Hoskins, R.A., Galle, R.F., George, R.A., Lewis, S.E., Richards, S., Ashburner, M., Henderson, S.N., Sutton, G.G., Wortman, J.R., Yandell, M.D., Zhang, Q., Chen, L.X., Brandon, R.C., Rogers, Y.H., Blazej, R.G., Champe, M., Pfeiffer, B.D., Wan, K.H., Doyle, C., Baxter, E.G., Helt, G., Nelson, C.R., Gabor, G.L., Abril, J.F., Agbayani, A., An, H.J., Andrews-Pfannkoch, C., Baldwin, D., Ballew, R.M., Basu, A., Baxendale, J., Bayraktaroglu, L., Beasley, E.M., Beeson, K.Y., Benos, P.V., Berman, B.P., Bhandari, D., Bolshakov, S., Borkova, D., Botchan, M.R., Bouck, J., Brokstein, P., Brottier, P., Burtis, K.C., Busam, D.A., Butler, H., Cadieu, E., Center, A., Chandra, I., Cherry, J.M., Cawley, S., Dahlke, C., Davenport, L.B., Davies, P., de Pablos, B., Delcher, A., Deng, Z., Mays, A.D., Dew, I., Dietz, S.M., Dodson, K., Doup, L.E., Downes, M., Dugan-Rocha, S., Dunkov, B.C., Dunn, P., Durbin, K.J., Evangelista, C.C., Ferraz, C., Ferriera, S., Fleischmann, W., Fosler, C., Gabrielian, A.E., Garg, N.S., Gelbart, W.M., Glasser, K., Glodek, A., Gong, F., Gorrell, J.H., Gu, Z., Guan, P., Harris, M., Harris, N.L., Harvey, D., Heiman, T.J., Hernandez, J.R., Houck, J., Hostin, D., Houston, K.A., Howland, T.J., Wei, M.H., Ibegwam, C., Jalali, M., Kalush, F., Karpen, G.H., Ke, Z., Kennison, J.A., Ketchum, K.A., Kimmel, B.E., Kodira, C.D., Kraft, C., Kravitz, S., Kulp, D., Lai, Z., Lasko, P., Lei, Y., Levitsky, A.A., Li, J., Li, Z., Liang, Y., Lin, X., Liu, X., Mattei, B., McIntosh, T.C., McLeod, M.P., McPherson, D., Merkulov, G., Milshina, N.V., Mobarry, C., Morris, J., Moshrefi, A., Mount, S.M., Moy, M., Murphy, B., Murphy, L., Muzny, D.M., Nelson, D.L., Nelson, D.R., Nelson, K.A., Nixon, K., Nusskern, D.R., Pacleb, J.M., Palazzolo, M., Pittman, G.S., Pan, S., Pollard, J., Puri, V., Reese, M.G., Reinert, K., Remington, K., Saunders, R.D., Scheeler, F., Shen, H., Shue, B.C., Sidén-Kiamos, I., Simpson, M., Skupski, M.P., Smith, T., Spier, E., Spradling, A.C., Stapleton, M., Strong, R., Sun, E., Svirskas, R., Tector, C., Turner, R., Venter, E., Wang, A.H., Wang, X., Wang, Z.Y., Wassarman, D.A., Weinstock, G.M., Weissenbach, J., Williams, S.M., WoodageT, null, Worley, K.C., Wu, D., Yang, S., Yao, Q.A., Ye, J., Yeh, R.F., Zaveri, J.S., Zhan, M., Zhang, G., Zhao, Q., Zheng, L., Zheng, X.H., Zhong, F.N., Zhong, W., Zhou, X., Zhu, S., Zhu, X., Smith, H.O., Gibbs, R.A., Myers, E.W., Rubin, G.M., Venter, J.C., 2000. The genome sequence of Drosophila melanogaster. Science 287, 2185–2195.

Akerboom, J., Carreras Calderón, N., Tian, L., Wabnig, S., Prigge, M., Tolö, J., Gordus, A., Orger, M.B., Severi, K.E., Macklin, J.J., Patel, R., Pulver, S.R., Wardill, T.J., Fischer, E., Schüler, C., Chen, T.-W., Sarkisyan, K.S., Marvin, J.S., Bargmann, C.I., Kim, D.S., Kügler, S., Lagnado, L., Hegemann, P., Gottschalk, A., Schreiter, E.R., Looger, L.L., 2013. Genetically encoded calcium indicators for multi-color neural activity imaging and combination with optogenetics. Front Mol Neurosci 6, 2.

Akerboom, J., Chen, T.-W., Wardill, T.J., Tian, L., Marvin, J.S., Mutlu, S., Calderón, N.C., Esposti, F., Borghuis, B.G., Sun, X.R., Gordus, A., Orger, M.B., Portugues, R., Engert, F., Macklin, J.J., Filosa, A., Aggarwal, A., Kerr, R.A., Takagi, R., Kracun, S., Shigetomi, E., Khakh, B.S., Baier, H., Lagnado, L., Wang, S.S.-H., Bargmann, C.I., Kimmel, B.E., Jayaraman, V., Svoboda, K., Kim, D.S., Schreiter, E.R., Looger, L.L., 2012. Optimization of a GCaMP Calcium Indicator for Neural Activity Imaging. J Neurosci 32, 13819–13840.

Allen, D.G., Lamb, G.D., Westerblad, H., 2008. Skeletal muscle fatigue: cellular mechanisms. Physiol. Rev. 88, 287–332.

Allen, M.J., Godenschwege, T.A., 2010. Electrophysiological recordings from the Drosophila giant fiber system (GFS). Cold Spring Harb Protoc 2010, pdb.prot5453.

Alonso, M.T., Barrero, M.J., Carnicero, E., Montero, M., Garcia-Sancho, J., Alvarez, J., 1998. Functional measurements of [Ca2+] in the endoplasmic reticulum using a herpes virus to deliver targeted aequorin. Cell Calcium 24, 87–96.

Alonso, M.T., Rodríguez-Prados, M., Navas-Navarro, P., Rojo-Ruiz, J., García-Sancho, J., 2017a. Using aequorin probes to measure Ca2+ in intracellular organelles. Cell Calcium 64, 3–11.

Alonso, M.T., Rojo-Ruiz, J., Navas-Navarro, P., Rodríguez-Prados, M., García-Sancho, J., 2017b. Measuring Ca2+ inside intracellular organelles with luminescent and fluorescent aequorin-based sensors. Biochim Biophys Acta Mol Cell Res 1864, 894–899.

Altun, M., Besche, H.C., Overkleeft, H.S., Piccirillo, R., Edelmann, M.J., Kessler, B.M., Goldberg, A.L., Ulfhake, B., 2010. Muscle wasting in aged, sarcopenic rats is associated with enhanced activity of the ubiquitin proteasome pathway. J. Biol. Chem. 285, 39597–39608.

Alzheimer's Association Calcium Hypothesis Workgroup, 2017. Calcium Hypothesis of Alzheimer's disease and brain aging: A framework for integrating new evidence into a comprehensive theory of pathogenesis. Alzheimers Dement 13, 178-182.e17.

Ambudkar, I.S., de Souza, L.B., Ong, H.L., 2017. TRPC1, Orai1, and STIM1 in SOCE: Friends in tight spaces. Cell Calcium 63, 33–39.

Andersson, D.C., Betzenhauser, M.J., Reiken, S., Meli, A.C., Umanskaya, A., Xie, W., Shiomi, T., Zalk, R., Lacampagne, A., Marks, A.R., 2011. Ryanodine receptor oxidation causes intracellular calcium leak and muscle weakness in aging. Cell Metab. 14, 196–207.

Ansved, T., Larsson, L., 1990. Quantitative and qualitative morphological properties of the soleus motor nerve and the L5 ventral root in young and old rats. Relation to the number of soleus muscle fibers. J. Neurol. Sci. 96, 269–282.

Arking, R., Wells, R.A., 1990. Genetic alteration of normal aging processes is responsible for extended longevity in Drosophila. Dev. Genet. 11, 141–148.

Arya, G.H., Weber, A.L., Wang, P., Magwire, M.M., Negron, Y.L.S., Mackay, T.F.C., Anholt, R.R.H., 2010. Natural variation, functional pleiotropy and transcriptional contexts of odorant binding protein genes in Drosophila melanogaster. Genetics 186, 1475–1485.

Augustin, H., Partridge, L., 2009. Invertebrate models of age-related muscle degeneration. Biochim. Biophys. Acta 1790, 1084–1094.

Aulestia, F.J., Alonso, M.T., García-Sancho, J., 2015. Differential calcium handling by the cis and trans regions of the Golgi apparatus. Biochem. J. 466, 455–465.

Austad, S.N., Fischer, K.E., 2016. Sex Differences in Lifespan. Cell Metab. 23, 1022–1033.

Baehr, L.M., West, D.W.D., Marcotte, G., Marshall, A.G., De Sousa, L.G., Baar, K., Bodine, S.C., 2016. Age-related deficits in skeletal muscle recovery following disuse are associated with neuromuscular junction instability and ER stress, not impaired protein synthesis. Aging (Albany NY) 8, 127–146.

Bai, J., Binari, R., Ni, J.-Q., Vijayakanthan, M., Li, H.-S., Perrimon, N., 2008. RNA interference screening in Drosophila primary cells for genes involved in muscle assembly and maintenance. Development 135, 1439–1449.

Barrero, M.J., Montero, M., Alvarez, J., 1997. Dynamics of [Ca2+] in the endoplasmic reticulum and cytoplasm of intact HeLa cells. A comparative study. J. Biol. Chem. 272, 27694–27699.

Barritt, G.J., 1999. Receptor-activated Ca2+ inflow in animal cells: a variety of pathways tailored to meet different intracellular Ca2+ signalling requirements. Biochem. J. 337 (Pt 2), 153–169.

Bartholomew, N.R., Burdett, J.M., VandenBrooks, J.M., Quinlan, M.C., Call, G.B., 2015. Impaired climbing and flight behaviour in Drosophila melanogaster following carbon dioxide anaesthesia. Sci Rep 5, 15298.

Bass, T.M., Grandison, R.C., Wong, R., Martinez, P., Partridge, L., Piper, M.D.W., 2007. Optimization of dietary restriction protocols in Drosophila. J. Gerontol. A Biol. Sci. Med. Sci. 62, 1071–1081.

Batelli, S., Kremer, M., Jung, C., Gaul, U., 2017. Application of MultiColor FlpOut Technique to Study High Resolution Single Cell Morphologies and Cell Interactions of Glia in Drosophila. J Vis Exp.

Baughman, J.M., Perocchi, F., Girgis, H.S., Plovanich, M., Belcher-Timme, C.A., Sancak, Y., Bao, X.R., Strittmatter, L., Goldberger, O., Bogorad, R.L., Koteliansky, V., Mootha, V.K., 2011. Integrative genomics identifies MCU as an essential component of the mitochondrial calcium uniporter. Nature 476, 341–345.

Bellinger, A.M., Reiken, S., Carlson, C., Mongillo, M., Liu, X., Rothman, L., Matecki, S., Lacampagne, A., Marks, A.R., 2009. Hypernitrosylated ryanodine receptor calcium release channels are leaky in dystrophic muscle. Nat. Med. 15, 325–330.

Bellinger, A.M., Reiken, S., Dura, M., Murphy, P.W., Deng, S.-X., Landry, D.W., Nieman, D., Lehnart, S.E., Samaru, M., LaCampagne, A., Marks, A.R., 2008. Remodeling of ryanodine receptor complex causes "leaky" channels: a molecular mechanism for decreased exercise capacity. Proc. Natl. Acad. Sci. U.S.A. 105, 2198–2202.

Beramendi, A., Peron, S., Casanova, G., Reggiani, C., Cantera, R., 2007. Neuromuscular junction in abdominal muscles of Drosophila melanogaster during adulthood and aging. J. Comp. Neurol. 501, 498–508.

Berridge, M.J., 2016. The Inositol Trisphosphate/Calcium Signaling Pathway in Health and Disease 96, 1261–1296.

Berridge, M.J., 2012. Calcium signalling remodelling and disease. Biochem. Soc. Trans. 40, 297–309.

Berridge, M.J., 2009. Inositol trisphosphate and calcium signalling mechanisms. Biochim. Biophys. Acta 1793, 933–940.

Berridge, M.J., 1997. Elementary and global aspects of calcium signalling. J. Physiol. (Lond.) 499 (Pt 2), 291–306.

Berridge, M.J., Bootman, M.D., Roderick, H.L., 2003. Calcium signalling: dynamics, homeostasis and remodelling. Nat. Rev. Mol. Cell Biol. 4, 517–529.

Bezprozvanny, I., Watras, J., Ehrlich, B.E., 1991. Bell-shaped calcium-response curves of Ins(1,4,5)P3- and calcium-gated channels from endoplasmic reticulum of cerebellum. Nature 351, 751–754.

Biressi, S., Rando, T.A., 2010. Heterogeneity in the muscle satellite cell population. Semin. Cell Dev. Biol. 21, 845–854.

Bischof, J., Maeda, R.K., Hediger, M., Karch, F., Basler, K., 2007. An optimized transgenesis system for Drosophila using germ-line-specific phiC31 integrases. Proc. Natl. Acad. Sci. U.S.A. 104, 3312–3317.

Bokov, A., Chaudhuri, A., Richardson, A., 2004. The role of oxidative damage and stress in aging. Mech. Ageing Dev. 125, 811–826.

Brand, A.H., Perrimon, N., 1993. Targeted gene expression as a means of altering cell fates and generating dominant phenotypes. Development 118, 401–415.

Brandt, A., Krohne, G., Grosshans, J., 2008. The farnesylated nuclear proteins KUGELKERN and LAMIN B promote aging-like phenotypes in Drosophila flies. Aging Cell 7, 541–551.

Bravo, R., Vicencio, J.M., Parra, V., Troncoso, R., Munoz, J.P., Bui, M., Quiroga, C., Rodriguez, A.E., Verdejo, H.E., Ferreira, J., Iglewski, M., Chiong, M., Simmen, T., Zorzano, A., Hill, J.A., Rothermel, B.A., Szabadkai, G., Lavandero, S., 2011. Increased ER-mitochondrial coupling promotes mitochondrial respiration and bioenergetics during early phases of ER stress. J. Cell. Sci. 124, 2143–2152.

Breen, L., Phillips, S.M., 2011. Skeletal muscle protein metabolism in the elderly: Interventions to counteract the "anabolic resistance" of ageing. Nutr Metab (Lond) 8, 68.

Brillantes, A.B., Ondrias, K., Scott, A., Kobrinsky, E., Ondriasová, E., Moschella, M.C., Jayaraman, T., Landers, M., Ehrlich, B.E., Marks, A.R., 1994. Stabilization of calcium release channel (ryanodine receptor) function by FK506-binding protein. Cell 77, 513–523.

Brini, M., Carafoli, E., 2011. The plasma membrane Ca^{2}+ ATPase and the plasma membrane sodium calcium exchanger cooperate in the regulation of cell calcium. Cold Spring Harb Perspect Biol 3.

Brini, M., Carafoli, E., 2009. Calcium pumps in health and disease. Physiol. Rev. 89, 1341–1378.

Brody, I.A., 1976. Regulation of isometric contraction in skeletal muscle. Exp. Neurol. 50, 673–683.

Brunk, U.T., Terman, A., 2002. Lipofuscin: mechanisms of age-related accumulation and influence on cell function. Free Radic. Biol. Med. 33, 611–619.

Bultynck, G., Kiviluoto, S., Henke, N., Ivanova, H., Schneider, L., Rybalchenko, V., Luyten, T., Nuyts, K., De Borggraeve, W., Bezprozvanny, I., Parys, J.B., De Smedt, H., Missiaen, L., Methner, A., 2012. The C terminus of Bax inhibitor-1 forms a Ca2+-permeable channel pore. J. Biol. Chem. 287, 2544–2557.

Cagan, R., 2009. Principles of Drosophila eye differentiation. Curr. Top. Dev. Biol. 89, 115–135.

Calvo-Rodríguez, M., García-Durillo, M., Villalobos, C., Núñez, L., 2016. In vitro aging promotes endoplasmic reticulum (ER)-mitochondria Ca2+ cross talk and loss of store-operated Ca2+ entry (SOCE) in rat hippocampal neurons. Biochim. Biophys. Acta 1863, 2637–2649.

Camello, C., Lomax, R., Petersen, O.H., Tepikin, A.V., 2002. Calcium leak from intracellular stores--the enigma of calcium signalling. Cell Calcium 32, 355–361.

Campbell, L.W., Hao, S.Y., Thibault, O., Blalock, E.M., Landfield, P.W., 1996. Aging changes in voltage-gated calcium currents in hippocampal CA1 neurons. J. Neurosci. 16, 6286–6295.

Carafoli, E., Garcia-Martin, E., Guerini, D., 1996. The plasma membrane calcium pump: recent developments and future perspectives. Experientia 52, 1091–1100.

Carreras-Sureda, A., Pihán, P., Hetz, C., 2018. Calcium signaling at the endoplasmic reticulum: fine-tuning stress responses. Cell Calcium 70, 24–31.

Catterall, W.A., 2011. Voltage-gated calcium channels. Cold Spring Harb Perspect Biol 3, a003947.

Chakraborty, S., Bartussek, J., Fry, S.N., Zapotocky, M., 2015. Independently controlled wing stroke patterns in the fruit fly Drosophila melanogaster. PLoS ONE 10, e0116813.

Chalil, S., Pierre, N., Bakker, A.D., Manders, R.J., Pletsers, A., Francaux, M., Klein-Nulend, J., Jaspers, R.T., Deldicque, L., 2015. Aging related ER stress is not responsible for anabolic resistance in mouse skeletal muscle. Biochem. Biophys. Res. Commun. 468, 702–707.

Chambers, J.P., Wayner, M.J., Rizopoulos, E., Gonzales, M.L., Taylor, R.B., Valdes, J.J., 1987. Partial characterization of two (Ca+2 + Mg+2)-dependent ATPase activities from bovine brain synaptic membrane homogenates. Brain Res. Bull. 18, 99–107.

Chandran, R., Kumar, M., Kesavan, L., Jacob, R.S., Gunasekaran, S., Lakshmi, S., Sadasivan, C., Omkumar, R.V., 2019. Cellular calcium signaling in the aging brain. J. Chem. Neuroanat. 95, 95–114.

Chaturvedi, D., Reichert, H., Gunage, R.D., VijayRaghavan, K., 2017. Identification and functional characterization of muscle satellite cells in Drosophila. Elife 6.

Chavous, D.A., Jackson, F.R., O'Connor, C.M., 2001. Extension of the Drosophila lifespan by overexpression of a protein repair methyltransferase. Proc. Natl. Acad. Sci. U.S.A. 98, 14814–14818.

Chen, T.-W., Wardill, T.J., Sun, Y., Pulver, S.R., Renninger, S.L., Baohan, A., Schreiter, E.R., Kerr, R.A., Orger, M.B., Jayaraman, V., Looger, L.L., Svoboda, K., Kim, D.S., 2013. Ultrasensitive fluorescent proteins for imaging neuronal activity. Nature 499, 295–300.

Chin, D., Means, A.R., 2000. Calmodulin: a prototypical calcium sensor. Trends Cell Biol. 10, 322–328.

Chorna, T., Hasan, G., 2012. The genetics of calcium signaling in Drosophila melanogaster. Biochim. Biophys. Acta 1820, 1269–1282.

Clancy, D.J., Gems, D., Hafen, E., Leevers, S.J., Partridge, L., 2002. Dietary restriction in long-lived dwarf flies. Science 296, 319.

Clapham, D.E., 2007. Calcium signaling. Cell 131, 1047–1058.

Cochemé, H.M., Quin, C., McQuaker, S.J., Cabreiro, F., Logan, A., Prime, T.A., Abakumova, I., Patel, J.V., Fearnley, I.M., James, A.M., Porteous, C.M., Smith, R.A.J., Saeed, S., Carré, J.E., Singer, M., Gems, D., Hartley, R.C., Partridge, L., Murphy, M.P., 2011. Measurement of H2O2 within living Drosophila during aging using a ratiometric mass spectrometry probe targeted to the mitochondrial matrix. Cell Metab. 13, 340–350.

Crameri, A., Whitehorn, E.A., Tate, E., Stemmer, W.P., 1996. Improved green fluorescent protein by molecular evolution using DNA shuffling. Nat. Biotechnol. 14, 315–319.

Cristea, A., Qaisar, R., Edlund, P.K., Lindblad, J., Bengtsson, E., Larsson, L., 2010. Effects of aging and gender on the spatial organization of nuclei in single human skeletal muscle cells. Aging Cell 9, 685–697.

Crompton, M., Künzi, M., Carafoli, E., 1977. The calcium-induced and sodium-induced effluxes of calcium from heart mitochondria. Evidence for a sodium-calcium carrier. Eur. J. Biochem. 79, 549–558.

Csordás, G., Renken, C., Várnai, P., Walter, L., Weaver, D., Buttle, K.F., Balla, T., Mannella, C.A., Hajnóczky, G., 2006. Structural and functional features and significance of the physical linkage between ER and mitochondria. J. Cell Biol. 174, 915–921.

Davidovic, M., Sevo, G., Svorcan, P., Milosevic, D.P., Despotovic, N., Erceg, P., 2010. Old age as a privilege of the "selfish ones." Aging Dis 1, 139–146.

de la Fuente, S., Fonteriz, R.I., Montero, M., Alvarez, J., 2013. Ca2+ homeostasis in the endoplasmic reticulum measured with a new low-Ca2+-affinity targeted aequorin. Cell Calcium 54, 37–45.

De Stefani, D., Raffaello, A., Teardo, E., Szabò, I., Rizzuto, R., 2011. A forty-kilodalton protein of the inner membrane is the mitochondrial calcium uniporter. Nature 476, 336–340.

Delbono, O., 2003. Neural control of aging skeletal muscle. Aging Cell 2, 21–29.

Demaurex, N., Lew, D.P., Krause, K.H., 1992. Cyclopiazonic acid depletes intracellular Ca2+ stores and activates an influx pathway for divalent cations in HL-60 cells. J. Biol. Chem. 267, 2318–2324.

Demontis, F., Perrimon, N., 2010. FOXO/4E-BP signaling in Drosophila muscles regulates organism-wide proteostasis during aging. Cell 143, 813–825.

Demontis, F., Piccirillo, R., Goldberg, A.L., Perrimon, N., 2013. Mechanisms of skeletal muscle aging: insights from Drosophila and mammalian models. Dis Model Mech 6, 1339–1352.

DiAntonio, A., 2006. Glutamate receptors at the Drosophila neuromuscular junction. Int. Rev. Neurobiol. 75, 165–179.

Dickinson, M.H., Lighton, J.R., 1995. Muscle efficiency and elastic storage in the flight motor of Drosophila. Science 268, 87–90.

DiPolo, R., Beaugé, L., 2006. Sodium/calcium exchanger: influence of metabolic regulation on ion carrier interactions. Physiol. Rev. 86, 155–203.

Doherty, K.R., McNally, E.M., 2003. Repairing the tears: dysferlin in muscle membrane repair. Trends Mol Med 9, 327–330.

Drago, I., Davis, R.L., 2016. Inhibiting the Mitochondrial Calcium Uniporter during Development Impairs Memory in Adult Drosophila. Cell Rep 16, 2763–2776.

Dubyak, G.R., el-Moatassim, C., 1993. Signal transduction via P2-purinergic receptors for extracellular ATP and other nucleotides. Am. J. Physiol. 265, C577-606.

Duffy, J.B., 2002. GAL4 system in Drosophila: a fly geneticist's Swiss army knife. Genesis 34, 1–15.

Eberl, D.F., Ren, D., Feng, G., Lorenz, L.J., Vactor, D.V., Hall, L.M., 1998. Genetic and Developmental Characterization of Dmca1D, a Calcium Channel α1 Subunit Gene in Drosophila melanogaster. Genetics 148, 1159–1169.

Efremov, R.G., Leitner, A., Aebersold, R., Raunser, S., 2015. Architecture and conformational switch mechanism of the ryanodine receptor. Nature 517, 39–43.

Einsiedel, L.J., Luff, A.R., 1992. Effect of partial denervation on motor units in the ageing rat medial gastrocnemius. J. Neurol. Sci. 112, 178–184.

Evans, D.S., Kapahi, P., Hsueh, W.-C., Kockel, L., 2011. TOR signaling never gets old: aging, longevity and TORC1 activity. Ageing Res. Rev. 10, 225–237.

Fabiato, A., 1983. Calcium-induced release of calcium from the cardiac sarcoplasmic reticulum. Am. J. Physiol. 245, C1-14.

Fang, Y., Bonini, N.M., 2015. Hope on the (fruit) fly: the Drosophila wing paradigm of axon injury. Neural Regen Res 10, 173–175.

Ferguson, M., Mockett, R.J., Shen, Y., Orr, W.C., Sohal, R.S., 2005. Age-associated decline in mitochondrial respiration and electron transport in Drosophila melanogaster. Biochem. J. 390, 501–511.

Fernandez-Sanz, C., De la Fuente, S., Sheu, S.-S., 2019. Mitochondrial Ca2+ concentrations in live cells: quantification methods and discrepancies. FEBS Lett. 593, 1528–1541.

Feske, S., Gwack, Y., Prakriya, M., Srikanth, S., Puppel, S.-H., Tanasa, B., Hogan, P.G., Lewis, R.S., Daly, M., Rao, A., 2006. A mutation in Orai1 causes immune deficiency by abrogating CRAC channel function. Nature 441, 179–185.

Fill, M., Copello, J.A., 2002. Ryanodine receptor calcium release channels. Physiol. Rev. 82, 893–922.

Foskett, J.K., 2010. Inositol trisphosphate receptor Ca2+ release channels in neurological diseases. Pflugers Arch. 460, 481–494.

Friedman, J.R., Voeltz, G.K., 2011. The ER in 3D: a multifunctional dynamic membrane network. Trends Cell Biol. 21, 709–717.

Friel, D.D., Tsien, R.W., 1992. A caffeine- and ryanodine-sensitive Ca2+ store in bullfrog sympathetic neurones modulates effects of Ca2+ entry on [Ca2+]i. J. Physiol. (Lond.) 450, 217–246.

Fuglevand, A.J., 2011. Mechanical properties and neural control of human hand motor units. J. Physiol. (Lond.) 589, 5595–5602.

Furuichi, T., Yoshikawa, S., Miyawaki, A., Wada, K., Maeda, N., Mikoshiba, K., 1989. Primary structure and functional expression of the inositol 1,4,5-trisphosphate-binding protein P400. Nature 342, 32–38.

Gallego-Sandín, S., Alonso, M.T., García-Sancho, J., 2011. Calcium homoeostasis modulator 1 (CALHM1) reduces the calcium content of the endoplasmic reticulum (ER) and triggers ER stress. Biochem. J. 437, 469–475.

Gant, J.C., Sama, M.M., Landfield, P.W., Thibault, O., 2006. Early and simultaneous emergence of multiple hippocampal biomarkers of aging is mediated by Ca2+-induced Ca2+ release. J. Neurosci. 26, 3482–3490.

Gao, S., Sandstrom, D.J., Smith, H.E., High, B., Marsh, J.W., Nash, H.A., 2013. Drosophila ryanodine receptors mediate general anesthesia by halothane. Anesthesiology 118, 587–601.

Gargano, J.W., Martin, I., Bhandari, P., Grotewiel, M.S., 2005. Rapid iterative negative geotaxis (RING): a new method for assessing age-related locomotor decline in Drosophila. Exp. Gerontol. 40, 386–395.

Gees, M., Owsianik, G., Nilius, B., Voets, T., 2012. TRP channels. Compr Physiol 2, 563–608.

Ghartey-Kwansah, G., Li, Z., Feng, R., Wang, L., Zhou, X., Chen, F.Z., Xu, M.M., Jones, O., Mu, Y., Chen, S., Bryant, J., Isaacs, W.B., Ma, J., Xu, X., 2018. Comparative analysis of FKBP family protein: evaluation, structure, and function in mammals and Drosophila melanogaster. BMC Dev. Biol. 18, 7.

Gilabert, J.A., Parekh, A.B., 2000. Respiring mitochondria determine the pattern of activation and inactivation of the store-operated Ca(2+) current I(CRAC). EMBO J. 19, 6401–6407.

Gillespie, D., Fill, M., 2008. Intracellular calcium release channels mediate their own countercurrent: the ryanodine receptor case study. Biophys. J. 95, 3706–3714.

Girardot, F., Lasbleiz, C., Monnier, V., Tricoire, H., 2006. Specific age-related signatures in Drosophila body parts transcriptome. BMC Genomics 7, 69.

Gladyshev, V.N., 2016. Aging: progressive decline in fitness due to the rising deleteriome adjusted by genetic, environmental, and stochastic processes. Aging Cell 15, 594–602.

Goddeeris, M.M., Cook-Wiens, E., Horton, W.J., Wolf, H., Stoltzfus, J.R., Borrusch, M., Grotewiel, M.S., 2003. Delayed behavioural aging and altered mortality in Drosophila beta integrin mutants. Aging Cell 2, 257–264.

Goldspink, G., Harridge, S.D.R., 2004. Growth factors and muscle ageing. Exp. Gerontol. 39, 1433–1438.

Gordon, S., Dickinson, M.H., 2006. Role of calcium in the regulation of mechanical power in insect flight. Proc. Natl. Acad. Sci. U.S.A. 103, 4311–4315.

Grabarek, Z., 2006. Structural basis for diversity of the EF-hand calcium-binding proteins. J. Mol. Biol. 359, 509–525.

Greenspan, R.J., 1997. Fly Pushing: The Theory and Practice of Drosophila Genetics. Cold Spring Harbor Laboratory Press.

Grotewiel, M.S., Martin, I., Bhandari, P., Cook-Wiens, E., 2005. Functional senescence in Drosophila melanogaster. Ageing Res. Rev. 4, 372–397.

Groth, A.C., Fish, M., Nusse, R., Calos, M.P., 2004. Construction of transgenic Drosophila by using the site-specific integrase from phage phiC31. Genetics 166, 1775–1782.

Grynkiewicz, G., Poenie, M., Tsien, R.Y., 1985. A new generation of Ca2+ indicators with greatly improved fluorescence properties. J. Biol. Chem. 260, 3440–3450.

Guarnieri, S., Morabito, C., Paolini, C., Boncompagni, S., Pilla, R., Fanò-Illic, G., Mariggiò, M.A., 2013. Growth associated protein 43 is expressed in skeletal muscle fibers and is localized in proximity of mitochondria and calcium release units. PLoS ONE 8, e53267.

Guerrero-Hernandez, A., Dagnino-Acosta, A., Verkhratsky, A., 2010. An intelligent sarco-endoplasmic reticulum Ca2+ store: release and leak channels have differential access to a concealed Ca2+ pool. Cell Calcium 48, 143–149.

Hales, K.G., Korey, C.A., Larracuente, A.M., Roberts, D.M., 2015. Genetics on the Fly: A Primer on the Drosophila Model System. Genetics 201, 815–842.

Hampel, S., Chung, P., McKellar, C.E., Hall, D., Looger, L.L., Simpson, J.H., 2011. Drosophila Brainbow: a recombinase-based fluorescence labeling technique to subdivide neural expression patterns. Nat. Methods 8, 253–259.

Hansford, R.G., 1994. Physiological role of mitochondrial Ca2+ transport. J. Bioenerg. Biomembr. 26, 495–508.

Hao, L., Rigaud, J.L., Inesi, G., 1994. Ca2+/H+ countertransport and electrogenicity in proteoliposomes containing erythrocyte plasma membrane Ca-ATPase and exogenous lipids. J. Biol. Chem. 269, 14268–14275.

Harman, D., 1956. Aging: a theory based on free radical and radiation chemistry. J Gerontol 11, 298–300.

Hasan, G., Rosbash, M., 1992. Drosophila homologs of two mammalian intracellular Ca(2+)-release channels: identification and expression patterns of the inositol 1,4,5-triphosphate and the ryanodine receptor genes. Development 116, 967–975.

Haug-Collet, K., Pearson, B., Webel, R., Szerencsei, R.T., Winkfein, R.J., Schnetkamp, P.P., Colley, N.J., 1999. Cloning and characterization of a potassium-dependent sodium/calcium exchanger in Drosophila. J. Cell Biol. 147, 659–670.

Hayashi, T., Rizzuto, R., Hajnoczky, G., Su, T.-P., 2009. MAM: more than just a housekeeper. Trends Cell Biol. 19, 81–88.

He, Y., Jasper, H., 2014. Studying aging in Drosophila. Methods 68, 129–133.

Henderson, C.A., Gomez, C.G., Novak, S.M., Mi-Mi, L., Gregorio, C.C., 2017. Overview of the Muscle Cytoskeleton. Compr Physiol 7, 891–944.

Hütter, E., Skovbro, M., Lener, B., Prats, C., Rabøl, R., Dela, F., Jansen-Dürr, P., 2007. Oxidative stress and mitochondrial impairment can be separated from lipofuscin accumulation in aged human skeletal muscle. Aging Cell 6, 245–256.

Hwee, D.T., Baehr, L.M., Philp, A., Baar, K., Bodine, S.C., 2014. Maintenance of muscle mass and load-induced growth in Muscle RING Finger 1 null mice with age. Aging Cell 13, 92–101.

Jang, Y.C., Van Remmen, H., 2011. Age-associated alterations of the neuromuscular junction. Exp. Gerontol. 46, 193–198.

Jeyaraju, D.V., Cisbani, G., Pellegrini, L., 2009. Calcium regulation of mitochondria motility and morphology. Biochim. Biophys. Acta 1787, 1363–1373.

Jiménez-Moreno, R., Wang, Z.-M., Gerring, R.C., Delbono, O., 2008. Sarcoplasmic reticulum Ca2+ release declines in muscle fibers from aging mice. Biophys. J. 94, 3178–3188.

Jiménez-Moreno, R., Wang, Z.-M., Messi, M.L., Delbono, O., 2010. Sarcoplasmic reticulum Ca2+ depletion in adult skeletal muscle fibres measured with the biosensor D1ER. Pflugers Arch. 459, 725–735.

Jin, K., 2010. Modern Biological Theories of Aging. Aging Dis 1, 72–74.

Jones, D.L., Rando, T.A., 2011. Emerging models and paradigms for stem cell ageing. Nat. Cell Biol. 13, 506–512.

Josephson, R.K., Malamud, J.G., Stokes, D.R., 2000. Asynchronous muscle: a primer. Journal of Experimental Biology 203, 2713–2722.

Joshi, A., Mueller, L.D., 1997. Adult crowding effects on longevity in Drosophila melanogaster: Increase in age-independent mortality. Current Science 72, 255–260.

Kang, H.-L., Benzer, S., Min, K.-T., 2002. Life extension in Drosophila by feeding a drug. Proc. Natl. Acad. Sci. U.S.A. 99, 838–843.

Kasture, A.S., Hummel, T., Sucic, S., Freissmuth, M., 2018. Big Lessons from Tiny Flies: Drosophila melanogaster as a Model to Explore Dysfunction of Dopaminergic and Serotonergic Neurotransmitter Systems. Int J Mol Sci 19.

Kaupp, U.B., Seifert, R., 2002. Cyclic nucleotide-gated ion channels. Physiol. Rev. 82, 769–824.

Kendall, J.M., Sala-Newby, G., Ghalaut, V., Dormer, R.L., Campbell, A.K., 1992. Engineering the CA(2+)-activated photoprotein aequorin with reduced affinity for calcium. Biochem. Biophys. Res. Commun. 187, 1091–1097.

Kennedy, B.K., Berger, S.L., Brunet, A., Campisi, J., Cuervo, A.M., Epel, E.S., Franceschi, C., Lithgow, G.J., Morimoto, R.I., Pessin, J.E., Rando, T.A., Richardson, A., Schadt, E.E., Wyss-Coray, T., Sierra, F., 2014. Geroscience: linking aging to chronic disease. Cell 159, 709–713.

Khachaturian, Z.S., 1994. Calcium hypothesis of Alzheimer's disease and brain aging. Ann. N. Y. Acad. Sci. 747, 1–11.

Kim, J.H., Johannes, L., Goud, B., Antony, C., Lingwood, C.A., Daneman, R., Grinstein, S., 1998. Noninvasive measurement of the pH of the endoplasmic reticulum at rest and during calcium release. Proc. Natl. Acad. Sci. U.S.A. 95, 2997–3002.

Kirischuk, S., Verkhratsky, A., 1996. Calcium homeostasis in aged neurones. Life Sci. 59, 451–459.

Kirkwood, T.B., 1977. Evolution of ageing. Nature 270, 301–304.

Kong, H., Wang, R., Chen, W., Zhang, L., Chen, K., Shimoni, Y., Duff, H.J., Chen, S.R.W., 2007. Skeletal and cardiac ryanodine receptors exhibit different responses to Ca2+ overload and luminal ca2+. Biophys. J. 92, 2757–2770.

Kostyuk, P., Pronchuk, N., Savchenko, A., Verkhratsky, A., 1993. Calcium currents in aged rat dorsal root ganglion neurones. J. Physiol. (Lond.) 461, 467–483.

Kreko-Pierce, T., Azpurua, J., Mahoney, R.E., Eaton, B.A., 2016. Extension of Health Span and Life Span in Drosophila by S107 Requires the calstabin Homologue FK506-BP2. J. Biol. Chem. 291, 26045–26055.

Kremer, M.C., Jung, C., Batelli, S., Rubin, G.M., Gaul, U., 2017. The glia of the adult Drosophila nervous system. Glia 65, 606–638.

Kretsinger, R.H., Nockolds, C.E., 1973. Carp muscle calcium-binding protein. II. Structure determination and general description. J. Biol. Chem. 248, 3313–3326.

Kuang, S., Gillespie, M.A., Rudnicki, M.A., 2008. Niche regulation of muscle satellite cell self-renewal and differentiation. Cell Stem Cell 2, 22–31.

Kushnir, A., Santulli, G., Reiken, S.R., Coromilas, E., Godfrey, S.J., Brunjes, D.L., Colombo, P.C., Yuzefpolskaya, M., Sokol, S.I., Kitsis, R.N., Marks, A.R., 2018. Ryanodine Receptor Calcium Leak in Circulating B-Lymphocytes as a Biomarker in Heart Failure. Circulation 138, 1144–1154.

Lacampagne, A., Liu, X., Reiken, S., Bussiere, R., Meli, A.C., Lauritzen, I., Teich, A.F., Zalk, R., Saint, N., Arancio, O., Bauer, C., Duprat, F., Briggs, C.A., Chakroborty, S., Stutzmann, G.E., Shelanski, M.L., Checler, F., Chami, M., Marks, A.R., 2017. Post-translational remodeling of ryanodine receptor induces calcium leak leading to Alzheimer's disease-like pathologies and cognitive deficits. Acta Neuropathol. 134, 749–767.

Lai, F.A., Erickson, H.P., Rousseau, E., Liu, Q.Y., Meissner, G., 1988. Purification and reconstitution of the calcium release channel from skeletal muscle. Nature 331, 315–319.

Lam, A.K.M., Galione, A., 2013. The endoplasmic reticulum and junctional membrane communication during calcium signaling. Biochim. Biophys. Acta 1833, 2542–2559.

Lang, S., Erdmann, F., Jung, M., Wagner, R., Cavalie, A., Zimmermann, R., 2011. Sec61 complexes form ubiquitous ER Ca2+ leak channels. Channels (Austin) 5, 228–235.

Lanner, J.T., Georgiou, D.K., Joshi, A.D., Hamilton, S.L., 2010. Ryanodine receptors: structure, expression, molecular details, and function in calcium release. Cold Spring Harb Perspect Biol 2, a003996.

Larsson, L., Ansved, T., 1995. Effects of ageing on the motor unit. Prog. Neurobiol. 45, 397–458.

Larsson, L., Degens, H., Li, M., Salviati, L., Lee, Y.I., Thompson, W., Kirkland, J.L., Sandri, M., 2019. Sarcopenia: Aging-Related Loss of Muscle Mass and Function. Physiol. Rev. 99, 427–511.

Lehmann, F.-O., Bartussek, J., 2017. Neural control and precision of flight muscle activation in Drosophila. J. Comp. Physiol. A Neuroethol. Sens. Neural. Behav. Physiol. 203, 1–14.

Lehmann, F.-O., Dickinson, M.H., 1997. The changes in power requirements and muscle efficiency during elevated force production in the fruit fly Drosophila melanogaster. Journal of Experimental Biology 200, 1133–1143.

Lehmann, F.-O., Skandalis, D.A., Berthé, R., 2013. Calcium signalling indicates bilateral power balancing in the Drosophila flight muscle during manoeuvring flight. J R Soc Interface 10, 20121050.

Lepock, J.R., Rodahl, A.M., Zhang, C., Heynen, M.L., Waters, B., Cheng, K.H., 1990. Thermal denaturation of the Ca2(+)-ATPase of sarcoplasmic reticulum reveals two thermodynamically independent domains. Biochemistry 29, 681–689.

Li, C., Wang, X., Vais, H., Thompson, C.B., Foskett, J.K., White, C., 2007. Apoptosis regulation by Bcl-x(L) modulation of mammalian inositol 1,4,5-trisphosphate receptor channel isoform gating. Proc. Natl. Acad. Sci. U.S.A. 104, 12565–12570.

Lindsay, T., Sustar, A., Dickinson, M., 2017. The Function and Organization of the Motor System Controlling Flight Maneuvers in Flies. Curr. Biol. 27, 345–358.

Linford, N.J., Bilgir, C., Ro, J., Pletcher, S.D., 2013. Measurement of lifespan in Drosophila melanogaster. J Vis Exp.

Liou, J., Kim, M.L., Heo, W.D., Jones, J.T., Myers, J.W., Ferrell, J.E., Meyer, T., 2005. STIM is a Ca2+ sensor essential for Ca2+-store-depletion-triggered Ca2+ influx. Curr. Biol. 15, 1235–1241.

Liu, C.-H., Chen, Z., Oliva, M.K., Luo, J., Collier, S., Montell, C., Hardie, R.C., 2020. Rapid Release of Ca2+ from Endoplasmic Reticulum Mediated by Na+/Ca2+ Exchange. J. Neurosci. 40, 3152–3164.

Liu, X., Kim, C.N., Yang, J., Jemmerson, R., Wang, X., 1996. Induction of apoptotic program in cell-free extracts: requirement for dATP and cytochrome c. Cell 86, 147–157.

Longo, V.D., Mitteldorf, J., Skulachev, V.P., 2005. Programmed and altruistic ageing. Nat. Rev. Genet. 6, 866–872.

López-Otín, C., Blasco, M.A., Partridge, L., Serrano, M., Kroemer, G., 2013. The hallmarks of aging. Cell 153, 1194–1217.

Lovick, J.K., Ngo, K.T., Omoto, J.J., Wong, D.C., Nguyen, J.D., Hartenstein, V., 2013. Postembryonic lineages of the Drosophila brain: I. Development of the lineage-associated fiber tracts. Dev. Biol. 384, 228–257.

Lytton, J., 2007. Na+/Ca2+ exchangers: three mammalian gene families control Ca2+ transport. Biochem. J. 406, 365–382.

MacLennan, D.H., Asahi, M., Tupling, A.R., 2003. The regulation of SERCA-type pumps by phospholamban and sarcolipin. Ann. N. Y. Acad. Sci. 986, 472–480.

Magwere, T., Pamplona, R., Miwa, S., Martinez-Diaz, P., Portero-Otin, M., Brand, M.D., Partridge, L., 2006. Flight activity, mortality rates, and lipoxidative damage in Drosophila. J. Gerontol. A Biol. Sci. Med. Sci. 61, 136–145.

Magyar, A., Bakos, E., Váradi, A., 1995. Structure and tissue-specific expression of the Drosophila melanogaster organellar-type Ca(2+)-ATPase gene. Biochem. J. 310 (Pt 3), 757–763.

Magyar, A., Váradi, A., 1990. Molecular cloning and chromosomal localization of a sarco/endoplasmic reticulum-type Ca2(+)-ATPase of Drosophila melanogaster. Biochem. Biophys. Res. Commun. 173, 872–877.

Malick, L.E., Kidwell, J.F., 1966. The effect of mating status, sex and genotype on longevity in Drosophila melanogaster. Genetics 54, 203–209.

Manno, C., Figueroa, L.C., Gillespie, D., Fitts, R., Kang, C., Franzini-Armstrong, C., Rios, E., 2017. Calsequestrin depolymerizes when calcium is depleted in the sarcoplasmic reticulum of working muscle. Proc. Natl. Acad. Sci. U.S.A. 114, E638–E647.

Mansouri, A., Muller, F.L., Liu, Y., Ng, R., Faulkner, J., Hamilton, M., Richardson, A., Huang, T.-T., Epstein, C.J., Van Remmen, H., 2006. Alterations in mitochondrial function, hydrogen peroxide release and oxidative damage in mouse hind-limb skeletal muscle during aging. Mech. Ageing Dev. 127, 298–306.

Marshall, C.B., Nishikawa, T., Osawa, M., Stathopulos, P.B., Ikura, M., 2015. Calmodulin and STIM proteins: Two major calcium sensors in the cytoplasm and endoplasmic reticulum. Biochem. Biophys. Res. Commun. 460, 5–21.

Martin, C.A., Krantz, D.E., 2014. Drosophila melanogaster as a genetic model system to study neurotransmitter transporters. Neurochem. Int. 73, 71–88.

Martinez, V.G., Javadi, C.S., Ngo, E., Ngo, L., Lagow, R.D., Zhang, B., 2007. Age-related changes in climbing behavior and neural circuit physiology in Drosophila. Dev Neurobiol 67, 778–791.

Marx, S.O., Reiken, S., Hisamatsu, Y., Jayaraman, T., Burkhoff, D., Rosemblit, N., Marks, A.R., 2000. PKA phosphorylation dissociates FKBP12.6 from the calcium release channel (ryanodine receptor): defective regulation in failing hearts. Cell 101, 365–376.

Matsuo, E., Kamikouchi, A., 2013. Neuronal encoding of sound, gravity, and wind in the fruit fly. J. Comp. Physiol. A Neuroethol. Sens. Neural. Behav. Physiol. 199, 253–262.

Medawar, P.B., 1952. An Unsolved Problem of Biology: An Inaugural Lecture Delivered at University College, London, 6 December, 1951. H.K. Lewis and Company.

Mei, Y., Xu, L., Kramer, H.F., Tomberlin, G.H., Townsend, C., Meissner, G., 2013. Stabilization of the skeletal muscle ryanodine receptor ion channel-FKBP12 complex by the 1,4-benzothiazepine derivative S107. PLoS ONE 8, e54208.

Meissner, G., 1986. Ryanodine activation and inhibition of the Ca2+ release channel of sarcoplasmic reticulum. J. Biol. Chem. 261, 6300–6306.

Meissner, G., McKinley, D., 1982. Permeability of canine cardiac sarcoplasmic reticulum vesicles to K+, Na+, H+, and Cl-. J. Biol. Chem. 257, 7704–7711.

Michno, K., Knight, D., Campusano, J.M., Campussano, J.M., van de Hoef, D., Boulianne, G.L., 2009. Intracellular calcium deficits in Drosophila cholinergic neurons expressing wild type or FAD-mutant presenilin. PLoS ONE 4, e6904.

Mikoshiba, K., 2007. IP3 receptor/Ca2+ channel: from discovery to new signaling concepts. J. Neurochem. 102, 1426–1446.

Miller, C., 1978. Voltage-gated cation conductance channel from fragmented sarcoplasmic reticulum: steady-state electrical properties. J. Membr. Biol. 40, 1–23.

Miller, M.S., Lekkas, P., Braddock, J.M., Farman, G.P., Ballif, B.A., Irving, T.C., Maughan, D.W., Vigoreaux, J.O., 2008. Aging enhances indirect flight muscle fiber performance yet decreases flight ability in Drosophila. Biophys. J. 95, 2391–2401.

Minta, A., Kao, J.P., Tsien, R.Y., 1989. Fluorescent indicators for cytosolic calcium based on rhodamine and fluorescein chromophores. J. Biol. Chem. 264, 8171–8178.

Miquel, J., Lundgren, P.R., Bensch, K.G., Atlan, H., 1976. Effects of temperature on the life span, vitality and fine structure of Drosophila melanogaster. Mech. Ageing Dev. 5, 347–370.

Mitra, R.D., Silva, C.M., Youvan, D.C., 1996. Fluorescence resonance energy transfer between blue-emitting and red-shifted excitation derivatives of the green fluorescent protein. Gene 173, 13–17.

Miyawaki, A., Furuichi, T., Maeda, N., Mikoshiba, K., 1990. Expressed cerebellar-type inositol 1,4,5-trisphosphate receptor, P400, has calcium release activity in a fibroblast L cell line. Neuron 5, 11–18.

Mockett, R.J., Orr, W.C., Rahmandar, J.J., Sohal, B.H., Sohal, R.S., 2001. Antioxidant status and stress resistance in long- and short-lived lines of Drosophila melanogaster. Exp. Gerontol. 36, 441–463.

Montell, C., Rubin, G.M., 1989. Molecular characterization of the Drosophila trp locus: a putative integral membrane protein required for phototransduction. Neuron 2, 1313–1323.

Montero, M., Alonso, M.T., Carnicero, E., Cuchillo-Ibáñez, I., Albillos, A., García, A.G., García-Sancho, J., Alvarez, J., 2000. Chromaffin-cell stimulation triggers fast millimolar mitochondrial Ca2+ transients that modulate secretion. Nat. Cell Biol. 2, 57–61.

Moore, G.A., McConkey, D.J., Kass, G.E., O'Brien, P.J., Orrenius, S., 1987. 2,5-Di(tert-butyl)-1,4-benzohydroquinone--a novel inhibitor of liver microsomal Ca2+ sequestration. FEBS Lett. 224, 331–336.

Morgan, T.H., 1910. SEX LIMITED INHERITANCE IN DROSOPHILA. Science 32, 120–122.

Muñoz-Alarcón, A., Pavlovic, M., Wismar, J., Schmitt, B., Eriksson, M., Kylsten, P., Dushay, M.S., 2007. Characterization of lamin mutation phenotypes in Drosophila and comparison to human laminopathies. PLoS ONE 2, e532.

Mureli, S., Fox, J.L., 2015. Haltere mechanosensory influence on tethered flight behavior in Drosophila. J. Exp. Biol. 218, 2528–2537.

Nair, K.S., 2005. Aging muscle. Am. J. Clin. Nutr. 81, 953–963.

Nakai, J., Ohkura, M., Imoto, K., 2001. A high signal-to-noise Ca(2+) probe composed of a single green fluorescent protein. Nat. Biotechnol. 19, 137–141.

Nakamura, K., Zuppini, A., Arnaudeau, S., Lynch, J., Ahsan, I., Krause, R., Papp, S., De Smedt, H., Parys, J.B., Muller-Esterl, W., Lew, D.P., Krause, K.H., Demaurex, N., Opas, M., Michalak, M., 2001. Functional specialization of calreticulin domains. J. Cell Biol. 154, 961–972.

Namiki, S., Dickinson, M.H., Wong, A.M., Korff, W., Card, G.M., 2018. The functional organization of descending sensory-motor pathways in Drosophila. Elife 7.

Navas-Navarro, P., Rojo-Ruiz, J., Rodriguez-Prados, M., Ganfornina, M.D., Looger, L.L., Alonso, M.T., García-Sancho, J., 2016. GFP-Aequorin Protein Sensor for Ex Vivo and In Vivo Imaging of Ca(2+) Dynamics in High-Ca(2+) Organelles. Cell Chem Biol 23, 738–745.

Nilwik, R., Snijders, T., Leenders, M., Groen, B.B.L., van Kranenburg, J., Verdijk, L.B., van Loon, L.J.C., 2013. The decline in skeletal muscle mass with aging is mainly attributed to a reduction in type II muscle fiber size. Exp. Gerontol. 48, 492–498.

Ogborn, D.I., McKay, B.R., Crane, J.D., Parise, G., Tarnopolsky, M.A., 2014. The unfolded protein response is triggered following a single, unaccustomed resistance-exercise bout. Am. J. Physiol. Regul. Integr. Comp. Physiol. 307, R664-669.

Ohkura, M., Sasaki, T., Sadakari, J., Gengyo-Ando, K., Kagawa-Nagamura, Y., Kobayashi, C., Ikegaya, Y., Nakai, J., 2012. Genetically encoded green fluorescent Ca2+ indicators with improved detectability for neuronal Ca2+ signals. PLoS ONE 7, e51286.

Ojima, K., 2019. Myosin: Formation and maintenance of thick filaments. Anim. Sci. J. 90, 801–807.

Ong, C., Yung, L.-Y.L., Cai, Y., Bay, B.-H., Baeg, G.-H., 2015. Drosophila melanogaster as a model organism to study nanotoxicity. Nanotoxicology 9, 396–403.

Palmer, A.E., Jin, C., Reed, J.C., Tsien, R.Y., 2004. Bcl-2-mediated alterations in endoplasmic reticulum Ca2+ analyzed with an improved genetically encoded fluorescent sensor. Proc. Natl. Acad. Sci. U.S.A. 101, 17404–17409.

Palmer, A.E., Qin, Y., Park, J.G., McCombs, J.E., 2011. Design and application of genetically encoded biosensors. Trends Biotechnol. 29, 144–152.

Palmer, A.E., Tsien, R.Y., 2006. Measuring calcium signaling using genetically targetable fluorescent indicators. Nat Protoc 1, 1057–1065.

Park, D.C., Yeo, S.G., 2013. Aging. Korean J Audiol 17, 39–44.

Partridge, L., Barton, N.H., 1993. Evolution of aging: testing the theory using Drosophila. Genetica 91, 89–98.

Patel, S., Joseph, S.K., Thomas, A.P., 1999. Molecular properties of inositol 1,4,5-trisphosphate receptors. Cell Calcium 25, 247–264.

Patron, M., Raffaello, A., Granatiero, V., Tosatto, A., Merli, G., De Stefani, D., Wright, L., Pallafacchina, G., Terrin, A., Mammucari, C., Rizzuto, R., 2013. The mitochondrial calcium uniporter (MCU): molecular identity and physiological roles. J. Biol. Chem. 288, 10750–10758.

Patterson, R.L., Boehning, D., Snyder, S.H., 2004. Inositol 1,4,5-trisphosphate receptors as signal integrators. Annu. Rev. Biochem. 73, 437–465.

Payne, A.M., Zheng, Z., González, E., Wang, Z.-M., Messi, M.L., Delbono, O., 2004. External Ca(2+)-dependent excitation--contraction coupling in a population of ageing mouse skeletal muscle fibres. J. Physiol. (Lond.) 560, 137–155.

Pérez, V.I., Bokov, A., Van Remmen, H., Mele, J., Ran, Q., Ikeno, Y., Richardson, A., 2009. Is the oxidative stress theory of aging dead? Biochim. Biophys. Acta 1790, 1005–1014.

Periasamy, M., Kalyanasundaram, A., 2007. SERCA pump isoforms: their role in calcium transport and disease. Muscle Nerve 35, 430–442.

Phillips, M.J., Voeltz, G.K., 2016. Structure and function of ER membrane contact sites with other organelles. Nat. Rev. Mol. Cell Biol. 17, 69–82.

Piccirillo, R., Demontis, F., Perrimon, N., Goldberg, A.L., 2014. Mechanisms of muscle growth and atrophy in mammals and Drosophila. Dev. Dyn. 243, 201–215.

Pittendrigh, C.S., Minis, D.H., 1972. Circadian systems: longevity as a function of circadian resonance in Drosophila melanogaster. Proc. Natl. Acad. Sci. U.S.A. 69, 1537–1539.

Powell, J.R., 1997. Progress and Prospects in Evolutionary Biology: The Drosophila Model. Oxford University Press.

Pozzan, T., Rizzuto, R., Volpe, P., Meldolesi, J., 1994. Molecular and cellular physiology of intracellular calcium stores. Physiol. Rev. 74, 595–636.

Prakriya, M., Lewis, R.S., 2015. Store-Operated Calcium Channels. Physiol. Rev. 95, 1383–1436.

Prins, D., Michalak, M., 2011. Organellar calcium buffers. Cold Spring Harb Perspect Biol 3.

Prins, D., Michalak, M., 2009. Endoplasmic reticulum proteins in cardiac development and dysfunction. Can. J. Physiol. Pharmacol. 87, 419–425.

Prochniewicz, E., Thompson, L.V., Thomas, D.D., 2007. Age-related decline in actomyosin structure and function. Exp. Gerontol. 42, 931–938.

Putney, J.W., 1986. A model for receptor-regulated calcium entry. Cell Calcium 7, 1–12.

Pyza, E., Meinertzhagen, I.A., 1993. Daily and circadian rhythms of synaptic frequency in the first visual neuropile of the housefly's (Musca domestica L.) optic lobe. Proc. Biol. Sci. 254, 97–105.

Reddish, F.N., Miller, C.L., Gorkhali, R., Yang, J.J., 2017. Calcium Dynamics Mediated by the Endoplasmic/Sarcoplasmic Reticulum and Related Diseases. Int J Mol Sci 18.

Reece, J.B., 2011. Campbell Biology. Benjamin Cummings / Pearson.

Rhodenizer, D., Martin, I., Bhandari, P., Pletcher, S.D., Grotewiel, M., 2008. Genetic and environmental factors impact age-related impairment of negative geotaxis in Drosophila by altering age-dependent climbing speed. Exp. Gerontol. 43, 739–748.

Ríos, E., 2018. Calcium-induced release of calcium in muscle: 50 years of work and the emerging consensus. J. Gen. Physiol. 150, 521–537.

Rizzuto, R., De Stefani, D., Raffaello, A., Mammucari, C., 2012. Mitochondria as sensors and regulators of calcium signalling. Nat. Rev. Mol. Cell Biol. 13, 566–578.

Rizzuto, R., Pozzan, T., 2006. Microdomains of intracellular Ca2+: molecular determinants and functional consequences. Physiol. Rev. 86, 369–408.

Rodriguez-Garcia, A., Rojo-Ruiz, J., Navas-Navarro, P., Aulestia, F.J., Gallego-Sandin, S., Garcia-Sancho, J., Alonso, M.T., 2014. GAP, an aequorin-based fluorescent indicator for imaging Ca2+ in organelles. Proc Natl Acad Sci U S A 111, 2584–2589.

Rodríguez-Prados, M., Rojo-Ruiz, J., Aulestia, F.J., García-Sancho, J., Alonso, M.T., 2015. A new low-Ca^{2+} affinity GAP indicator to monitor high Ca^{2+} in organelles by luminescence. Cell Calcium 58, 558–564.

Rooyackers, O.E., Adey, D.B., Ades, P.A., Nair, K.S., 1996. Effect of age on in vivo rates of mitochondrial protein synthesis in human skeletal muscle. Proc. Natl. Acad. Sci. U.S.A. 93, 15364–15369.

Rossi, D., Barone, V., Giacomello, E., Cusimano, V., Sorrentino, V., 2008. The sarcoplasmic reticulum: an organized patchwork of specialized domains. Traffic 9, 1044–1049.

Royer, L., Ríos, E., 2009. Deconstructing calsequestrin. Complex buffering in the calcium store of skeletal muscle. J. Physiol. (Lond.) 587, 3101–3111.

Ruan, H., Tang, X.D., Chen, Mai-Lei, Joiner, M.-L.A., Sun, G., Brot, N., Weissbach, H., Heinemann, Stefan H., Iverson, L., Wu, C.-F., Hoshi, T., Chen, M.-L., Joiner, M.A., Heinemann, Stephen H., 2002. High-quality life extension by the enzyme peptide methionine sulfoxide reductase. Proc. Natl. Acad. Sci. U.S.A. 99, 2748–2753.

Rubin, D.M., Mehta, A.D., Zhu, J., Shoham, S., Chen, X., Wells, Q.R., Palter, K.B., 1993. Genomic structure and sequence analysis of Drosophila melanogaster HSC70 genes. Gene 128, 155–163.

Rubin, G.M., Spradling, A.C., 1982. Genetic transformation of Drosophila with transposable element vectors. Science 218, 348–353.

Rudolf, R., Magalhães, P.J., Pozzan, T., 2006. Direct in vivo monitoring of sarcoplasmic reticulum Ca2+ and cytosolic cAMP dynamics in mouse skeletal muscle. J. Cell Biol. 173, 187–193.

Ruknudin, A., Valdivia, C., Kofuji, P., Lederer, W.J., Schulze, D.H., 1997. Na+/Ca2+ exchanger in Drosophila: cloning, expression, and transport differences. Am. J. Physiol. 273, C257-265.

Santulli, G., Marks, A.R., 2015. Essential Roles of Intracellular Calcium Release Channels in Muscle, Brain, Metabolism, and Aging. Curr Mol Pharmacol 8, 206–222.

Sanyal, S., Consoulas, C., Kuromi, H., Basole, A., Mukai, L., Kidokoro, Y., Krishnan, K.S., Ramaswami, M., 2005. Analysis of conditional paralytic mutants in Drosophila sarco-endoplasmic reticulum calcium ATPase reveals novel mechanisms for regulating membrane excitability. Genetics 169, 737–750.

Sanyal, S., Jennings, T., Dowse, H., Ramaswami, M., 2006. Conditional mutations in SERCA, the Sarco-endoplasmic reticulum Ca2+-ATPase, alter heart rate and rhythmicity in Drosophila. J. Comp. Physiol. B, Biochem. Syst. Environ. Physiol. 176, 253–263.

Schatzmann, H.J., 1966. ATP-dependent Ca++-extrusion from human red cells. Experientia 22, 364–365.

Schiaffino, S., 2012. Tubular aggregates in skeletal muscle: just a special type of protein aggregates? Neuromuscul. Disord. 22, 199–207.

Schnetkamp, P.P.M., 2004. The SLC24 Na+/Ca2+-K+ exchanger family: vision and beyond. Pflugers Arch. 447, 683–688.

Schwaller, B., 2010. Cytosolic Ca2+ buffers. Cold Spring Harb Perspect Biol 2, a004051.

Seo, A.Y., Xu, J., Servais, S., Hofer, T., Marzetti, E., Wohlgemuth, S.E., Knutson, M.D., Chung, H.Y., Leeuwenburgh, C., 2008. Mitochondrial iron accumulation with age and functional consequences. Aging Cell 7, 706–716.

Seo, M.-D., Enomoto, M., Ishiyama, N., Stathopulos, P.B., Ikura, M., 2015. Structural insights into endoplasmic reticulum stored calcium regulation by inositol 1,4,5-trisphosphate and ryanodine receptors. Biochim. Biophys. Acta 1853, 1980–1991.

Shah, S.Z.A., Zhao, D., Khan, S.H., Yang, L., 2015. Regulatory Mechanisms of Endoplasmic Reticulum Resident IP3 Receptors. J. Mol. Neurosci. 56, 938–948.

Sharma, V., O'Halloran, D.M., 2014. Recent structural and functional insights into the family of sodium calcium exchangers. Genesis 52, 93–109.

Shcherbata, H.R., Yatsenko, A.S., Patterson, L., Sood, V.D., Nudel, U., Yaffe, D., Baker, D., Ruohola-Baker, H., 2007. Dissecting muscle and neuronal disorders in a Drosophila model of muscular dystrophy. EMBO J. 26, 481–493.

Shefer, G., Rauner, G., Yablonka-Reuveni, Z., Benayahu, D., 2010. Reduced satellite cell numbers and myogenic capacity in aging can be alleviated by endurance exercise. PLoS ONE 5, e13307.

Shigetomi, E., Patel, S., Khakh, B.S., 2016. Probing the Complexities of Astrocyte Calcium Signaling. Trends Cell Biol. 26, 300–312.

Shimomura, O., Johnson, F.H., 1972. Structure of the light-emitting moiety of aequorin. Biochemistry 11, 1602–1608.

Shimomura, O., Johnson, F.H., Saiga, Y., 1962. Extraction, purification and properties of aequorin, a bioluminescent protein from the luminous hydromedusan, Aequorea. J Cell Comp Physiol 59, 223–239.

Shuttleworth, T.J., 2009. Arachidonic acid, ARC channels, and Orai proteins. Cell Calcium 45, 602–610.

Simon, A.F., Liang, D.T., Krantz, D.E., 2006. Differential decline in behavioral performance of Drosophila melanogaster with age. Mech. Ageing Dev. 127, 647–651.

Sinha, M., Hasan, G., 1999. Sequencing and exon mapping of the inositol 1,4,5-trisphosphate receptor cDNA from Drosophila embryos suggests the presence of differentially regulated forms of RNA and protein. Gene 233, 271–276.

Skulachev, V.P., 1999. Phenoptosis: programmed death of an organism. Biochemistry Mosc. 64, 1418–1426.

Smith, L.A., Wang, X., Peixoto, A.A., Neumann, E.K., Hall, L.M., Hall, J.C., 1996. A Drosophila calcium channel alpha1 subunit gene maps to a genetic locus associated with behavioral and visual defects. J. Neurosci. 16, 7868–7879.

Smith, M.J., 1992. Nucleotide sequence of a Drosophila melanogaster gene encoding a calreticulin homologue. DNA Seq. 3, 247–250.

Smyth, J.T., Hwang, S.-Y., Tomita, T., DeHaven, W.I., Mercer, J.C., Putney, J.W., 2010. Activation and regulation of store-operated calcium entry. J. Cell. Mol. Med. 14, 2337–2349.

Soares, L., Parisi, M., Bonini, N.M., 2014. Axon injury and regeneration in the adult Drosophila. Sci Rep 4, 6199.

Sohal, R.S., Orr, W.C., 2012. The redox stress hypothesis of aging. Free Radic. Biol. Med. 52, 539–555.

Somlyo, A.V., Gonzalez-Serratos, H.G., Shuman, H., McClellan, G., Somlyo, A.P., 1981. Calcium release and ionic changes in the sarcoplasmic reticulum of tetanized muscle: an electron-probe study. J. Cell Biol. 90, 577–594.

Sørensen, J.G., Loeschcke, V., 2001. Larval crowding in Drosophila melanogaster induces Hsp70 expression, and leads to increased adult longevity and adult thermal stress resistance. J. Insect Physiol. 47, 1301–1307.

Sorrentino, V., 2011. Sarcoplasmic reticulum: structural determinants and protein dynamics. Int. J. Biochem. Cell Biol. 43, 1075–1078.

Sorrentino, V., 2004. Molecular determinants of the structural and functional organization of the sarcoplasmic reticulum. Biochim. Biophys. Acta 1742, 113–118.

Southall, T.D., Terhzaz, S., Cabrero, P., Chintapalli, V.R., Evans, J.M., Dow, J.A.T., Davies, S.-A., 2006. Novel subcellular locations and functions for secretory pathway Ca2+/Mn2+-ATPases. Physiol. Genomics 26, 35–45.

Srikanth, S., Wang, Z., Tu, H., Nair, S., Mathew, M.K., Hasan, G., Bezprozvanny, I., 2004. Functional properties of the Drosophila melanogaster inositol 1,4,5-trisphosphate receptor mutants. Biophys. J. 86, 3634–3646.

Stein, W.D., 1967. The movement of molecules across cell membranes. Academic Press.

Stenholm, S., Harris, T.B., Rantanen, T., Visser, M., Kritchevsky, S.B., Ferrucci, L., 2008. Sarcopenic obesity: definition, cause and consequences. Curr Opin Clin Nutr Metab Care 11, 693–700.

Strehler, E.E., Treiman, M., 2004. Calcium pumps of plasma membrane and cell interior. Curr. Mol. Med. 4, 323–335.

Stump, C.S., Short, K.R., Bigelow, M.L., Schimke, J.M., Nair, K.S., 2003. Effect of insulin on human skeletal muscle mitochondrial ATP production, protein synthesis, and mRNA transcripts. Proc. Natl. Acad. Sci. U.S.A. 100, 7996–8001.

Stutzmann, G.E., Smith, I., Caccamo, A., Oddo, S., Laferla, F.M., Parker, I., 2006. Enhanced ryanodine receptor recruitment contributes to Ca2+ disruptions in young, adult, and aged Alzheimer's disease mice. J. Neurosci. 26, 5180–5189.

Sun, B., Stewart, B.D., Kucharski, A.N., Kekenes-Huskey, P.M., 2019. Thermodynamics of Cation Binding to the Sarcoendoplasmic Reticulum Calcium ATPase Pump and Impacts on Enzyme Function. J Chem Theory Comput 15, 2692–2705.

Suzuki, J., Kanemaru, K., Ishii, K., Ohkura, M., Okubo, Y., Iino, M., 2014. Imaging intraorganellar Ca2+ at subcellular resolution using CEPIA. Nat Commun 5, 4153.

Sztretye, M., Yi, J., Figueroa, L., Zhou, J., Royer, L., Allen, P., Brum, G., Ríos, E., 2011. Measurement of RyR permeability reveals a role of calsequestrin in termination of SR Ca(2+) release in skeletal muscle. J. Gen. Physiol. 138, 231–247.

Takahashi, A., Camacho, P., Lechleiter, J.D., Herman, B., 1999. Measurement of intracellular calcium. Physiol. Rev. 79, 1089–1125.

Takeshima, H., Nishi, M., Iwabe, N., Miyata, T., Hosoya, T., Masai, I., Hotta, Y., 1994. Isolation and characterization of a gene for a ryanodine receptor/calcium release channel in Drosophila melanogaster. FEBS Lett. 337, 81–87.

Talbot, J., Maves, L., 2016. Skeletal muscle fiber type: using insights from muscle developmental biology to dissect targets for susceptibility and resistance to muscle disease. Wiley Interdiscip Rev Dev Biol 5, 518–534.

Tang, S., Wong, H.-C., Wang, Z.-M., Huang, Y., Zou, J., Zhuo, Y., Pennati, A., Gadda, G., Delbono, O., Yang, J.J., 2011. Design and application of a class of sensors to monitor Ca2+ dynamics in high Ca2+ concentration cellular compartments. Proc. Natl. Acad. Sci. U.S.A. 108, 16265–16270.

Taylor, C.W., Tovey, S.C., 2010. IP(3) receptors: toward understanding their activation. Cold Spring Harb Perspect Biol 2, a004010.

Taylor, M.V., 2013. Comparison of Muscle Development in Drosophila and Vertebrates. Landes Bioscience.

Thastrup, O., Dawson, A.P., Scharff, O., Foder, B., Cullen, P.J., Drøbak, B.K., Bjerrum, P.J., Christensen, S.B., Hanley, M.R., 1989. Thapsigargin, a novel molecular probe for studying intracellular calcium release and storage. Agents Actions 27, 17–23.

Thibault, O., Gant, J.C., Landfield, P.W., 2007. Expansion of the calcium hypothesis of brain aging and Alzheimer's disease: minding the store. Aging Cell 6, 307–317.

Thibault, O., Landfield, P.W., 1996. Increase in single L-type calcium channels in hippocampal neurons during aging. Science 272, 1017–1020.

Tian, L., Hires, S.A., Mao, T., Huber, D., Chiappe, M.E., Chalasani, S.H., Petreanu, L., Akerboom, J., McKinney, S.A., Schreiter, E.R., Bargmann, C.I., Jayaraman, V., Svoboda, K., Looger, L.L., 2009. Imaging neural activity in worms, flies and mice with improved GCaMP calcium indicators. Nat. Methods 6, 875–881.

Timerman, A.P., Ogunbumni, E., Freund, E., Wiederrecht, G., Marks, A.R., Fleischer, S., 1993. The calcium release channel of sarcoplasmic reticulum is modulated by FK-506-binding protein. Dissociation and reconstitution of FKBP-12 to the calcium release channel of skeletal muscle sarcoplasmic reticulum. J. Biol. Chem. 268, 22992–22999.

Tinel, H., Cancela, J.M., Mogami, H., Gerasimenko, J.V., Gerasimenko, O.V., Tepikin, A.V., Petersen, O.H., 1999. Active mitochondria surrounding the pancreatic acinar granule region prevent spreading of inositol trisphosphate-evoked local cytosolic Ca(2+) signals. EMBO J. 18, 4999–5008.

Toescu, E.C., Verkhratsky, A., 2003. Neuronal ageing from an intraneuronal perspective: roles of endoplasmic reticulum and mitochondria. Cell Calcium 34, 311–323.

Toescu, E.C., Vreugdenhil, M., 2010. Calcium and normal brain ageing. Cell Calcium 47, 158–164.

Toroser, D., Orr, W.C., Sohal, R.S., 2007. Carbonylation of mitochondrial proteins in Drosophila melanogaster during aging. Biochem. Biophys. Res. Commun. 363, 418–424.

Toyoshima, C., 2009. How Ca2+-ATPase pumps ions across the sarcoplasmic reticulum membrane. Biochim. Biophys. Acta 1793, 941–946.

Toyoshima, C., Nomura, H., Sugita, Y., 2003. Crystal structures of Ca2+-ATPase in various physiological states. Ann. N. Y. Acad. Sci. 986, 1–8.

Tsien, R.Y., 1981. A non-disruptive technique for loading calcium buffers and indicators into cells. Nature 290, 527–528.

Tu, H., Nelson, O., Bezprozvanny, A., Wang, Z., Lee, S.-F., Hao, Y.-H., Serneels, L., De Strooper, B., Yu, G., Bezprozvanny, I., 2006. Presenilins form ER Ca2+ leak channels, a function disrupted by familial Alzheimer's disease-linked mutations. Cell 126, 981–993.

Vajente, N., Norante, R., Pizzo, P., Pendin, D., 2020. Calcium Imaging in Drosophila melanogaster. Adv. Exp. Med. Biol. 1131, 881–900.

van Heemst, D., 2010. Insulin, IGF-1 and longevity. Aging Dis 1, 147–157.

Vandecaetsbeek, I., Vangheluwe, P., Raeymaekers, L., Wuytack, F., Vanoevelen, J., 2011. The Ca2+ pumps of the endoplasmic reticulum and Golgi apparatus. Cold Spring Harb Perspect Biol 3.

Vangheluwe, P., Raeymaekers, L., Dode, L., Wuytack, F., 2005. Modulating sarco(endo)plasmic reticulum Ca2+ ATPase 2 (SERCA2) activity: cell biological implications. Cell Calcium 38, 291–302.

Vanterpool, C.K., Vanterpool, E.A., Pearce, W.J., Buchholz, J.N., 2006. Advancing age alters the expression of the ryanodine receptor 3 isoform in adult rat superior cervical ganglia. J. Appl. Physiol. 101, 392–400.

Venkatachalam, K., Wong, C.-O., Zhu, M.X., 2015. The Role of TRPMLs in Endolysosomal Trafficking and Function. Cell Calcium 58, 48–56.

Venkiteswaran, G., Hasan, G., 2009. Intracellular Ca2+ signaling and store-operated Ca2+ entry are required in Drosophila neurons for flight. Proc. Natl. Acad. Sci. U.S.A. 106, 10326–10331.

Vervliet, T., 2018. Ryanodine Receptors in Autophagy: Implications for Neurodegenerative Diseases? Front Cell Neurosci 12, 89.

Vijg, J., Campisi, J., 2008. Puzzles, promises and a cure for ageing. Nature 454, 1065–1071.

Viña, J., Borrás, C., Miquel, J., 2007. Theories of ageing. IUBMB Life 59, 249–254.

Volterra, A., Liaudet, N., Savtchouk, I., 2014. Astrocyte Ca^{2+} signalling: an unexpected complexity. Nat. Rev. Neurosci. 15, 327–335.

Vonhoff, F., Keshishian, H., 2017. In Vivo Calcium Signaling during Synaptic Refinement at the Drosophila Neuromuscular Junction. J. Neurosci. 37, 5511–5526.

Wagner, N., Laugks, U., Heckmann, M., Asan, E., Neuser, K., 2015. Aging Drosophila melanogaster display altered pre- and postsynaptic ultrastructure at adult neuromuscular junctions. J. Comp. Neurol. 523, 2457–2475.

Walkinshaw, E., Gai, Y., Farkas, C., Richter, D., Nicholas, E., Keleman, K., Davis, R.L., 2015. Identification of genes that promote or inhibit olfactory memory formation in Drosophila. Genetics 199, 1173–1182.

Wandrag, L., Siervo, M., Riley, H.L., Khosravi, M., Fernandez, B.O., Leckstrom, C.A., Martin, D.S., Mitchell, K., Levett, D.Z.H., Montgomery, H.E., Mythen, M.G., Stroud, M.A., Grocott, M.P.W., Feelisch, M., Caudwell Xtreme Everest Research Group, 2017. Does hypoxia play a role in the development of sarcopenia in humans? Mechanistic insights from the Caudwell Xtreme Everest Expedition. Redox Biol 13, 60–68.

Wang, Q.-C., Zheng, Qiaoxia, Tan, H., Zhang, B., Li, X., Yang, Y., Yu, J., Liu, Y., Chai, H., Wang, X., Sun, Z., Wang, J.-Q., Zhu, S., Wang, F., Yang, M., Guo, C., Wang, H., Zheng, Qingyin, Li, Y., Chen, Q., Zhou, A., Tang, T.-S., 2016. TMCO1 Is an ER Ca(2+) Load-Activated Ca(2+) Channel. Cell 165, 1454–1466.

Wang, S., Trumble, W.R., Liao, H., Wesson, C.R., Dunker, A.K., Kang, C.H., 1998. Crystal structure of calsequestrin from rabbit skeletal muscle sarcoplasmic reticulum. Nat. Struct. Biol. 5, 476–483.

Wangler, M.F., Yamamoto, S., Bellen, H.J., 2015. Fruit flies in biomedical research. Genetics 199, 639–653.

Webb, S., Tribe, M.A., 1974. Are there major degenerative changes in the flight muscle of ageing diptera? Exp. Gerontol. 9, 43–49.

Weitkunat, M., Brasse, M., Bausch, A.R., Schnorrer, F., 2017. Mechanical tension and spontaneous muscle twitching precede the formation of cross-striated muscle in vivo. Development 144, 1261–1272.

White, K.E., Humphrey, D.M., Hirth, F., 2010. The dopaminergic system in the aging brain of Drosophila. Front Neurosci 4, 205.

Xin, H.B., Timerman, A.P., Onoue, H., Wiederrecht, G.J., Fleischer, S., 1995. Affinity purification of the ryanodine receptor/calcium release channel from fast twitch skeletal muscle based on its tight association with FKBP12. Biochem. Biophys. Res. Commun. 214, 263–270.

Xiong, J., Verkhratsky, A., Toescu, E.C., 2002. Changes in mitochondrial status associated with altered Ca2+ homeostasis in aged cerebellar granule neurons in brain slices. J. Neurosci. 22, 10761–10771.

Xu, L., Mann, G., Meissner, G., 1996. Regulation of cardiac Ca2+ release channel (ryanodine receptor) by Ca2+, H+, Mg2+, and adenine nucleotides under normal and simulated ischemic conditions. Circ. Res. 79, 1100–1109.

Yao, K.M., Samson, M.L., Reeves, R., White, K., 1993. Gene elav of Drosophila melanogaster: a prototype for neuronal-specific RNA binding protein gene family that is conserved in flies and humans. J. Neurobiol. 24, 723–739.

Yazawa, M., Ferrante, C., Feng, J., Mio, K., Ogura, T., Zhang, M., Lin, P.-H., Pan, Z., Komazaki, S., Kato, K., Nishi, M., Zhao, X., Weisleder, N., Sato, C., Ma, J., Takeshima, H., 2007. TRIC channels are essential for Ca2+ handling in intracellular stores. Nature 448, 78–82.

Yoshihara, M., Ensminger, A.W., Littleton, J.T., 2001. Neurobiology and the Drosophila genome. Funct. Integr. Genomics 1, 235–240.

Yui, R., Ohno, Y., Matsuura, E.T., 2003. Accumulation of deleted mitochondrial DNA in aging Drosophila melanogaster. Genes Genet. Syst. 78, 245–251.

Zalk, R., Lehnart, S.E., Marks, A.R., 2007. Modulation of the ryanodine receptor and intracellular calcium. Annu. Rev. Biochem. 76, 367–385.

Zatti, G., Burgo, A., Giacomello, M., Barbiero, L., Ghidoni, R., Sinigaglia, G., Florean, C., Bagnoli, S., Binetti, G., Sorbi, S., Pizzo, P., Fasolato, C., 2006. Presenilin mutations linked to familial Alzheimer's disease reduce endoplasmic reticulum and Golgi apparatus calcium levels. Cell Calcium 39, 539–550.

Zhang, X., Hu, M., Yang, Y., Xu, H., 2018. Organellar TRP Channels. Nat Struct Mol Biol 25, 1009–1018.

Zhou, Y., Frey, T.K., Yang, J.J., 2009. Viral calciomics: interplays between Ca2+ and virus. Cell Calcium 46, 1–17.

Zhu, H., Bhattacharyya, B.J., Lin, H., Gomez, C.M., 2011. Skeletal muscle IP3R1 receptors amplify physiological and pathological synaptic calcium signals. J. Neurosci. 31, 15269–15283.